N81-71117

APPLICATIONS REVIEW PANEL:

HIGH RESOLUTION PASSIVE MICROWAVE SATELLITES

FINAL REPORT

14 APRIL 1978

PREPARED FOR OFFICE OF APPLICATIONS
NASA HEADQUARTERS
J. LEHMANN: CO-ORDINATOR
P. GLOERSEN: CONTRACT MONITOR
UNDER CONTRACT NAS5-23677

EDITED BY: DAVID H. STAELIN (617)253-3711
PHILIP W. ROSENKRANZ (617)253-3073

RESEARCH LABORATORY OF ELECTRONICS
MASSACHUSETTS INSTITUTE OF TECHNOLOGY
CAMBRIDGE, MASSACHUSETTS 02139

REPRODUCED BY
NATIONAL TECHNICAL
INFORMATION SERVICE
U.S. DEPARTMENT OF COMMERCE
SPRINGFIELD, VA. 22161

Errata

page

5-32, 6-39 Rosenkranz, Staelin, and Grody, J. Geophys. Res. 83 (1978): change "in press" to "pp. 1857-1868".

6-3 Line 2: change "17" to "18".
Line 5: change "five" to "six".

6-4 Line 15: change "Scanned" to "Scanning".

6-14 Line 1: change "Atmospheric" to "Aeronautics".

6-24 Equation (8) should read:

$$\frac{R}{f}\frac{\partial T_B}{\partial \eta} = \int_{-\infty}^{\ell n P_s} V \frac{d\, W(\nu,P)}{d\, \ell n\, P}\, d\, \ell n\, P - V_s\, W(\nu,P_s)$$

6-33 Table 6.1: at end of caption add "(NEMS or SCAMS channels)".

7-66 Crutzen, Isaksen, and McAfee, J. Geophys. Res.: change "in press, 1977" to "83, 345-363, 1978".

7-69 Wofsy, S. C.: change "preprint draft dated February 1977" to "J. Geophys. Res. 83, 364-378, 1978".

APPLICATIONS REVIEW PANEL:
HIGH RESOLUTION PASSIVE MICROWAVE SATELLITES

CHAIRMAN:

D. H. Staelin[D]	Systems (Chapter 8)

SUBCOMMITTEE CHAIRMEN:

P. Gloersen[E]	Monitoring of Sea and Land Ice (Chapter 2)
N. Grody[G]	Applications to Synoptic Meteorology and Climatology (Chapter 6)
T. J. Schmugge[E]	Applications to Land Parameters (Chapter 3)
C. T. Swift[F,H]	Monitoring of the Ocean and Other Aquatories (Chapter 4)
J. W. Waters[C]	Applications to the Stratosphere, Mesosphere, and Lower Thermosphere (Chapter 7)
T. T. Wilheit[E]	Monitoring of Severe Storms (Chapter 5)

MEMBERS:

R. F. Adler[E]	W. F. Mitchell[N]	G. Schaerer[E]
J. Alishouse[H]	T. S. Nelson[N]	W. Shenk[E]
R. Burpee[I]	R. W. Newton[K]	R. Sheets[I]
W. J. Campbell[M,O]	E. G. Njoku[C]	J. C. Shiue[E]
J. Echerman[E]	R. C. Olson[A]	H. Siddalingaiah[E]
J. Gustincic[C]	P. W. Rosenkranz[D]	F. Y. Sorrell[J]
J. C. King[E]	J. W. Rouse[K]	D. W. Thiele[E]
J. L. King[E]	R. C. Savage[L]	J. Theon[E]
C. Laughlin[E]		S. C. Wofsy[B]
D. F. McGinnis[G]		J. Zwally[E]

A. Aerojet Electrosystems Company
B. Harvard University
C. Jet Propulsion Laboratory, California Institute of Technology
D. Massachusetts Institute of Technology
E. NASA/Goddard Space Flight Center
F. NASA/Langley Research Center
G. NOAA/National Environmental Satellite Service
H. NOAA/Environmental Research Laboratories
I. NOAA/National Hurricane and Experimental Meteorological Laboratory
J. North Carolina State University
K. Texas A&M University
L. USAF/Global Weather Center
M. United States Geological Survey
N. USN/Fleet Weather Facility, Suitland
O. University of Puget Sound

CONTENTS

CHAPTER 1. INTRODUCTION AND SUMMARY

1.1 Introduction and Overview 1-1

1.2 Executive Summary 1-2

CHAPTER 2. MONITORING OF SEA AND LAND ICE

2.1 Executive Summary 2-1

2.2 Present Important Observables 2-3

2.3 Competitive and Complementary Techniques 2-21

2.4 Requirements 2-27

2.5 Users 2-31

2.6 Required Future Work 2-33

2.7 References 2-36

CHAPTER 3. APPLICATIONS OF MICROWAVE RADIOMETRY TO LAND PARAMETERS

3.1 Executive Summary 3-1

3.2 Application Areas 3-3

3.3 Parameters To Be Measured 3-14

3.4 References 3-29

CHAPTER 4. MONITORING OF THE OCEAN AND OTHER AQUATORIES

4.1 Executive Summary 4-1

4.2 Applications 4-5

4.3 Anticipated Impacts of High Resolution Microwave Measurements 4-30

4.4 Acknowledgments 4-44

4.5 Bibliography 4-45

CHAPTER 5. MONITORING OF SEVERE STORMS

5.1 Executive Summary 5-1

5.2 Introduction 5-3

5.3 Observables 5-4

5.4 Applications to Tropical Cyclones 5-12

5.5 Application to Severe Local Storms 5-26

5.6 References 5-32

CHAPTER 6. MICROWAVE RADIOMETRY APPLIED TO SYNOPTIC METEOROLOGY AND CLIMATOLOGY

6.1 Executive Summary 6-1

6.2 Background 6-3

6.3 Measurement Techniques and Evaluation 6-14

6.4 Recommendation for High Resolution Instruments . 6-34

6.5 Acknowledgments 6-37

6.6 Bibliography 6-38

CHAPTER 7. APPLICATIONS OF HIGH RESOLUTION PASSIVE MICROWAVE SATELLITE SYSTEMS TO THE STRATOSPHERE, MESOSPHERE, AND LOWER THERMOSPHERE

7.1 Summary 7-1

7.2 Earth's Upper Atmosphere: A Summary Description 7-2

7.3 Major Problems Related to the Stratosphere, Mesosphere, and Lower Thermosphere 7-5

7.4 Applications of Microwave Radiometric Techniques to Upper Atmospheric Sensing 7-23

7.5 Results to Date Obtained from Microwave Sensing of the Upper Atmosphere 7-26

7.6 High Resolution Satellite Systems for Microwave Sensing of the Upper Atmosphere 7-40

7.7 Recommendations and Impact 7-59

7.8 Acknowledgments 7-65

7.9 References 7-66

CHAPTER 8. SYSTEMS

8.1 Executive Summary 8-1

8.2 Introduction 8-3

8.3 History of Passive Microwave Sensors in Space . . 8-3

8.4 Survey of Current Instrument Technology 8-5

8.5 Summary of Applications 8-8

8.6 Analysis of a Baseline Observatory System 8-10

8.7 Representative Proposed System Concepts 8-17

8.8 Alternative Mission Purposes 8-23

8.9 Cost-Effectiveness 8-26

8.10 Recommendations 8-29

8.11 References 8-37

APPENDIX A. ORBIT SELECTION FOR EARTH OBSERVATION MISSIONS

A.1 General A-1

A.2 Orbit Plane Precession A-1

A.3 Coverage Pattern Selection A-3

APPENDIX B. GENERAL THEORETICAL ASPECTS OF PASSIVE MICROWAVE REMOTE SENSING

B.1 The Forward Problem B-1

B.2 The Inverse Problem B-4

B.3 Bibliography B-10

CHAPTER 1

INTRODUCTION AND SUMMARY*

1.1 Introduction and Overview

The technology and demonstrated utility of passive microwave sensor systems has now advanced such that it is appropriate to invest in larger more powerful satellite systems serving an expanded community of users. Because such investments must be made carefully, a panel was assembled by NASA to review and authoritatively document user needs for improved passive microwave systems in space. The panel first met in January, 1977, and this report documents the results of those and subsequent deliberations. We believe that development of an expanded microwave observatory capability is well justified; the relative merits of various systems alternatives are described in this report.

The report is divided into chapters, each authored by two or more panel members representing microwave technology and the associated user community; user areas include severe storms, sea and land ice, synoptic meteorology and climatology, oceanology, soil conditions, and the high atmosphere. Each chapter contains a survey of what has been, can be, and needs to be monitored with passive microwave techniques in order to best serve users and the public. Recommendations concerning both systems and technology development are presented for each chapter, and the last chapter integrates the various opportunities into distinct and representative systems options.

The panel assigns the highest priority to development of a microwave observatory which achieves global coverage in 6-12 hours with $\sim$ 5-25 km resolution at several wavelengths in the 1.4-185 GHz region; the priority is high because of the wide range of users that would be uniquely and importantly served by such a novel system.

*Prepared by D. H. Staelin.

1.2 Executive Summary

1.2.1 Systems

More than 12 passive microwave spectrometers and imaging systems will have flown in space before 1979, and current instrument technology is adequate to support most contemplated future missions. Selected areas for further development include low-noise millimeter and sub-millimeter wavelength receivers and the design of large multi-frequency antennas.

The experiments now in space, together with aircraft and other research programs, have clearly demonstrated the competence and utility of passive microwave systems, and with the advent of a shuttle-launch capability, it is appropriate to capitalize on that expanded payload capability for the national welfare. In particular, it will be practical to launch larger antennas that can achieve spatial resolution much more appropriate to user requirements than was possible with the first small experimental satellites.

Because of the wide range of important documented applications, highest priority is assigned to development of an imaging multi-frequency observatory system covering the region $\sim$ 1.4-185 GHz with $\sim$ 5-25 km resolution on most channels, full earth coverage in $\sim$ 6-12 hours, and a $\sim$ 3-4 meter mechanically scanned antenna.

Several important special purpose systems also have high priority. A limb-scanning spectrometer for precise mapping of trace atmospheric constituents and temperature at 12-120 km altitude has very high priority because of the extensive and unique abilities of microwave sensors and the growing importance of understanding this atmospheric region. High priority is also accorded: 1) a large phased array ($\gtrsim$ 10 m) operating near 1.4 GHz for sensing soil moisture, 2) a 100-200 GHz imaging spectrometer for monitoring severe storms through high clouds at $\sim$ 1 hr intervals from geostationary orbit, and 3) study and development of an

experimental multi-channel 5-mm radar transmissometer for measuring atmospheric pressure over ocean.

Of less immediate priority is the study and possible development of a wide-swath low-resolution synthetic aperture radar to provide a "zoom" capability for a passive microwave observatory. Low priority was accorded to development of ∿ 100 m antenna systems because of their present high cost; development should follow conceptual designs with hope for significant cost reduction.

1.2.2 Sea and Land Ice

Sea ice concentration can be measured with a few percent accuracy, and several types of ice can be distinguished. Resolution of ∿ 1-5 km every 6-12 hours would be quite useful for 1) offshore facilities developers, 2) polar marine navigators (microwave data has been used operationally for over 2 years in this work), and 3) climatologists and modelers of ocean and atmosphere dynamics. The land ice data is useful primarily for climatology.

The greatest future needs are for 1) continued operational availability of microwave sea ice coverage maps, 2) continued spectral observations of sea and land ice with ground truth support, 3) development of a means for quantitative determination of the water equivalent in a snow pack, and 4) development of an improved operational high resolution system for sea-ice monitoring for navigation and climatological purposes.

1.2.3 Soil Moisture, Snow Cover, and Frozen Ground

Soil moisture has been measured with modest precision if the vegetation is not too thick, and snow cover and frozen ground can be classified at least approximately. Resolution of ∿ 3-25 km at intervals of ∿ 12-72 hours should be useful for 1) crop yield forecasts, 2) watershed runoff estimates, 3) climatology, and 4) land trafficability analyses. None of these applications has been demonstrated operationally,

but they appear promising on the basis of aircraft, spacecraft, and ground-based experiments.

The greatest future needs are for additional tests and validation of 1) soil moisture measurement techniques and the effects of vegetation, soil type and roughness, and penetration depth, 2) methods for utilizing such data in crop yield forecasts, general circulation models, watershed management, etc., and 3) signature measurement techniques for snow and frozen soil. Land measurement objectives should certainly be incorporated in any general microwave observatory system; such an experiment is necessary in order to develop the statistical confidence desirable before making operational commitments. A special-purpose large antenna for low frequencies has utility for the soil moisture objectives.

1.2.4 Oceans and Other Aquatories

Demonstrated measurement accuracies over ocean are believed to be approximately 1) 2-5 ms^{-1} for surface wind, 2) 0.5-2 K for surface temperature, and 3) $\sim$ 1 ppt for surface salinity. In open ocean, resolution of $\sim$ 10-50 km at $\gtrsim$ 12 hour intervals would be useful to the Fleet Numerical Weather Facility and to the National Meteorological Center in their preparation of operational analyses and forecasts. The fishing and shipping industries would be important beneficiaries. In coastal zones, fresh water areas, or oil spills, much higher resolutions of $\sim$ 1 km would require antennas of $\sim$ 100 m diameter.

Future needs are for 1) simulated or actual operational tests of SMMR data for oceanographic purposes, 2) further theoretical and experimental studies and validation of sea temperature, wind speed, salinity, and pollution measurements, 3) incorporation of ocean measurement objectives in any microwave observatory system, and 4) incorporation of a passive microwave system in any oceanographic observatory.

1.2.5 Severe Storms

Over oceans it has been demonstrated that precipitation, humidity, and oceanic parameters can each be measured and mapped with useful accuracy that illuminates the dynamic structure and behavior of severe storms; this would be very useful in supporting NMC, GWC, and FNWC operational services, particularly in remote locations. There is some evidence such storms over land can also be mapped, but much more crudely, and primarily by virtue of their precipitation patterns and associated temperature anomalies. Resolution of $\sim$ 2-50 km and a revisit time of 0.5-6 hours requires two satellites in low earth orbit to obtain the spatial resolution, and a synchronous satellite to obtain the time resolution.

The greatest future needs are for 1) simulated operational use of satellite data for severe storms, 2) high resolution microwave data over severe storms; aircraft and spacecraft are the appropriate platforms, 3) inclusion of severe storm objectives in any microwave observatory system, and 4) inclusion of a cloud-penetrating microwave imaging spectrometer in any severe storm observatory.

1.2.6 Synoptic Meteorology and Climatology

Satellites and other systems have demonstrated the ability of microwaves to penetrate most clouds and to yield 1) atmospheric temperature profile estimates with $\sim$ 1-5 K accuracy, 2) precipitable water vapor over ocean with $\sim$ 0.1-0.4 cm rms accuracy, 3) liquid water over ocean with $\sim$ 0.01 cm rms accuracy, and 4) precipitation rate, surface wind over ocean, and oceanic surface temperature with accuracies sufficient to define the character of meteorological situations.

Resolution of 15-50 km and 6-12 hour revisit times are sufficient to resolve most meteorological phenomena of

interest and are quite feasible to achieve. Such a system would support improved NMC, GWC, and FNWC operational products and would support the collection of uniform global climatological data. Most unique and valuable for climatology would be statistics concerning atmospheric water transport, sea ice canopy, snow coverage, and temperatures of the air and ocean in remote regions; the considerable potential of passive microwaves to monitor the high atmosphere is discussed separately below.

The greatest future needs are for 1) trial and operational use of microwave satellite data for synoptic and climatological purposes, 2) more high resolution data from aircraft to support (1) above, 3) development of a multipurpose microwave observatory component for any future synoptic or climatological observatory, and 4) inclusion of synoptic meteorology and climate objectives in any general microwave observatory program.

1.2.7 Stratosphere, Mesosphere, and Lower Thermosphere

Atmospheric temperature can be measured at altitudes of $\sim$ 10-110 km and variables such as wind, pressure reference level, magnetic field, and the abundances of O, O_2, O_3, CO, NO, ClO, OH, H_2O, H_2O_2, N_2O, NO_2, HNO_3, CH_4, and others can be measured over portions of this range; the accuracies generally exceed those available using other remote sensing techniques, partly because of a somewhat greater insensitivity to aerosols and non-equilibrium excitations. Such uniquely accurate data could increase very significantly man's understanding of the chemistry and dynamics of this atmospheric region, and synoptic monitoring with microwaves should provide a sensitive indicator for man-induced influences.

The greatest future needs are for 1) a modular limb-scanning microwave observatory with a $\sim$ 1-2 m antenna and

spectrometers for several molecular resonances; basic satellite research data would be very helpful, even from brief shuttle missions, 2) improved space-qualified detectors for 100-3000 GHz having noise temperatures of one to ten times the frequency in GHz, and 3) laboratory spectrum measurements of important atmospheric molecules that are not yet well studied.

CHAPTER 2

MONITORING OF SEA AND LAND ICE*

2.1 Executive Summary

2.1.1 Summary of Measurement Capability

A. Priorities	Nominal Desired Spatial Resolution (km)	Frequencies (GHz)	Sensitivities (°K rms)	Achievable Measurement Accuracy
Sea Ice Concentration	1-5*	6-100	< 1	∿ 2-3%
Ice Type; Sea and Land	1-5	10-100 (3 freq.)	< 1	Several Types

*Zoom capability to 100 m resolution would be desirable.

B. The operational viewing interval should be ∿ 12^h, although 6^h intervals would facilitate sea ice navigation. The best viewing angle would be constant near 50° zenith, with vertical and horizontal polarizations being measured separately, although cross-track scanning (with varying incidence angle) could be employed with degraded performance.

C. Principal users would be 1) marine navigators and off-shore facility developers at regional centers [ESMR data from the Nimbus-5 Satellite has been used over 2 years operationally in this work], and 2) climatologists and other modelers (ocean and atmosphere dynamics).

D. The operational use of Nimbus-5 ESMR microwave data (∿ 25 km resolution) for ice-pack monitoring and ship navigation has been quite successful, and it appears that higher resolution data would be even more so. High-resolution land ice monitoring has not been demonstrated operationally; climatological applications appear to be the most important.

*Prepared by P. Gloersen, H. J. Zwally, and W. J. Campbell.

2.1.2 Future Needs

A. Support of continued operational use of passive microwave data for ship navigation, e.g. the use of Nimbus-5 ESMR data by the Navy. A substitute data source will be required when ESMR data ceases.

B. Continue support for multi-wavelength microwave aircraft flights over sea and land ice to study ice signatures with high spatial resolution and appropriate ground truth.

C. Commence development of an improved passive microwave system to meet the continued and additional needs of sea-ice monitoring for navigation and climatological purposes.

D. Develop a means for quantitative determination of the water equivalent in a snow pack.

2.2 Present important observables

In the cryosphere there are three parameters which can be inferred from microwave brightness temperatures which at this time appear to be of particular importance: temporal and spatial variations of sea ice concentration, and type, horizontal and vertical temperature distributions and snow accumulation rates on the ice sheets of Greenland and Antarctica, and water equivalent in large-scale snow packs over terrain. Of these, the first two appear to be tractable; the third will require additional work in the future to establish its viability.

There are a number of basic electromagnetic properties of the ice in the cryosphere which are common to the retrieval of all of these parameters. The physical processes involved include reflection at the atmosphere-ice boundary and ice-substrate boundary, and emission, absorption and volume scattering of the radiation within the volume of the ice. Modeling of these processes makes use of the complex index of refraction: the real part of the index of refraction for surface reflection (except in extreme cases of high imaginary component), and the imaginary part for explaining volume emission and absorption within the ice layer; hence these phenomena may be understood on a macroscopic basis. A macroscopic approach also can be used for volume scattering by arbitrarily invoking a scattering albedo without any supporting physics. The scattering albedo, however, can be derived from various microscopic models which include taking into account density fluctuations within the ice layer (Stogryn, 1970), Tsang and Kong (1976), Fisher (1977) or Mie scattering (Chang et al., 1976).

2.2.1 Sea ice concentration

The ability to determine sea ice concentration from microwave brightness temperatures is derived from the large differences in emissivity of open water which is

approximately 0.5 and completely consolidated sea ice which is approximately 0.9. At the present time, it is possible to infer sea ice concentration from a single frequency measurement to a reasonably good approximation, about 15 percentage points, at a wavelength of 1.55 cm (Nimbus 5 Electrically Scanned Microwave Radiometer [ESMR-5]) by utilizing the fact that the brightness temperature of open water at this wavelength is 130 K (including an average atmospheric term) and using a priori seasonal values of the ice surface temperature at a given location. These two points define zero ice concentration and 100% ice concentration, respectively. Thus, instantaneous fields of view (IFOV) containing mixtures of open water and ice floes which are not resolved by the instrument will result in intermediate values of the brightness temperature. The present spatial resolution capability of the Nimbus 5 ESMR is approximately 35 km, which is useful for determining sea ice concentration both for applications to climate modeling and to passage of special marine transport systems. In connection with the latter application, such relatively coarse spatial resolution might at first seem inadequate, but by observing the temporal variation of the ice concentration it is possible to determine whether the ice pack is in a state of compression or divergence, an essential and probably the primary element in determining navigability within the pack. Converging ice is difficult or impossible to negotiate even with an ice breaker, whereas diverging ice presents little impediment to a properly designed vessel.

During the U.S./U.S.S.R. BESEX experiment in April 1973, the "Galileo I" aircraft obtained four mesoscale microwave images (10,000 km^2) of parts of the Bering Sea ice pack near the time of its maximum extent. The pack ice in this region is all first-year ice, with thicknesses ranging from a few centimeters to a meter. In addition, this ice is subject to rapid dynamic changes because it is

unbounded on its southern edge. Figure 2.1 shows the 19 GHz image for 20 February 1973 with a N-S orientation of polynyas that had formed as the pack drifted rapidly southward during the preceding six days. The amount of open water indicated by this image is 16%.

The uncertainty within each IFOV in determining sea ice concentration is ∿ 15% for low spatial resolution, single-channel spacecraft data, when using a priori values of the surface brightness temperature. This uncertainty may be reduced slightly by observing the time variation of brightness temperature and assuming that the maximum brightness temperature at a given location observed over relatively long time periods represents the brightness temperature of fully consolidated sea ice at that location. This particular method is under investigation at the present time and results of the improvement in accuracy are not yet available.

2.2.2 Sea ice type

If significantly improved values for sea ice concentration are required, as is the case for climate studies, it will be necessary to take into account certain complications that occur in the ice pack. There are at least three distinct sea ice types, radiometrically speaking, that occur: first year (FY) sea ice, which is on the average half a meter to two meters thick with snow cover; multiyear (MY) sea ice, which is generally thicker than first year ice, and first year thin (FT) sea ice which is substantially less than half a meter in thickness and has no snow cover. These three ice types each have a characteristic emissivity. These emissivity differences arise from differences in the surface properties of these various ice types as well as from internal differences. In first year ice, the microwave radiation emanates largely from the brine-laden sea ice and the snow layer. The imaginary part of the index of refraction is sufficiently large for FY sea ice that the optical thickness is the order of a wavelength at

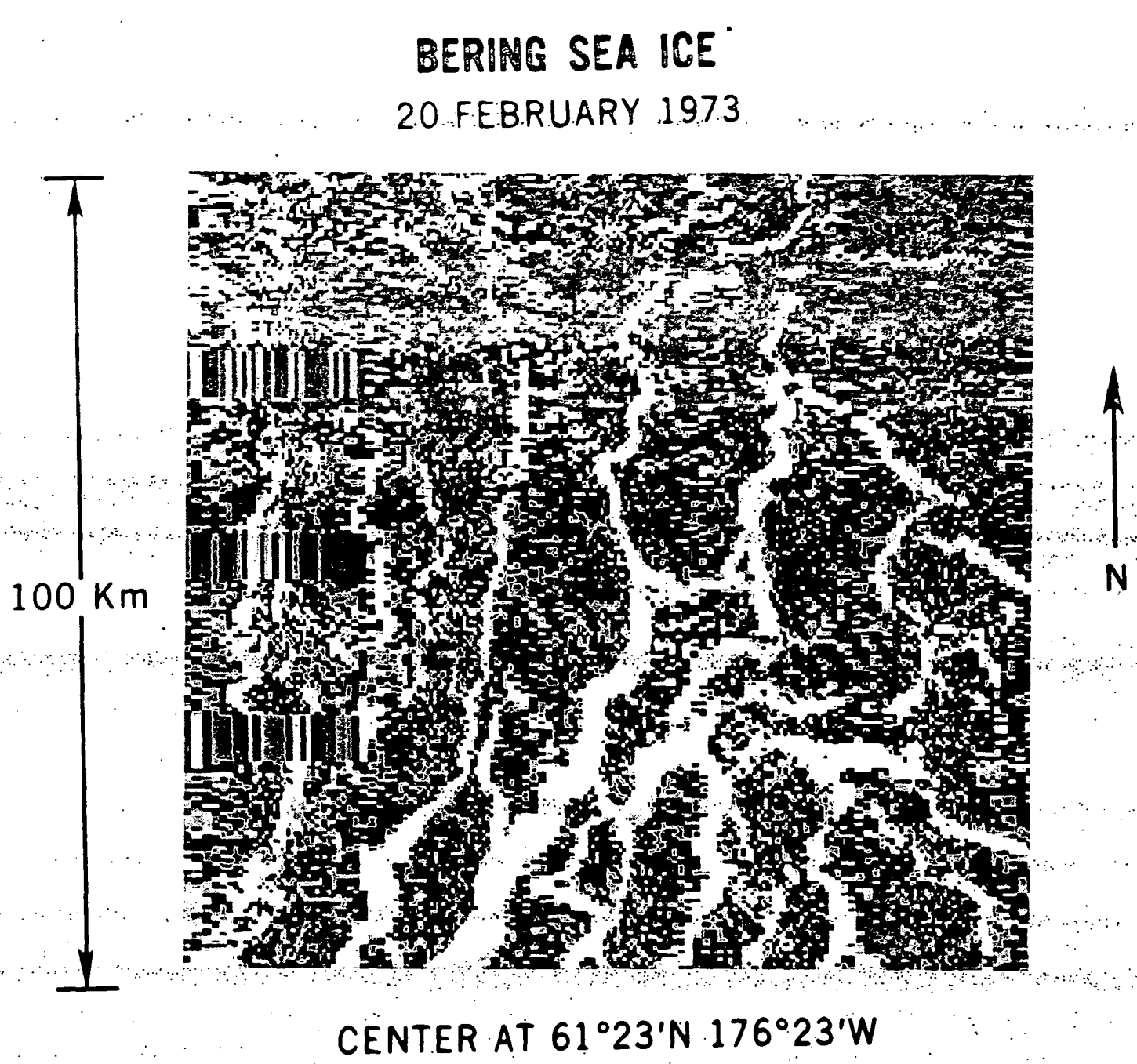


Figure 2.1. False-color ESMR image collected on 20 February 1973 on NASA CV-900 aircraft over the BESEX area, Bering Sea. The image is centered near 61° 24'N, 176° 24'W. (Original in color.)

a temperature of about -10°C. The optical thickness varies by an order of magnitude over the temperature interval -5 to -30°C. This radiation is modified principally by reflections and absorption at the snow/air interface which give rise to the polarization properties observed at the longer wavelengths. At a wavelength of 0.8 cm, surface roughness apparently causes depolarization. The difference between FY and FT emissivities can also be accounted for entirely on the basis of surface properties. Due to the absence of snow on FT, the exposed surface has a significantly higher real part of the index of refraction than FY, due to the presence of liquid brine throughout the freeboard layer of the FT. This higher real part of the index results in higher surface reflectivity and lower emissivity.

In addition, the FT sea ice will have a generally higher surface temperature than the two thicker types due to significant conduction of heat through the FT layer. FT ice occurs in highly dynamic regions of the ice canopy through formation and refreezing of leads. During the Arctic Ice Dynamics Joint Experiment (AIDJEX), such ice types were found to comprise approximately 30% of the total area within the AIDJEX triangle on some occasions.

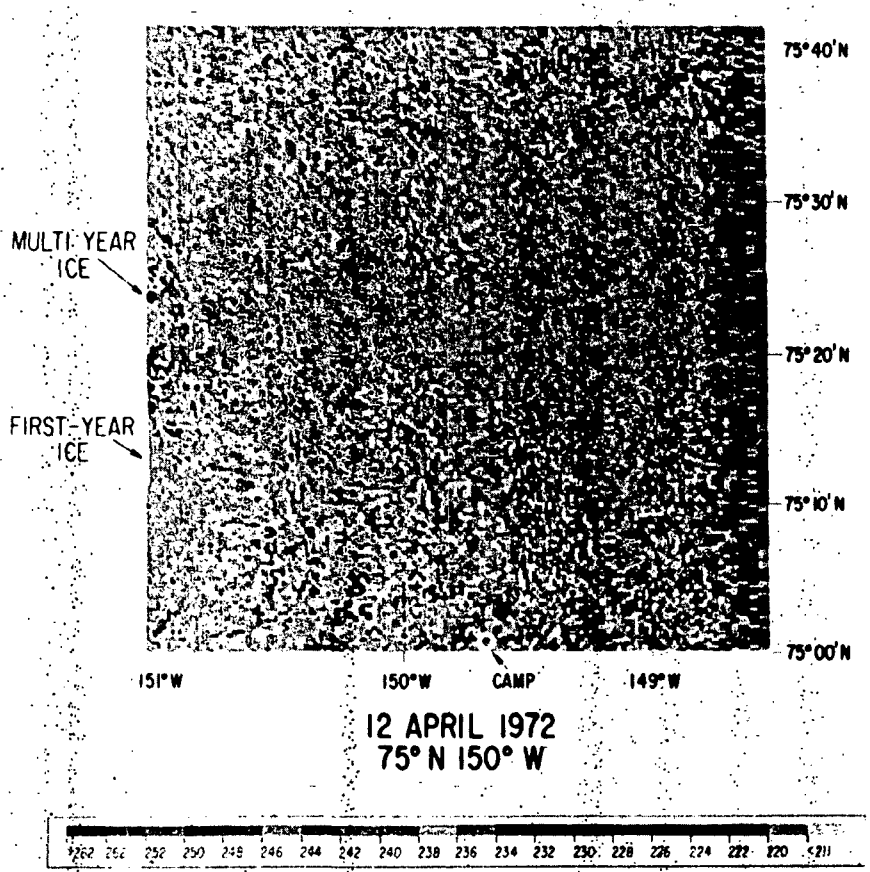
In MY, the freeboard portion of the ice is largely devoid of brine due to its drainage in previous summers to below sea level. Thus, the index of refraction is nearly that of fresh water ice in the freeboard layer. As a result, the optical thickness of the freeboard layer is on the order of tens of wavelengths. At or near the sea level, the brine concentration increases to approximately 0.1%, which markedly increases the imaginary part of the index, and hence the optical thickness in the submarine portion of MY

is the order of a wavelength. Thus, the radiation emanating from multiyear sea ice originates mostly near sea level in a layer of ice about one wavelength thick. In the freeboard portion of the ice itself, the emanating radiation is modified both by reflection at the snow/air interface and by volume scattering resulting from the presence of air pockets in the MY that were left behind as a result of brine drainage in previous summers. The wavelength dependence of the MY emissivity arises from both the variation with wavelength of the scattering cross-section and the finite thickness of the freeboard portion of the ice (the order of 30 cm).

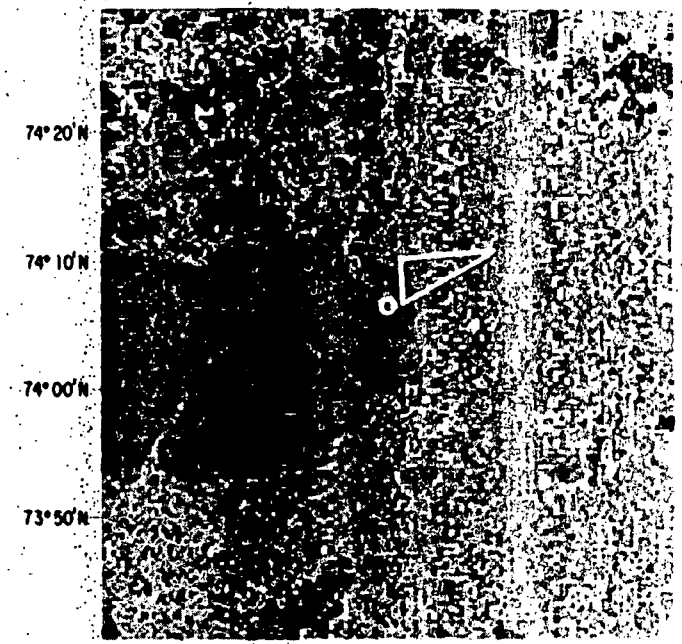
Figure 2.2 (right) shows a 19 GHz microwave image depicting the observed emissivities of a large ice area (10,000 km^2) of the eastern Beaufort Sea. The multiyear floes, having an average thickness of 3-4 m, have cold (blue) brightness temperatures while the warm (yellow) temperatures are associated with first-year floes having average thicknesses of less than 2 m. Figure 2.2 (left) shows a microwave image of the 1972 AIDJEX area in the western Beaufort Sea. A comparison of this image with one obtained a year earlier in the eastern Beaufort Sea reveals a markedly different morphological makeup of the ice in that no large multiyear floes were present. Campbell et al. (1975a) noted that numerous small multiyear floes, smaller than the radiometer footprint of 500 m, were observed in the area, and by matching and averaging radiometer signatures of the various ice types they found that the 1972 AIDJEX area was made up of approximately equal amounts of multiyear and first-year ice.

Separation of the contributions by the various components and recognition of the role of atmospheric effects are necessary in order to improve substantially on the 15

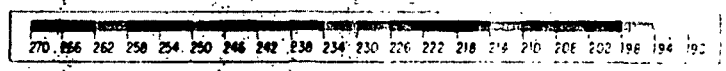
COMPOSITE MICROWAVE (λ=1.55 cm) IMAGES OF BEAUFORT SEA ICE TAKEN FROM 10km HEIGHT



12 APRIL 1972
75° N 150° W



15 MARCH 1971
74° N 131° W



percentage points accuracy presently available. This requires the use of multispectral microwave observation techniques (Gloersen and Barath, 1977; Gloersen et al., 1977). A number of different algorithm forms are presently under consideration but will not be listed here due to their preliminary nature.

A time sequence of microwave mosaic images of the sea ice extending from Harrison Bay, on the north of Alaska, north into the Beaufort Sea for 350 km is shown in Figure 2.3. The seven images cover the time from 4 to 23 April 1972. Three distinct zones of sea ice can be observed in each image: (1) a shore-fast zone made up of undisturbed first-year ice having a uniformly high brightness temperature; (2) a shear zone composed of three distinct ice types -- multiyear floes with cold brightness temperatures, refrozen polynyas with brightness temperatures similar to those of shore-fast ice and a mixture of first-year and unresolvable chunks of multiyear ice having a brightness temperature between those of the two ice types; and (3) a mixed zone of first-year ice and unresolvable floes of multiyear ice with many refrozen polynyas. The extremely dynamic nature of the shear zone is clearly seen, with its width doubling in 19 days.

The Electronically Scanning Microwave Radiometer (ESMR) on Nimbus-5 has provided the first large-scale synoptic views of the polar sea ice packs. These have been interpreted in light of the AIDJEX-NASA and BESEX findings revealing that both the morphology and dynamics of these major ice masses are more complex than had hitherto been assumed. Since its launch on 11 December 1973 Nimbus-5 has provided a wealth of data on the variations of these packs at time scales ranging from several days to seasons. Figure 2.4 shows a pair of ESMR images of the Arctic at

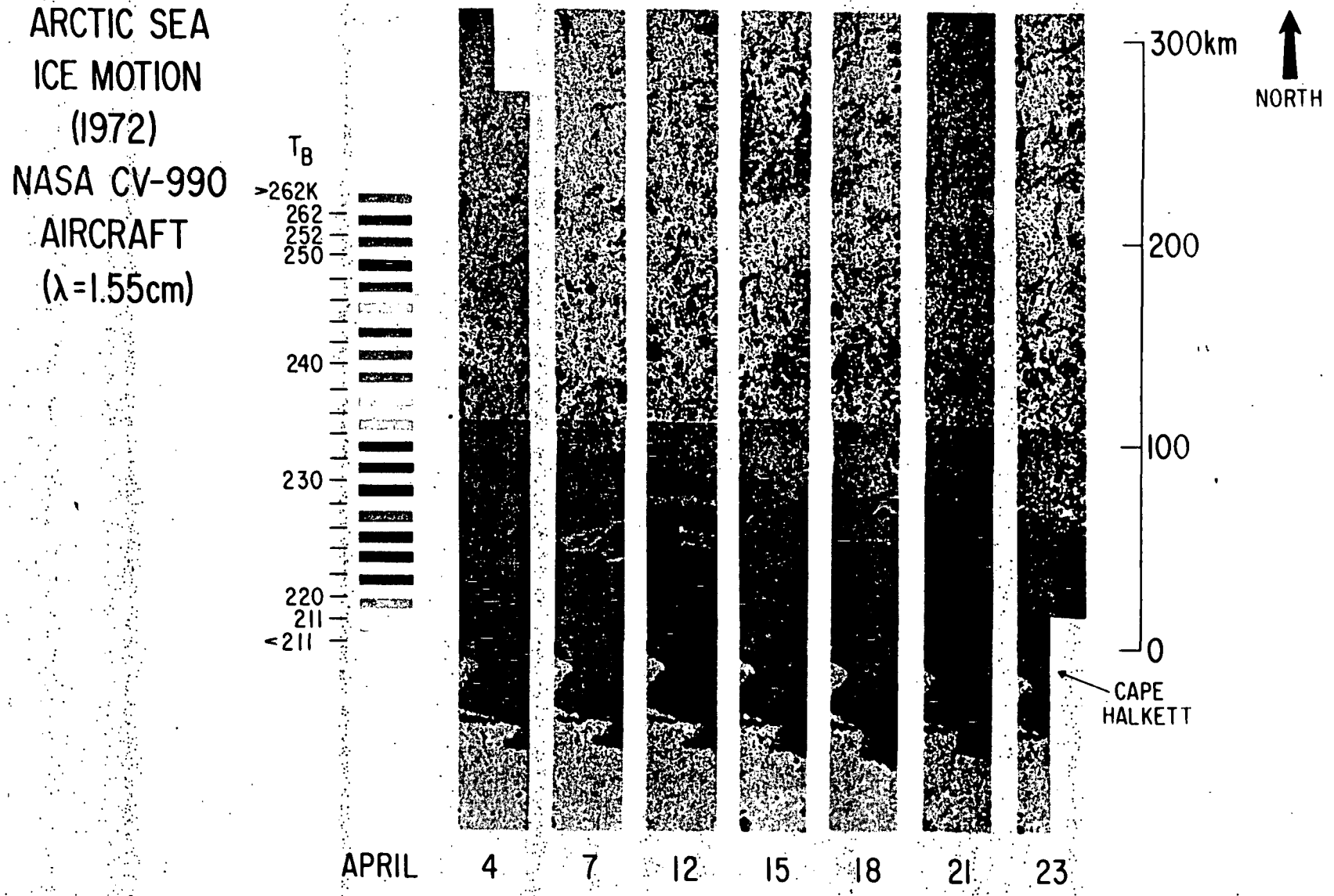


Figure 2.3. Successive false-color ESMR image strips collected between 4 and 23 April 1972 of sea ice of the western Beaufort Sea from Harrison Bay, Alaska to 74° N. (Original in color.)

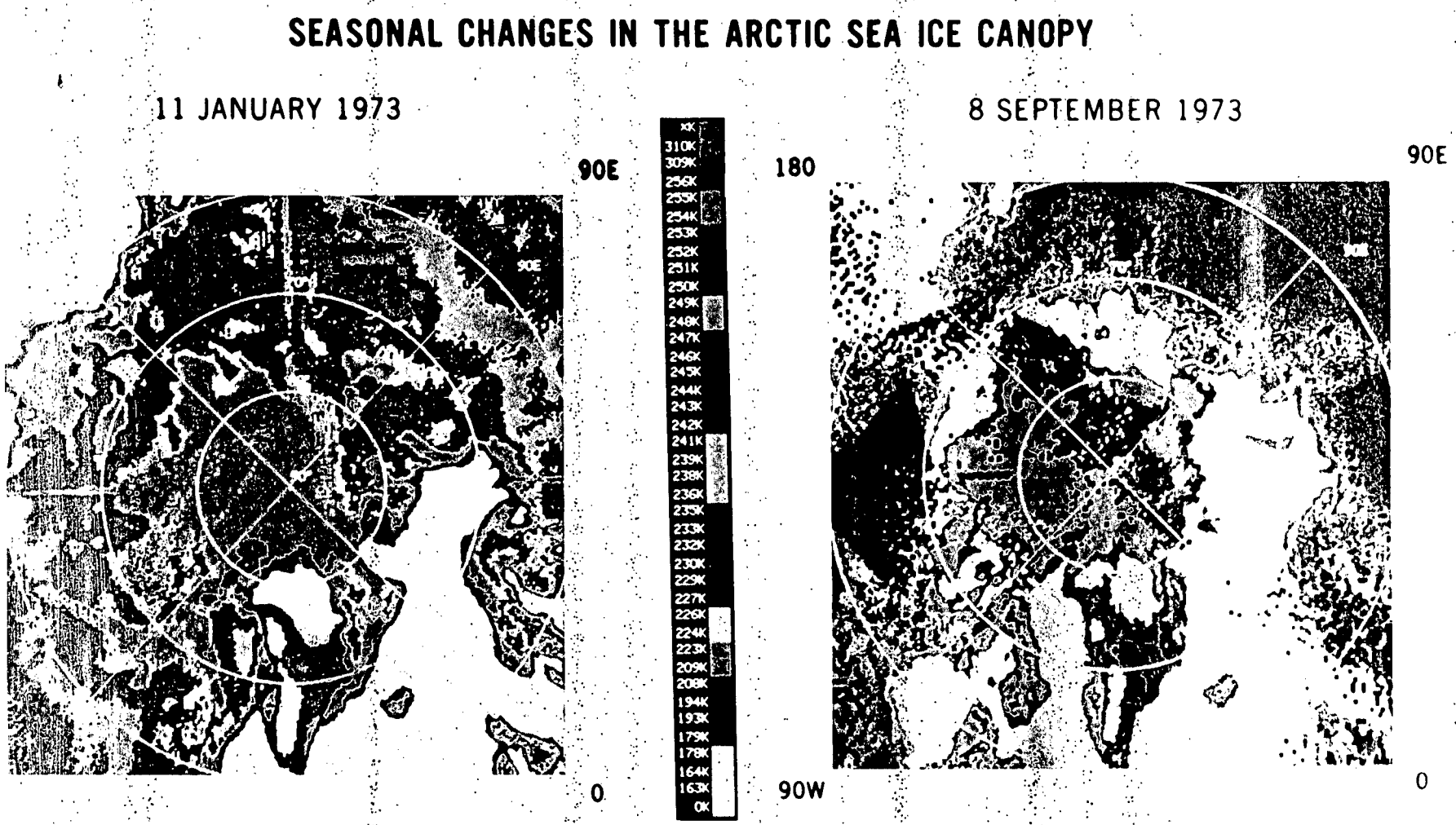


Figure 2.4. False-color ESMR mosaics collected over the northern hemisphere on 11 January 1973 and 8 September 1973 depicting seasonal changes in the Arctic sea ice canopy. (Original in color.)

different seasons. The winter image of 11 January 1973 shows the ice canopy to be composed of two general types of ice: the principally multiyear ice covering the main portion of the Arctic Ocean, with brightness temperatures ranging from 209 to 223 K, and either first-year or first-year/multiyear mixtures with higher brightness temperatures covering the southern portion of the marginal seas (i.e. the Beaufort, Chukchi, East Siberian, Laptev, Kara and Barents Seas). Note that the multiyear ice extends far south into the eastern Beaufort Sea. By using a combination of ESMR and LANDSAT-1 images combined with the AIDJEX-NASA data, Campbell et al. (1973) have shown that the Beaufort Sea ice cover is made up of large multiyear floes in its eastern sector while its western sector consists of small, fragmented first-year and multiyear floes.

By the end of the summer melt season the ESMR image for 8 September 1973 (Figure 2.4) shows that most of the ice that covered the marginal seas had melted. The area of the end-of-summer pack is approximately half of that of the winter pack. Analysis of these and other ESMR images by Gloersen et al. (1974) reveals that not all of the first-year/multiyear ice mixture melted. Figure 2.5 shows an analysis of the near-maximum ice extent (10 February 1973) and near-minimum ice extent (9 September 1973) based on the ESMR images. The areas of the pack in which the first-year/multiyear ice mixture survived the summer melt are source areas for multiyear ice which is advected into the multiyear pack. This process thereby allows the ice pack to maintain a steady-state mass by balancing the volume of ice that is advected out of the Arctic Ocean by the East Greenland current. The analysis also shows that the summer pack extended closer to Svalbard than did the winter pack, suggesting a strong summer ocean surface current flowing southward in this region. Note that the ESMR image for the Arctic in the winter of 1973 (Figure 2.4) shows that the

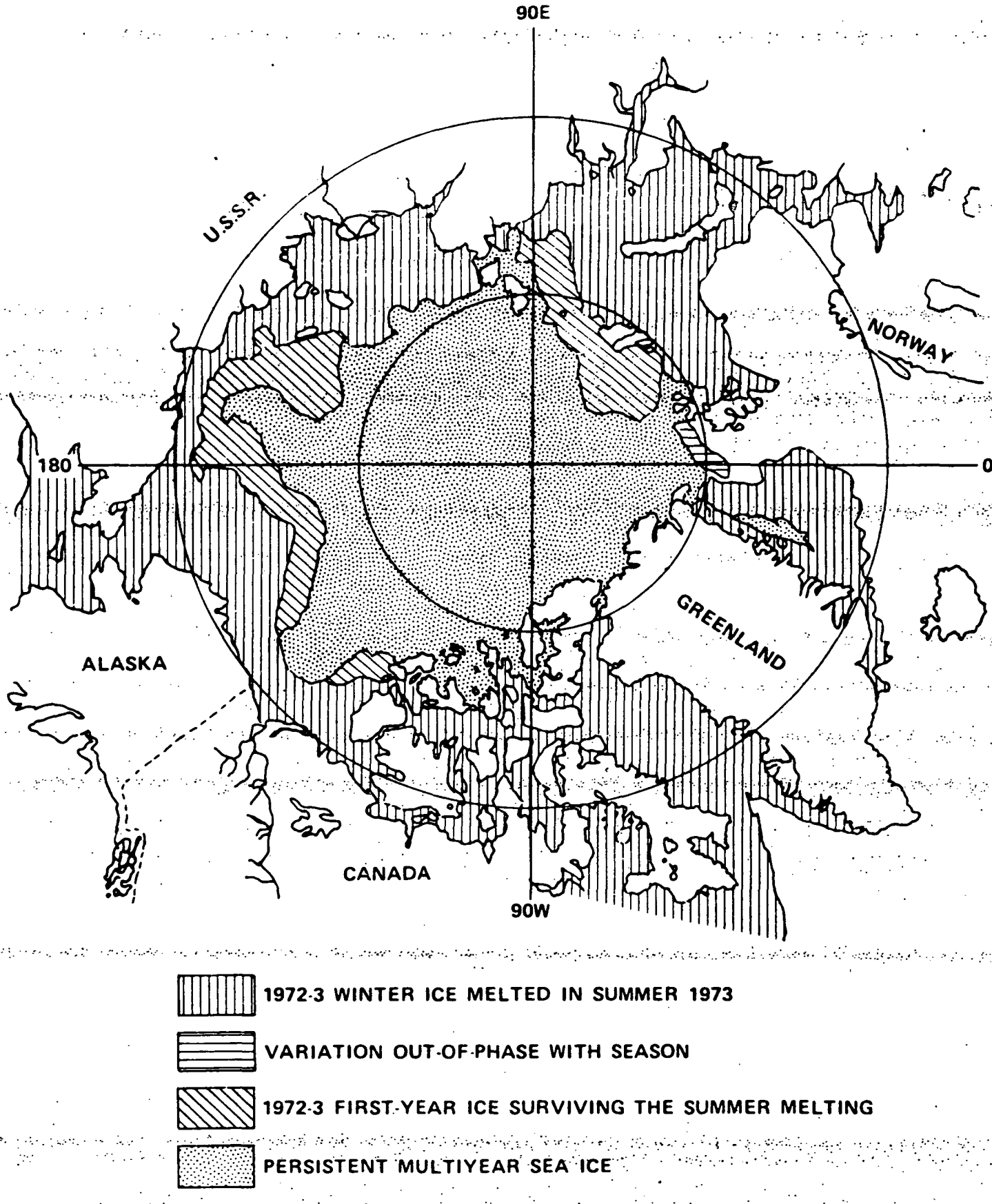


Figure 2.5. Seasonal variations of sea ice in the northern hemisphere.

ice cover of the Bering Sea, which was made up of first-year and younger ice, has a cold radiometric signature similar to that of the multiyear ice of the Arctic Ocean. The reason for this is that the large (35 km) footprint of ESMR is covering a mixture of ice and open water, and the average brightness temperature appears cold because the water signature is much colder than that of the first-year ice.

The ESMR images of the Antarctic are equally useful as those of the Arctic for studying large-scale ice morphology and dynamics. Figure 2.6 shows both a winter and summer image of the Antarctic. The winter image indicates that the ice cover is made up largely of first-year ice, except in the Weddell Sea. By late in the following melt season (10 February 1973), the ESMR image indicates that approximately 80% of the ice cover has melted. This is shown in the analysis given in Figure 2.7 in which the near-minimum (10 February 1973) and near-maximum (16 July 1973) ice extents are delineated. The observations at first seem to indicate the formation of multiyear ice where ice remains at the end of the melt season. Analysis of ESMR images in Austral Spring 1972 and Austral Winter 1973 by Gloersen et al. (1974) indicate that no multiyear ice was present, thus the regions where ice remains at the end of the melt season are accumulation regions in a system of steady depletion and replenishment. An alternate explanation may be that some of the remaining ice never undergoes a surface melt during summer, causing a retention of brine in the freeboard portion from one year to the next.

While there is utility in the spatial resolution presently available from satellites, there would be significant improvement in the utility of the parameter retrievals for the purposes both of maritime operations and climate studies if the spatial resolution were to be improved. For maritime operations, location of specific large leads in the ice pack

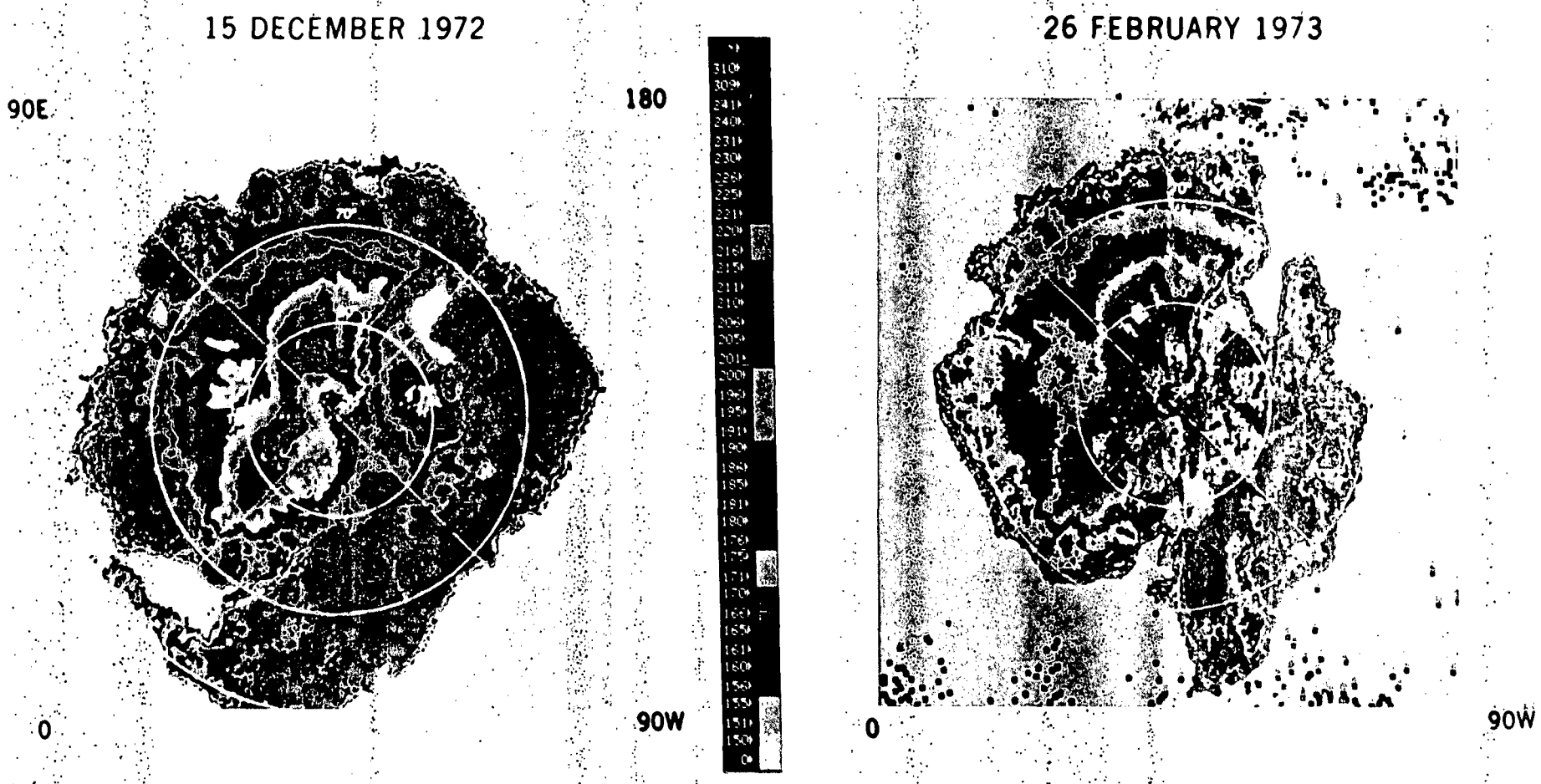


Figure 2.6. False color ESMR mosaics collected over the southern hemisphere on 15 December 1972 and 26 February 1973 depicting seasonal changes in the Antarctic sea ice canopy. (Original in color.)

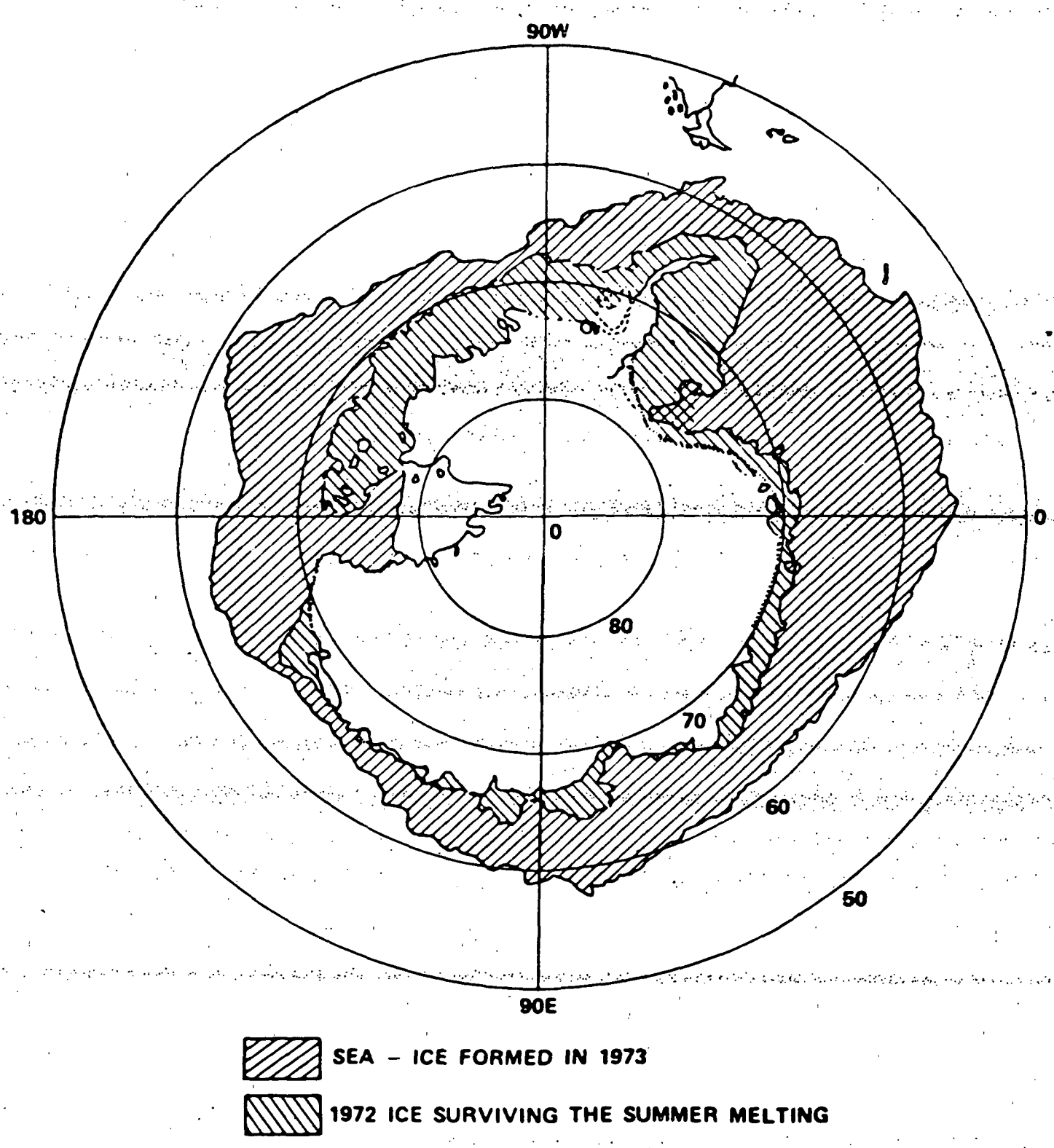


Figure 2.7. Seasonal variations of sea ice in the southern hemisphere.

would be particularly useful for offshore surface transport in the Arctic Basin by conventional barges. For climate studies, more accurate ice concentration measurements are required. The multispectral parameter retrieval processes are inherently non-linear, but linear approximations are required to determine the ice concentration and other parameters. If the three basic ice types can be partly separated by utilizing higher spatial resolution, the linear approximation becomes valid over a larger interval.

2.2.3 Continental ice sheet properties

The continental ice sheets of Greenland and Antarctica represent 85% of the total fresh water on the earth. Substantial variations in this stored water can have profound effects on sea level and global climate. Passive multispectral microwave techniques promise to permit monitoring changes and important characteristics of these continental ice sheets. Important parameters that can be inferred from microwave brightness temperatures are the horizontal and vertical distributions of physical temperature and the average snow accumulation rates, which are required for studies of the growth of the ice sheets. To date, the single wavelength observations such as those shown in Figures 2.4 and 2.6 made using the Nimbus 5 ESMR have given indications of the variability of snow accumulation rates on both Greenland and Antarctica (Chang et al., 1976; Zwally and Gloersen, 1976). In addition, spectral signatures are distinctly evident in the Nimbus-5 NEMS data (Kunzi et al., 1976).

Snow accumulation rates are inferred from the average snow particle size in the snow layer covering the ice sheet and the average temperature within the snow layer (Chang et al., 1976; Zwally, 1977; Zwally and Gloersen, 1976). Again, multispectral brightness temperature observations will be

required in order to determine simultaneously the physical temperature distribution. Such multispectral techniques are presently under investigation at Goddard Space Flight Center in connection with the NASA climate program and the ocean dynamics program.

2.2.4 Snow-covered terrain

Extent of the winter snow pack in the northern hemisphere is currently a standard product provided by NOAA, and is based on visual and infrared observations from spacecraft in addition to surface and airborne observation. Such observations can be made sufficiently systematically through breaks in the cloud cover. However, the extent of the snow pack gives little indication of its water content. It is here that the microwave techniques show promise. At this point in time, a convincing demonstration that quantitative determination of the water equivalent in the snow pack can be obtained by using microwave brightness temperatures obtained from space has not yet been carried out. Model calculations of the sensitivity of the technique are in progress. A very limited number of multispectral microwave observations of snow pack using airborne sensors have been made and the data are presently under analysis. Some preliminary indications of this potential have been discussed (Chang and Gloersen, 1975; Schmugge et al., 1974; Edgerton et al., 1971).

The physical situation in such a snow pack is somewhat analogous to the case of multiyear ice in which the snow pack bears a rough analogy to the freeboard portion of MY and the substrate for the snow cover is analogous to the portion of the MY below sea level. In order to determine the water equivalent of such a snow pack, observations must be made when the internal temperature of the snow pack is well below freezing. Otherwise, the imaginary part of the index is sufficiently large to restrict significantly the penetration of

microwave radiation through the snow cover. The physical state of the substrate is also important in interpreting brightness temperatures, since frozen substrate would result in relatively high emissivity, and a moist substrate somewhat lower emissivity. Again multispectral observations are essential for separation of the various components that contribute to the brightness temperature. A concerted effort is being made to develop the appropriate algorithms for these determinations in connection with the Scanning Multichannel Microwave Radiometer (SMMR) scheduled to be flown on both the Nimbus G and the SEASAT-A satellites in 1978.

2.3 Competitive and complementary techniques

Here we will briefly discuss the capabilities of a number of satellite systems that are either currently operational or presumably will be so in the near future. The characteristics of the sensors are summarized in Table 2.1, reproduced from Campbell et al. (1975b).

2.3.1 Visible and near infrared

2.3.1.1 LANDSAT

LANDSAT (formerly known as ERTS) imagery is of cartographic quality on a scale of $1:10^6$. Each image is 185 km on a side. The Multi-Spectral Scanner (MSS) sensor system collects information in 4 spectral bands ranging from visual (0.5 μm) to near IR (1.1 μm) with a stated surface resolution of 100 m. Experience has, however, shown that high contrast linear features such as leads with widths significantly smaller than this are commonly visible in the imagery. Because of its scale, resolution, and map-like accuracy, LANDSAT imagery is ideally suited for studying lead patterns, ice drift and deformation.

The drawbacks of the LANDSAT imagery are that the MSS is limited by cloud cover. It is also limited by darkness, although present indications are that highly useful data can be obtained at much lower light levels (sun angles) than those at which the satellite is normally operated. Another major drawback inherent in LANDSAT imagery is its lack of continuity. At the equator LANDSAT images exactly the same area once every 18 days. In the polar regions the orbital overlap permits coverage of the same site during 3 to 5 consecutive days (depending on the latitude) followed by a 13 to 15 day "holiday" before the satellite returns to the study area. When the days lost because of cloud cover are

Table 2.1. Characteristics of present or planned sensors particularly useful in sea ice studies and their vehicles.

Vehicle	Sensor	Wavelength	Surface Resolution	Repetitive Coverage	Maximum Latitude	Restricted by	Features of Note	Status as of Sept. 1975
LANDSAT	Multi-spectral Scanning System (MSS)	0.5-1.1μm	80 m	Daily for 2 to 5 days, followed by a 13 to 16 holiday	81° N	Clouds/Darkness	High resolution cartographic quality	Operational
NOAA	Scanning Radiometer	0.5-0.7μm 10.5-12.5μm	3.5 km 8 km	2 X daily 2 X daily	Near Polar Orbit	Clouds/Darkness Clouds	— Thermal IR	Operational
	Very High Resolution Radiometer	0.5-0.7μm 10.5-12.5μm	1 km 1 km	Daily Daily		Clouds/Darkness Clouds	— Thermal IR	
DMSP	Line-scan Radiometer	0.4-1.1μm 8-13μm	0.6 or 3.7 km 0.6 or 3.7 km	4 X daily 4 X daily	Near Polar Orbit	Clouds/Darkness Clouds	— Thermal IR	Operational
Nimbus 5	Electronically Scanned Microwave Radiometer (ESMR)	1.55 cm (19.35 GHz)	32 km	2 X daily	Near Polar Orbit		All Weather	Operational
	Temperature-Humidity Infrared Radiometer (THIR)	6.5-7μm 10.5-12.5μm	22 km 7.5 km	2 X daily 2 X daily		Clouds Clouds	Thermal IR Thermal IR	
Nimbus 6	ESMR	0.8 cm (37 GHz)	25 km	2 X daily	Near Polar Orbit		All Weather	Operational
	THIR	See Nimbus 5						
Nimbus G	Scanning Multichannel Microwave Radiometer (SMMR)	0.8-6 cm (5 bands, 10 channels)	16 to 87 km as a function of frequency	2 X daily	Near Polar Orbit		All Weather	1978
	THIR	See Nimbus 5						
SEASAT-A	Synthetic Aperture Radar (SAR)	22 cm (L band)	25 m	36 hours	75° N		All Weather (100 km swath)	1978
	Radar Altimeter	2.2 cm (K band)	1.6-12 km				All Weather	
	Microwave Scatterometer	2.2 cm	50 km				All Weather (400 km swath)	
	SMMR	See Nimbus G						
	Visible/IR Scanner	0.49-0.94μm 10.5-12.5μm	3 km 5 km			Clouds/Darkness Clouds		
Earth Observatory Satellites (EOS)	MSS		10 m	6-9 days at equator		Clouds/Darkness		1980s
	SAR		15 m				All Weather	
Close Grid Geodynamic Measurement Satellite System (CLOGEOS)	Determines differential motion of passive targets.		< 10 cm	?	Near Polar Orbit	Clouds		1980s

added to these "holiday" periods, LANDSAT coverage has, in fact, proven to be quite spotty. To obtain the optimum use of LANDSAT, identifiable ice features must be located on sequential images. The long-holiday periods make this identification difficult except during periods of exceptional weather which, of course, are not periods of storm passage when most interesting changes occur in the ice pack. Nevertheless, even with these drawbacks, LANDSAT imagery has, because of its cartographic quality and good resolution, proven to be the satellite system that is presently most useful for quantitative studies of ice drift and deformation.

2.3.1.2 NOAA

The NOAA satellite series has also produced a large amount of imagery that is useful in the study of sea ice. These satellites operate at appreciably higher altitudes than do satellites in the LANDSAT series (1465 km above the earth's surface as compared with 900 km). The prime sensor involved for sea ice studies is a dual channel very high resolution radiometer (VHRR) which obtains information in both the visible (0.5-0.7 μm) and the infrared (10-12.5 μm) regions. The images produced are 2000 km on a side and have a surface resolution of 1 km. In the polar regions a given area is usually imaged once daily. These satellites also carry a scanning radiometer that gives a twice daily image of any location on the earth's surface in both the visible and IR but at a reduced resolution (8 km).

The advantages of NOAA imagery are that during both light and dark periods, it provides regular broad scale coverage of the polar regions on a scale at which many useful large ice features can still be distinguished. The disadvantages are that images cannot be obtained through a cloud cover, the resolution and scale are sufficiently large so that many interesting and important ice features are lost, and finally the projection of the image is such that quantitative drift and deformation measurements are difficult.

2.3.1.3 DMSP (Defense Meteorological Satellite Program)

This satellite series which was formerly called DAPP (Data Acquisition and Processing Program) is operated by the U.S. Air Force for the U.S. Department of Defense. The principal purpose of the satellites is the observation of cloud patterns. The imagery is collected by both high resolution and very high resolution 2 channel radiometers operating in both the visual (0.4 to 1.1 μm) and the IR (8 to 13 μm) ranges. The satellites orbit at a slightly lower altitude (833 km) than satellites in the LANDSAT series and significantly lower than those in the NOAA series. Usually two DMSP satellites are in orbit at the same time which provides coverage of any spot on the earth's surface four times daily. The VHRR system which is of primary interest here has a spatial resolution of 0.6 km at nadir. DMSP imagery provides a view of sea ice on a scale that is intermediate between that of LANDSAT and of NOAA. Several images are obtained each day, darkness is not a limitation, and the map format, while not as convenient as LANDSAT, is easier to use than NOAA. In addition there are a variety of options available for specially processing both the visual and the IR data, so that the imagery has a higher apparent resolution and the temperature (or albedo) scale is expanded relative to some arbitrarily set base value such as the freezing temperature of sea water. The principal limitations of the sensing system are that it does not penetrate clouds and does not possess as high a spatial resolution as might be desired.

2.3.2 Thermal infrared

As discussed in the previous sections both the NOAA (and its predecessor ITOS) and the DMSP satellites have thermal IR systems operating respectively in the ranges of 10.5-12.5 μm and 8-13 μm and with resolutions of 1.0 and 0.6 km. Other satellites with IR systems of interest are

in the Nimbus series. The THIR system has a ground resolution of 7 km for the temperature channel. Nimbus G will also fly a scanning radiometer operating in a similar range (10.5 to 12.5 μm) with a resolution of 0.8 km.

The first IR sensors were useful only at night and had a low resolution, while the more recent versions operate successfully either during the day or night with increasing resolution. Because of their resolution limitations the IR systems on the early satellites were primarily useful for the mapping of gross ice boundaries such as the edge of the pack or the location of large polynyas. Even as the resolution of the IR systems improved to values of 1 km or less so that detailed observations of features within the pack became possible, little was done with the IR imagery except use it during dark periods as a replacement for visual imagery which was usually of an even better resolution. This was done by simply noting that open water or thin ice areas that appeared dark on visual imagery (low albedo) also appeared warm on the IR imagery. However, these studies indicated that the large reflectance changes that made the water-ice transition so clear in the visual range often corresponded to much less obvious thermal contrasts as recorded by the IR system. This was particularly true when the IR image was displayed by distributing the distinguishable gray shades over the 100 C of interest for meteorological purposes.

2.3.3 Active microwave sensors

2.3.3.1 Scatterometer

The microwave scatterometer is emerging as a powerful tool for determining ice type. The scatterometer is a calibrated down-looking radar which can be used to measure the backscatter coefficient σ, as a function of aspect angle along a strip of terrain under an aircraft or spacecraft. The proposed scatterometer for SEASAT will undoubtedly yield

useful information concerning ice type distribution on the mesoscale in the Arctic Ocean.

The scatterometer forms a very powerful tool for use in determination of sea ice type in combination with passive microwave radiometer data. There is about a 60° difference in brightness temperature between first-year ice and multi-year ice and about 20 dB difference in backscattering cross-section as observed by the scatterometer.

2.3.3.2 Radar altimeter

This sensor which is scheduled to be operated on SEASAT-A will determine the distance between the spacecraft and the ice-ocean surface to an rms precision of roughly ± 10 cm. Inasmuch as the footprint of the radar is a 2 × 7 km spot, the results will not resolve individual roughness elements in the sea ice such as ridges and leads as is possible via an aircraft-borne laser profilometer. Nevertheless it may be possible to discern both spatial and temporal variations in the average (2 × 7 km) elevation of the surface of ice covered seas. These variations would presumably correlate with the intensity of ice deformation which has been shown to vary significantly between different provinces in the Arctic Ocean (Hibler, 1975). Other interesting studies that will be possible once SEASAT is launched concern the inter-relations between the results of the radar altimeter, the scatterometer, and the synthetic aperture radar.

2.3.3.3 SAR (Synthetic Aperture Radar)

A number of countries (U.S.A., Canada, and countries of the European Space Agency) are carrying out programs with the aim of putting SAR's into space. The U.S. SEASAT-A program is aimed at launching a SAR, complemented by a scatterometer, radar altimeter, multi-frequency microwave radiometer and a visible/IR radiometer in early 1978.

Canada plans to put a SAR with complementary sensors (payload not defined yet) into space by spring 1984.

The SEASAT-SAR will operate in the L-band range and is expected to have a resolution as low as 25 m and a swath width of 100 km. At the present time the proposed circular orbit at an altitude of 800 km will allow SAR imagery to be obtained as far north as 75° N with repeat coverage every 36 hours. If current orbit proposals are not altered, a large part of the Arctic Ocean will not be imaged by the SAR.

From the work accomplished so far and including the forthcoming results of the main AIDJEX experiment, some projections can be made of the kind of SAR product one may expect from SEASAT-A. Leads, ice boundaries, as well as a variety of ice features such as ridges and rubble fields should be readily identifiable. Major ridging of first-year ice should be clearly seen, but multiyear ice ridges will not be as distinguishable. What would be difficult to determine are ice types, particularly the difference between first-year and multiyear ice. The successive tracking of the identifiable features will, however, permit quantitative information on ice drift and deformation to be obtained on an all-weather basis.

2.4 Requirements

2.4.1 Frequency of observations

2.4.1.1 Sea ice

Frequency of operations required on the sea ice canopy depends to some degree on the spatial resolution at hand. Based on present day knowledge, translations of the ice pack the order of 10 km per day are not unusual in the Arctic Basin. In the ice packs surrounding Antarctica, ESMR-5 images used in connection with producing a time-lapse motion study of the sea ice have indicated that three-day averages

in some cases result in significant jumps in the position of the pack. Thus, it seems that a reasonable observation frequency for sea ice packs is once per day for most cases. In certain unusual circumstances, e.g. during and immediately after the passage of a severe storm, more frequent coverage would be desirable, say, two or three times a day.

2.4.1.2 Continental ice sheet

There are a number of time scales of interest for observing properties of continental ice sheets in Greenland and Antarctica. Observations of the snow accumulation rate and temperature distribution probably would not require more than one or two observations per month. For following the melt line during the spring, summer, and fall seasons there are periods of rapid change where weekly or bi-weekly observations should be made.

2.4.1.3 Snow-covered terrain

Generally speaking, one to two observations per week should suffice for most purposes of weather, climate, and hydrology. In the melting season, however, for potential flood control, it would be important to make the observations on a more frequent basis since the onset of melting can be quite sudden under certain conditions.

This higher frequency of observation would also be desired in water resource management for power generation in the vicinities of glaciers used for this purpose (e.g. in Norway).

2.4.2 Required radiometer characteristics

Generally speaking, for the cryospheric observables it is desirable to use a constant angle scan to avoid unwanted variation of the emissivity with angle. The nature of this variation depends on the particular target observed and therefore would have to be separated from the variations of greater interest when applying algorithms to retrieve

geophysical parameters. Maintaining a constant incidence angle during the scan simplifies the task of geophysical parameter retrieval from the data.

In general, the brightness temperatures display a polarization effect when observing smooth surfaces. For all of the cryospheric applications except sea ice, the vertical polarization channels would be the most desirable since the surface effects are relatively constant for all forms of ice in the wavelength region under consideration. This choice of polarization minimizes the effect of surface reflection and maximizes the ability to observe radiation from the volume of the snow layer. In the case of sea ice, the observation of both polarizations enhances the distinction of open water from sea ice since the real part of the index of refraction is an order of magnitude higher for liquid water than it is for ice and hence the polarization is considerably greater.

In terms of the appropriate wavelengths for making such observations, the present techniques have concentrated on the use of a wavelength of 1.55 cm (the Nimbus 5 ESMR). This wavelength is near ideal for single-channel determination of sea ice concentration and variations in the emissivity of the continental ice sheets of Greenland and Antarctica. On the other hand, no convincing evidence has been obtained to date that would indicate that this wavelength is useful for observing snow cover over terrain. In the latter case, investigations carried out on a limited basis utilizing the Nimbus 6 ESMR, which is dual-polarized and operates at a wavelength of 0.8 cm, have indicated that this shorter wavelength can consistently detect snow cover on terrain. Since there are several contributions to the variation of brightness temperature in all observations in the cryosphere, it is clear that a multispectral dual-polarization approach is required for more precise retrieval of geophysical parameters. The Scanning Multichannel

Microwave Radiometer (SMMR) to be flown on the Nimbus G and SEASAT-A satellites (Table 2.1) is a step in the direction of such multispectral retrievals (Gloersen and Barath, 1977).

In terms of future instruments, the question arises as to whether the wavelength range of the observations should be extended at either end of the spectrum. There is little doubt that shorter wavelengths, say in the 0.3 cm window, would be very useful in increasing the sensitivity of the observations of snow cover over terrain. The atmospheric interference is considerably greater at this wavelength in the presence of cloud cover, however, which may limit the utility of such determinations. In the case of sea ice, shorter wavelength observations would also be advantageous, since the spatial resolution for a given aperture size would be greater due to the shorter wavelength. Again, however, the greater sensitivity to the presence of clouds might nullify this potential advantage. This shorter wavelength would offer limited additional advantage for observation of the continental ice sheets since it is the subsurface features that are of interest.

At the other end of the spectrum, going to longer wavelengths, e.g. 21 cm, would be advantageous in all of the cryospheric areas if it would be possible to achieve 10 to 20 km spatial resolution. Such spatial resolution is achievable by utilizing the larger payload capabilities of the shuttle free-fliers to be launched into polar orbit. Observations on the continental ice sheet at this wavelength would permit determination of the so-called 10-m temperature, which is independent of seasonal variations and is an important parameter to be determined both for climatological and glaciological purposes. Over sea ice, there would be an increased sensitivity to FT due to the greater optical depth at longer wavelengths.

2.4.3 Ancillary data

In principle, all of the geophysical parameter retrievals can be made without the use of ancillary data once the techniques have been validated. Of course, in the validation of the techniques, ancillary data are essential. These can be provided both by underflights of an instrumented aircraft and certain field measurements. The instrumented aircraft should include radiometers which simulate those on board the spacecraft, as is the case for the SMMR simulator on board the NASA CV-990 at the present time. In addition, obtaining simultaneous data at much higher spatial resolution with airborne instruments permits easier retrievals, since there tends to be less mixing of the various phenomena when data are obtained in this manner. The airborne instruments should also include a thermal infrared radiometer (11 μm band) for determinations of surface temperature, and various observations of the surface conditions at visual wavelengths.

Field measurements generally consist of determining the precise nature of the targets that are observed from both the aircraft and the spacecraft. In the case of sea ice, it consists of determining ice types and thickness for spot-checking the aircraft determinations. On continental ice sheets and snow-covered terrain, measurements of the particle size variation both in the vertical and horizontal directions in the snow cover, and the temperature variation with depth, are required.

2.5 Users

2.5.1 Sea ice

The U.S. Navy Fleet Weather Facility has been using Nimbus 5 ESMR microwave data in preparing their weekly charts on an operational basis since 1973. These charts are used by both military, commercial and overseas maritime

interests to facilitate shipping in ice-infested areas. Such operational use is expected to increase with the advent of more advanced microwave systems and with improved techniques for extracting the ice concentration appearing on these charts. Also contributing to the increased interest in this area is the recent extension of the offshore limit to 200 miles and the increasing incentive for developing offshore resources in the cryospheric environment. Present activities within this 200 mile limit include fisheries in the Arctic region, resupply of military bases using commercial vessels, resupply of the Prudhoe Bay oil complex, resupply of Indian settlements along the Alaskan coastline, and commerical support of research activities on the continental shelf by the U.S.G.S. The most immediate increase in activity in this area will result from the extraction of continental shelf oil utilizing offshore platforms in regions which become covered with sea ice. The operational aspects of monitoring sea ice within the 200 mile limit fall under the purview of the Marine Weather Services Branch of the Ocean Services Division of the National Weather Service, NOAA.

In terms of non-commercial usage, the sea ice parameters are essential ingredients for climate and global weather models. In addition there is effort in the area of modeling sea ice dynamics, which requires such input for both operational interests and studies of climate processes.

2.5.2 Continental ice sheets

There are no known commercial users of the physical parameters derived from the continental ice sheets. However, such data are of great importance for understanding global climate, as has been outlined in the NASA Climate Plan dated April 22, 1977 and Understanding Climatic Change, a program plan published by the National Academy of Sciences (1975).

2.5.3 Snow cover over terrain

Knowledge of the volume of water within the snow pack on terrain is essential for management of the global water supply. Some success has been achieved to date predicting runoff characteristics by observing simply the spatial extent of the snow cover on LANDSAT images (Gloersen and Salomonson, 1975). Such a technique, however, requires careful calibration of the specific characteristics of the area which relate snow depth to elevation, extent, and time of occurrence of the snow cover. A potentially more accurate technique and one more readily adaptable to larger areas of snow cover would be the utilization of microwave techniques for determining the water equivalent of the snow cover as described in section 2.2.4.

Further into the future, additional applications that would become practical when higher spatial resolution (the order of 1 km) becomes available would include the management of water resources for hydroelectric power generation from glacial runoff.

2.6 Required future work

2.6.1 Science

The general principles required to retrieve geophysical parameters from microwave brightness temperatures in the cryospheric environment are at hand. However, additional work in determining more precisely the microwave properties of snow and ice are certainly justified in terms of improving the accuracy of the parameter retrieval. For instance, the complex index of refraction of pure water ice has not been determined over all the wavelengths of interest. However, Vant (1976) reports new measurements at a wavelength of 3 cm and over a wavelength range from 7 to 3000 cm. In the limited data available in this reference, there are indications that both the imaginary and the real part of

the index of refraction are functions of frequency as well as physical temperature. Thus, extensive additional measurements are required to cover the entire wavelength range of interest in order to permit more precise parameter retrievals.

Other areas where additional basic research is required include the modeling and testing of surface roughness effects and various volume scattering mechanisms. More precise knowledge in these areas would certainly permit increasing the precision of retrieval of geophysical parameters.

2.6.2 Instrument development

The clearest immediate need in instrument development is the design and implementation of multispectral radiometer systems with increased spatial resolution which could eventually be flown on free-fliers launched by the Shuttle. Further into the future, larger systems of this sort could be assembled in orbit by man-in-space techniques. In terms of radiometry, the present-day sensitivity figures are adequate for many purposes. However, improvement in this area can always be utilized for improved retrieval accuracy. In order to be useful, such improvement must be accompanied by improvements in instrument stability, particularly with regard to varying temperatures in the components ahead of the radiometer. Perhaps a more important area of concern at this time is the development of techniques to avoid RFI from surface-based sources, such as telecommunication links and surveillance radars.

2.6.3 Real-time applications

Present multispectral microwave radiometer systems and those contemplated for the near future assume the use of ground stations for analyzing the data prior to distribution to the user community. Once a geophysical parameter

retrieval algorithm set is sufficiently developed, it would be relatively simple to implement an inexpensive microcomputer receiver system which could receive spacecraft data directly and provide geophysical parameters of a nearby area on an immediate basis. This could conceivably be of use in certain maritime operations requiring passage through sea ice or warning of impending high dynamic activity within the ice pack (for instance in the case of oil platforms in the 200 mile zone off the Alaskan north slope), or of use in warning of floods due to sudden melting of snow packs. However, such usage might require more training of local observers in interpretation techniques than would be practical.

2.7 References

Campbell, W. J., P. Gloersen, W. Nordberg, and T. T. Wilheit, Dynamics and morphology of Beaufort Sea ice determined from satellites, aircraft, and drifting stations. In "Symposium on Approaches to Earth Sciences through Use of Space Technology" (P. Bock, ed.), Konstanz, F.R.G. 23-25 May 1973, pp. 311-327, Akademi-Verlag.

Campbell, W. J., W. F. Weeks, R. O. Ramseier, and P. Gloersen, Geophysical studies of floating ice by remote sensing, J. Glaciology, 15, 305-328, 1975a.

Campbell, W. J., R. O. Ramseier, W. F. Weeks, and P. Gloersen, An integrated approach to the remote sensing of floating ice, Proc. Int. Astron. Fed., Lisbon, 1975b.

Chang, T. C., P. Gloersen, T. Schmugge, T. T. Wilheit, and H. J. Zwally, Microwave emission from snow and glacier ice, J. Glaciology, 16, 23-39, 1976.

Edgerton, A. T., A. Stogryn, and G. Poe, Microwave investigation of snowpacks, Final Report 1285 R-4, USGS contract 14-08-001-11828, Aerojet General Corporation, El Monte, Cal., 1971.

Fisher, A. D., A model for microwave intensity propagation in an inhomogeneous medium, IEEE Trans. Antennas Propag., AP-25, 876-882, 1977.

Gloersen, P., T. C. Chang, T. T. Wilheit, and W. J. Campbell, Polar sea ice observations by means of microwave radiometry, Proc. Inter-disciplinary Symp. on Advanced Concepts and Techniques in the Study of Ice and Snow Resources, Monterey, Cal., pp. 541-550, National Academy of Science, 1974.

Gloersen, P. and V. V. Salomonson, Satellites -- new global observing techniques for ice and snow, J. Glaciology, 15, No. 73, 373-389, 1975.

Gloersen, P. and F. Barath, A scanning multichannel microwave radiometer for Nimbus-G and Seasat-A, IEEE J. of Oceanic Engineering, Vol. OE-2, No. 2, 172-178, 1977.

Gloersen, P., H. J. Zwally, A. T. C. Chang, D. K. Hall, W. J. Campbell, and R. O. Ramseier, Time-dependence of sea-ice concentration and multiyear ice fraction in the Arctic basin, Boundary-Layer Meteorology, 13, (1977).

Hibler, W. D., Characterization of cold regions terrain using airborne laser profilometry, J. Glaciology, 15, 329-347, 1975.

Kunzi, K. F., A. D. Fisher, D. H. Staelin, and J. W. Waters, Snow and ice surfaces measured by the Nimbus 5 Microwave Spectrometer, J. Geophys. Res., 81, 4965-4980, 1976.

Schmugge, T. J., P. Gloersen, T. Wilheit, and F. Geiger, Remote sensing of soil moisture with microwave radiometers, J. Geophys. Res., 79, 317-323, 1974.

Stogryn, A., The brightness temperature of a vertically structured medium, Radio Science, 5, 1397-1406, 1970.

Tsang, L., and J. A. Kong, Thermal microwave emission from half-space random media, Radio Science, 11, 599-609, 1976.

Vant, M. G., A combined empirical and theoretical study of the dielectric properties of sea ice over the frequency range 100 MHz to 40 GHz, Technical Report, Environment Canada, 1976.

Zwally, H. J., Microwave emissivity and accumulation rate of polar firn, J. Glaciology, 18, 195-215, 1977.

Zwally, H. J., and P. Gloersen, Passive microwave images of the polar regions and research applications, Polar Record, 18, 431-450, 1976.

CHAPTER 3

APPLICATIONS OF MICROWAVE RADIOMETRY TO LAND PARAMETERS: SOIL MOISTURE, SNOW COVER AND FROZEN GROUND*

3.1 Executive Summary

3.1.1 Summary of Measurement Capability

A.

Priorities	Nominal Desired Spatial Resolution (km)	Frequencies (GHz)	Sensitivities (°K rms)
Soil Moisture	25*	1.4**	1
Snow Cover (Water Equivalent and Ripeness)	25*	3-90 (∿ 4 channels)	1

*3 km for watersheds.

**Multiple wavelengths 5 cm and longer are highly desirable.

B. The operational viewing interval can be ∿ 2-3 days. However, diurnal observations would be useful for soil moisture purposes and for snow condition monitoring especially during thawing. View angles less than 35°-40° are not critical and the horizontal polarization is desired. Both polarizations would yield increased information over this angular range. A conically scanning system receiving dual polarization at constant incidence angle would yield superior performance but at a sacrifice in spatial resolution.

C. Principal operational uses would be for crop yield forecasts, watershed runoff estimates, climatology, and land trafficability analyses. None of these applications have been demonstrated operationally, but they appear plausible based on demonstrated satellite measurement capabilities.

3.1.2 Recommendations

The review of passive microwave sensing of land parameters as presented in this chapter leads us to make the following recommendations:

*Prepared by T. J. Schmugge, R. W. Newton, D. McGinnis, and E. G. Njoku.

A. Continue support of efforts to test and validate microwave soil moisture estimates, and to better ascertain the effects of vegetation, soil type, soil roughness, and depth of penetration. Initiate an investigation to determine techniques of incorporating microwave data into crop yield forecasts and general circulation models. Continue to support efforts to develop techniques of utilizing microwave data for watershed management.

B. Continue support of efforts to monitor snow signatures at multiple wavelengths under conditions of good ground truth.

C. Incorporate land parameter objectives in any high-resolution passive microwave satellite system developed for purposes such as those recommended elsewhere in this report. There is general agreement that soil moisture information can be obtained for a spaceborne microwave system. However, the relationship between this soil moisture information and the soil moisture parameters needed for management decisions is not fully understood. The understanding and documentation of this relationship cannot be obtained without spaceborne data. The need for average soil moisture values over large areas for crop yield and general circulation models which has not been satisfied by existing means justifies proceeding with an experimental space system.

3.2 Application areas

3.2.1 Water resources

3.2.1.1 General

An increasing world population imposes greater demands on available water supplies. Variations in climate leading to floods or drought create havoc with the proper allocation of water in maintaining the present quality of life. Reasonable estimates of future water use and demand indicate a 3-5 times increase by the year 2000. To meet this increased demand, existing water supplies for a given region will have to be managed more efficiently with intelligent transfers of water from regions having excess supplies to areas of scarcity.

A system that can effectively monitor and inventory water supplies would be attractive for many government agencies at all levels in meeting priority needs where mandated responsibilities exist. These needs for water resource information will include assessing flood potential and watershed yield, crop yield prediction, irrigation efficiency improvement, snowpack monitoring, reservoir management, watershed planning, and waterworks design. In most cases these data are necessary as input into models used by agencies as their major management decision-making mechanisms. Although these watershed models are limited by the accuracy and timeliness of their input data, they are the major mechanisms used for watershed management such as in decisions on water release and storage, and water allocation policies. Therefore, improvements are needed in acquiring the input data for these models.

Since 1960 satellites have proved their worth by contributing data for

water resources management. The early visible camera systems were later supplemented with infrared and near-infrared sensors. Unfortunately these sensors are restricted by clouds from viewing the Earth and limited in the number of hydrologic parameters they can adequately observe. Variables such as soil moisture, snowpack density, snow wetness, precipitation distribution, and timely observations of floods are not amenable to these shorter wavelength sensors.

3.2.1.2 Soil moisture

The microwave portion of the electromagnetic spectrum offers potential for monitoring several of these parameters which are inputs to the models. Microwave observations are less dependent on atmospheric conditions, penetrate soil profiles and vegetation, and are very responsive to changes in the dielectric properties of various media such as snow and soil, caused by changes in the water content. One of the most needed observations for a broad range of applications is that of soil moisture. Hydrologists are particularly interested in soil moisture data because it defines the antecedent conditions needed for partitioning rainfall into its runoff and infiltration components. There is a substantial amount of results from investigations of passive microwave observations showing that microwave responses are sensitive to soil moisture variations at depths of a few centimeters. Although this approach is still in the developmental stage, the results are sufficiently encouraging to visualize microwave sensors on board operational satellites of the near future collecting data that would provide responsible estimates of soil moisture conditions for watersheds in excess of 12,000 km^2. The availability of such data to various governmental agencies would supply vital information that had previously been crudely estimated or inferred

from point precipitation measurements.

3.2.1.3 Snow water equivalent

Accurate data pertaining to the water equivalent of snowpacks is a highly critical parameter in the western United States. As in other parts of the world, such as Scandinavia and Switzerland, meltwater from mountainous snowpacks provides much needed water for hydropower generation and irrigation. As great as 70 percent of the 11 western states' water supply is directly derived from the spring runoff of snowpacks. As demonstrated by two consecutive years of record or near-record light snowpacks, determination of the water volume in the snowpack in advance of the runoff period is necessary to implement a program for proper management of the expected runoff. Such knowledge can permit an equitable allocation and distribution of the meager water supply available to the multipurpose reservoir systems.

Of importance also is the protection from excessive cold and drying winds provided by snowcover in the Plains of the United States and Canada. Russia and China have large wheat growing regions that likewise depend on the protection of the snowcover. The meltwater provided in the spring recharges the upper soil mantle for spring wheat and other grains planted in the spring. Information on the water content of these non-mountainous snowpacks could indicate areas of potential moisture deficiencies and the susceptibility to the hazard of wind erosion endangering newly emerged crops.

Sensors on board present operational satellites scan the Earth in only the visible, near infrared and thermal infrared portions of the spectrum. None of these sensors can monitor the water equivalent of snow. The microwave portion of the electromagnetic spectrum has shown considerable potential for monitoring snowpack density (or water equivalent) and wetness [Rango, 1977].

3.2.1.4 User agencies and requirements

Some documented federal agency needs are given below in Table 3.1.

Table 3.1: Documented Federal Agency Needs for Water Resources

Land Parameters	National Agency	Needs
SOIL MOISTURE	NOAA/Off. of Hydr./RFC's	Observe and model soil moisture for river stage forecasts, including flood forecasts.
	NOAA/Agriculture Wea. Service	Soil moisture levels for formulating agricultural weather advisories and for modeling crop-weather relationships.
	Bureau of Reclamation	Soil moisture values for irrigation drainage investigation planning.
	USDA/Soil Conserv. Serv.	Soil moisture content on plowed or fallow areas to indicate susceptibility to wind erosion.
	USDA/Forest Service	Soil moisture in plant zone for predicting biomass productivity.
SNOW, ICE, FROZEN GROUND	US Army Corp of Engineers	Snow and ice monitoring for trafficability in polar regions and detection of permafrost.
	NOAA/Off. of Hydrology/RFCs	Snow cover monitoring for contributions to runoff for river stage forecasting.
	Bureau of Reclamation	Snowfield mapping for runoff prediction, river ice for ice jams for flooding.
	USGS/Water Resources Div.	Seasonal snowcover monitoring, glacier monitoring for hazardous behavior.
	USDA/SCS	Snow surveys.
	USDA/Forest Service	Snowpack monitoring for avalanche prediction and flood forecasting.
LAND/ WATER INTERFACE	Bureau of Reclamation	Watershed surface drainage characteristics.
	USGS/Water Resources Div.	Identification of water surfaces to delineate flood hazard area.
	USDA/Soil Conservation Service	Flood delineation during peak flow.

In addition to these federal agencies, state agencies such as the Texas Water Development Board, the California Department of Water Resources and the Colorado Division of Water Resources also need basic hydrologic data for watersheds within their jurisdiction. Not only do state agencies require basic hydrologic data that can be converted to water supply/control information, but county, municipal and special water related districts also need such information. A recent report by the Landsat Follow-on Applications Survey Group (1976) estimated that $27,580,000 are being expended annually by such local governments solely for inventory and parameter estimate studies associated with water development projects. This figure was based on the approximage expenditures of 56 Standard Metropolitan Statistical Areas (SMSA). Within these SMSA's there were 174 county governments, 2,902 municipal governments, 1,470 township governments, 3,844 special districts and an additional 2,486 special water related districts.

For water resources applications there is no sharp cutoff on the required spatial resolution of a satellite sensor since watershed dimensions range from less than 1 km to hundreds of kilometers. Resolution of 3 to 5 km is highly desirable, with greater than 10 km resolution being of marginal utility. Proper monitoring of soil moisture requires observations at least weekly, but preferably every 3 to 4 days. Information on snowpack conditions is necessary bi-weekly in winter and every week during the spring melt season.

3.2.2 Climate

3.2.2.1 General

One of the most important variables which affects agriculture and hence man, is climate. Subtle variations from normal of various climatic parameters can wreak havoc with crop production. Precipitation, whether in the form of snow whose melt waters may fill reservoirs, permitting irrigation during periods of scarce rainfall; or in the form of showers to maintain soil moisture at adequate levels to supply continued growth, can cause years of tremendous surpluses or deficits by small deviations from normal patterns.

During the 1950's oceanographers working with the seasonal changes in the heights of sea levels concluded that a vast quantity of water, some 5.0×10^{18} g, was removed from the oceans between fall and spring each year and returned, of course, to the oceans between spring and fall. This resulted in an annual variation in mean sea level of about 1.4 cm when spread evenly over all the oceans of the world. Little of this moisture is stored in the atmosphere at any time and the change in atmospheric storage from winter to summer (considering both hemispheres together) is quite negligible. Storage in rivers, lakes, and other surface water reservoirs does not change significantly through the year. Therefore, the only place where this amount of water can be held is in the soil itself, (Mather, 1974).

This exchange of moisture from the soil to the oceans and back through the atmosphere will have a large effect on the climate. At the present time the climate models treat the interaction of the atmosphere with underlying land or ocean surfaces relatively crudely (Schneider, 1974).

It is clear that the moisture content of the upper few centimeters of the soil has a strong effect on the soil thermal properties, on evapotranspiration rates from the soil, and thus on the resulting heat and moisture transport at the atmosphere-earth boundary. For example, studies of severe thunderstorms indicate that the inflow air source region is from the near surface layer of the atmosphere (Davies-Jones, 1974). The addition of either heat or moisture to the inflow air adds energy to the storm. It has been found that the tornado frequency maxima in the Texas panhandle were centered in the region of intense irrigation and the maxima attributed to the increase water vapor content of the lower atmosphere as a result of evapotranspiration from the irrigated fields (Beebe, 1974). This particular effect needs to be verified with more studies that would be possible with remotely sensed soil moisture data. Recent sensitivity studies with general circulation models (Charney, 1977) have shown that the local evaporative flux included in the model was a major factor in influencing the precipitation amounts predicted.

3.2.2.2 Agency roles and requirements

Three major agencies are involved in the development of the U.S. climate plan. (See Table 3.2). The elements of the climate program involve: (1) establishing a climatic impact warning system, (2) improving existing climate prediction, (3) computer simulation and predictions of climate and (4) developing a global monitoring system for climate.

Table 3.2: Major Agency Roles in U.S. Climate Plan

Agency	Development Role
NSF	Physics of climate dynamics.
NOAA	Climate impact warning system. Operational climate forecasting.
NASA	Development of satellite instruments and systems for climate observations. Sensitivity studies. Climate data sets.

For climate and meteorological studies the surface resolution of a spaceborne soil moisture sensor should be comparable to the spatial scale of the soil moisture variation. In areas where the dominant form of rain is convective storms, it is not uncommon for there to be significant differences in the rainfall measurements of gages separated by as little as 10km. Therefore, to accurately observe soil moisture variations caused by storms of this type resolutions of the order of 10-20 km are necessary. Monthly averages of such resolution cells over areas of up to 100km can be considered to be a minimal requirement.

3.2.3 Agriculture

3.2.3.1 General

Agricultural resource and regulatory agencies in all levels of government from federal to local as well as private organizations require information on crop type, acreage, status and expected production throughout the growing season. Much of the required agricultural information is amenable to remote sensing. The use of infrared and visible sensors on Landsat for such purposes is discussed in Billingsley et al. (1976), and the potential of active microwave sensors for crop discrimination and plant moisture estimation is discussed in a series of publications produced by the University of Kansas (e.g., Bush and Ulaby, 1976). The role of passive microwave sensors is discussed below.

3.2.3.2 LACIE program

A large test program involving NOAA's Center for Climatic and Environmental Assessments (CCEA), NASA and the USDA is currently underway to develop techniques of improving global wheat production forecasts. The test program utilizes remote sensing technology and is called the Large Area Crop Inventory Experiment (LACIE). This is a project utilizing remote sensing technology that will result in an operational system in which a user agency is providing a portion of the supporting funds. This fact demonstrates the user agency interest and the need for remote sensing technology. In the discussion below, the LACIE program is used as the framework within which the requirements for soil moisture information are depicted.

The primary objectives of LACIE are to develop techniques of identifying wheat, determine the acreage, determine its status throughout

the growing season and estimate its productivity. Soil moisture data are vital to the accurate estimation of crop yield. Passive microwave sensors undoubtedly have the potential for providing soil moisture information that would be of more benefit than the weather/climate information that is currently used as a substitute for soil moisture.

The current technique utilized in the LACIE program is to construct computerized models by comparing years of historical data on weather and yield and establish a statistical linkage between them. These models are area dependent and they allow for a trend to high yields resulting from improved farming practices, new grain varieties and variation in fertilizer applications. Weather data for the current year are collected by crop district, county or equivalent crop area and are used with the regression model to predict yields for the coming harvest.

Temperature and water available to the crop are currently obtained through the dependence of these parameters on current weather information. The primary parameter is precipitation which is obtained from the point observations of the WMO grid and from estimates made from satellite cloud observations. As a result, the moisture input for yield models is unsatisfactory for regions from which only limited precipitation data is available.

The only method of providing a reliable and direct estimate of soil moisture is with microwave sensors. In fact, there is evidence that microwave sensors have the potential of providing an estimate of soil matric potential which is a direct measurement of the water available to the plant. Although it does not appear feasible to estimate the soil moisture in the root zone as is desired, a multifrequency sensor could provide information on the soil moisture gradient in the near surface

soil layers. Repeated measurements of this gradient could be used without other precipitation or runoff information to estimate the soil moisture in the root zone.

The utilization of microwave data for the remote measurement of soil moisture in the root zone will require the development of a water budget model that uses as its input only surface soil moisture profile gradient information and soil texture information. Even without such a water budget model, it only appears logical that a direct measurement of soil moisture in the near surface layer, if acquired often enough, would provide correlations to wheat yield that are superior to the gross precipitation information that is currently used.

3.2.3.3 User agencies and requirements

The number of agricultural resource and regulatory agencies and private organizations requiring agricultural information is large, and is described in the TERSSE report (1974) and in the Landsat Follow-on Application Survey Group report (1976). Most of these agencies will benefit from the improved crop information through incorporation of soil moisture measurements from space into the yield models. Most yield forecasting is done on a regional rather than farm by farm basis, thus the 20 to 30 km resolution available with a 10m L-band antenna from space would provide much useful data for these applications.

3.3 Parameters to be measured

3.3.1 Soil moisture

3.3.1.1 Physical basis

A microwave radiometer measures the thermal emission from the surface, and at these wavelengths the intensity of the observed emission is proportional to its brightness temperature (Rayleigh-Jeans approximation). The brightness temperature T_B observed by a radiometer from a height above the surface is:

$$T_B = \tau\left[r T_{sky} + T_e\right] + T_{atm}$$

The term in brackets includes the reflected component of the downwelling sky brightness temperature (cosmic background plus atmospheric contribution) and the brightness temperature of the radiation emitted by the earth's surface. These are modified by the transmittance τ of the layer of atmosphere between the surface and the radiometer. The final term in the expression is the contribution of this layer of atmosphere to the upwelling radiation reaching the radiometer. At the longer wavelengths, i.e. those best suited for soil moisture sensing, the atmospheric effects are minimal and will be neglected in this discussion.

Thermal microwave emission from soils is generated within the soil volume. The amount of energy generated at any point within the volume is dependent on the soil dielectric properties (or soil moisture) and the soil temperature at that point. As energy propagates upward through the soil volume from its point of origin, it is affected by the dielectric (soil moisture) gradients along the path of propagation. In addition, as the energy crosses the surface boundary it is reduced by the effective transmission coefficient which is determined by the dielectric characteristics close to the surface.

The brightness temperature of the surface can be written in terms of an integral over the half-space (Njoku and Kong, 1977)

$$T_B = \int_{-\infty}^{0} T(z)\, F[\varepsilon_r(z)]\, dz$$

where $T(z)$ is the subsurface temperature profile and $\varepsilon_r(z)$ is the dielectric constant profile. $F[\varepsilon_r(z)]$ is in the form of a weighting function which includes the effects of the surface reflectivity. The depths from which the emitted radiation originates and its radiation temperatures are governed by the relative shape of the weighting function, which in turn depends primarily on the dielectric loss profile. The magnitude of the weighting function is dependent on the surface reflectivity, which in most cases is governed by the dielectric properties in a region close to the surface. The depth of this region and the subsurface extent of the weighting function are frequency dependent, thus lower frequencies are sensitive to dielectric properties at greater depths in the soil. Further theoretical and experimental work is needed to determine the dependence of the "sensing depth" on frequency and moisture profile.

When $T(z)$ is uniform, the weighting function integral can be evaluated to give the emissivity, e, which is related to the surface reflectivity, r. The brightness temperature can then be written as:

$$T_B = T \int_{-\infty}^{0} F[\varepsilon_r(z)]\, dz$$

$$\text{or} \quad T_B = eT = (1 - r)T$$

For a smooth surface the emissivity can be approximated to a high degree of accuracy using numerical techniques for a layered medium.

This expression for brightness temperature is widely used and is sufficiently accurate for most applications. In areas where a large subsurface increase or decrease of temperature occurs over the region defined by the weighting function an average temperature must be used for T rather than the surface temperature.

The presence of soil moisture causes a marked change in soil dielectric properties, resulting in a decrease in emissivity over that of a dry soil. In addition to the presence of moisture, surface roughness and vegetation cover also have significant effects, generally tending to increase the surface emissivity.

3.3.1.2 Soil dielectric properties

A number of soil dielectric constant measurements have been made in recent years as functions of moisture content, frequency and soil type (e.g. Leschanskii et al., 1971; Lundien, 1971; Wiebe, 1971; Hipp, 1974; Hoekstra and Delaney, 1974; Newton and McClellan, 1975; Njoku and Kong, 1977). A compilation of some of the earlier measurements is found in the report by Cihlar and Ulaby (1974). Figure 3.1 shows the dependence of the real and imaginary parts of the dielectric constant as functions of moisture content at wavelengths of 1.55 and 21 cm. There is some difference between the dielectric constants measured for different soil types when plotted against moisture percent by weight especially at the longer wavelengths (Figure 3.1). This is due to the different strengths by which water molecules adhere to the soil particles. Thus when plotted against soil water matric potential the dielectric constant becomes essentially independent of soil type (Newton, 1976). For this reason brightness temperature data are often plotted as a function of percentage

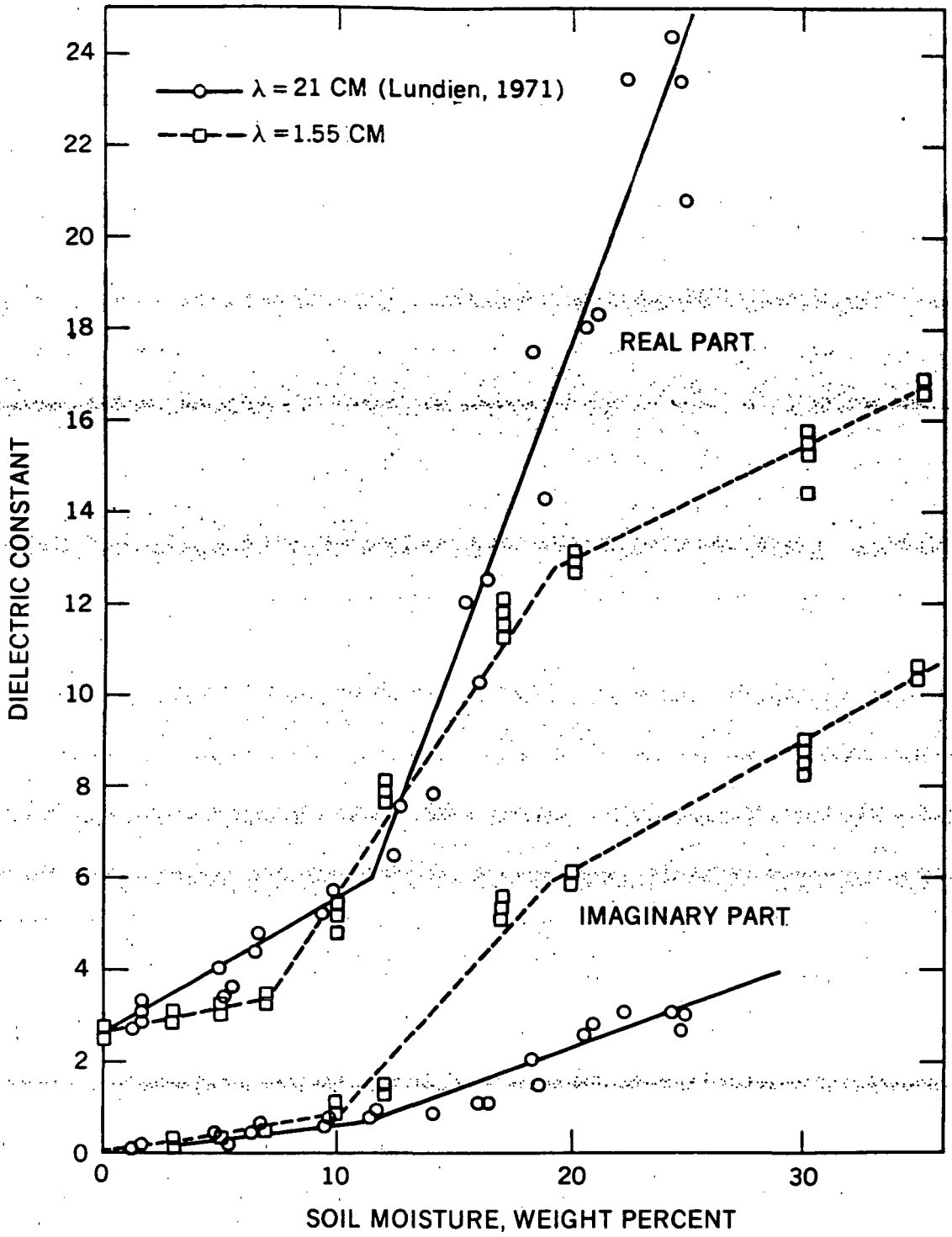


Figure 3.1. Representative soil dielectric constant measurements as functions of moisture content at wavelengths of 1.55 and 21 cm (Schmugge, 1977).

field capacity (which is directly related to soil water matric potential) (Schmugge, 1976). This is further desirable because matric potential (and percentage field capacity) are parameters that describe the water availability to plants and the degree of soil saturation, which are of primary importance to agriculturalists and hydrologists.

The range of dielectric constants presented in Figure 3.1 produces a change in emissivity from greater than 0.9 for a dry soil to less than 0.6 for a wet soil, assuming an isotropic soil with a smooth surface. This change in emissivity for a soil has been observed by truck mounted radiometers in field experiments (Poe, 1971; Newton, 1976), and by radiometers in aircraft (Schmugge, 1974) and satellites (Eagleman, 1976). In no case were emissivities as low as 0.6 observed for real surfaces. It is believed that this is primarily due to the effects of surface roughness.

As can be seen in Figure 3.1 there is a greater range of dielectric constant for soils at the 21 cm wavelengths. This fact combined with a larger soil moisture sampling depth and better ability to penetrate a vegetative canopy make the longer wavelength sensors better suited for soil moisture sensing.

3.3.1.3 Ground based experiments

Measurement programs utilizing ground-based radiometers have been performed for a number of years. The more comprehensive measurement programs have been executed by Aerojet-General Corporation (Poe, et al., 1971), Jet Propulsion Laboratory (Blinn and Quade, 1972; Blinn et al., 1972; Njoku, 1977) and Texas A & M University (Newton, 1976; Newton and Tesch, 1976; Newton et al., 1974).

In Figures 3.2(a) and (b) the field measurements of Newton (1976) are plotted versus angle of observation for various moisture contents and

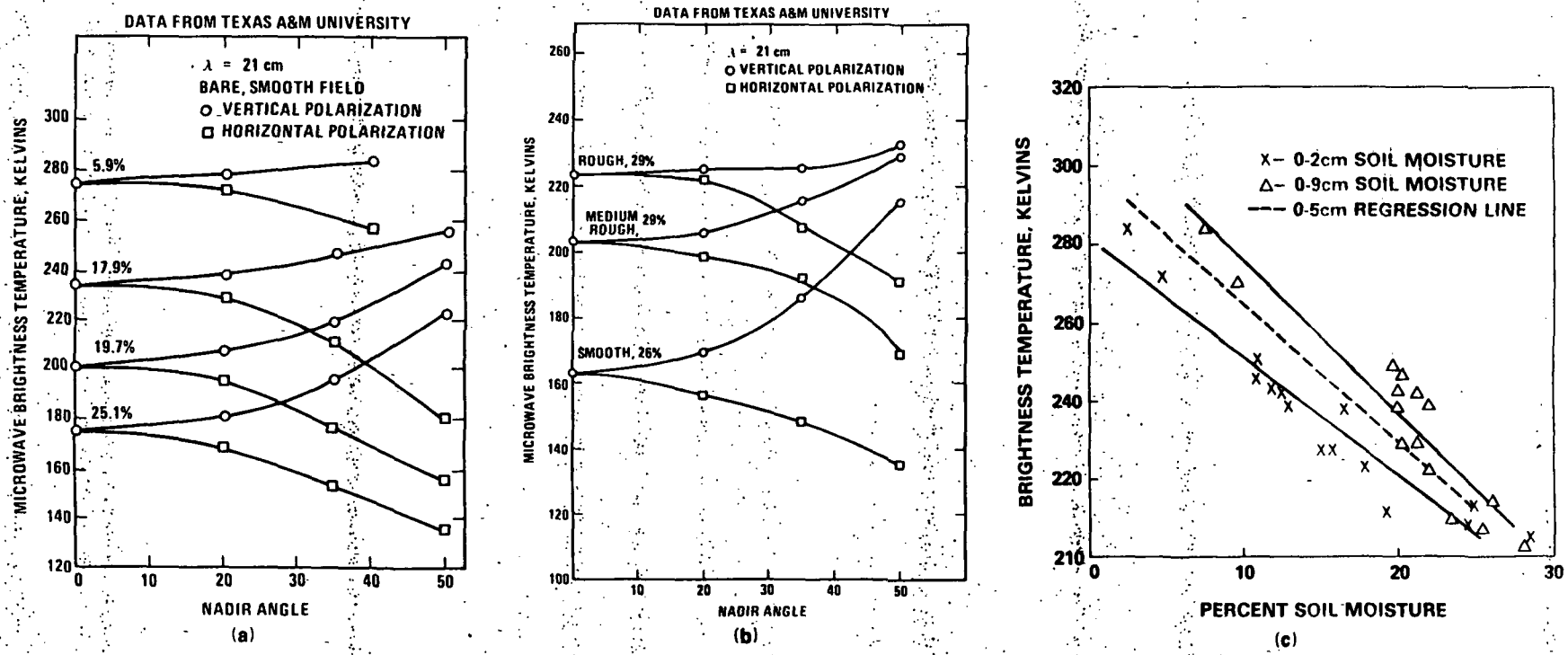


Figure 3.2. Results from field measurements performed at Texas A & M University: (a) T_B versus angle for different moisture levels; (b) T_B versus angle for different surface roughness at about the same moisture level; (c) T_B versus soil moisture in different layers for the medium rough field (Newton, 1976).

for three levels of surface roughness. The horizontal polarization is that for which the electric field of the wave is parallel to the surface and the vertical polarization is perpendicular to it. These results indicate the effect of moisture content on the observed values of T_B and the effect of surface roughness, which is to increase the effective emissivity at all angles and to decrease the difference in T_B for the two polarizations at the larger angles. Thus, by making the polarization measurements it may be possible to separate the effects of surface roughness and soil moisture.

When the brightness temperatures for a single roughness are plotted versus soil moisture in the 0 - 2 cm layer there is an approximately linear decrease of T_B, Figure 3.2(c). As the thickness of the layer increases both the slope and the intercept of the linear regression result also increase. This is because the moisture content for the high T_B cases increases, while it remains essentially the same for the low T_B or wet cases. This type of behavior was also seen in the results obtained from aircraft platforms and has led to the belief that the soil moisture sampling depth is in the 2 - 5 cm range for the 21 cm wavelength. This is in agreement with the predictions of theoretical results for radiative transfer in soils (Wilheit, 1975; Burke and Paris, 1975).

3.3.1.4 Aircraft and satellite experiments

Significant improvements in the understanding of the effects of individual scene parameters on the relationship of brightness temperature to soil moisture have been achieved using ground-based measurements acquired during controlled experiments. However, demonstration of the potential of passive microwave sensors for estimating soil moisture on an operational basis must be performed with aircraft and spacecraft sensors that integrate

large areas of natural, non-idealized terrain. A series of aircraft experiments performed over the last several years by a number of investigators demonstrates the sensitivity of microwave radiometers to soil moisture in agricultural terrain. Skylab and Nimbus satellites have also provided significant results for very large areas of integration.

The results from aircraft experiments are summarized in Figure 3.3 where results from aircraft flights in February 1973 (Figure 3.3(a)) and March 1975 (Figure 3.3(b)) over Phoenix, Arizona are presented (Schmugge, 1976). The values are plotted versus soil moisture expressed as a percent of field capacity to normalize the effect of soil texture differences. The agreement of the slopes for the three regressions indicates that the results are repeatable. The differences in the intercepts are due to differences in soil temperature between the 1975 a.m. and p.m. results.

The effect of a vegetative canopy will be that of an absorbing layer that depends on the amount of the vegetation and the wavelength of observations. In Figure 3.3(c) the results from vegetated fields for the two years are presented. The vegetation was either alfalfa or wheat with wheat being 20 - 30 cm high in 1973 and 50 - 60 cm high for the 1975 data. The slope of the curve is in good agreement with those for the bare fields. The intercept is lower due to the cooler soil temperatures. Thus sensitivity to soil moisture is maintained through the moderate vegetative canopies considered here. This result is supported by the field measurements of Newton (1976) who found the sensitivity maintained through 125 cm of a closely planted Sorghum field.

Studies of the Nimbus-5 satellite ESMR data at 1.55 cm wavelength have shown that it has limited applicability for soil moisture sensing (Meneely, 1977). The limitation is primarily caused by a vegetative canopy

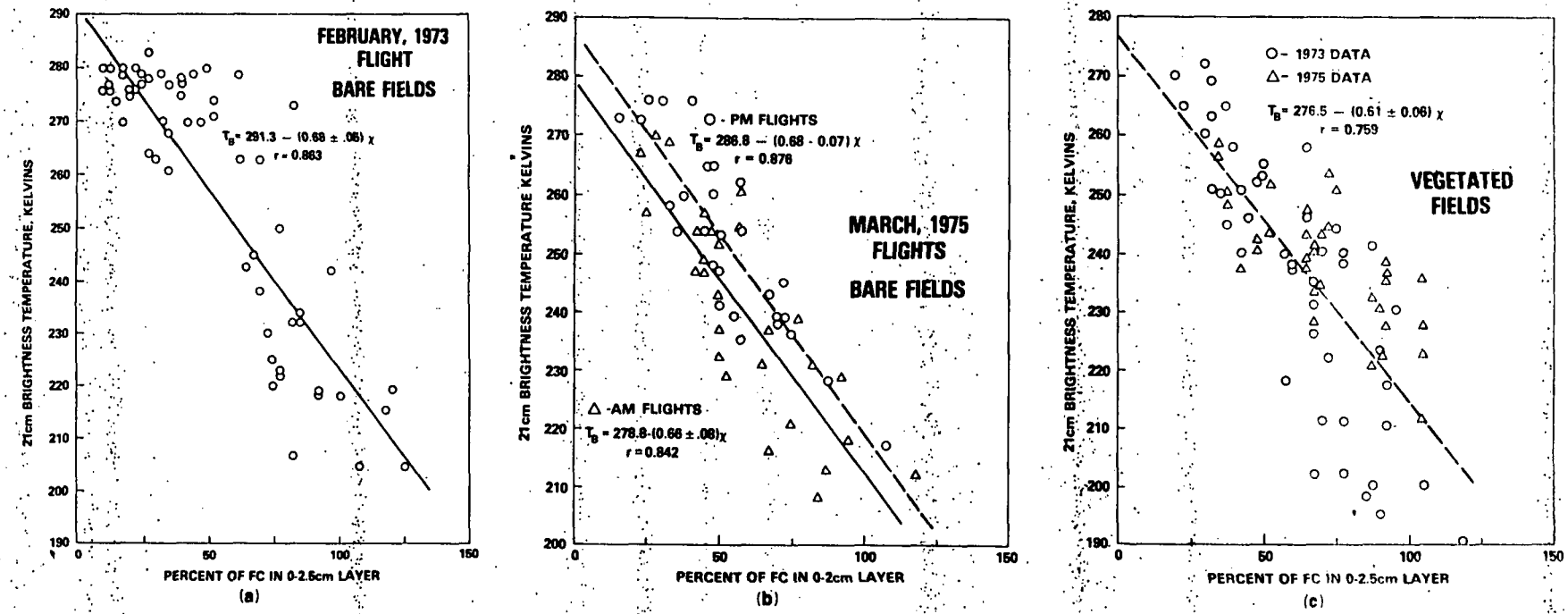


Figure 3.3. Aircraft observations of T_B over agricultural fields around Phoenix, Arizona: (a) bare field results from 1973 flight; (b) bare field results from 1975 flights; (c) vegetated field results from both years (Schmugge, 1976).

over the soil. For situations where there is a significant amount of bare ground the ESMR brightness temperature has shown significant correlations with soil moisture (McFarland and Blanchard, 1977; Schmugge et al., 1977). These situations arise in agricultural areas before the crops are planted and during the early stages of growth.

Studies using the 21 cm data obtained by the S-194 instrument on board Skylab have shown significant correlations with soil moisture variations. The latter were determined either by moisture budget models (Eagleman and Lin, 1976) or by using the antecedent precipitation index (McFarland, 1976). This was a limited data set and its interpretation was hampered by the coarse spatial resolution (~115km) of the sensor. However the results are encouraging for the potential use of a sensor operating at this wavelength for soil moisture sensing.

3.3.2 Snow cover

The use of microwaves for the remote sensing of snow parameters is still at an early stage. Early field experiments by Edgerton et al (1970) at a wavelength of about 1 cm observed anomalously low brightness temperatures for dry snow compared to what would be expected on the basis of the dielectric properties of the snow. They also noted a sharp rise in brightness temperature when the snow began to melt due to the presence of liquid water in the snow. The lowering of T_B has been explained as being due to volume scattering by the snow grains (England, 1974; Chang et al., 1976; Tsang and Kong, 1976).

The potential of microwave sensors for the remote sensing of snow depends on the observations of the lowered T_B for a sufficiently thick snowpack. The required thickness will depend on the wavelength. Figure 3.4 shows the decrease in brightness temperature as snow mass per unit area increases above a frozen ground surface. The indication is that

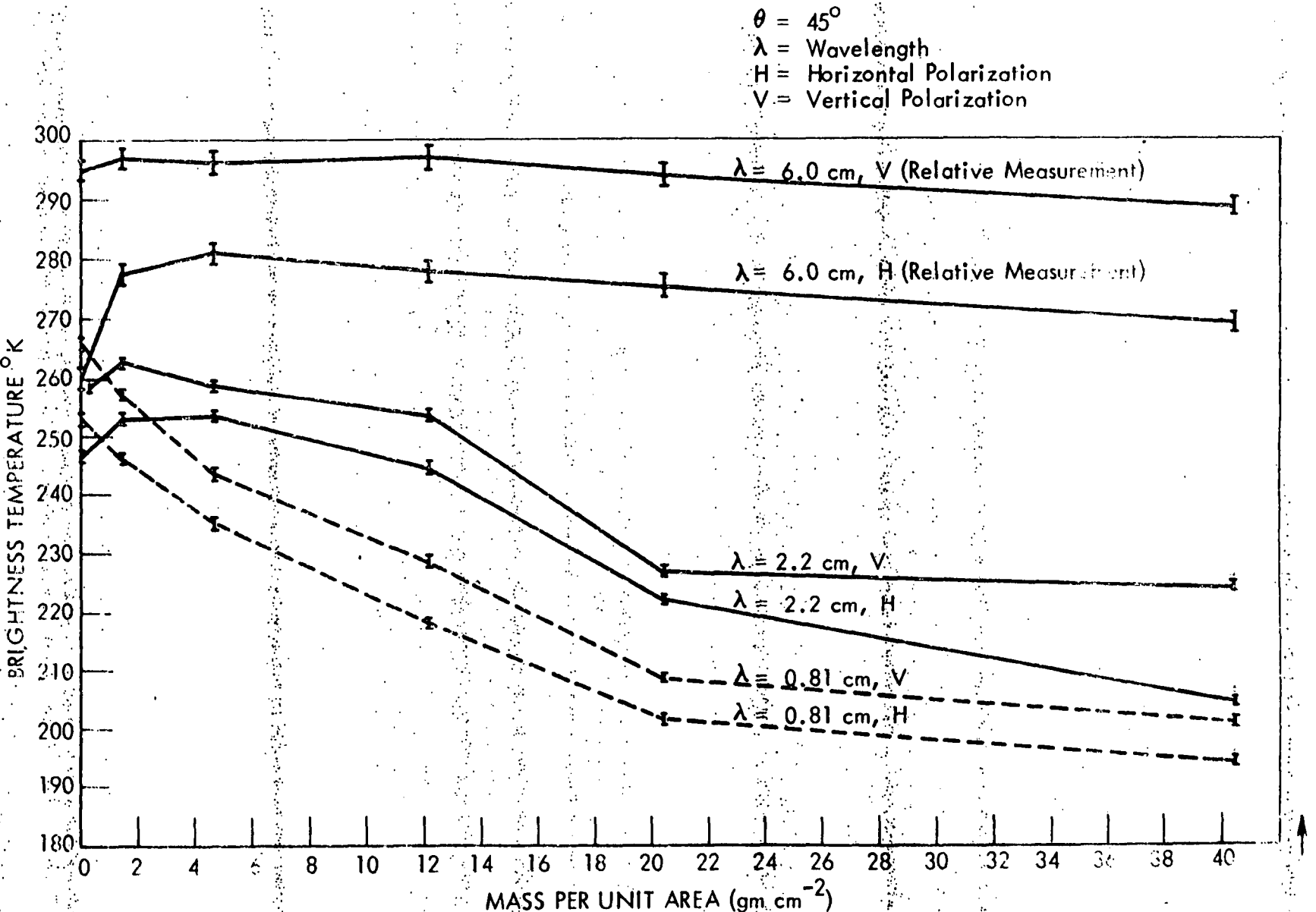


Figure 3.4. Measured brightness temperature as a function of snow mass per unit area (water equivalent) for dry snow (Edgerton et al., 1971).

multispectral observations at centimeter wavelengths may yield information on snow depth or water equivalent. When the nature of the underlying surface is unknown a long wavelength channel in the decimeter range will be desirable to infer the characteristics of underlying media. This is illustrated in figure 3.5 which shows the multispectral response obtained during aircraft flights over three different types of substrata underlying the snow targets; wet soil, a frozen lake and a continental glacier. The 11 and 21 cm radiometer show the greatest change as they respond to the different dielectric properties of the underlying media. The 0.8 and 1.55 cm results showed least variation indicating a response to the dry snow surface layer.

The increase of T_B as the snow melts is caused by the increased absorption of water on the snow grains producing a rise in the emissivity (figure 3.6). The ability to detect the presence of liquid water in snow makes it possible to determine the onset of melt in the snowpack which is important for determining when the snow will contribute to runoff. Field experiments currently in progress should substantially improve the capabilities of microwave radiometry in monitoring snow cover parameters.

Satellite data from Nimbus 5 and 6 have provided snow cover information on a global scale (Kunzi et al., 1976). Much work needs to be done before quantitative measurements of snow parameters such as depth and water equivalent can be made from space.

3.3.3 Frozen ground

Work performed by England and Johnson (1975) has shown that frozen soil appears dry radiometrically so that the frost line divides materials of different dielectric properties, viz. frozen soil from non-frozen soil.

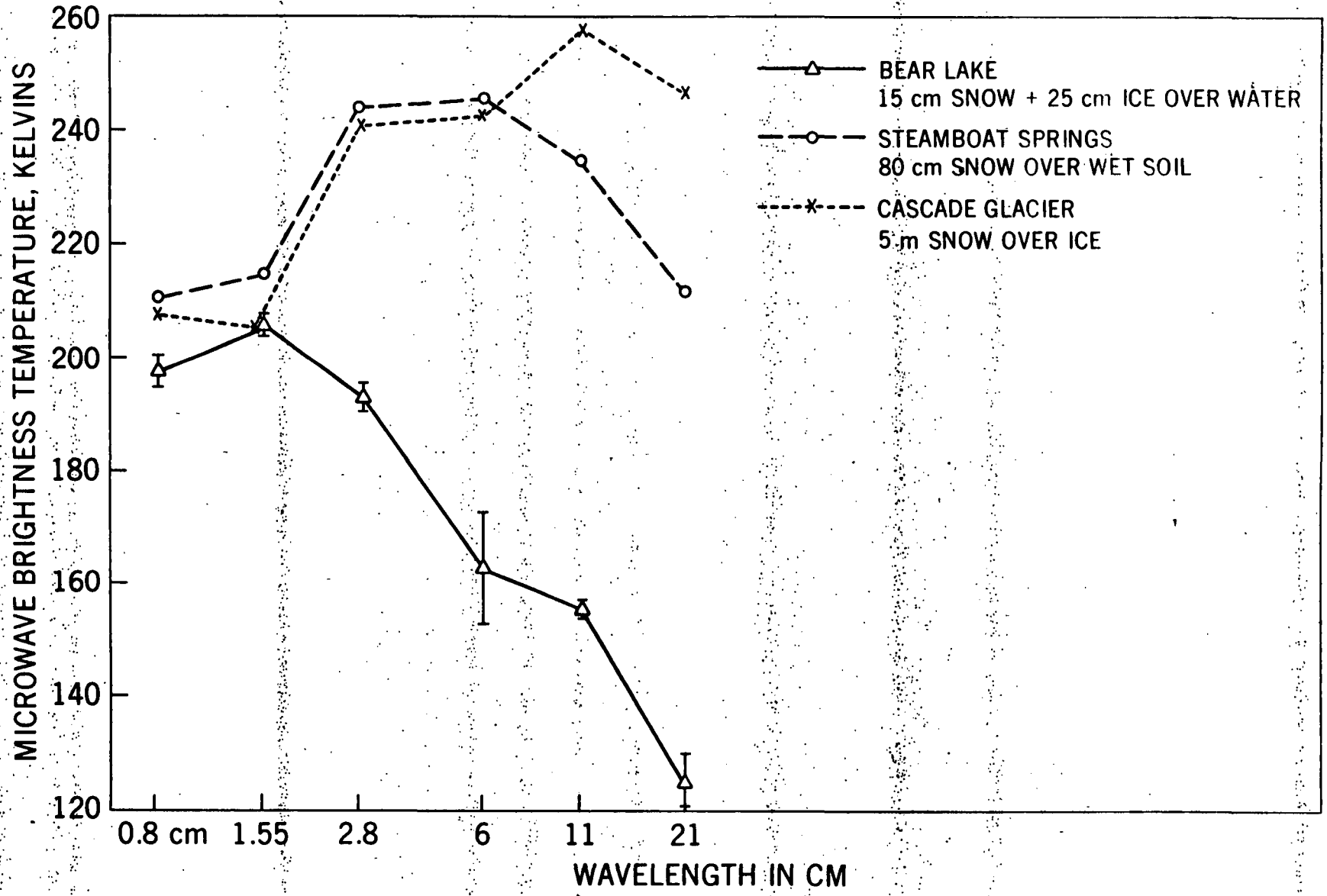


Figure 3.5. Aircraft multispectral measurements of snow overlying different kinds of substrata (Schmugge, 1973).

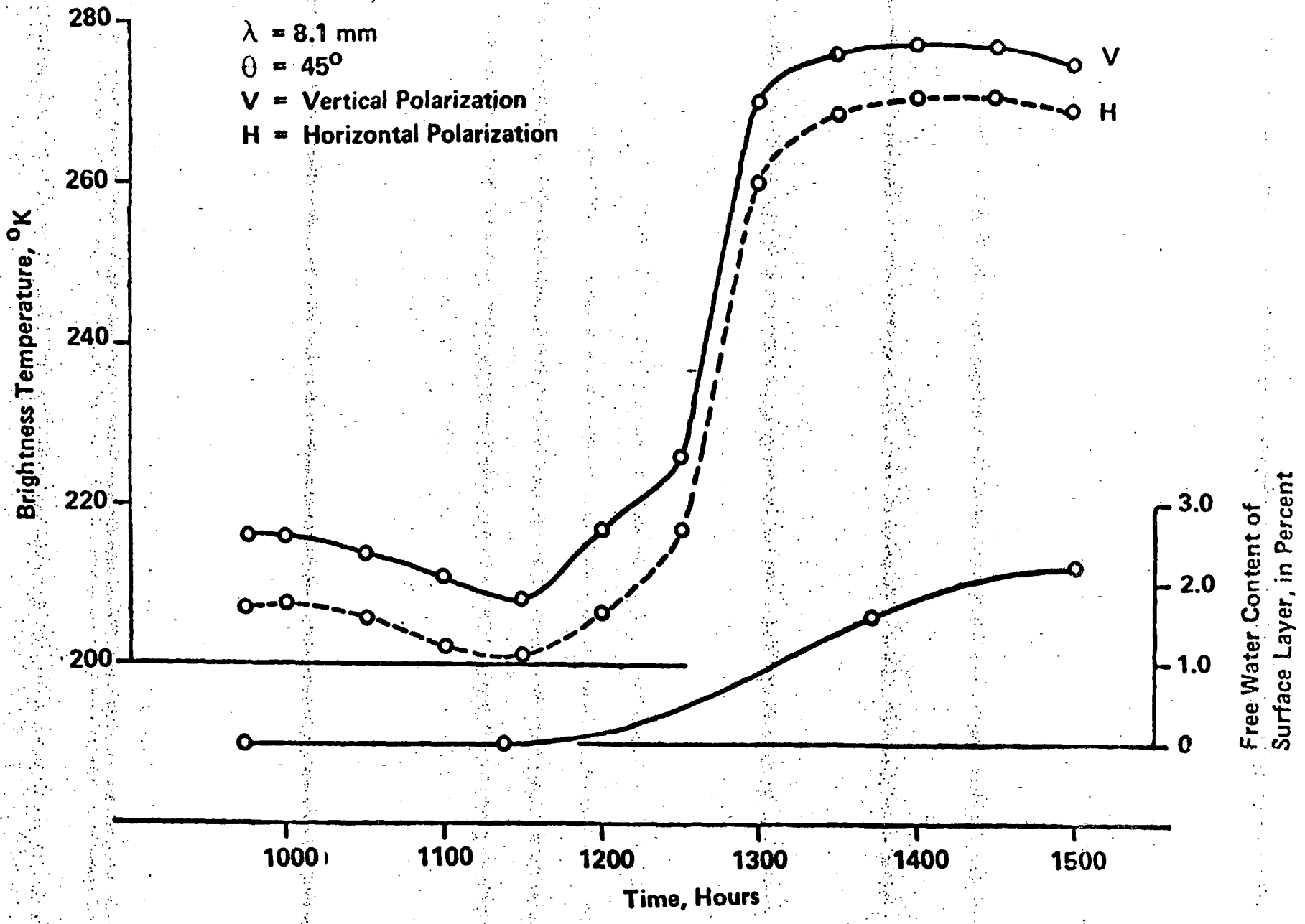


Figure 3.6. Brightness temperature and surface free water changes during the warming of a cold snow pack. (Wavelength 0.8 cm; snowpack thickness 0.8 m, density 517 kg/m^3) (Edgerton et al., 1971).

Such information can be of assistance in locating a path of non-permafrost in an area where patches of the frozen earth exist. Construction projects such as the location of oil pipelines (e.g. trans-Alaskan line) and even housing units could benefit from a rapid check of an area for small pockets of permafrost. Military maneuvers would also benefit from knowledge of frozen-non frozen terrain. Very little work has been done so far on this application of microwave radiometry.

3.4 References

Beebe, R.C., Large scale irrigation and severe storm enhancement, Symposium on Atmospheric Diffusion and Air Pollution, American Meteorological Society, Boston, Mass., 1974.

Billingsley, F.C., M.R. Helton, and V.M. O'Brien, Landsat follow-on: A report by the applications survey groups, NASA Technical Memorandum 33-803, Jet Propulsion Laboratory, California Institute of Technology, Pasadena, Cal., December 1976.

Blinn, J.C., and J.G. Quade, Microwave properties of geological materials: Studies of penetration depth and moisture effects, 4th Annual Earth Resource Program Review, NASA Johnson Space Center, Houston, Texas, January 17-21, 1972.

Burke, W.J., and J.F. Paris, A radiative transfer model for microwave emission from bare agricultural soils, NASA Technical Memorandum TM X-58166, NASA Johnson Space Center, Houston, Texas, 1975.

Bush, T.F., and F.T. Ulaby, Radar return from a continuous vegetation canopy, IEEE Transactions on Antennas and Propagation, AP-24, May 1976.

Chang, T.C., P. Gloersen, T. Schmugge, T.T. Wilheit, and H.J. Zwally, Microwave emission from snow and glacier ice, Journal of Glaciology, 16, 23-29, 1976.

Charney, J., W.J. Quirk, S. -H. Chow, and J. Kornfield, A comparative study of the effects of albedo change on drought in semi-arid regions, J. Atmos. Sci., 34, 1366-1385, 1977.

Cihlar J., and F.T. Ulaby, Dielectric properties of soils as a function of moisture content, RSL Technical Report 177-47, University of Kansas Center for Research, Inc., Lawrence, Kansas, 1974.

Davies-Jones, R.P., Discussion of measurements inside high-speed thunderstorm updrafts, Journal of Applied Meteorology, 13, 710 - 717, 1974.

Eagleman, J.R., and W. C. Lin, Remote sensing of soil moisture by a 21 cm passive radiometer, Journal of Geophysical Research, 81, 3660-3666, 1976.

Edgerton, A.T., A. Stogryn, and G. Poe, Microwave investigation of snowpacks Final Report 1285 R-4, USGS contract 14-08-001-11828, Aerojet General Corporation, El Monte, Cal., 1971.

England, A.W., Thermal microwave emission from a half-space containing scatters, Radio Science, 9, 447-454, 1974.

England, A.W., and G.R. Johnson, Thermal microwave detection of near-surface thermal anomalies, Proceedings of the U.N. Geothermal Symposium, 971-977, 1975.

Hipp, J.E., Soil electromagnetic parameters as a function of frequency, soil density, and soil moisture, Proceedings of the IEEE, 62, 98-103, 1974.

Hoekstra, P., and A. Delaney, Dielectric properties of soils at UHF and microwave frequencies, Journal of Geophysical Research, 79, 1699-1708, 1974.

Kunzi, K.F., A.D. Fisher, D.H. Staelin and J.W. Waters, Snow and ice surfaces measured by the Nimbus 5 Microwave Spectrometer, Journal of Geophysical Reasearch, 81, 4965-4980, 1976.

Leschanskii, Y.I., G.N. Lebedeva, and V.D., Schumilin, Electrical parameters of sandy and loamy soils in the range of centimeter, decimeter and meter wavelengths, Izvestiya Vysshikh Uchebnykh Zavedenii, Radiofizika, 14, 562-569, 1971.

Lundien, J.R., Terrain analysis by electromagnetic means, Technical Report 3-693, Report 5, U.S. Army Waterways Experiment Station, Vicksburg, Miss., 1971.

Mather, J.K., Climatology fundamentals and applications, McGraw Hill, 151-153, 1974.

McFarland, M.J., and B.J. Blanchard, Temporal correlation of antecedent precipitation with Nimbus 5 ESMR brightness temperatures, 2nd Hydrometeorlogy conference, Toronto, Canada, October 1977.

McFarland, M.J., The correlation of Skylab L-band brightness temperatures with antecedent precipitation, Proceedings of the Conference on Hydrometeorology, Fort Worth, Texas, April 1976.

Meneely, J.M., Application of the electrically scanning microwave radiometer (ESMR) to classification of the moisture condition of the ground, Earth Satellite Corporation, Final Report, Contract NAS5-22328, March 1977.

NASA, Definition of the Total Earth Resources System for the Shuttle Era: Volumes 1-7, Final Report NASA contract NAS9-13401, Earth Resources Program Office, NASA Johnson Space Center, Houston, Texas, 1974.

Newton, R.W., S.L. Lee, J.W. Rouse, and J.F. Paris, On the feasibility of remote monitoring of soil moisture with microwave sensors, 9th International Symposium on Remote Sensing of Environment, University of Michigan, Ann Arbor, Mich., April 1974.

Newton, R.W., and E.A. Tesch, Joint Soil Moisture Experiment: Ground-based measurements at Texas A&M University, July 13-25, 1975, Technical Report RSC-71, Remote Sensing Center, Texas A & M University, College Station, Texas, 1976.

Newton, R.W., Microwave remote sensing and its application to soil moisture detection, Technical Report RSC-81, Remote Sensing Center, Texas A & M University, College Station, Texas, 1976.

Njoku, E.G., and J.A. Kong, Theory for passive microwave remote sensing of near-surface soil moisture, Journal of Geophysical Research, 82, 3108-3118, 1977.

Poe, G., and A.T. Edgerton, Determination of soil moisture content using microwave radiometry, Final Report, 1684FR-1 DOC contract 0-35239, Aerojet General Corp., El Monte, Calif., 1971.

Rango, A., Remote sensing: Snow monitoring tool for today and tomorrow, NASA Goddard Space Flight Center, X-913-77-57, (preprint), 1977.

Schmugge, T.J., Microwave signatures of snow, Proceedings of Annual Science and Technology Review at GSFC, NASA SP-361, 193-195, 1973.

Schmugge, T.J., P. Gloersen, T. Wilheit, and F. Geiger, Remote sensing of soil moisture with microwave radiometers, Journal of Geophysical Research, 79, 317-323, 1974.

Schmugge, T.J., T. Wilheit, W. Webster, and P. Gloersen, Remote sensing of soil moisture with microwave radiometers II, NASA Technical Note TN D-8321, 1976.

Schmugge, T.J., J.M. Meneely, A. Rango, and R. Neff, Satellite Microwave observations of soil moisture variations, Water Resources Bulletin, 13, 265, 1977.

Schmugge, T.J., Remote sensing of surface soil moisture, 2nd Hydrometeorology Conference, Toronto, Canada, October 1977.

Schneider, S.H., and R.E. Dickinson, Climate modelling, Review of Geophysics and Space Physics, 12, 447, 1974.

Tsang, L., and J.A. Kong, Thermal microwave emission from half-space random media, Radio Science, 11, 559-609, 1976.

Wiebe, M.L., Laboratory measurements of the complex dielectric constant of soils, Technical Report RSC-23, Texas A & M University, College Station, Texas, 1971.

Wilheit, T.T., Radiative transfer in a plane stratified dielectric, NASA Technical Memorandum TMX-71051, 1975.

CHAPTER 4

MONITORING OF THE OCEAN AND OTHER AQUATORIES*

4.1 Executive Summary

4.1.1 Summary of Measurement Capability

A.

Priorities	Nominal Desired Spatial Resolution (km)		Radiometer Frequencies (GHz)	Radiometer Sensitivities (°K rms)	Achievable Measurement Accuracy (rms)
	Open Ocean	Coastal Zones			
Surface wind	20-50	2-5	1.4-10 (3 freq.)	1	2-5 ms^{-1}
Surface temperature	20-50	1	1.4-10 (3 freq.)	0.3	0.5-2°K
Surface salinity	5-10	0.5-1	1.4-10 (3 freq.)	0.3	∿1 ppt.
Surface and volume pollution	-	0.5	1.4-10 (3 freq.) +19, 37	0.3-2	-
Fresh water ice		0.5	1.4*	2	-

*(Plus several narrow band, closely spaced channels for thickness measurement.)

B. Depending upon the parameter to be measured, the viewing interval ranges from 12 hours to weekly. The choice of viewing angle is driven by the measurement of ocean surface roughness. Dual linear polarization at an angle of incidence near 55° will provide a unique measurement of and approximate correction for, roughness at any frequency. A nadir measurement (0° incidence angle) at circular polarization would greatly improve the spatial resolution, but would require several frequencies to correct for roughness.

C. Surface wind and temperature data would be useful to the Fleet Numerical Weather Facility and to the National

*Prepared by C. T. Swift and F. Y. Sorrell.

Meteorological Center in preparation of operational analyses and forecasts. Salinity and pollution information appear to be of interest to the EPA and the States (Departments of National Resources, Fisheries, and Pollution Control).

D. The complementary and unique roles of microwave sensors of the ocean and other aquatories are summarized below:

Surface Wind - The competing technique is the radar scatterometer. However, radar may have an upper limit of $\sim$ 25 m/sec because the radar responds to the rms height of capillary waves, which do not grow without limit. On the other hand, the radiometer infers winds also through increased emission from surface foam coverage, which monotonically increases for wind speeds up to at least 70 m/sec.

Surface Temperature - The competing technique here is the infrared radiometer. The obvious advantage of the microwave radiometer is its ability to penetrate clouds. Indeed, the atmosphere is so transparent at the lower microwave frequencies, that corrections are small except during extreme weather conditions.

Surface Salinity - Thus far, a microwave radiometer has provided the only demonstrated remote sensing technique for synoptically measuring salinity in coastal zones. Optical techniques, such as Raman scattering of a laser beam, have been proposed, but not yet demonstrated.

Surface and Volume Pollution - The Coast Guard has demonstrated operational use of a radar imaging scatterometer to detect oil spills (the radar cross section is reduced due to damping of capillary waves by the oil). In addition to the detection of oil spills, microwave radiometers offer demonstrated capability for measuring oil slick thickness. There is also experimental evidence that microwave radiometers can detect concentrated volume pollutants, such as acid dumps.

Optical systems compete; however, microwaves offer near all-weather and night-time operation. Microwave radiometers also respond to changes in the dielectric constant, and therefore offer the possibility of measuring "colorless" pollutants.

Fresh Water Ice - Imaging scatterometers can detect ice boundaries, and short-pulse altimeters have been proposed as a technique to measure thickness at nadir. Microwave radiometers offer the possibility of measuring thickness over a swath. Optical techniques can measure ice boundaries, but not ice thickness.

The economic significance of the radiometric monitoring of ocean surface temperature and wind fields has been well documented in several NASA workshops dating back to 1967 (Woods Hole, Williams College, Houston). These studies have shown that the remotely sensed data would, for example (a) impact the four billion dollar fishing industry, (b) contribute toward 1 to 2 week forecasts, which, if possible, might have as much as a one billion cost benefit to agriculture, forestry, municipal water supplies and construction industry, to name a few, and (c) perhaps save the shipping industry hundreds of millions of dollars per year through knowledge of sea state.

It is important to note that remote sensors collect synoptic data in a very short period of time. Equivalent data obtained by any other method would require enormous expenditures. Thus it is very difficult to precisely determine the economic benefits of remote sensors. The alternate cost is just so high that the data simply would not be obtained.

4.1.2 Recommendations

A. Support continued efforts to demonstrate microwave

capabilities for ocean surface measurements; especially use of the Nimbus-G and SeaSat data for simulated or actual operational purposes.

B. Support continued theoretical and experimental studies to determine ultimate capabilities of passive microwave sensors for oceanic observations including observations, from aircraft or other appropriate platforms, of the fine spatial structure of the observed surface parameters.

C. Study the feasibility of a radiometer imaging system to achieve a 1-km spatial resolution. Such a system would require a 100-300 m antenna in space to provide usable geophysical data in the coastal zones. An alternative approach would be to use high-altitude aircraft for coastal zone remote sensing.

D. Continue to support the development of an analytical model of emission from foam and heavy seas in order to quantify the measurement of surface wind speed.

E. Develop a better understanding of the effect of pollutants on the dielectric constant of sea water.

F. Verify, through field experiments, the ability of radiometers to measure fresh water ice thickness and other layered media. These measurements will require a radiometer with several narrow-band, closely spaced channels.

4.2 Applications

4.2.1 Demonstrated measurements

4.2.1.1 Sea surface temperature

A precision 2.6 GHz radiometer has been developed under the NASA Advanced Applications Flight Experiments program for the purpose of all-weather measurement of sea surface temperature (Hidy et al., 1972; Hardy et al., 1974). Since the emissivity of the ocean at this frequency is $\sim$ 0.3, the accuracy of radiometric measurements must be approximately three times better than the desired accuracy of inferred surface temperature. As a demonstration of the instrument performance, this radiometer was flown down the length of Chesapeake Bay in conjunction with extensive surface truth measurements (Blume et al., 1977a). The surface truth values of salinity and temperature were used to calculate the brightness temperature of a flat ocean surface, with corrections for sky radiation, antenna losses, and beam efficiency. Comparison between calculation and measurement over a calm sea showed an average difference of 0.3 K.

While the 2-3 GHz range is perhaps the best for single-channel retrievals of sea surface temperature, antenna requirements for acceptable spatial resolution from a satellite bias a choice of frequency toward higher values, at least for near-term applications. The peak sensitivity to changes in sea surface temperature actually occurs in the interval of 4-7 GHz. Although sensitivity to atmospheric interference is also higher there than in the 2-3 GHz range, sensitivity to salinity variations is less, and antenna design is more tractable. Atmospheric effects can be corrected by using higher frequency channels. Such multichannel sea surface temperature retrievals should be at least comparable to single channel measurements in the 2-3 GHz interval (Gloersen and Barath, 1977).

In a subsequent series of flights, Blume et al. (1977b) added a 1.4 GHz radiometer to their system. This frequency is more sensitive to salinity of the surface layer, whereas 2.6 GHz is more sensitive to the temperature. Thus the two measurements were simultaneously inverted for temperature and salinity. The aircraft flew a series of parallel east-west flight lines over the Chesapeake Bay area, with calm sea conditions. The resultant isotherms are plotted on the map in Figure 4.1. These microwave retrievals were compared with surface truth at 11 stations. The mean discrepancy between in-situ and remotely sensed temperature was 0.56°C, with a standard deviation of 0.59°C.

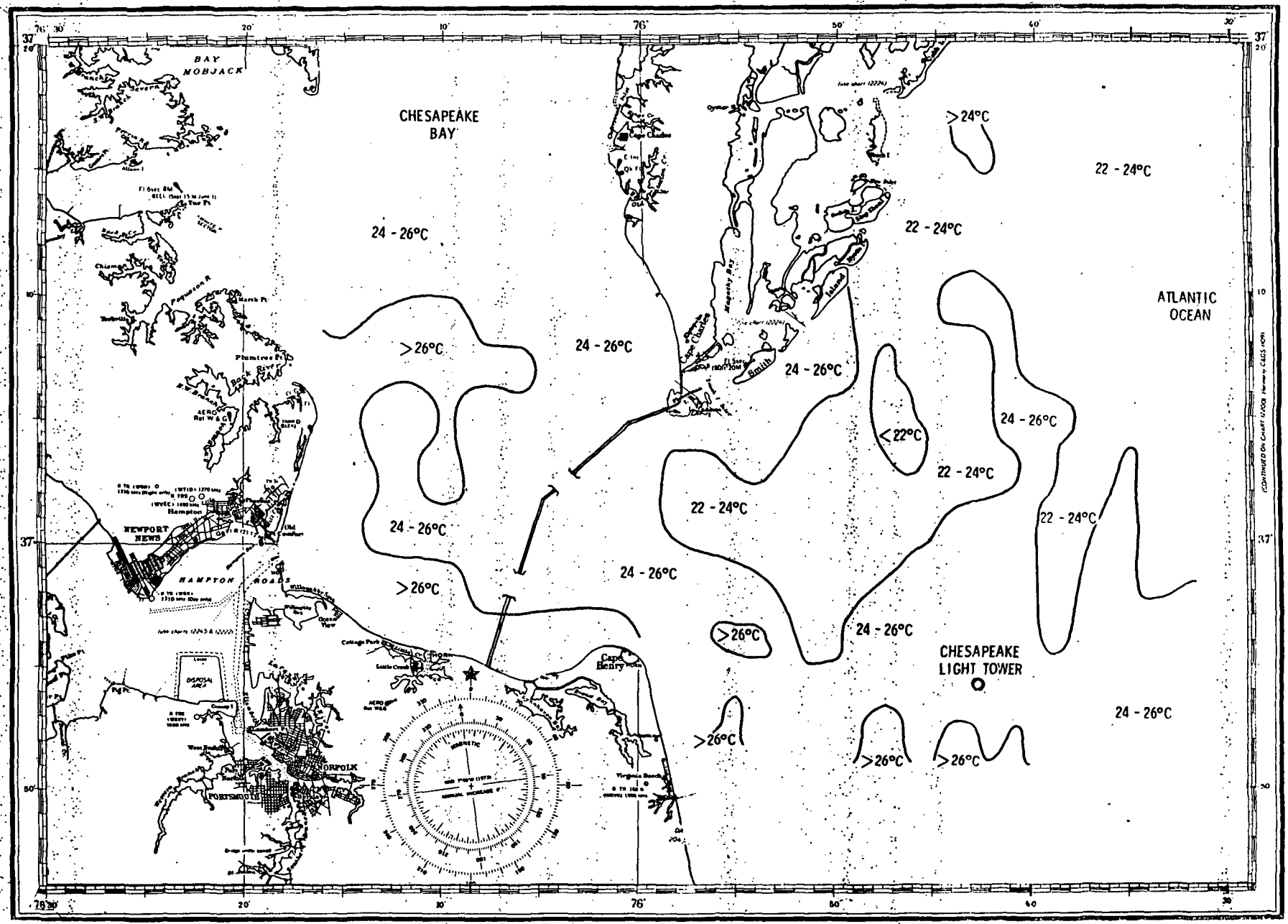


Fig. 4.1. Isotherms in lower Chesapeake Bay on August 24, 1976, obtained from microwave measurements (Blume et al., 1977b).

4.2.1.2 Salinity

The Blume et al. (1977b) map of isohalines is shown in Figure 4.2. Increments are 2 ppt. Comparison of these retrieved values with chemical analysis of samples taken at the 11 surface stations gave a mean discrepancy of 0.52 ppt, with a standard deviation of 0.91 ppt. Considered together, Figures 4.1 and 4.2 suggest a physically reasonable situation: salinity increases as the relatively warmer bay water mixes with and merges into the cooler coastal ocean water.

Other measurements of salinity have been reported by Thomann (1976). Single flight lines were made along the Mississippi sound, with continuous comparisons between aircraft measurements and surface samples. Good agreement was obtained for salinity concentrations ranging from 5 ppt to 30 ppt. In these flights surface temperature variations were corrected by using infrared measurements.

4.2.1.3 Rough Surface Emission/Sun Glitter

The thermal emission from rough surfaces as a function of viewing angle, polarization and electromagnetic frequency was demonstrated by the classic Argus Island experiments (Hollinger, 1971), and later verified by experiments conducted from a railroad bridge spanning the Cape Cod Canal (Swift, 1974). The results summarizing these two data sets are shown in Figure 4.3. As a most relevant experiment, Hollinger set his radiometer array at a viewing angle of 55° where the vertically polarized channel is theoretically invariant with surface roughness (Stogryn, 1967) and collected data vs. windspeed for both polarization states. The results in Figure 4.4 indicate that the vertically polarized channel is roughness independent and the horizontally polarized channel is not. Thus, the vertically polarized channel should provide a unique measurement of temperature, and the horizontal channel should provide roughness information in open

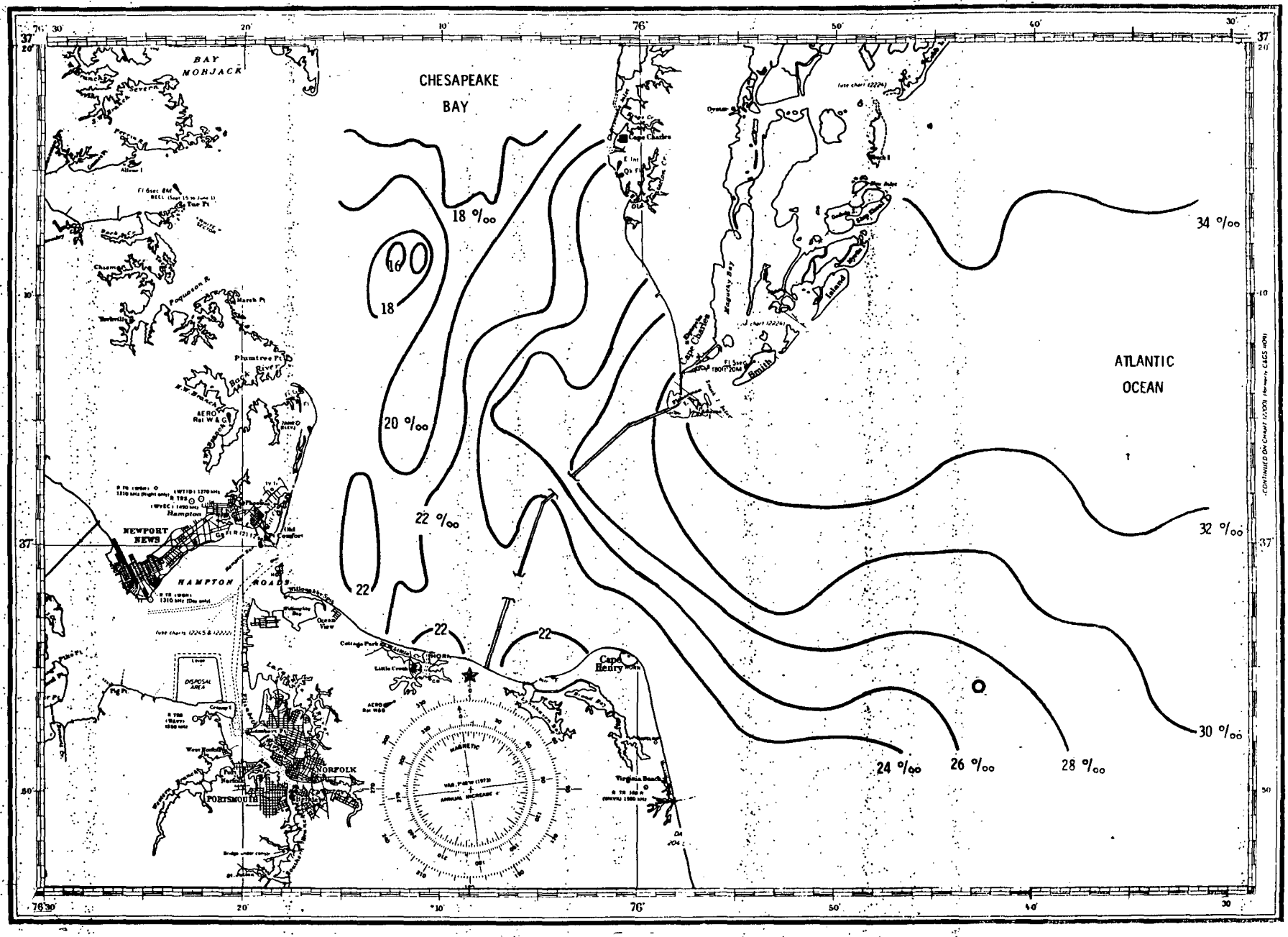


Fig. 4.2. Isohalines in lower Chesapeake Bay on August 24, 1976, in increments of 2 ppt., obtained from microwave measurements (Blume et al., 1977b).

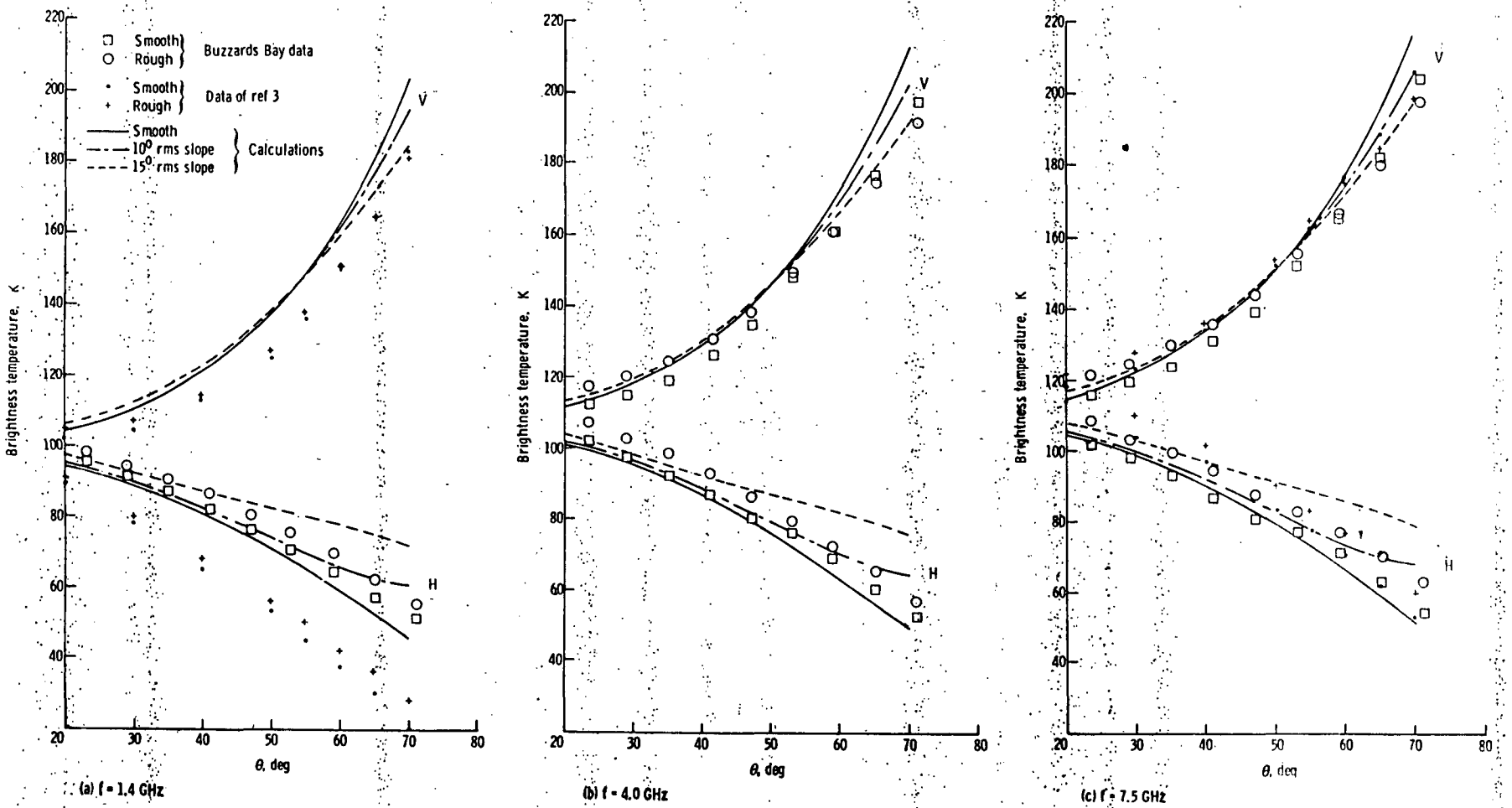


Fig. 4.3. Plots of radiometric brightness temperature vs. viewing angle. The calculations are based on equations developed by Stogryn (1967) (V = vertical polarization, H = horizontal polarization). The dots and crosses are data of Hollinger (1971).

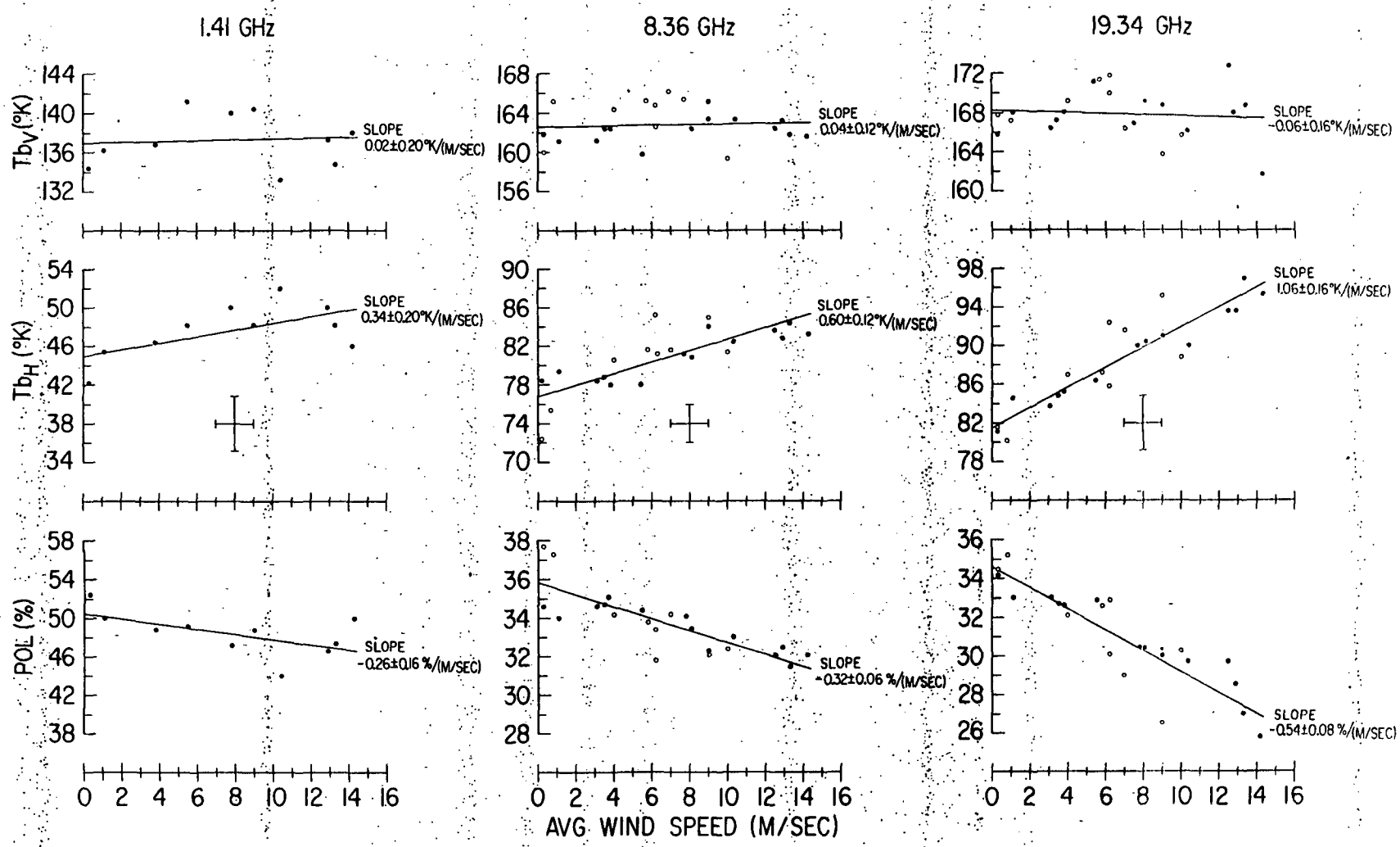


Fig. 4.4. Brightness temperature vs. wind speed (fetch-limited) at viewing angle of 55°, for vertical polarization (top) and horizontal polarization (middle).

ocean areas where salinity is relatively constant. Hollinger's multi-spectal data also suggest that the contribution due to roughness decreases with decreasing electromagnetic frequency.

Several years ago, it was shown (Cox and Munk, 1954) that the degree of roughness of the ocean surface can be inferred by measuring the glitter pattern of sunlight as recorded on film. Indeed, it was shown that the slope statistics could be measured from photographs taken at various angles away from specular. It was later shown that similar results (Swift, 1974) could be achieved at microwave frequencies. It is certain that such microwave glitter patterns can be developed from space with the added benefit of all-weather capability.

4.2.1.4 Wind Speed as Derived from Ocean Surface Foam Emission

In 1969, Nordberg flew a 19 GHz radiometer over a wind-driven Salton Sea in order to verify the theory of emission from rough ocean surfaces. The results showed that the experimental values were tens of degrees Kelvin higher than predicted by Stogryn's theory (Nordberg et al., 1969). Nordberg correctly attributed this discrepancy to increased emission due to surface foam. In later experiments, data were collected over a variety of wind speed conditions, also at 19 GHz, and the correlation of increased brightness temperature with increasing foam coverage is shown in Figure 4.5. Multifrequency measurements have recently been reported (Webster et al., 1976), and windspeed sensitivity vs. frequency for two incident angles, nadir and 38°, is shown in Figure 4.6. These data indicate that the horizontally polarized channel at 38° is more sensitive to changes in windspeed. It is also of interest to note that the windspeed sensitivity increases at higher frequencies, therefore suggesting that surface temperature, salinity, and windspeed can independently be measured by an appropriate selection of at least three microwave frequencies.

4.2.1.5 Emission from Oil Spills

Measurements of oil slick thickness have been made under both laboratory and field conditions (Hollinger and Mennella,

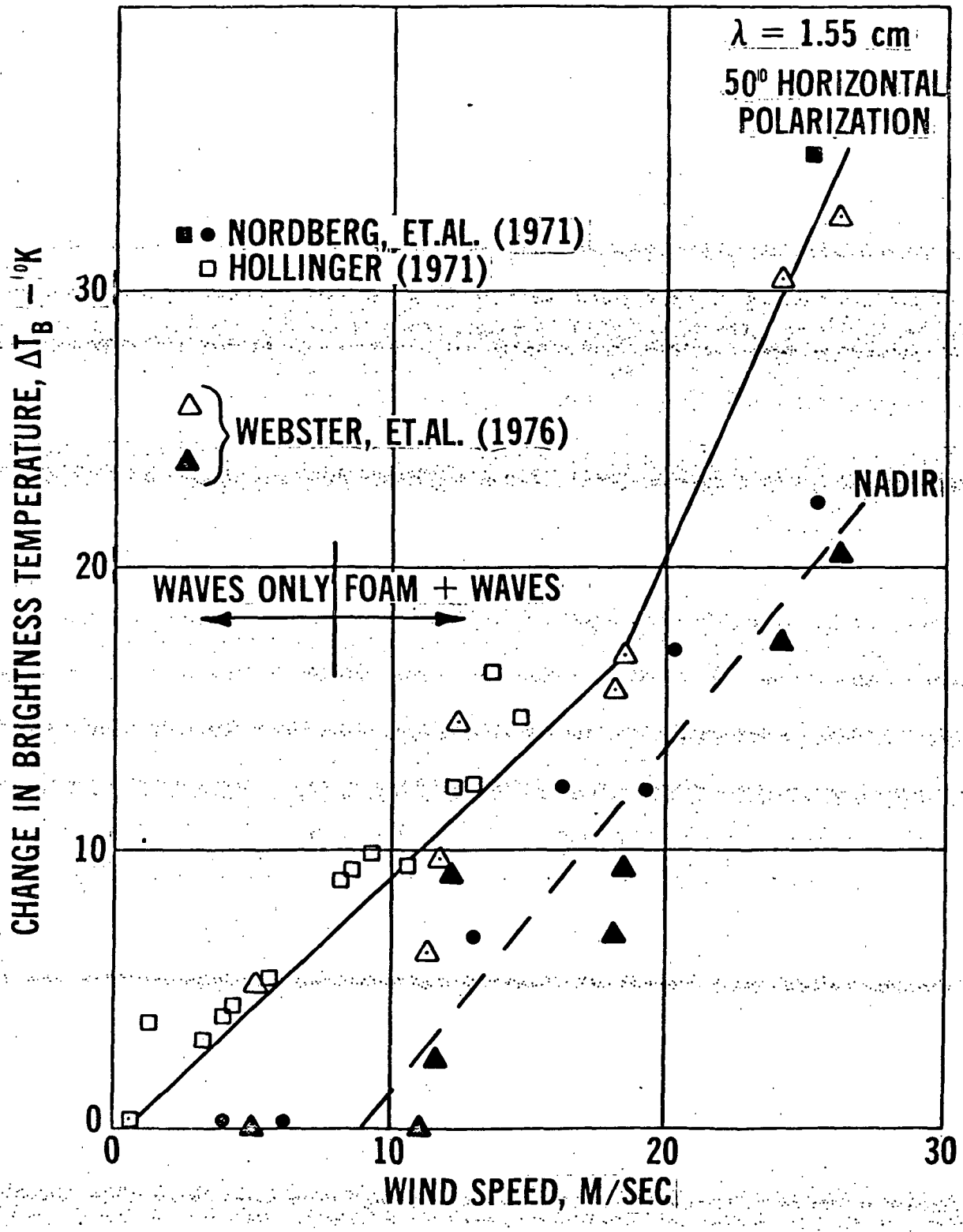


Fig. 4.5. Increased radiometric brightness temperature at 19 GHz, versus wind speed. (Gloersen and Barath, 1977)

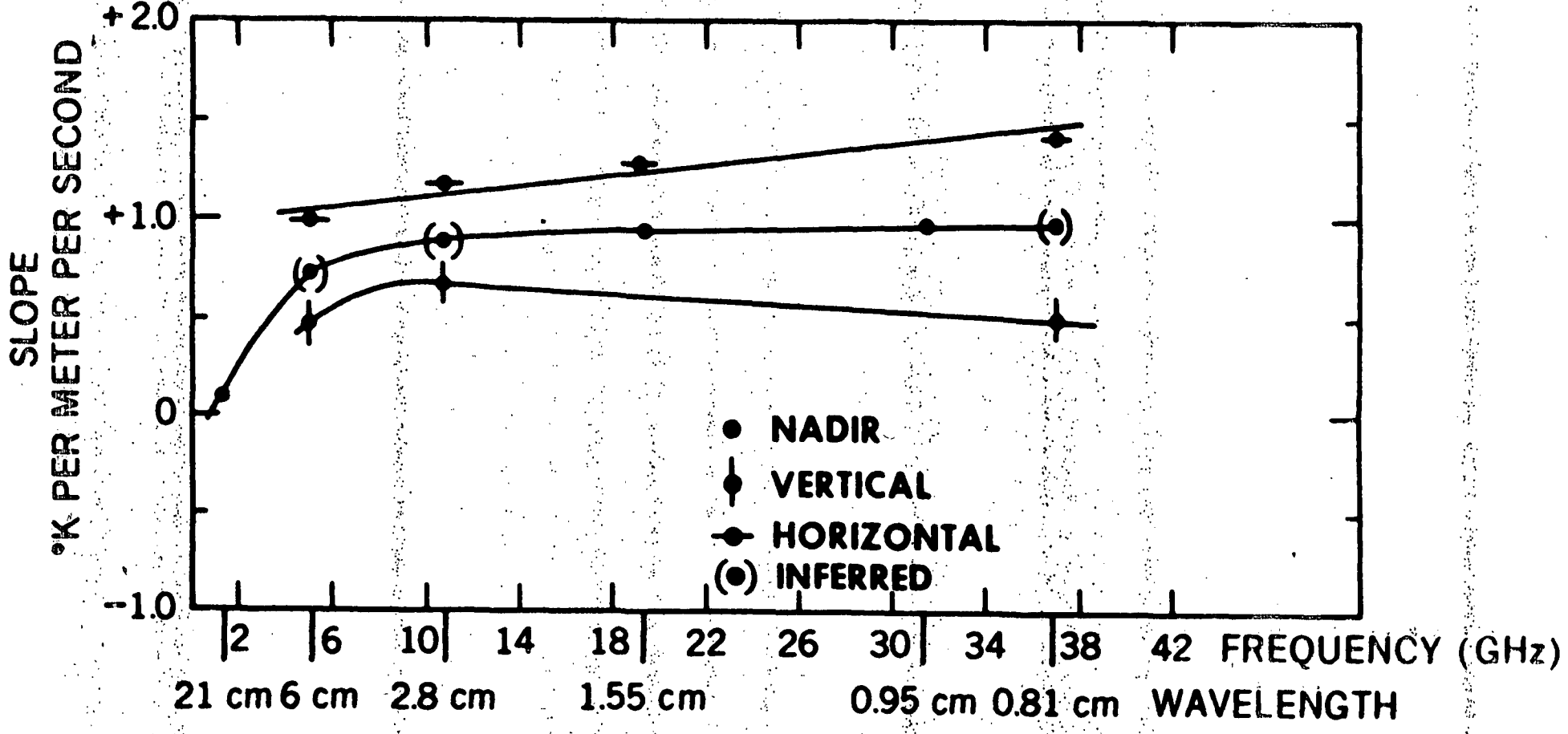


Fig. 4.6. Relationship between brightness temperature and wind speed versus electromagnetic frequency (fully developed sea). (Webster et al., 1976.) Vertical and horizontal measurements are at 38° incidence angle.

1973), (Hollinger, 1974). In conducting the laboratory experiments, the radiometer viewed a square tank of water, and the oil was poured into the tank and allowed to spread evenly into a layer of uniform thickness. Data were then collected at two microwave frequencies as a function of slick thickness. The results are shown in Figure 4.7. The experimental data are in good agreement with theoretical calculations, and illustrate the alternate matching and mismatching effect of the layer as the slick thickness increases by intervals of 1/4 of an electromagnetic wavelength. A co-operative program was then initiated between the Naval Research Laboratory, the Virginia Institute of Marine Sciences, NASA/Wallops and the U.S. Coast Guard to observe the time development of a controlled oil spill. Some of the typical radiometric results are shown in Figure 4.8. This figure shows (1) the visible slick with contours representing changes in the optical reflectance; (2) isotherms of brightness temperature at 31 GHz; (3) isotherms of brightness temperature at 19.3 GHz; and (4) inferred values of oil thickness. These results indicate that microwave radiometers can be used to measure slick thicknesses of less than a millimeter under field conditions.

4.2.1.6 Emission from Fresh Water Ice

It was demonstrated some years ago that the emission from fresh water ice produces the characteristic oscillatory signature of layered media as the ice thickness increases Edgerton et al., 1971). More recent studies (Apinis and Peake, 1976) have concluded that if sufficient radiometer frequencies are available, fresh water ice thickness can be uniquely measured by observing the resultant quarter-wave maxima/minima in the emissivity. Computational results are shown in Figure 4.9, where the reflection coefficient (1-emissivity) is plotted vs. microwave frequency. These calculations show that the number of oscillations of the reflection coefficient per bandwidth increase with increasing ice thickness. The upper limit on the measurement of thickness is thus limited by the bandwidth of the radiometer and the center frequency -

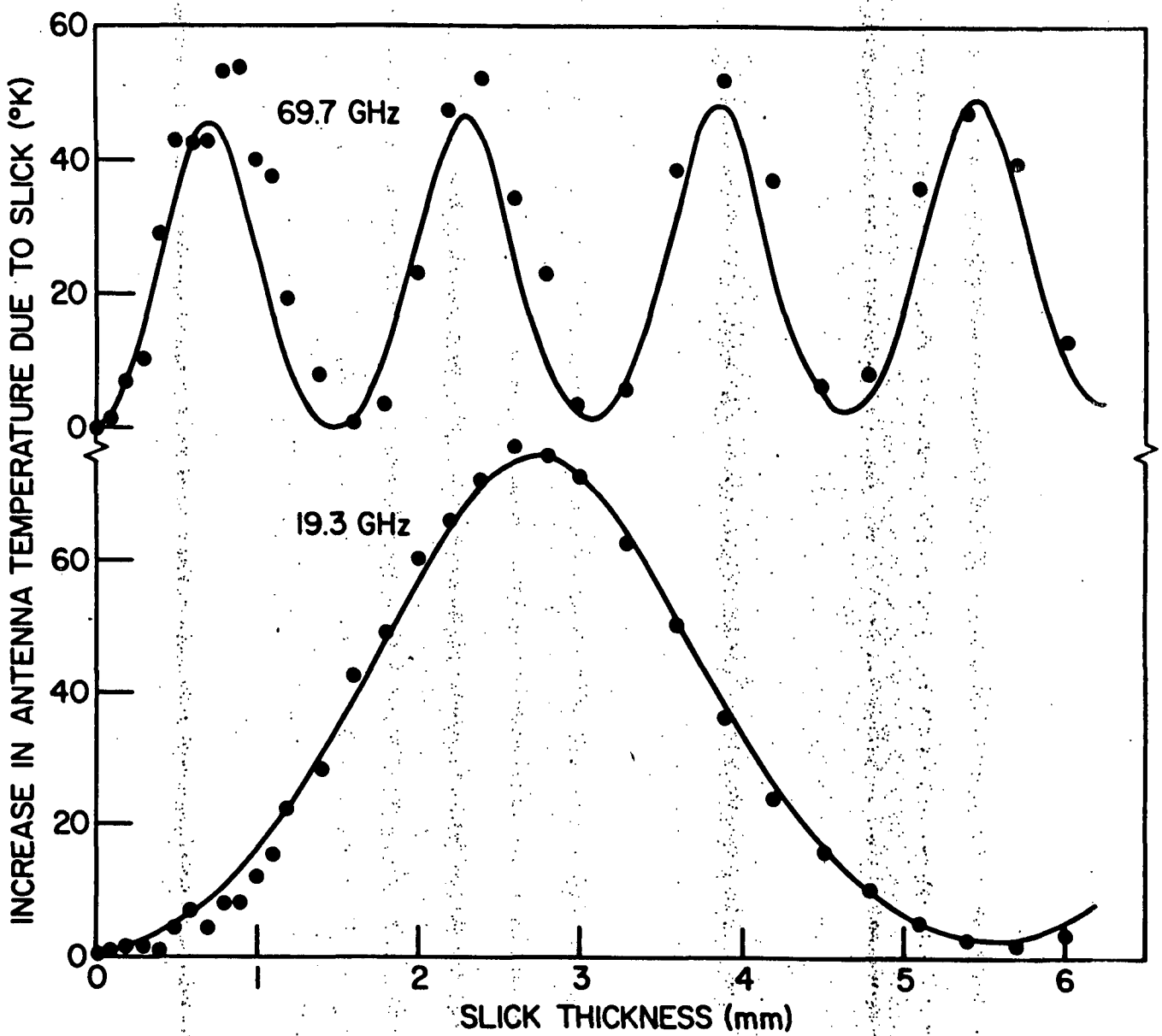


Fig. 4.7. Increased brightness temperature vs. oil slick thickness at 69.7 GHz and 19.3 GHz.

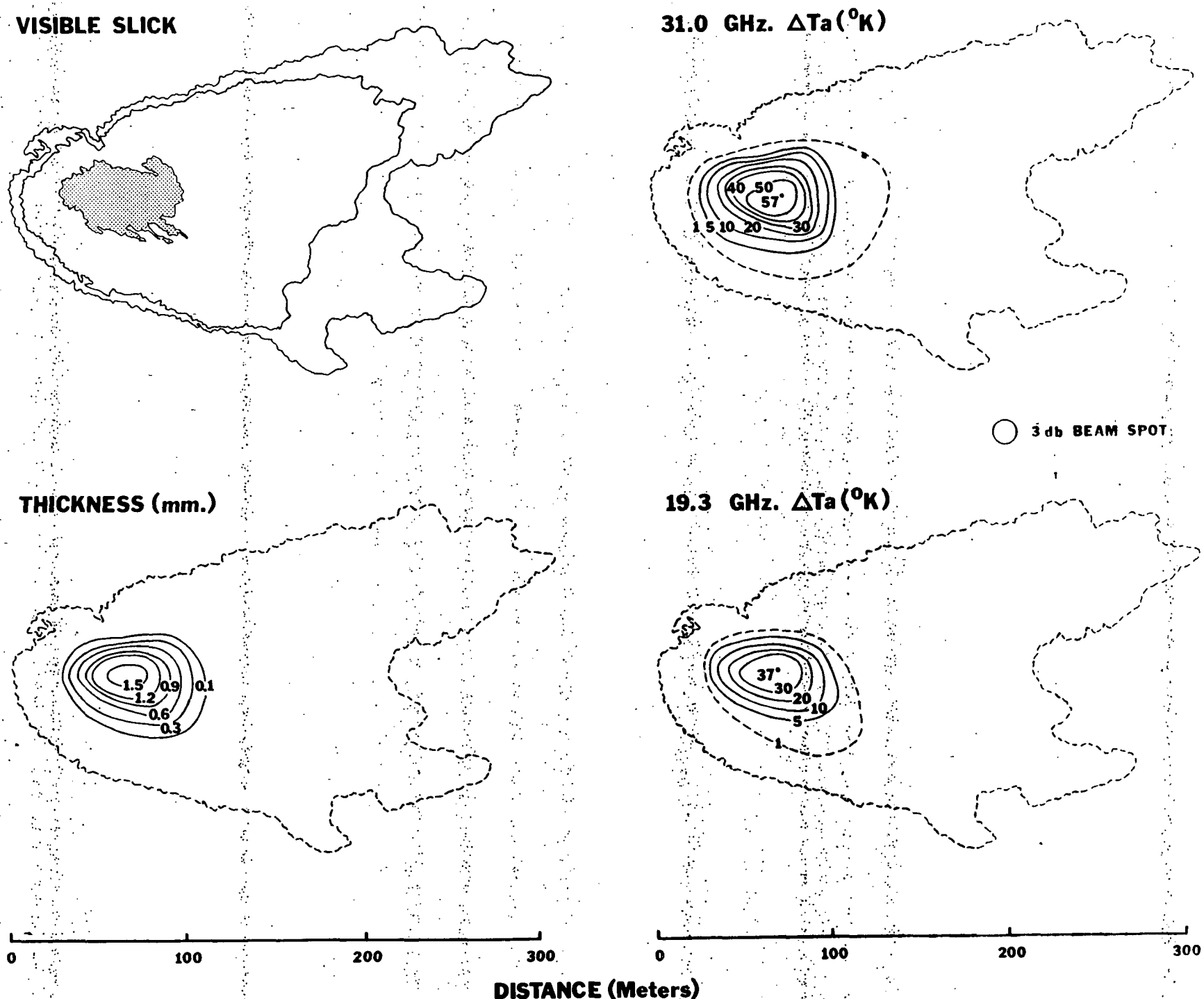


Fig. 4.8. Sketch of visible oil slick, radiometric isotherms at 31.0 GHz and 19.3 GHz, and inferred thickness. (Hollinger and Mennella, 1973.)

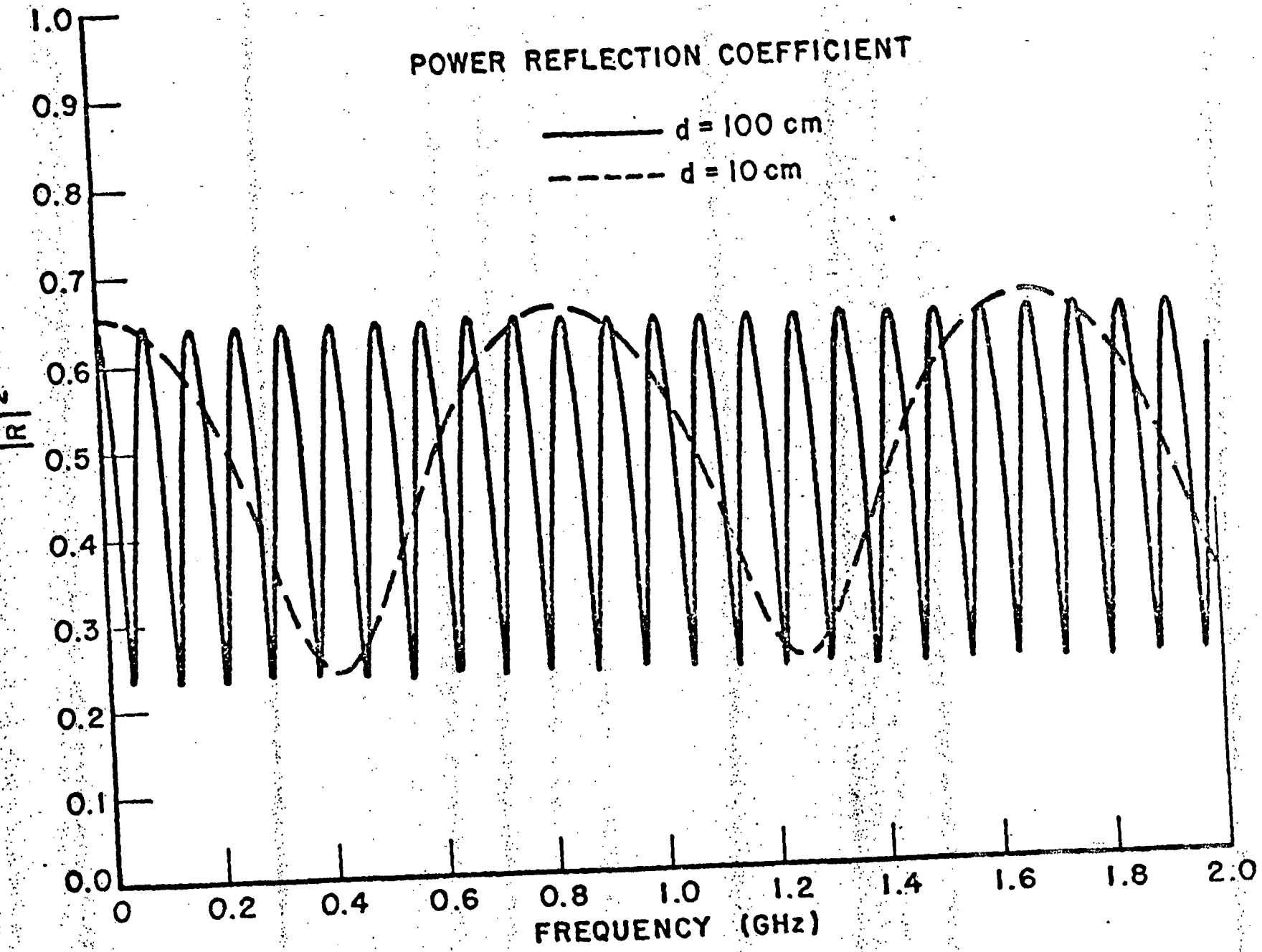


Fig. 4.9. The power reflection coefficient as a function of frequency for two different ice layer thicknesses.

spacing of adjacent measurements.

4.2.1.7 Emission from Polluted Water

The dielectric constant of pollutants, such as sludge and industrial wastes, is not known. However, since the dielectric constant of most materials is substantially less than that of water, the flow of pollutants near ocean dump sites can possibly be observed if concentrated to the extent that the dielectric constant of the water-waste mixture is changed by as much as 0.2%.

In an effort to detect pollutants, the NASA Langley S/L band radiometer system was flown over the New York bight dumping area in 1975. Seven parallel lines were flown, three of which were north of the dumping area. The test was unsuccessful from the viewpoint of achieving quantitative results because of S-band radar interference and long-term instabilities of the L-band instrument. However, qualitative results suggest a southerly flow of pollutants from the dumping area.

4.2.2 Competitive and Complementary Techniques

4.2.2.1 Ocean Temperature

Infrared measurements can provide surface temperature measurements with spatial resolution that is much finer than can be achieved with microwave radiometers. The smaller wavelength reduces the physical size of diffraction limited optics, and there is more fractional bandwidth available at the infrared wavelength to allow substantial reduction in integration time for imaging. Also the emissivity of sea water is close to unity and the black body temperature is directly measured, independent of roughness and foam coverage. The disadvantage of infrared techniques is that the data is obscured by clouds, haze, and is biased by the attenuating atmospheric column.

The depth of penetration of water is less than a millimeter at infrared wavelengths, compared to 1 centimeter at 3 GHz. Penetration less than a millimeter can result in additional errors of a few tenths of a degree due to temperature gradients

in the top mm of the ocean.

4.2.2.2 Salinity

A laser technique has been proposed in recent years which indirectly infers salinity by measuring the Raman scattering from sulphates dissolved in sea water. The basis of the measurement is that the sulphate concentration is directly proportional to the salt concentration. This activity seems to have ceased because background noise is much higher than the scattered data signal.

4.2.2.3 Surface Roughness

Both large scale and small scale surface roughness can be independently measured by radars. For viewing angles extending from nadir to approximately 20°, the scattering is dominated by the large waves, and the mechanism is governed by geometric optics. The degree of roughness, i.e., the rms slope of the waves, can be inferred by measuring the decreased scattering at nadir, and the increased scattering within 20° of nadir.

If the radar is pointed at angles greater than approximately 20°, scattering results from resonance with ocean waves that are of the order of the electromagnetic wavelength. These ocean waves are relatively small and are essentially in equilibrium with the local wind vector. The degree of scattering is proportional to the rms height of these scatters, which increases with increasing wind speed. It is clear, however, that the height of these wavelengths cannot increase without limit; thus an upper limit on the remote measurement of wind speed with active systems is suggested.

Radiometers, on the other hand, could provide high wind measurements from foam emission. Radiometric data from typhoon June (discussed in Chapter 5) are consistent with an interpretation that extrapolates the emissivity vs. wind speed relation linearly to velocities of ~75 ms^{-1}.

4.2.2.4 Oil/Ice Detection

Active systems can detect oil spills, because the slick modifies the surface viscosity and damps the capillary waves. The damping of capillaries essentially removes the ensemble of small scale scatters, thus substantially reducing the back-scatter at viewing angles beyond 20°. Oil thickness is unlikely to be measured by radar techniques.

Radars have proven useful over the Great Lakes, where a SLAR is used to routinely measure ice coverage and texture due to changes in the scattering coefficient. The complementary role of radiometry is that the emissivity strongly depends upon thickness, which is an added parameter of interest.

4.2.3 Requirements

4.2.3.1 Temporal and Spatial Resolution and Accuracy of Inferred Parameters

The time and space scales of ocean surface phenomena range through many orders of magnitude (see, for example, Pierson, 1976) and form rather continuous spectra in frequency and length scales. Fortunately, however, many of the more important phenomena tend to be banded or grouped in certain ranges. These bands or ranges are generally caused by the different scales and driving mechanisms in the open ocean and coastal zones. Because of this it is convenient to consider these as two distinct physical areas and discuss the remote sensing requirements of each separately. One is cautioned to remember, however, that there is a very large and continuous range of time and length scales involved and that this simplification may, on occasion, omit some important and interesting phenomena.

4.2.3.1.1 Coastal Areas

The motion and resulting density and temperature structure in the coastal zone is generally produced or driven by the tides, winds, open ocean currents on the seaward side, and in some cases coastal rivers. The bounding ocean currents

(for example, the Gulf Stream on the East Coast) interact with the coastal topography to produce eddy motions. The interaction of these eddies to produce smaller scale coastal currents is not well understood, but it is clear that the scale of the eddy motion is largely dependent on topography. The most common example of this is the eddy motion from the Gulf Stream and the resulting currents induced in the coastal zone. An indication of the extent and scale of this is shown in Figure 4.10, which depicts the Gulf Stream and topography-induced eddies from measurements of Sea Surface Temperature (SST). This figure also indicates the general scale of coastal zone motions. It is interesting to note that much of the data to develop this figure was obtained via the NOAA IR radiometer. Finally, some currents, and density and temperature structure are generated by the passage of atmospheric fronts.

The motion resulting from these driving forces is a combination of natural oscillations of the particular coastal area and the oscillations forced by the previously mentioned driving mechanisms. The along-shore motions are typically on scales that occur in the open ocean (these are discussed in the next section), while the cross-shelf motions, both forced and natural, are largely imposed by the dimensions of the topography of the area. This results in a length scale for most cross-shelf phenomena that is roughly the distance to the shelf break. Typically, this is a distance or length scale of 50-150 km. An indication of this is provided in Figure 4.10. Therefore, the most useful swath width or field of view for remotely sensed data should be on the order of this length. Required resolution depends to some extent on the phenomena of concern but it generally dictates a spatial resolution (footprint) of 0.5-2.0 km. The appropriate time resolution is more dependent on the phenomenon than is spatial resolution, but it ranges from 1/4 of a day for tides to at least several days for eddy motions. The surface phenomena of

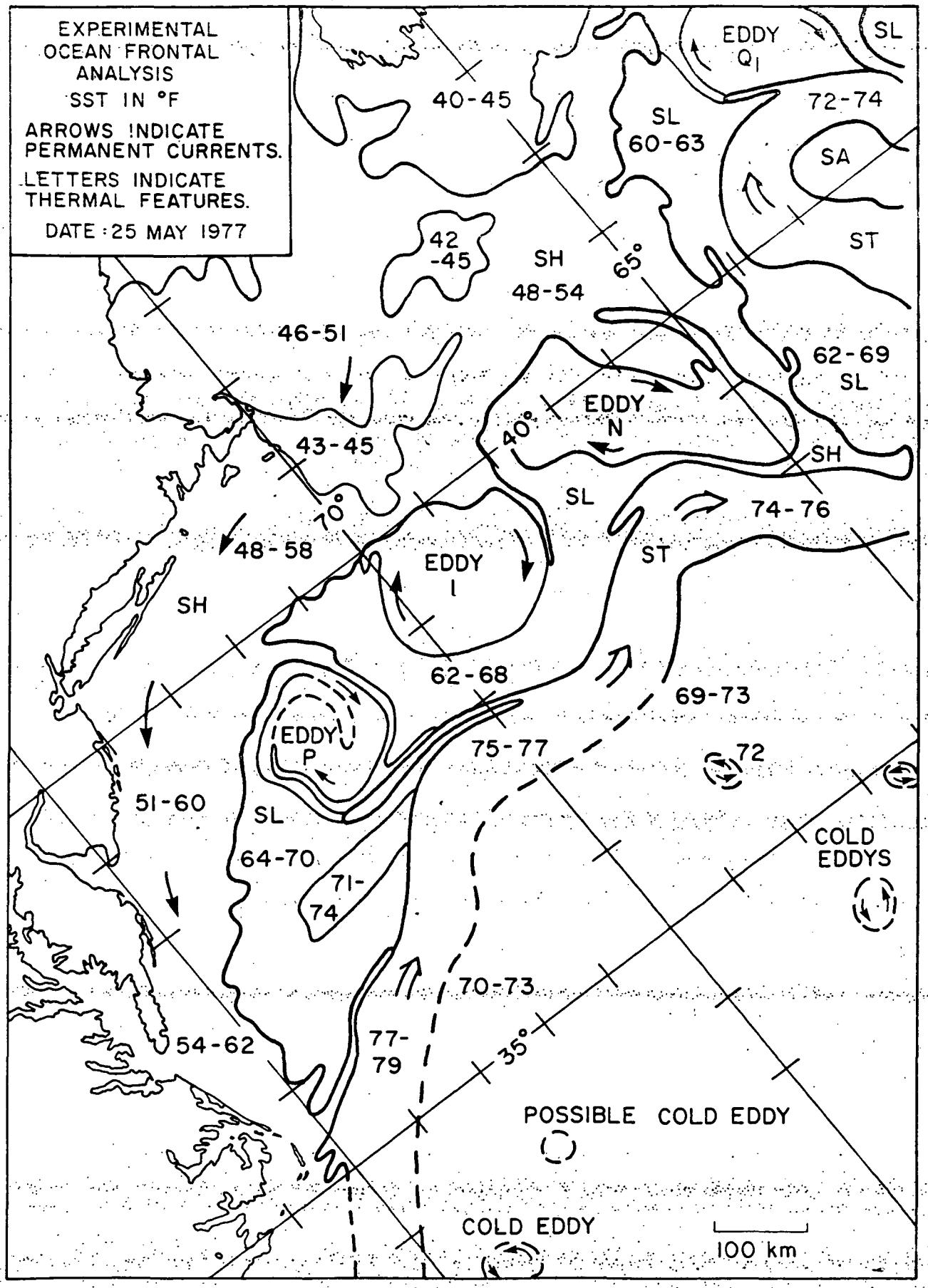


Fig. 4.10. Example of scale of coastal zone motions.

most interest are sea surface temperature, surface wind speed or wind stress, gravity waves, currents (measured or inferred), and in some cases salinity. The most immediate needs are for surface winds and sea surface temperature. As a result of discussions with potential users as well as data obtained from the "Follow-on SeaSat User Needs Report" (1976), Table 4.1, which is a summary of user requirements for the coastal zone, was developed. (Specific user needs and programs are discussed in Section 4.3.3.)

With respect to pollution, the primary use of a satellite system will be for monitoring. That is, the pollution will probably be first detected by satellites, but thereafter it will be measured by aircraft and/or ground sensors. Therefore, the remote sensing requirements are for early detection of any pollutant signature. This could be surface slicks resulting from reduced surface tension or a reduction in dielectric constant due to pollutant. The relation between various pollutants and the accompanying decrease in dielectric constant has not been quantitatively developed. Thus, at the present time most user requirements for pollution detection are in the preliminary stages. However, a general indication of the expected user needs for pollution detection are included in Table 4.1. The requirements in Table 4.1 are specifically for detection of pollutants. Detailed measurements are expected to be carried out using ships or aircraft. Pollution or water quality modeling requires an understanding of the currents and density structure of the region, but these data presumably will be obtained via appropriate techniques, independently of the ultimate application.

Detection of lake and estuary ice is also basically a coastal phenomenon and has similar length scales and spatial resolution requirements. In addition to ice detection, it may also be possible to measure fresh water ice thickness. Several of the world's major shipping routes are covered by lake or brackish ice for several months a year (i.e., Gulf of St. Lawrence and Baltic Sea), and great efforts are being made

MEASUREMENT	RANGE	ABSOLUTE ACCURACY	RELATIVE ACCURACY	REQUIRED RESOLUTION	SWATH OR FOV	TEMPORAL COVERAGE
SEA SURFACE TEMPERATURE	0-35°C	1°C	0.5°C	1 km	100-150 km	48-72 hrs.
SURFACE WINDS	0-50 m/s	2-4 m/s	1-2 m/s	2-5 km	150 km	24 hrs.
SALINITY	5-40 ppt.	2 ppt	0.5-1 ppt.	0.5-1 km	100-150 km	72 hrs.
POLLUTION	-	-	-	0.5 km	100 km	24 hrs.
ICE	-	-	-	0.5 km	100 km	Weekly

Table 4.1. Remote sensing requirements for coastal zones.

to extend the navigable season in these areas. To do this, remotely sensed ice thickness and location are needed for two purposes: (1) As input into numerical models of ice dynamics and thermodynamics, and (2) as routing maps to direct ship traffic through the thinnest ice in an area. If the measurement of ice thickness becomes sufficiently quantitative, it should also be possible to determine when ship or ice breaker operations are possible in an area.

4.2.3.1.2 Open Ocean

In the open ocean large scale motions, which are often possible forcing mechanisms for the coastal zones, are driven by mean (large scale) winds, coriolis acceleration, and thermal gradients. The resulting motion and structure are the result of natural oscillations, which are determined by the dimensions of the particular ocean basin of concern and the motions induced by the forcing. The length scale of the basins is on the order of thousands of km and thus the coverage required is also on this scale. Fortunately the time scale is from days to weeks and thus the desired area coverage can be accomplished by using a somewhat smaller field of view (FOV) and sweeping the area several times within the desired time period. Thus the desired swath (or total FOV) in the open ocean ranges from several hundred to a thousand or so km. Time scales are generally greater than 24 hours, and usually weeks.

Superimposed on these large scale motions are more detailed or smaller structures. These are caused by the passage of ocean fronts and possible eddies shed by large scale ocean currents from local topographic features. The motions are more on the time and space scales of coastal phenomena, and the remote sensing user requirements for the coastal zones applies almost directly. The only exception is perhaps slightly more stringent requirements on salinity accuracy.

By far the most dominant, and thus most interesting

phenomena, in the open ocean are the large scale phenomena. In addition these motions are the hardest to measure, particularly when using conventional ship techniques. The primary reason is that the phenomena have spatial scales on the order of 1000's of km and time scales of days to years. An example is sea surface temperature anomalies. Such anomalies have been shown to have important consequences in long-range weather forecasting and can be a fundamental cause of short period climatic variations (cf. Namias, 1972).

The large scale motions are generally geostrophic and are generated by large scale wind and coriolis forces; in addition, the baroclinic structure has approximately the same scale. Therefore, the most important surface parameters of concern are surface winds, temperatures, and sea surface topography, with somewhat less interest in obtaining gravity wave information. Sea surface temperature is of great importance for large scale modeling applications because the heat budget of the oceans represents a significant fraction of the solar energy transport from equator to pole. In addition, the Navy has an operational interest in sea surface temperature as related to undersea acoustics. Table 4.2 provides a summary of user requirements to observe typical large scale motions. These were obtained from the same sources as Table 4.1. It should be emphasized that these requirements are for observation of the large scale motions; if ocean fronts or specific eddy motions are of concern, requirements in Table 4.1 are more applicable.

4.2.3.2 Radiometer Requirements

Of all surface parameters that can be measured, those relating to the volume properties of the ocean and other aquatories present the most stringent demands on the performance of the microwave radiometer. For example, measurements of ocean temperature accurate to within 1 K, and of coastal salinity to within 1 ppt., require brightness temperature to be measured with an rms accuracy of 0.3-0.5 K.

MEASUREMENT	RANGE	ABSOLUTE ACCURACY	RELATIVE ACCURACY	REQUIRED RESOLUTION	SWATH OR FOV*	TEMPORAL COVERAGE
SEA SURFACE TEMPERATURE	0-30°C	1°C	0.5°C	20-50 km	500-1000 km	76 hrs.
SURFACE WINDS	0-50 m/s	3-5 m/s	2-4 m/s	20-50 km	1000 km	48 hrs.
SALINITY	5-40 ppt.	0.5-1 ppt.	0.2-0.5 ppt.	5-10 km	500 km	76 hrs.

*SMALLER FOV ACCEPTABLE W/INCREASED TEMPORAL COVERAGE.

Table 4.2. Remote sensing requirements in the open ocean.

4.2.3.3 Accuracy of Emission Models

The dielectric constant of sea water is presumably known to within 0.2% at microwave frequencies lower than X-band (Klein and Swift, 1977). If the ocean is not contaminated with concentrated pollutants or its surface undisturbed by wind forces, this 0.2% accuracy in the dielectric constant will allow surface temperature and salinity to be measured to within 1 K and 1 ppt., respectively.

Models which describe the emission due to uniformly layered media, such as oil and ice, are based upon well established analytical models, and have been checked by laboratory experiments. The major uncertainties that exist are changes in emission caused by lateral inhomogeneities in the layer thickness (such as "globs" of oil and formation of oil/water emulsions). The magnitude of these uncertainties can only be assessed through comprehensive field experimentation.

The changes in the emissivity due to surface roughness are inadequately explained by the physical optics/geometric optics model of rough surface emission. For example, experiments indicate that the thermal emission from very rough ocean surfaces is 5 K higher than the simple geometric optics model predicts. The composite model of large scale plus small scale roughness seems to account for this discrepancy (Wentz, 1975). However, until the validity of the assumptions used in the composite model are articulated, empirical corrections (Blume et al., 1977a) must be used or else the instrument should be pointed at the angle of incidence where the vertically polarized signature is more nearly roughness invariant.

It has been observed (Nordberg et al., 1971) that the presence of foam over the ocean can cause an increase of tens of degrees Kelvin in brightness temperature. This observation suggests that microwave radiometers can be used to

measure wind speed over the ocean using this effect too, because the percentage foam over the ocean surface monotonically increases with wind speed (Ross and Cardone, 1974).

To date, the level of effort expended upon the modeling of foam emission has been relatively low, and there are still questions concerning the physics of emission (Webster et al., 1976; Rosenkranz and Staelin, 1972; Ross and Cardone, 1974). More effort is required in this area to better quantify the radiometric signature vs. wind speed and to determine if ocean temperature measurements can be made to within 1 K in the presence of foam.

4.3 Anticipated Impacts of High Resolution Microwave Measurements

4.3.1 General Significance

Prior to the availability of remotely sensed data, virtually all physical information of the ocean and coastal areas was obtained via measurements made from ships. (The development of dropable, expendable transmitters occurred almost simultaneously with early sensing methods). Through the use of ships over extended periods of time there has evolved a very general qualitative understanding of the nature of the currents and the seas. Although some quantitative data does exist, most of it is confined to certain spatially restricted areas and has usually been gathered for only a short period historically. These data have supported evaluation of some specific theoretical concepts and analytical techniques; in addition they have established rather accurate baseline conditions for specific areas. However, it is often difficult to use the data for the development of predictive models. This is largely because the observations were necessarily over a spatially restricted area, and thus information on one or several important external driving mechanisms was not obtained simultaneously.

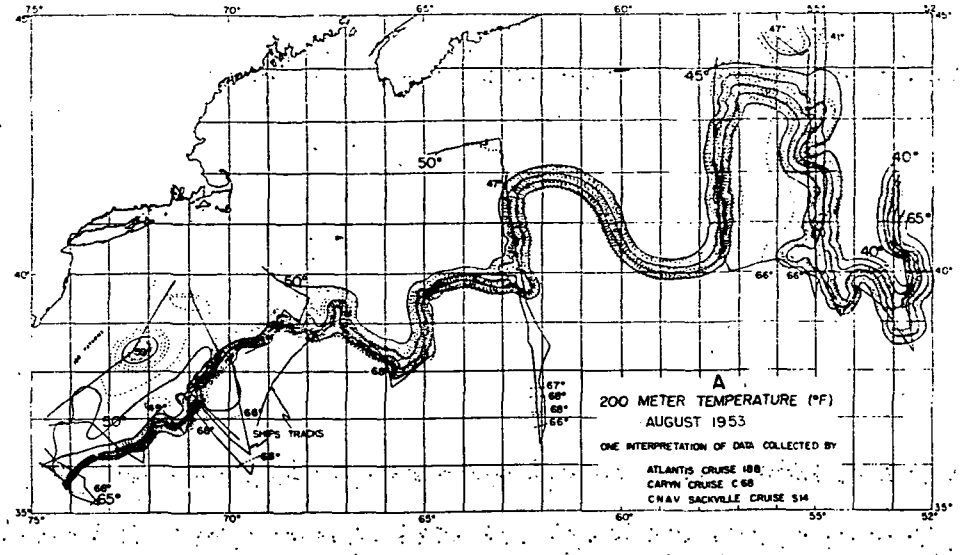
Most data, and thus an understanding of the governing phenomena, have been developed over a rather long time period. Therefore, if some new area suddenly becomes of concern (parts of the eastern continental shelf presently considered for oil drilling, for example), then ships alone would require considerable time before the area is well understood and accurately described. Moreover, it is now realized that many phenomena previously considered to be local are at least partially governed by large scale driving forces. A complete description of these phenomena requires simultaneous measurement of the large scale motions. This becomes more and more evident when one looks at the recent directions taken by climate and weather models. Thus the ultimate goal becomes a quantitative description of an entire ocean area. By comparing the area that can be covered by a ship in a reasonable amount of time to the total ocean area, one concludes that trying to understand the ocean by using conventional ship methods alone is equivalent to trying to understand the nature of a very large forest by painstaking examination of each tree.

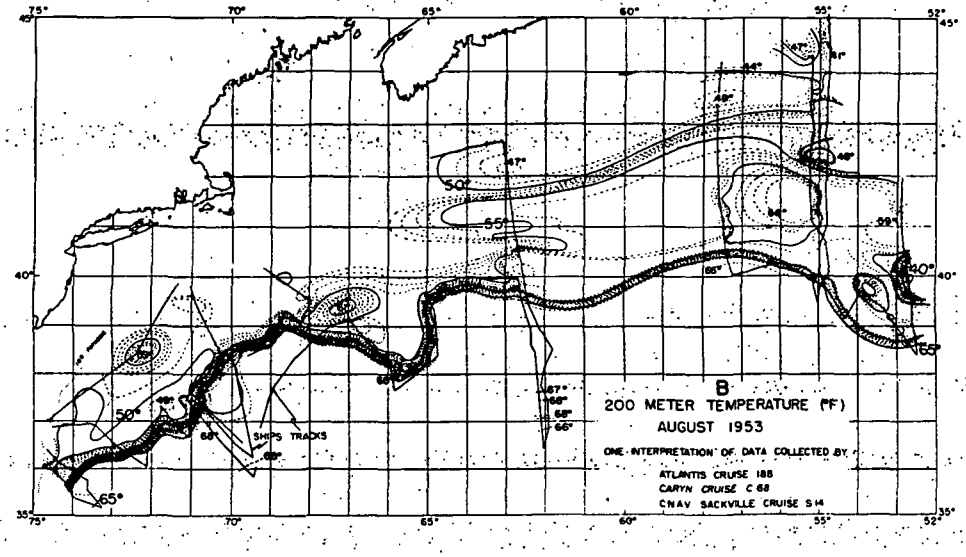
Obviously, the environment of the ocean is a complicated one; all the physical processes in the ocean are controlled by both surface and subsurface parameters. These parameters act and interact to produce the phenomena actually observed. Remote sensing techniques are only effective in measuring those phenomena controlled by surface parameters. However, by a combination of large scale remote sensing and conventional ship methods an understanding of most phenomena can be obtained. This is possible, in part, because most of the crucial problems in physical oceanography are predominantly driven by either surface or well understood (for example coriolis) forces. Furthermore, some subsurface phenomena such as internal waves can be inferred indirectly from microwave measurements of the surface (e.g., Apel et al., 1976). Therefore, remote sensing of the proper parameters with the necessary resolution will extend our quantitative understanding of the ocean over tremendously larger areas, with an accompanying predictive

capability for both large scale and local phenomena.

The discussion so far has centered on the spatial requirements necessary to view large scale motions. However, the most severe deficiency of the traditional methods is the time factor. All ocean and coastal phenomena change with time as well as space. The traditional methods, because they are shipbound, are highly time constrained and thus they cannot produce any synoptic (in the oceanographic sense) data of global scale. As a result, most of the so-called global data are actually patched up works from different times and different cruises. As an example of this deficiency one need not consider very large scale motion. As early as 1955, Fuglister demonstrated it was possible to make totally different interpretations of temperature measurements of the Gulf Stream from the same data (taken by a ship). Figure 4.11 shows three alternative analyses made by Fuglister (1955), and clearly demonstrates the problem. This problem could have been removed by one simultaneous measurement of relative ocean surface temperature. Therefore, remote sensing can resolve one of the most severe problems associated with all shipbound measurements, that of not being able to make or accurately reconstruct synoptic measurements. This suggests the tremendous power of augmenting traditional ship point sampling techniques with synoptic remote-sensing techniques.

Because synoptic data obtained by any other method would require enormous expenditures, it is difficult to precisely determine the economic benefits of various remote-sensing techniques. One cannot determine economic benefits simply by the reduction in cost that occurs from using remote sensing methods, because the alternate cost is so high the data simply would not be obtained. Instead, the value of the knowledge gained must be inferred. This, of course, can only be done by looking at specific applications, which is done in Section 4.3.3. One should note, however, that history has shown benefit analysis to be an uncertain business.





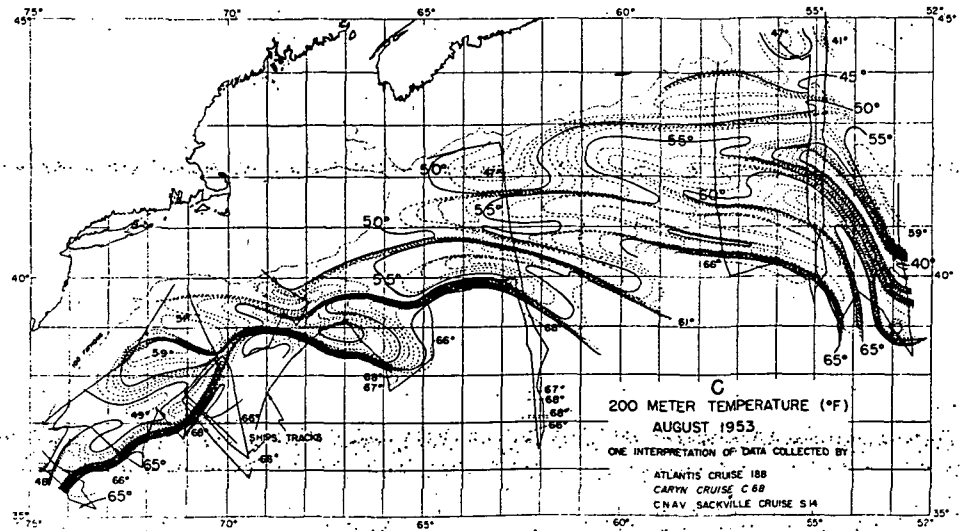


Fig. 4.11. Three alternative analyses of the temperature fields (°F), at a depth of 200 m in the Gulf Stream between 75° and 52° west long. (After Fuglister, 1955.)

4.3.2 Present State of the Art

Before undertaking a description of the anticipated use or impact of passive high resolution systems, it is well to review briefly the remote sensing capability to be provided by SeaSat and Nimbus G, both due to be launched in 1978. A complete definition of SeaSat mission capability is given in the NOAA Program Development plan for SeaSat-A (1977), and a rather concise summary of SeaSat-A instrument capabilities is provided in Table 4.3. As indicated in Table 4.3, SeaSat will fly a variety of instruments, including a Scanning Multichannel Microwave Radiometer (SMMR) (Gloersen and Barth, 1977). This instrument, also to be flown on Nimbus-G, will provide the first opportunity to test the feasibility of simultaneously retrieving sea surface temperature (SST), ocean wind speed, and atmospheric vapor and liquid water content. Data on ice age and extent will also be provided. Expected measurement accuracies are also provided in Table 4.3, with a more complete description of the microwave radiometer provided in Table 4.4.

A review of Table 4.1, "Remote Sensing Requirements for Coastal Zones," of Table 4.2,"Remote Sensing Requirements for the Open Ocean," and Table 4.3, "SeaSat-A Instrument Capability," reveals that SeaSat is well suited to data acquisition of many large scale or open ocean phenomena. However, for large scale phenomena the spatial resolution or IFOV is marginal with some instruments, in particular the radiometer used for SST and surface winds. In most of the applications for coastal areas the resolution is so poor that there is at best very limited applicability.

The "Follow-on SeaSat User Needs Report" (1976), from which Figure 4.12 is excerpted, indicates the most widely needed data are for surface winds and sea surface temperature. It is believed that most users assumed instrument capabilities similar to those of SeaSat-A. SeaSat can obtain high resolution SST via the IR radiometer, but this instrument does not have all-weather capability. Because many smaller scale phenomena are caused by frontal or rapidly changing weather

MEASUREMENT			RANGE	PRECISION	RESOLUTION OR IFOV	TOTAL FOV	COMMENTS
TOPOGRAPHY	ALTIMETER	GEOID	7 cm - 200 m	± 10 cm	1.6 - 12 km SPOT	NADIR ONLY	2 GRIDS SAMPLED THROUGHOUT ONE YEAR
		CURRENTS, SURGES, ETC.	7 cm - 10 m	± 10 cm	1.6 - 12 km SPOT	NADIR ONLY	ALONG SUBSATELLITE TRACK ONLY
SURFACE WINDS	MICROWAVE RADIOMETER	AMPLITUDE	7-50 m/s	± 2 m/s, ± 10%	121 km SPOT	679-km SWATH OFFSET 22° FROM NADIR	
	SCATTER-OMETER	AMPLITUDE	4 -28 m/s	± 2 m/s, ± 10%	<50 km SPOT	250/500/400 /500/250 km	400 km CENTER BLOCK 500 km FULL WINDS 250 km HIGH WINDS ONLY
		DIRECTION	0-360°	± 20°			
GRAVITY WAVES	ALTIMETER	HEIGHT	1.0 - 20 m	± 0.5 m or ± 10%	1.6 - 12 km SPOT	NADIR ONLY	ALONG SUBSATELLITE TRACK ONLY
	IMAGING RADAR	LENGTH	50 - 1000 m	± 10%	25-m RESOLUTION	100 x 4000 km	SELECTED COVERAGE (IN VIEW OF COMPATIBLE STATION)
		DIRECTION	0-360°	± 15°			
SURFACE TEMPERATURE	V&IR RADIOMETER	ABSOLUTE	-2° TO +35°C	± 2°C	4 km (IR) IFOV	2127*-km SWATH ABOUT NADIR	(CLEAR AIR ONLY)
	MICROWAVE RADIOMETER	ABSOLUTE	0° TO 35°C	± 2°C	121 km SPOT	638-km SWATH OFFSET 22° FROM NADIR	(CLOUDS; LT RAIN)
SEA ICE CLOUDS LOCATION AND OCEAN FEATURE	MICROWAVE RADIOMETER	EXTENT	N/A	21 km	21 km	638-km SWATH OFFSET 22° FROM NADIR	GLOBAL IMAGES, ALL WEATHER
	V&IR RADIOMETER	EXTENT	N/A	2 km	2 km (VISIBLE) 4 km (IR)	2127*-km SWATH	BROADLY SAMPLED IMAGES, CLEAR AIR
	IMAGING RADAR	LEADS	N/A	± 25 m	25 m	100 km	REAL TIME TRANSMISSION ALL WEATHER
		ICEBERGS					

*DATA SWATH WIDTH FOR QUOTED ACCURACIES IS ONLY ABOUT 1500 km

Table 4.3. SeaSat-A instrument capability.

NIMBUS-G/SEASAT-A SCANNING MULTIFREQUENCY MICROWAVE RADIOMETER (SMMR)

PURPOSE:	IMAGE SURFACE RADIATION AT 5 MICROWAVE FREQUENCIES DETERMINE SEA SURFACE TEMP. TO 2°K ABSOLUTE, 1°K RELATIVE DETERMINE OCEAN SURFACE WIND SPEED 0-50 M/S TO +2 M/S DETERMINE INTEGRATED LIQUID WATER CONTENT DETERMINE INTEGRATED WATER VAPOR CONTENT DETERMINE RAIN RATE DETECT ICE AGE, EXTENT, CONCENTRATION AND DYNAMICS					
FREQUENCY:	6.6 GHz	10.7 GHz	18.0 GHz	21.0 GHz	37.0 GHz	
BANDWIDTH:	100 MHz					
SPOT SIZE (IFOV):	NIMBUS G	95x148 km	59x91 km	41x55 km	30x46 km	18x27 km
	SEASAT-A	79x121 km	49x74 km	29x44 km	25x38 km	14x21 km
COVERAGE:	NIMBUS G 820-km SWATH CENTERED ON NADIR SEASAT-A 600-km SWATH TO RIGHT OF NADIR					
EARTH INCIDENCE ANGLE:	NIMBUS G: 50°; SEASAT-A: 49°					
DATA RATE:	2 KBITS/SEC					

Table 4.4. SeaSat-A microwave radiometer description.

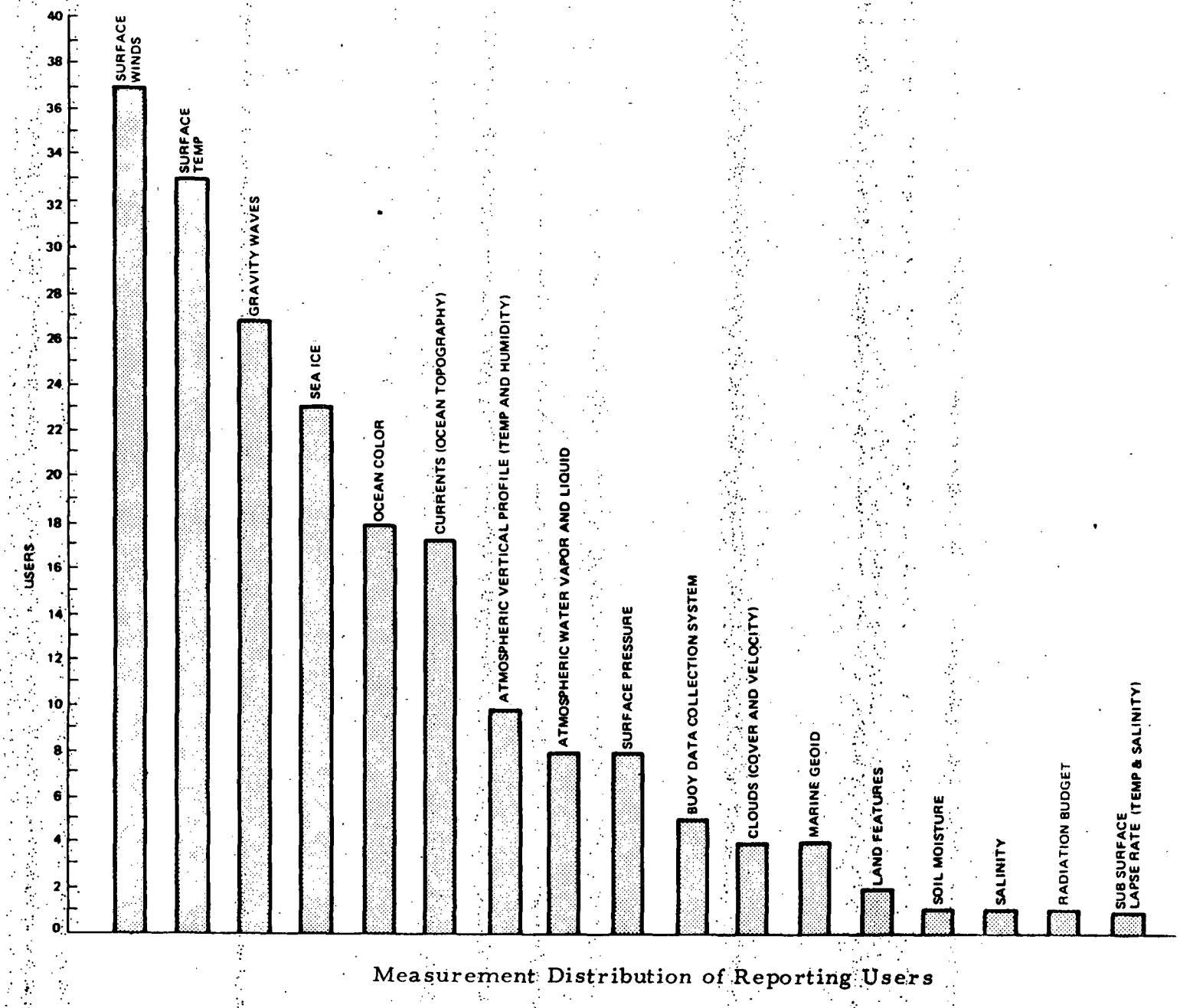


Fig. 4.12. User interest in specific surface phenomena (from Follow-on SeaSat user needs report).

conditions, these periods are usually accompanied by extensive cloud cover. Therefore the conditions in which high resolution measurements are needed most are those in which IR coverage is least likely to be available. Using the techniques described in Chapter 8, it should be possible to develop a passive microwave radiometer with a resolution of 0.5 to 1 km and a swath width of 100 to 150 km. The expected SST accuracies are on the order of $0.5^{o}K$ relative accuracy and 1 to $2^{o}K$ absolute accuracy. This capability is well suited for measurement of coastal zone phenomena and small scale ocean phenomena, whose surface sensing requirements are given in Table 4.1.

One of the instruments on SeaSat for measurement of ocean surface wind is the microwave scatterometer. This instrument has adequate spatial resolution for most open ocean measurements and is also expected to have adequate measurement accuracy. The technique does tend to have greater errors at high wind speeds and thus a tendency to "saturate" above a certain wind speed. Because wind speeds under storm condition are a major need, this can be a significant limitation. User requirements for wind speed in the coastal zone (Table 4.1) are for higher resolution than is presently available with scatterometers.

The brightness temperature of the ocean surface varies with wind-generated surface roughness (Section 4.2.1.3) and very strongly with the generation of sea foam (Section 4.2.1.4). Thus, as discussed earlier, the microwave radiometer can be utilized for the measurement of surface winds. Present results are encouraging (Webster et al., 1976), but probably some additional work is needed to produce an operational system.

The advantages of a high resolution passive system would be: (1) adequate resolution and swath or FOV for the coastal zones (Table 4.2) and (2), a system with larger swath or FOV that could provide open ocean data without the probability of saturation.

4.3.3 Specific Immediate Applications

The impact and economic benefits of any system obviously depend to a certain extent on the specific application and how the system is applied. In order to provide a more accurate assessment of potential impacts, an informal survey of possible users and user applications was made. It was not possible to conduct a complete survey and thus these examples should be considered as illustrations of the probable acceptance and use of high resolution systems, rather than a complete tabulation. Specific examples are divided by requirements into coastal zone and open ocean applications.

4.3.3.1 Examples of Applications in the Coastal Zone

4.3.3.1.1. Salinity Measurements

Strong interest in salinity measurements was expressed by physical oceanographers working in the coastal zones. A high resolution system would provide the necessary resolution and FOV for most applications; and the present measurement accuracy of 0.5 ppt. is well suited for measurements in estuaries and adequate for the near coastal zone. For example, the features in Figure 4.10 are obtained primarily by IR surface temperature measurements. In the winter the temperature differences between shelf and slope water are large and IR measurements provide good definition. In the summer, however, the temperature differences are small and the data become much more difficult to interpret. Salinity measurements with a relative accuracy of 0.5 ppt. would provide independent confirmation of these features as well as all-season (summer) capability. Salinity data would also supply fundamental information on mixing processes in the coastal zone and on one of the driving forces (coastal rivers).

Some of the potential users indicated only a limited interest in salinity measurements. This may be partially attributed to their only recently becoming aware of the possibility, and also because the present measurement accuracy of 0.5 ppt. is only marginal in the open ocean. Another possibility

is that the SeaSat follow-on survey (1976) did not contact the true users of the data. For example, Figure 4.12 shows a low interest profile in soil moisture, yet the U.S. Department of Agriculture is very interested in measurements of soil moisture. In order to verify the possibility that many real users were not contacted, the map of the isohalines shown in Figure 4.2, and a description of the experiment were sent to a total of 166 attendees of a 1975 EPA Conference on Estuary Pollution Control, along with a return postcard inquiring whether or not such salinity data would be useful to them. The response rate was 40% with 76% of the respondees expressing a positive need. The principal uses of the data related to off-shore drilling, siting of off-shore power stations, monitoring shell-fish health, fish spawning, and modeling. The principal users appear to be the EPA and the states (Departments of Natural Resources, Fisheries, and Pollution Control).

4.3.3.1.2 Physical Mechanisms of Eastern Coastal Currents

Studies are being undertaken at John Hopkins University and Woods Hole to obtain data on Northeastern Coast mesoscale shelf dynamics. These studies involve ship measurements of currents, temperature, and salinity structure in an effort to understand the interchange of shelf and slope waters as related to the general mesoscale phenomena of the area. While this has many applications, the research is basic with an understanding and description of the phenomena as the primary goal. Satellite sensed SST will be of particular benefit, if provided with coastal zone resolution. Surface winds are needed to determine wind stress as well as Gulf stream location via SST and altimetry.

4.3.3.1.3 Southeastern Coast Ecosystem Studies

Currently there are numerous studies of the Southeastern Continental shelf ecosystem. The goal of the studies is an understanding of the transport and location of marine nutrients

and the resulting marine biological and ecological systems. The work requires a rather complete understanding of the currents, salinity and temperature structure. One immediate application of the results is location of possible waste disposal sites. Synoptic coastal zone measurements of surface temperature and wind are needed. The present program uses Naval Frontal Analysis (Figure 4.10) and NOAA/NESS data to help locate the Gulf Stream. High resolution all weather information is desperately needed.

4.3.3.1.4 U.S. Coast Guard

The Coast Guard flies regular infrared temperature transects in their "Airborne Radiation Thermometer Program." These are combined with ship measurement and used to provide Air-Sea Rescue Charts. Much of this information could be provided by satellite systems, providing spatial resolution of ~10 km were available. Economic benefits to improve ship operations and Air-Sea rescue are significant, but difficult to estimate.

4.3.3.1.5 East Coast Baseline Studies

The expected initiation of off-shore oil drilling on the Eastern U.S. continental shelf has produced an immediate need for the establishment of baseline conditions in this area. Moreover, an increased understanding of the driving mechanisms for currents and the resulting variability in currents and winds is required to design and operate oil wells. The area has not been extensively studied in the past and this is an excellent example of an immediate need for baseline or average conditions. This will clearly require that large amounts of synoptic data be taken in the next few years. Obviously the area is a coastal zone with the accompanying need for high resolution measurements.

A risk analysis by the oil industry (Satellite Data Collection User Requirements Workshop, 1975) indicates potential savings of $750K to 2M per oil drilling platform can be

achieved by improved knowledge of wind and current variability.

4.3.3.1.6 Support to NOAA/NESS

Presently NESS provides user information in the form of Ice Surveillence, Frontal Analysis; and Gulf Stream Charts. These are used by the Marine transport industry, the Coast Guard for Air-Sea rescue, and for Naval Operations. These are global data, but many present users are concerned with the coastal zone. Most of the input data are supplied by visible and IR radiometers, but these cannot provide all-weather data. They specifically state that SeaSat-A microwave radiometer data will have limited to zero use at NOAA/NESS because of this instrument's poor spatial resolution. A higher resolution system with all-weather capability is certainly needed and enthusiastically supported.

The use of remote sensed data on ice location and thickness to extend the shipping season in Northern routes has a significant economic benefit. Presently these data are published primarily by NOAA/NESS and obtained from ship reports and visible and IR radiometers. Economic benefits of extended shipping seasons range between $45M and $145M (Active Microwave Workshop Report, 1975).

4.3.3.2 Examples of Applications in the Open Oceans

4.3.3.2.1 Naval Use of Sea Surface Temperature

The Navy has operational requirements for SST to provide input data on underwater acoustics and fog generation. Desired resolution is 1 km with 0.5^{o} relative and $1^{o}C$ absolute accuracy. 10-km resolution should suffice for most purposes. Most of these data are presently obtained by ship reports and IR radiometry, but the lack of all-weather capability is a severe limitation. There is a particular need for these data in and near frontal activity where there are extreme weather conditions and thus extensive cloud cover.

4.3.3.2.2 Weather Forecasting

A crucial part of large scale weather forecasting is the

heat budget between the atmosphere and ocean. The most important single parameter in determining this energy balance is Sea Surface Temperature. In fact Namias (1973) has used SST departures from normal to help forecast Hurricane Agnes. Crucial to his analysis is a definition of what constitutes normal SST. This requires that an extremely large amount of data be averaged by months and seasons. It is clear that remote sensing is the only economically feasible way to do this. Present remotely sensed data are marginal since the IR radiometer cannot measure SST under cloud cover and thus may appreciably distort the average. Present microwave radiometer data provide adequate-to-marginal spatial resolution and marginal-to-inadequate absolute accuracy.

4.3.3.2.3 Ship Routing

Computerized ship routing is currently in use by the U.S. Navy and many commercial operators. Reasonably accurate analytical models to predict sea state exist, if surface wind conditions are known. Currently these models work with available weather data as input. The SeaSat scatterometer will make a contribution here, but it tends to saturate at high wind speeds where sea state becomes most critical to ships. Also, its spatial resolution is marginal for this purpose, even in the open ocean. Previous studies of this application (Corte and Warren, 1975) estimate potential annual worldwide savings from optimized commercial ship routing at: $500 to $900 million in fuel consumption (from a total of $18.6 billion at $12 per barrel); $800 to $1500 million in hull damage (from a total of $2.4 billion); and $200 million in cargo damage (from a total of $2 billion). Of the world merchant fleet, 5% (by tonnage) flies the U.S. flag, and ∿ 11% is more or less U.S. owned. Savings to the Navy are not included in these figures.

Reduced oil spills would also be a result of improved ship routing to avoid storms. Assigning a dollar value to this type of benefit is very difficult.

4.4 Acknowledgements

G. S. Janowitz and Tom Curtin of North Carolina State University for many helpful discussions on Coastal and Ocean phenomena. Bill Boicourt, Johns Hopkins, John Ruzzecki and C. Welch, Virginia Institute for Marine Sciences, for description of current East Coast physical oceanography programs. J. Namias for a discussion of climate and weather models. J. P. Hollinger for critiquing the physics and applications section on microwave radiometry.

4.5 BIBLIOGRAPHY

Active Microwave Workshop Report, NASA SP-376, 1975.

Apel, J. R., H. M. Byrne, J. R. Proni, and R. L. Charnell, "Observations and Interpretation of a High Frequency Internal Wave Packet and Surface Slick Pattern," J. Geophys. Res.,, 80 (6), p. 865 (1975).

Apinis, J. J., and W. H. Peake, Passive Microwave Mapping of Ice Thickness, Rep. 3892-2, 17, The Ohio State Univ., Columbus, OH, 1976.

Blume, H. C., A. W. Love, M. J. Van Melle, and W. W. Ho, Radiometric Observations of Sea Temperature at 2.65 GHz over the Chesapeake Bay, IEEE Trans. Antennas Propag., AP-25, 121, 1977a.

Blume, H. C., B. M. Kendall, and J. C. Fedors, Measurement of Ocean Temperature and Salinity via Microwave Radiometry, Boundary Layer Meteorology, 1977b, in press.

Corte, A. B., and C. J. Warren, Policy Issues and Data Communications for NASA Earth Observation Missions until 1985. Center for Policy Alternatives, Research Program on Communications Policy; M.I.T., Cambridge, Ma., Nov. 1975.

Cox, C., and W. Munk, Measurements of the Roughness of the Sea Surface from Photographs of the Sun's Glitter, J. Opt. Soc. Amer., 44, 838 (1954).

Debye, P., Polar Molecules, Dover, 1941 (originally pub. Reinhold Publishing Corp., 1929).

Edgerton, A. T., F. Ruskey, D. Williams, A. Stogryn, G. Poe, D. Meeks, and O. Russell, Microwave Emission Characteristics of Natural Materials and the Environment, Rep. 9016R-8, Aerojet-General Corp., El Monte, CA., 1971.

Eskite and De Rycke, Requirements for marine-related data which may be obtained by satellite remote sensing in the period 1980-85 and beyond, March 20, 1977 (NOAA).

Follow-on SEASAT User Needs Report, JPL Report 624-1, October 6, 1976.

Fuglister, F. C., "Alternative Analysis of Current Surveys," Deep Sea Res., 2, 213 (1955).

Gloersen, P., and F. T. Barath, "A Scanning Multichannel Microwave Radiometer for Nimbus-G and SeaSat-A," IEEE J. Oceanic Eng., OE-2, 172, 1977.

Hardy, W. N., K. W. Gray, and A. W. Love, An S-Band Radiometer Design with High Absolute Precision, IEEE Trans. Microwave Theory and Techniques, MTT-22, 382, 1974.

Hidy, G. M., W. F. Hall, W. N. Hardy, W. W. Ho, A. C. Jones, A. W. Love, M. J. Van Melle, H. H. Wang, and A. E. Wheeler, Development of a Satellite Microwave Radiometer to Sense the Surface Temperature of the World Oceans, NASA Contractor Rep. CR-1960, 1972.

Hollinger, J. P., Passive Microwave Measurements of Sea Surface Roughness, IEEE Trans., Geoscience Elect., GE-9, 165, July, 1971.

Hollinger, J. P., and R. A. Mennella, Oil Spills: Measurements of Their Distributions and Volumes by Multifrequency Microwave Radiometry, Science, 181, 54, July 6, 1973.

Hollinger, J. P., The Determination of Oil Slick Thickness by Means of Multifrequency Passive Microwave Techniques, Rep. 2953, Naval Research Laboratory, Washington, D.C., 1974.

Klein, L. A., and C. T. Swift, An Improved Model for the Dielectric Constant of Sea Water at Microwave Frequencies, IEEE Trans., Antennas and Propag., AP-25, 104, 1977.

Namias, Jerome, "Experiments in Objectively Predicting Some Atmospheric and Oceanic Variables for the Winter of 1971-72," J. Applied Meteorology, 11, 1164 (1972).

Namias, Jerome, "Hurricane Agnes -- An event shaped by large scale air-sea systems generated during anticedent months," Quart. J. Royal Meteorological Soc., 19, (221), 506 (1973).

NOAA Program Development Plan for SEASAT-A Research and Applications, U.S. Department of Commerce, 1977.

Nordberg, W., J. Conaway, and P. Thaddeus, Microwave Observations of Sea State from Aircraft, Quart. J. Royal Meteorological Soc., 95, 408 (1969).

Nordberg, W., J. Conaway, D. B. Ross, and T. Wilheit, Measurements of Microwave Emission from a Foam-Covered, Wind-Driven Sea, J. Atmos. Sci., 28, 429 (1971).

Peake, W. H., Interaction of Electromagnetic Waves with Some Natural Surfaces, IRE Trans., Antennas and Propag. (Special Suppl.), AP-7, S324, 1959.

Pierson, Willard J., "The Theory and Applications of Ocean Wave Measuring Systems at and Below the Sea Surface on the Land, From Aircraft and From Spacecraft," NASA CR-2646, 1976.

Rosenkranz, P. W., and D. H. Staelin, "Microwave emissivity of ocean foam and its effect on nadiral radiometric measurements," J. Geophys. Res., 77, 6528 (1972).

Ross, D. B., and V. J. Cardone, Observations of Oceanic Whitecaps and their Relation to Remote Measurements of Surface Wind Speed, J. Geophys. Res., 79, 444, 1974.

Ruck, G. T., D. E. Barrick, W. D. Stuart, and C. K. Krichbaum, Radar Cross Section Handbook, Vol. 2, Chap. 9, Plenum Press, 1970.

Stogryn, The Apparent Temperature of the Sea at Microwave Frequencies, IEEE Trans., Antennas and Propag., AP-15, 278, 1967.

Stratton, J. A., Electromagnetic Theory, McGraw-Hill Book Co., 1941.

Swift, C. T., Microwave Radiometer Measurements of the Cape Cod Canal, Radio Sci., 9, 641 (1974).

Thomann, G. C., Experimental Results of the Remote Sensing of Sea-Surface Salinity at 21-cm Wavelength, IEEE Trans., Geosci. Electronics, GE-14, 198, 1976.

Webster, W. J., T. T. Wilheit, D. B. Ross, and P. Gloersen, Spectral Characteristics of the Microwave Emission From a Wind-Driven Foam-Covered Sea, J. Geophys. Res., 81, 3095 (1976).

Wentz, F. J., A Two-Scale Scattering Model for Foam-Free Sea Microwave Brightness Temperatures, J. Geophys. Res., 80, 3441, 1975.

Wolff, E. A., C. E. Cote, and J. E. Painter, "Satellite Data Collection User Requirement Workshop," Goddard Space Flight Center Report, May 21, 1975.

CHAPTER 5

MONITORING OF SEVERE STORMS*

5.1 Executive Summary

5.1.1 Summary of Measurement Capability

A. Priorities	Nominal Desired Spatial Resolution (km)	Frequencies (GHz)	Sensitivities (°K rms)
Tropical Cyclones (rain maps, temperature and humidity profiles, sea temperature, wind)	3-50	10-90 (2 or 3 window channels)	1
		60 or 118 (∿7 channels)	0.3
		22 and 183 GHz (1-5 channels)	1
		3, 5 GHz	0.3
Severe Local Storms (Temperature and humidity profiles, soil moisture, rain (as feasible)	2-30	60 or 118 (∿7 channels)	0.3
		183 (2-5 channels)	1
		1.4	0.3
		90-150 (2 channels)	1

Chapters 4 and 6 summarize obtainable parameter accuracies.

B. The viewing interval should be in the range 0.5-6 hr for tropical cyclones, with 6 hours often being acceptable. One hour is an appropriate revisit time for severe local storms; this implies a synchronous system. The viewing angle and polarization is not very critical above 10 GHz, but should be ∿ 50° zenith with vertical and horizontal polarizations measured separately for oceanic observations below ∿10 GHz.

C. Such data would be very useful in supporting improved NMC, GWC, and FNWC operational services, particularly in remote locations.

D. Experience with the Nimbus-5 and Nimbus-6 satellites provides confidence that most of the parameters above can

*Prepared by T. T. Wilheit, R. F. Adler, R. Burpee, R. Sheets, W. E. Shenk, and P. W. Rosenkranz.

be determined to useful accuracies, with the exception of the oceanic surface parameters, for which present data (and theoretical studies) are encouraging, but incomplete.

5.1.2 Recommendations

A. Support aircraft observations over tropical cyclones and severe local storms, especially at those wavelengths for which little such data exists with high spatial resolution. Theoretical studies are important and cost-effective, but cannot replace such observations.

B. Support trial efforts to use occasional Nimbus and Seasat data for simulated severe storm operational purposes, with ground truth.

C. Support efforts to incorporate high spatial resolution microwave capabilities in operational severe storm sensing systems -- at either synchronous or polar orbiter altitudes. Pre-operational test of such systems on shuttle sortie missions would also yield useful data.

D. Support incorporation of passive microwave severe storm monitoring capabilities in any general purpose high resolution passive operational microwave satellite system.

5.2. Introduction

The phenomena relevant to severe storms which are addressable by passive microwave techniques are:

Precipitation
Water Vapor
Atmospheric Temperature Profile
Sea Surface Temperature
Wind Speed at Sea Surface
Soil Moisture Content

In this chapter, we will limit our emphasis to the first three of these as the others are dealt with in other chapters.

It is inherent in severe storms that the time scales of interest are short and similarly the spatial scales are fine. Establishing firm lower limits of "requirements" is not really possible, yet knowledge of the information content of the various time and space scales is essential in order to make meaningful cost/benefit estimates for the justification of operational systems. Therefore, experiments which examine these scales are an important part of any remote sensing program.

Although it is true that any increment in capabilities above the existing state of the art would be useful, on the basis of what is currently known we can specify that time resolution of the order of an hour and space resolution of the order of 10 km, with uncertainty of about a factor of three, are needed for full specification of severe storm dynamics. There will, of course, be some variation from parameter to parameter, and for certain applications, such as definition of precursor conditions, these requirements can be relaxed by an order of magnitude.

In order to address the one hour time frame, either a geostationary platform or an unreasonably large family

of low orbiters is needed. The simultaneous requirement of tens of kilometers of resolution places severe requirements on an antenna system placed into geostationary orbit due to the large distance (3.6×10^4 km). One approach to meeting these requirements is to use the 100-200 GHz range with an antenna size of 4.4m (the largest that can be fit into the Shuttle). Thus the 118 GHz molecular oxygen line and the 183 GHz water vapor line became particularly relevant to severe storm applications.

In this chapter we will show examples demonstrating, albeit at inadequate temporal and spatial resolution, the technical feasibility of measuring rain, wind, and thermal anomalies.

5.3. Observables

The principal components in the atmosphere contributing to the upwelling brightness temperature are molecular oxygen, water vapor and liquid water droplets. Ice, as in cirrus clouds, is not a significant factor in the microwave frequency range. For water droplets, two cases must be considered, raining and non-raining. In the non-raining case, the small droplet (Rayleigh) limit is applicable (Gunn and East, 1954) and the net absorption coefficient becomes proportional to the net density of liquid water, independent of the droplet size distribution, as long as there are no particles larger than about 100μm. A typical stratus cloud containing 20 mg/cm^2 of liquid water would have an opacity of about 10^{-3} at 5 GHz and would vary approximately as the frequency squared. The raining case will be considered later.

5.3.1. Temperature Profile

Molecular oxygen has a series of resonances between 50 and 70 GHz which at sea level pressure merge to form an absorption band and a single isolated resonance, designated 1^-, at 118.75 GHz. In Chapter 6, the application of the

50-70 GHz oxygen spectrum to the measurement of the atmospheric temperature profile will be discussed. For reasons discussed in the introduction, the 118 GHz line becomes particularly relevant to monitoring of severe storms.

In Figure 5.1, a set of weighting functions is shown. The number by each weighting function is the frequency, in MHz, away from the center of the 118 GHz line. Simulation of temperature profile retrievals using this set of frequencies indicate that they will do substantially as well as the channels chosen for the operational microwave sounding unit which is to be launched on TIROS-N, that is, about 2°C accuracy.

5.3.2. Water Vapor

Water vapor has a weak resonance at 22.235 GHz, a strong resonance at 183.3 GHz and many strong ones at even higher frequencies. The 22.235 GHz line has been exploited to measure total integrated water vapor content in the NEMS and SCAMS experiment on Nimbus-5 and 6 respectively. Water vapor accuracies of ≤ 0.4 g/cm^2 have been demonstrated with such a system. Chapter 6 discusses retrieval accuracies in more detail.

The strength of the 183 GHz line makes it ill suited for measurement of total water vapor content, but it is quite sensitive to gradients in water vapor above about 2 km. A situation which is relevant to both severe local storms and to hurricanes is a layer of dry air overlaying a layer of moist, essentially saturated air. It is of interest in these situations to monitor the height of the interface. Calculations have been performed wherein we assume a moist layer (75% relative humidity) with a lapse rate of 6.22°K/km from the surface to a height h, a thin inversion layer from h to h + 0.25 km with a lapse rate of -4°K/km and humidity decreasing linearly to 30% at h + 0.25 km and a dry layer from h + 0.25 km to 12 km with a lapse

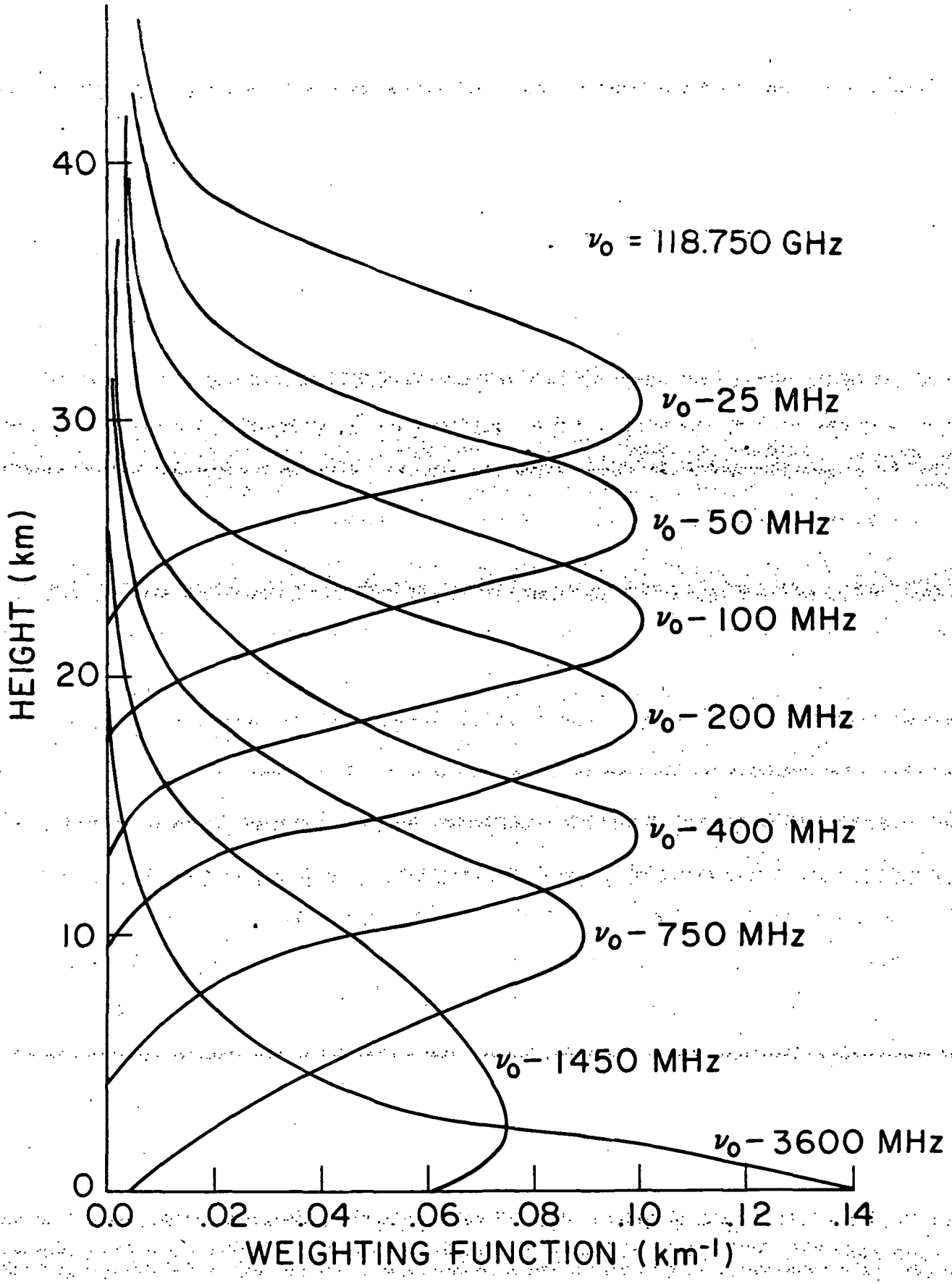


Figure 5.1. Temperature weighting functions near the 118 GHz oxygen line.

rate of 6.71°K/km and humidity decreasing linearly to 0% at 12 km. This is a generalization of the tropical atmosphere found in the Handbook of Geophysics and Space Environments (AFCRL 1965). The results are shown in Figure 5.2 for various frequencies near the 183 GHz line. The maximum sensitivity to this height is observed for frequencies about 6-15 GHz from line center.

5.3.3. Precipitation

The Nimbus-5 Satellite was launched December 12, 1972. One of the instruments aboard was an Electrically Scanning Microwave Radiometer (ESMR). This instrument, operating at a frequency of 19.35 GHz (λ=1.55 cm), scans from 50° to the left of the spacecraft track through to 50° to the right of the spacecraft track every four seconds with a resolution at nadir of 25 km. In the images produced from these data over the ocean, features were noted which could not be explained by reasonable values for atmospheric water vapor, surface wind speed or non-raining liquid water content. It was readily demonstrated that these features corresponded to rain (Wilheit et al. 1976). Rain has an enhanced effect over non-raining liquid water primarily because the particle size is larger than in non-raining clouds and also because a non-raining cloud typically does not have as much water content as a raining one. A quantitative theory for this has been developed by Wilheit et al. (1977). In their model, a Marshall-Palmer (1948) distribution of rain drops is assumed from the surface to freezing level along with reasonable distribution of water vapor and non-raining cloud. The Marshall-Palmer distribution is scaled inversely to the fall velocity as a function of height in order to establish a constant rain rate from the surface to the freezing level. They found quantitative agreement between this model and radar observations as shown in Figure 5.3. In this figure, the black dots show the comparison between rain rate as measured by the WSR-57

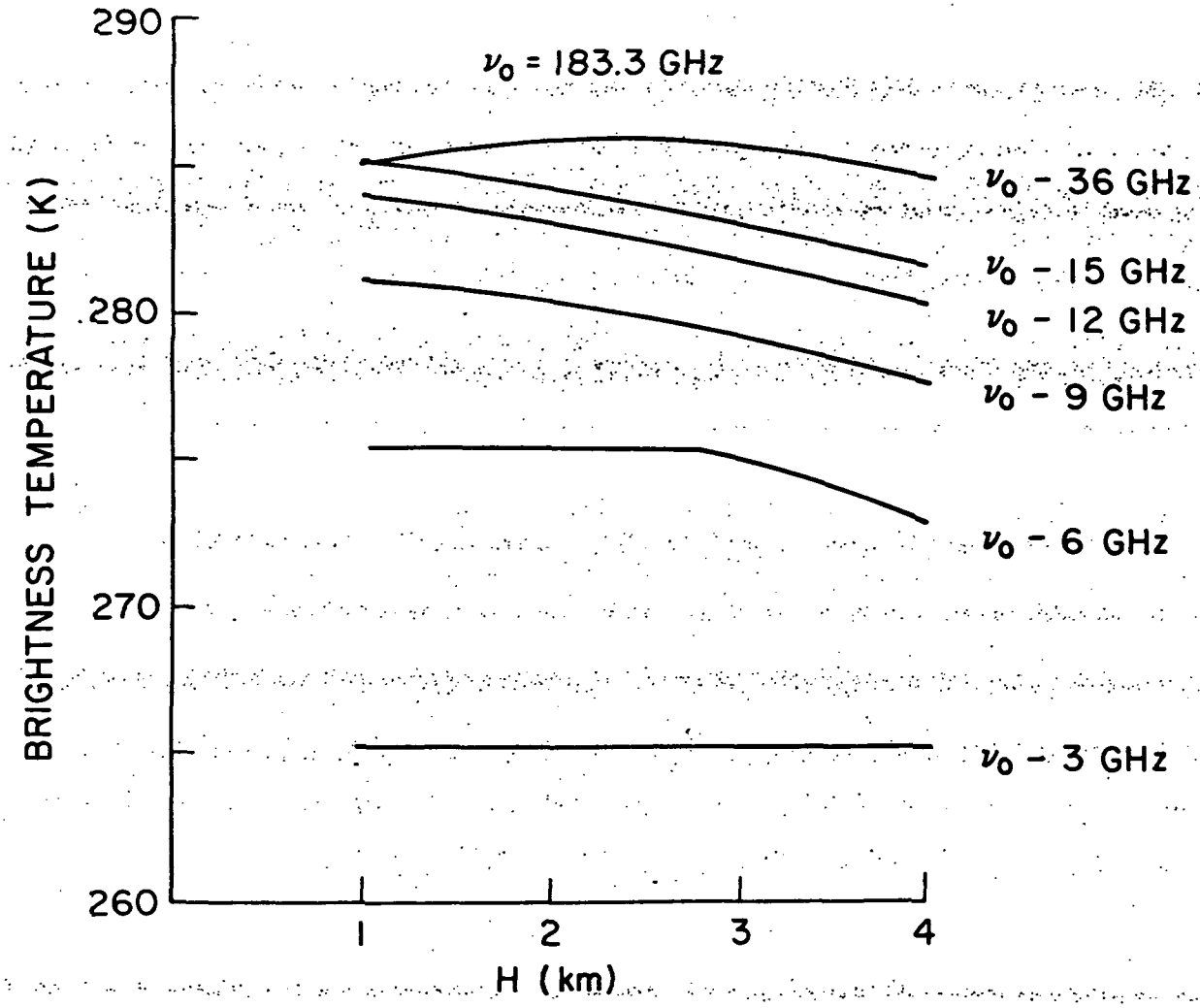


Figure 5.2. Brightness temperature with trade inversion at height H over ocean.

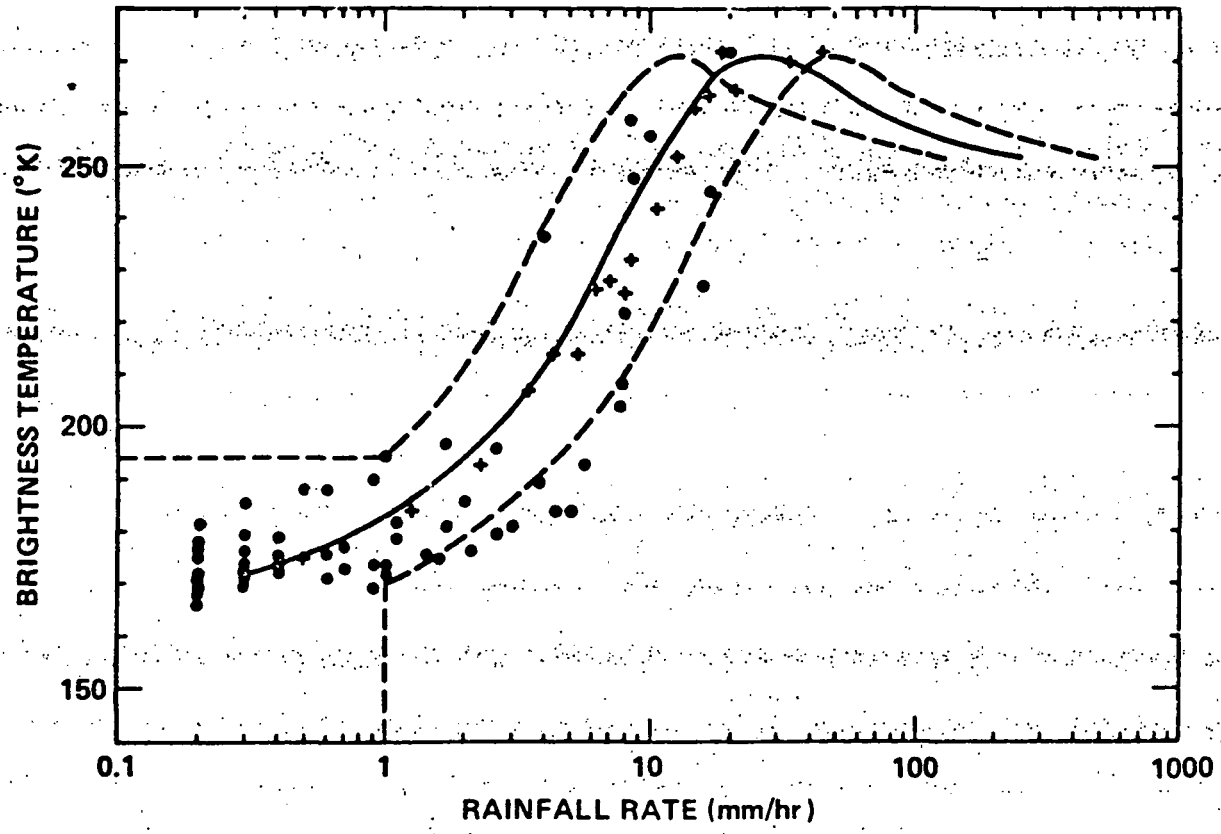


Figure 5.3. Brightness temperature as a function of rain rate:
• Nimbus-5 ESMR vs. WSR-57 radar;
+ inferred from ground based measurements of brightness temperature and direct measurements of rain rate.
The solid line is the calculated brightness temperature for a 4 km freezing level. The dashed lines represent departure of 1 mm/hr or a factor of two in rain rate (whichever is greater) from the calculated curve.

radar at the National Hurricane and Experimental Meteorology Laboratory at Miami, Florida and the brightness temperature measured by the Nimbus-5 ESMR. The solid line is theoretical relationship between brightness temperature and rain rate for the appropriate freezing level (4 km). The dashed lines show an envelope of a factor of two in rain rate (the typically quoted accuracy of the WSR-57) or a minimum of 1 mm/hr. The crosses are points inferred from a ground based radiometer experiment with direct rain rate measurements. Arguments presented in the Wilheit et al. (1977) paper suggest that the relationship between rain rate and brightness temperature at this frequency should be very insensitive to details of the particle size distribution.

The insensitivity of the Nimbus-5 ESMR results to particle size distribution derives from the fact that the brightness temperature at this frequency is determined by the absorption coefficient of the rain and that the effect of scattering is only a minor correction. However, at higher frequencies the effect of scattering becomes more significant. This effect has been exploited by Savage and Weinman (1975) to obtain maps of rain over land using the data of Nimbus-6 ESMR (37 GHz). If one goes to higher frequencies, above the 60 GHz oxygen complex, the effect is striking. In Figure 5.4 we show calculations for nadir viewing brightness temperature in the frequency range 75 to 175 GHz. Here, the brightness temperatures are calculated for a land or ocean background with no rain or 20 mm/hr rain rate. Note that the rain depresses the brightness temperature with either background. Thus it would be easy to map rain at any frequency in this range except within about 2 GHz of the 1^- line of molecular oxygen (118.75 GHz). Since this mapping depends on the scattering properties of the rain drop, hail having a size large compared to raindrops and very low loss, would provide an even more striking effect.

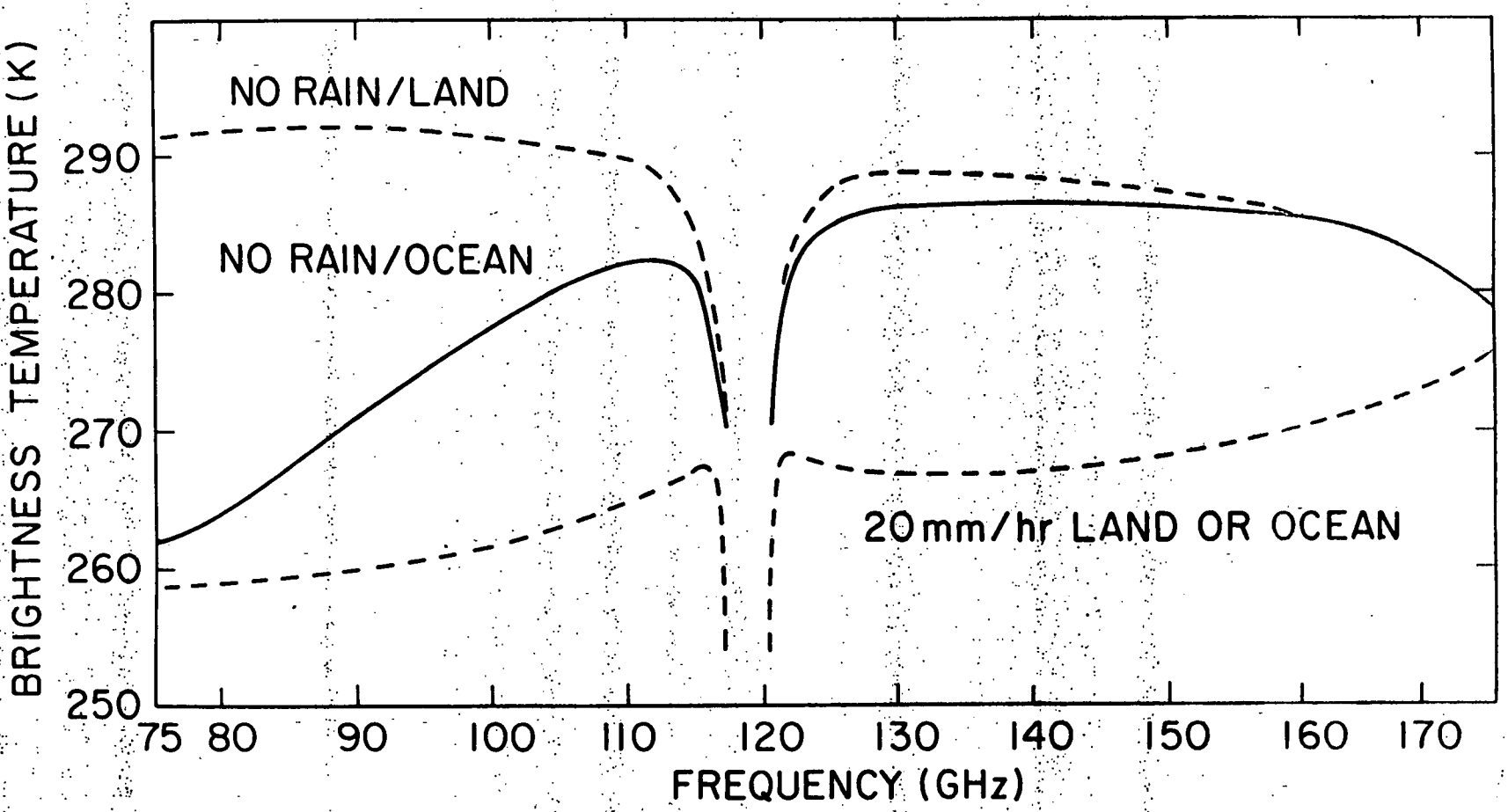


Figure 5.4. Brightness temperatures near the oxygen line, with and without rain.

5.4. Applications to Tropical Cyclones

The potential benefits of improved information on the intensity, position and rainbands of tropical cyclones for use in forecasting are significant. Tropical cyclones cause considerable human suffering that includes loss of life. The loss of property now averages more than $500 million annually (see Figure 5.5). Although the loss of lives in the United States has been relatively low, the loss of both lives and property are even greater in other nations of the world.

Any means that would improve the forecasting and warnings for these destructive weather systems would result in significant savings. For example, increased accuracy in storm track forecasts would permit smaller areas to be warned. Even small improvements (10-15%) in the forecasts of the point of landfall would result in considerable savings. That is, the estimated cost for preparing a coastline for a forecast hurricane landfall now exceeds $25 million. The normal area warned is 300 nmi in length. Therefore, just a 10 percent improvement in the forecast accuracies could result in a savings of 2.5 million in preparation costs alone. The microwave instrumentation on Nimbus-5 and 6 has demonstrated the potential applications of microwave data products to tropical cyclone problems. The results already obtained from these satellites indicate that higher resolution microwave instrumentation has the potential to improve tropical cyclone forecasts and warnings.

5.4.1. Demonstrated and Feasible Applications

Satellite borne passive microwave measurement systems have demonstrated the capability to provide valuable information about tropical cyclones. Because of resolution limitations of current microwave systems most of these measurements have been more qualitative than quantitative.

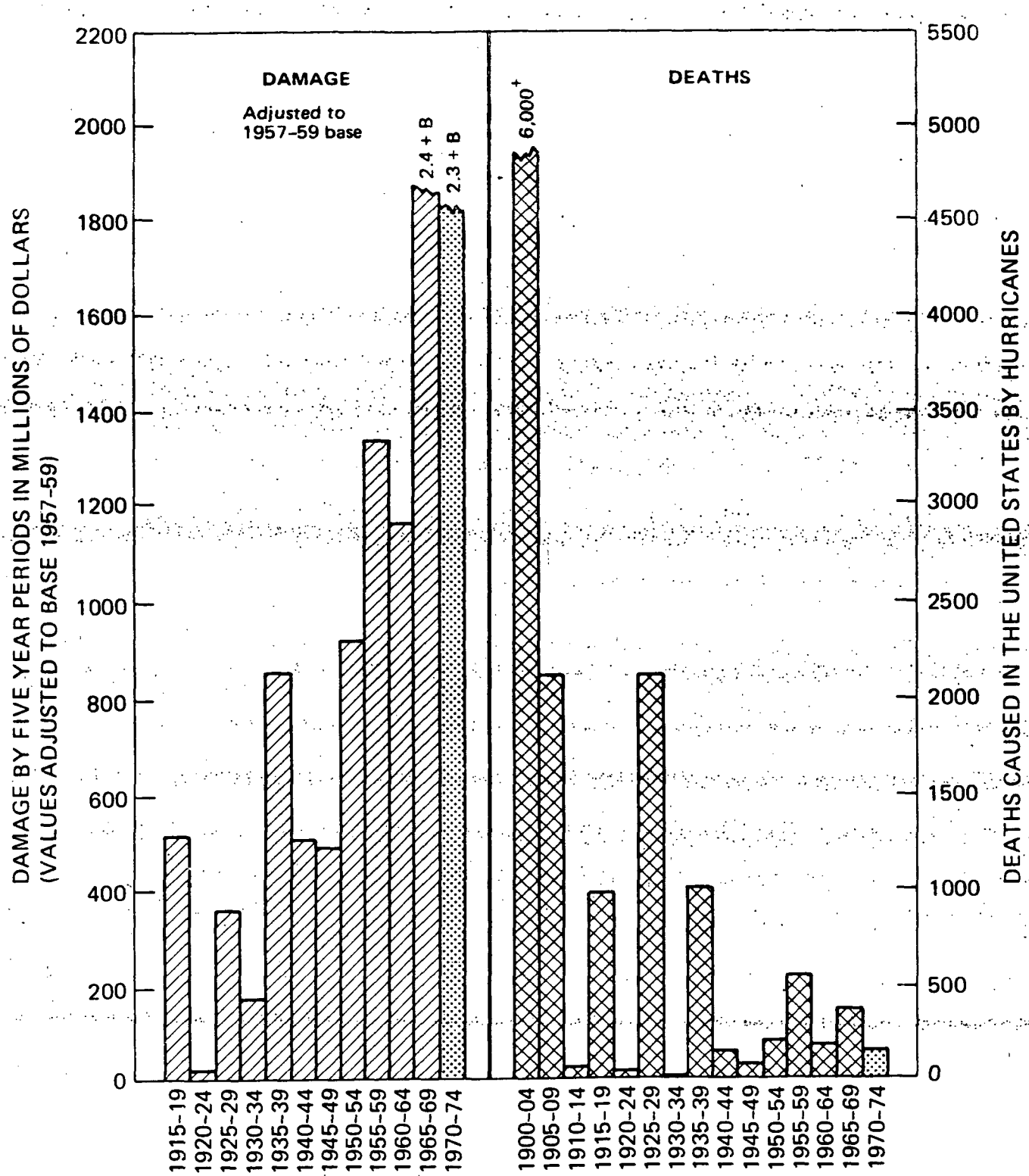


Figure 5.5. Damage and loss of life from hurricanes in the United States by five year periods. A reduction in deaths has resulted from improved warning services, but property damage has risen due to development of exposed coastal areas. (National Research Council, 1977)

An example of the potential of multifrequency measurements of tropical storms (Rosenkranz et al. 1978) was provided when typhoon June was observed by the Scanning Microwave Spectrometer (SCAMS) on Nimbus-6. This typhoon formed in the Philippine Sea in November 1975; its central sea level pressure reached a minimum value of 876 mb on the 19th, a record low. Surface winds in excess of 150 knots were estimated by reconnaissance aircraft on the same day.

The SCAMS instrument provides data that can be used to estimate the temperature pattern in the upper troposphere, atmospheric precipitable water and cloud liquid water. The measurements in the oxygen band at 55.45 GHz correspond approximately to 200 mb and can be used to determine the temperature field at this level. Mature tropical cyclones have a warm central core in the upper troposphere that is related to storm intensity. This warm core structure is evident in Figure 5.6 even though the SCAMS resolution of approximately 150 km near the center of its scan is too coarse to resolve the temperature structure completely.

In the part of the spectrum where the atmosphere is semi-transparent, the spectrometer has one channel centered on the 22.23 GHz water vapor line, and a "window" channel at 31.65 GHz, which is particularly sensitive to clouds. Since both channels are affected by water vapor and cloud droplets, the data for both channels can be solved simultaneously for two variables that are called α and β. These are shown in Figure 5.7 with solid lines for α contours and dotted lines for β contours. With a reasonably smooth sea surface and absence of rain, the atmospheric precipitable water vapor and liquid water (small droplet clouds) can be estimated by

$$\text{vapor (mm)} = 72 + 12\,\alpha$$

$$\text{liquid (mm)} = 0.4\,\beta$$

where the value of 72 mm is the saturation point for a tropical model atmosphere. Thus α is normally negative.

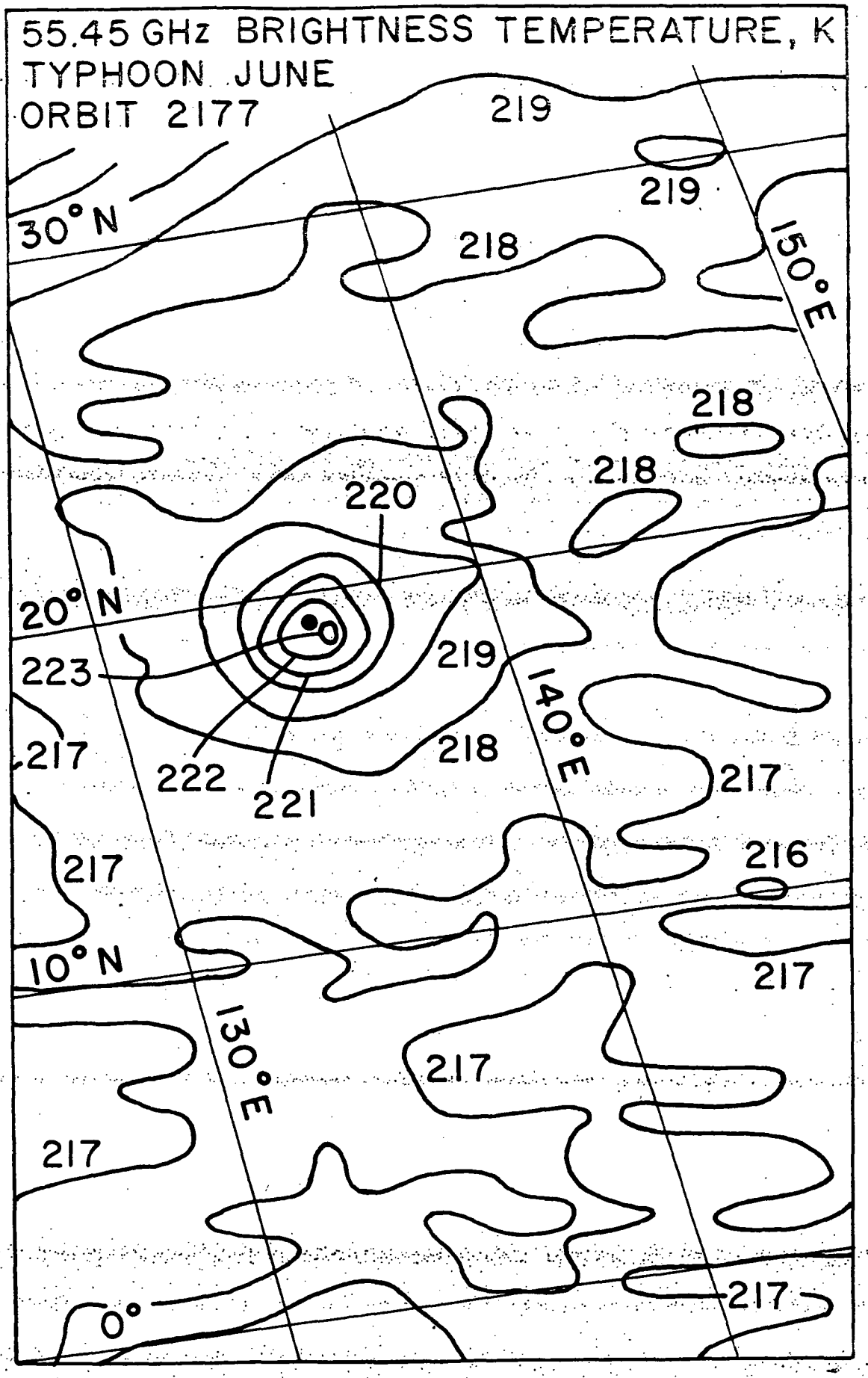


Figure 5.6. 55.45 GHz brightness temperature, corrected for scan angle, from typhoon June on November 21, 1975. The black dot represents the eye location reported by reconnaissance aircraft.

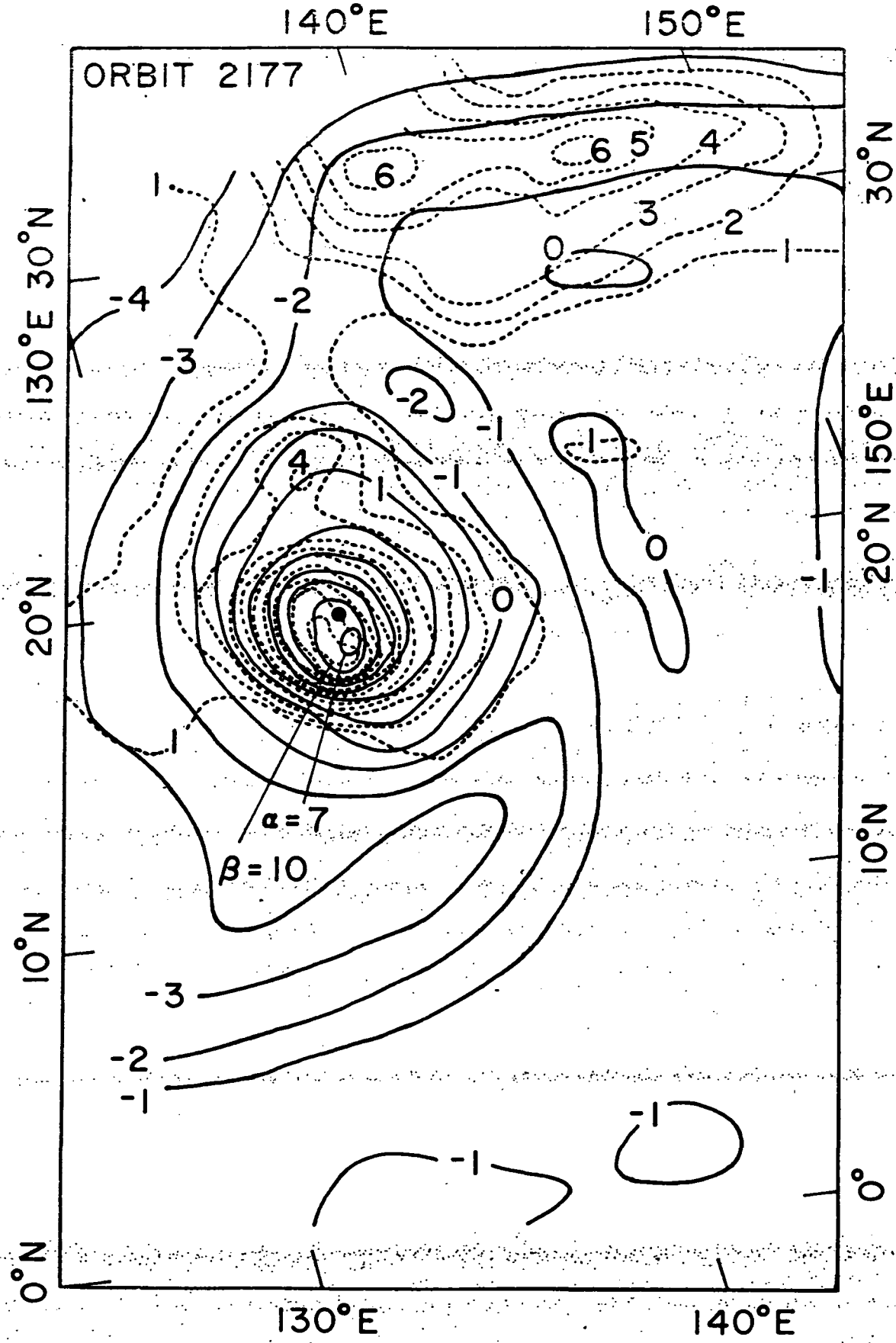


Figure 5.7. α (solid lines) and β (dotted lines) for typhoon June on November 21, 1975.

Inside the typhoon, α reaches positive values. These positive values are probably the result of increased surface emissivity due to sea state, and of rain cells of high microwave opacity. The latter tend to look much the same as sea state since the spectrometer's spot size is much larger than the typical rain cell and thus averages them with the surrounding regions. Measurements from other orbits indicate that the effect of sea state on α is greater than the rain for this typhoon, probably because opaque rain cells do not cover a large fraction of the beam spot area (18000 km^2). If one assumes that the troposphere inside the typhoon contains 72 mm of precipitable water vapor and interprets the maximum value of α in Figure 5.7 as entirely due to sea state, a surface wind speed of 130 knots is inferred. This is very close to the estimate made earlier that day (November 21) by observers on aircraft.

Figure 5.8 shows hurricane Eloise at 1635 GMT on September 22, 1975 as it was depicted in the Gulf of Mexico by the microwave imager ESMR on-board Nimbus-5. Nearly simultaneous observations from research aircraft into Hurricane Eloise indicate that the microwave sensor was able to depict the major areas of precipitation in a gross sense. Figure 5.9 is a much higher resolution visible spectra depiction of Hurricane Eloise about four hours later than the microwave data. It shows more clearly the band of cloudiness that streams outward from the storm's center toward the north, but is strongly influenced by the cirrus patterns at the top of the storm rather than the rainbands. More of the details of the individual convective elements in the elongated precipitation area to the north of Eloise are indicated in a radar display composited from the research aircraft (Figure 5.10) that is superimposed on a visible spectra picture. It is obvious from a comparison of Figures 5.8 and 5.10 that much of the detail of the precipitation area of Eloise has been "smeared" by



Figure 5.8. Microwave depiction of Hurricane Eloise in the Gulf of Mexico at 1625 GMT on September 22, 1975.

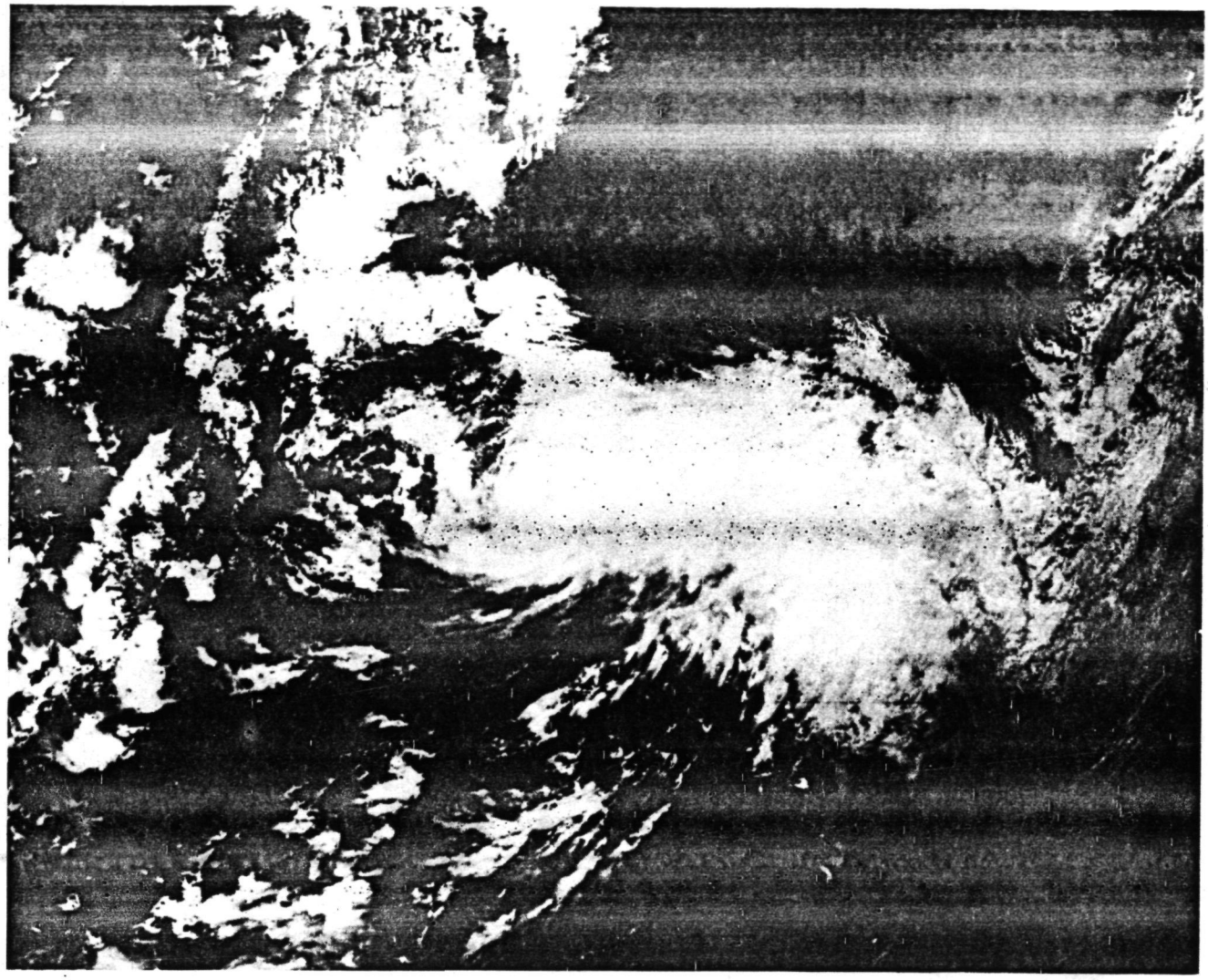


Figure 5.9. Satellite depiction of Hurricane Eloise at 2029 GMT on September 22, 1975.



Figure 5.10. GOES-I depiction of Hurricane Eloise at 2300 GMT on September 22, 1975 with superimposed 5 cm radar pattern composited from a nearly simultaneous research aircraft flight into the storm.

the poor resolution of the microwave imager on Nimbus-5. Obviously, a satellite borne microwave system cannot match the resolution of an air-borne radar system, but improved resolution of satellite microwave systems to a horizontal scale of about 10 km would be very useful to tropical cyclone researchers and forecasters since it would resolve large isolated convective elements as well as the rainbands around the storm.

Calculations have already been made that demonstrate the potential impact of future microwave systems with higher resolution. Adler and Rogers (1977) used the Nimbus-5 ESMR data to make calculations of the latent heat release in a tropical cyclone. They concluded that these observations were potentially useful in monitoring tropical cyclones for observing the change from a weak system to a strong system. For one particular storm they found that the rainfall rates increased near the storm center as the storm intensified and that the more intense the cyclone and the greater the latent heat release, the greater was the contribution from larger rainfall rates. Unpublished results indicate that this result is more general.

5.4.2 Importance of Information

The above-mentioned studies indicate some of the types of investigations attempted with the microwave type sensors. The two major deficiencies of this system are inadequate space and time resolution. If a spatial resolution of a few kilometers ($\sim$10) and a temporal resolution of approximately one hour could be obtained, there would be many areas of application for research where major voids now exist. In addition, if the processing of the data were automated so that analyses could be produced in a matter of minutes, these systems would have considerable potential as operational observations and could help to improve tropical cyclone forecasting.

5.4.3. Comparison with Competitive and Complementary Techniques

5.4.3.1. Storm Intensity

The present means of determining the very important parameter of storm intensity are: (1) direct measurements by aerial reconnaissance flights into the tropical cyclones and (2) estimates of the storm's intensity from the structure observed by the visible and infrared spectra satellite products. The latter method (Dvorak technique) is based upon storm structure as observed from the satellite, past 24 hour structure and empirical "model" developments. This scheme has proven quite good for average type storm development. It has its greatest difficulties with rapidly changing, very intense, and apparently less organized weaker systems.

The major problem with the visible and infrared spectra satellite depictions of a hurricane is that the interior convective structure of the storm is often masked by cirrus clouds. This feature is easily recognized by the comparison of simultaneous radar and satellite depictions of a mature storm with a large cirrus canopy. With the proper spatial resolution, the microwave system could produce a representation of the storm structure similar to that produced by airborne or land based radar. The internal convective structure would then be revealed which should result in significant improvements in satellite estimates of storm intensity. Furthermore, with a temporal resolution of approximately an hour, it is likely that short-term intensity forecast schemes would be possible, particularly in rapidly changing systems.

5.4.3.2. Storm Location

The present means of determining storm positions out over the water areas is through direct measurements by aerial reconnaissance, land radars, and visible and

infrared spectra satellite observations. Aerial reconnaissance is not always available for tracking storms and ground based radars are limited to ranges of about 300 km. Hence, satellites have been relied upon more frequently for tracking tropical cyclones in recent years. These satellite observations again suffer from the fact that the central storm structure is often obscured by cirrus, and in the absence of a well-defined eye, the position estimate may be considerably in error. A means which would provide a depiction of the interior convective banded structure and the warm spot associated with the eye would again provide considerable improvement over present satellite techniques for position estimates.

Statistical techniques presently used to forecast storm motion are strongly dependent upon past 12 hour movements. Instantaneous spot observations from aircraft can sometimes be misleading due to short-term oscillations in the storm track. This factor is illustrated in the storm track for Hurricane Carla (Figure 5.11). A microwave system that could provide adequate temporal and spatial resolution could be used to obtain the more usable "smoothed" storm tracks. The result could be more accurate storm track forecasts that would permit smaller areas to be warned.

5.4.3.3. Precipitation

Estimates of precipitation are now made operationally for tropical weather systems through use of visible and infrared satellite products (Griffith et al. 1976). These estimates are more qualitative than quantitative since they are based upon the reflectivity, infrared temperatures and the extent of the cloud tops associated with the weather system. The major deficiency of this system is resolution caused by the averaging inherent to the technique and the fact that non-precipitating clouds can and often

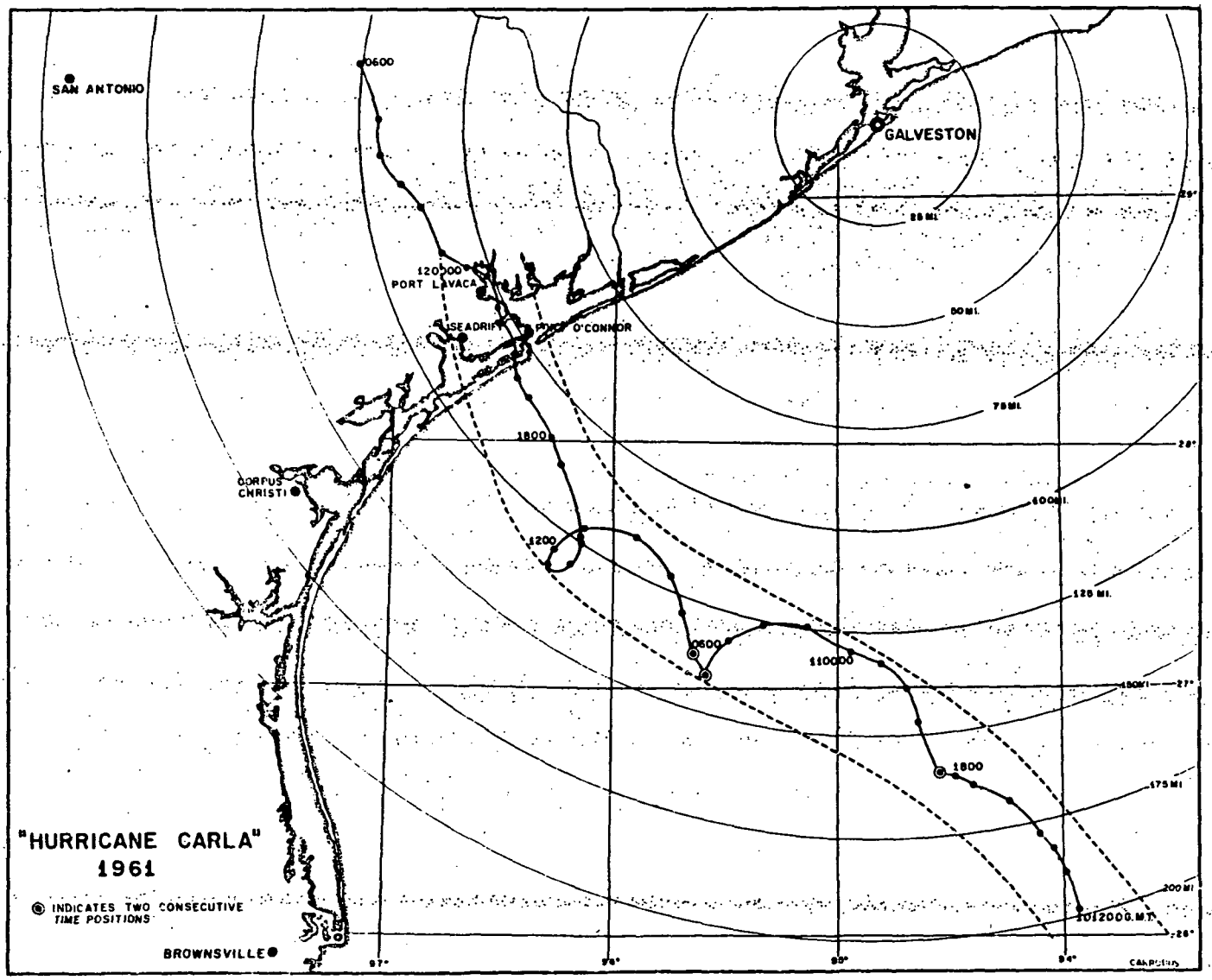


Figure 5.11. Storm track of the eye of hurricane Carla (1961) as determined by land based radar and aircraft reconnaissance.

do have temperatures and reflectivities similar to precipitating clouds. Again, a system with the proper spatial and temporal resolution which would more closely depict actual precipitating areas would be quite useful both from an operational point of view and for research purposes. Rain mapping with this spatial resolution and with temporal resolution on the order of a few tens of minutes would permit tracking of precipitation cells from which mid-level winds beneath the cloud canopy could be derived. It is this possibility which provides the most stringent demands on the spatial and temporal resolution of a severe storm microwave system.

The three major contributors to damage resulting from a hurricane are the winds, the storm surge and the inland flooding resulting from the heavy rainfall associated with these systems. The microwave systems should be capable of providing improvements in the precipitation and perhaps the position forecasts for hurricanes prior to landfall. That is, one should not only be able to distinguish wet storms from dry storms prior to landfall, but also should be able to determine the spatial distribution and partially to quantify rain rates for various sectors of the storms. These measurements, along with empirical studies of orographic and synoptic effects, could be used to compute the possible flooding potential of the land-falling storm. The results may be more qualitative than quantitative initially until more knowledge is gained about the interaction of the tropical system with orographic and synoptic scale features. Measurements of rain over land which appear possible with measurements in the 90 GHz range would improve such determinations also.

5.4.3.4. Storm Development

The differences in the characteristics of weak tropical systems that develop into tropical cyclones and those that do not strengthen are poorly understood.

Microwave systems with improved spatial and temporal coverage could provide considerable insight into the processes that distinguish between developing and non-developing tropical disturbances. For instance, potentially useful information would include spatial and temporal distributions of latent heat release as well as detailed depiction of the convective organization of the weather system. These two factors should result in significant improvements in estimations of storm strength as well as the ability to detect characteristics that would be used in forecasting rapid changes in intensity or determining if a storm is likely to intensify or weaken within the next few hours.

5.4.4. Summary

If a satellite borne microwave system can be devised with a spatial resolution approaching 10 km and a temporal resolution of approximately one hour, it could result in significant advances in research associated with tropical weather systems, particularly tropical cyclones. Furthermore, if "real time" analysis techniques were developed for the potential microwave sensor outputs, these products could be of considerable benefit for use in operational forecasts and warnings. The satellite borne microwave systems appear to have great potential for depicting the internal convective structure of tropical weather systems, including tropical cyclones, in a temporal and spatial resolution desired for research and operational purposes. The critical factors, of course, are whether or not the desired spatial and temporal resolutions are compatible.

5.5. Application to Severe Local Storms

5.5.1. Demonstrated and Feasible Applications

Data from passive microwave instruments have the potential to add substantial information to the study of severe local storms, or severe thunderstorms. However,

the analysis of thunderstorm activity is restricted due to the lack of temporal resolution when using a low orbiting spacecraft. Despite this, the microwave data can be very useful in two main ways: 1) to help define precursor conditions useful as input to dynamical and statistical models to aid in the prediction of severe thunderstorms, and 2) to test concepts of detection and monitoring that if proved feasible would be best suited to geostationary orbits.

5.5.1.1. Precursor Conditions

The three dimensional distribution of temperature and atmospheric water in the form of water vapor, cloud liquid water and rainfall along with surface boundary conditions of surface temperature and surface moisture are needed to define precursor conditions for thunderstorm activity. These atmospheric and surface conditions can then be used in models to predict the where and when of convective activity. One of the principal types of models is the regional-scale dynamical model. Recent evidence has indicated that the distribution of water in the atmosphere is a critical parameter.

The principal advantage of temperature retrieval from microwave sensors is the capability that information can be obtained even when ice clouds are present. The optimum system will, of course, be a combination of microwave and infrared sensors. Moisture information over land has limitations in the low layers due to surface effects. This is where the information is most needed and, therefore, an effort must be made to limit this drawback.

For defining these precursor conditions the high time resolution provided by geostationary orbit is helpful but not essential. The information from low-orbiting microwave instruments combined with other data, both satellite and conventional, would provide a better estimate of these conditions than is presently available. This would presumably result in better forecasts by the models.

5.5.1.2. Tests of Concepts

The microwave portion of the electromagnetic spectrum also holds the potential for having properties usable in the detection and monitoring of severe thunderstorms. To be of practical value the features of importance must be viewed frequently. This points to geostationary orbit; but the concepts could, at least, be tested in low orbiters.

5.5.1.2.1. Temperature Anomaly Detection

One such idea is the detection of areas of subsidence around thunderstorms. These are related to the blocking of the ambient flow by the thunderstorm itself (Fritsch et al. 1976) and may be indicators of thunderstorm intensity. The microwave sensors would be valuable in the detection of these anomalies, because of the capability of "seeing" through the cirrus cloud anvil spreading out from the thunderstorm. Infrared sensors would have difficulty detecting these features.

5.5.1.2.2. Thunderstorm Buoyancy

The buoyancy in a thunderstorm is an indicator of its vigor. Microwave measurements of the temperature anomalies within updraft cores above the influence of supercooled water could provide a buoyancy estimate. This could be especially valuable in determining whether a cell could later become a hail or tornado producer. The achievable horizontal resolution of the microwave sounder may limit this application.

5.5.1.2.3. Rain and Hail Detection

Brightness temperatures emerging from both rain clouds and from bodies of water are depressed in comparison with window brightness temperatures from dry land. However, polarization characteristics give rain a unique signature, as shown in Figure 5.12. In this figure, brightness temperatures measured by the Nimbus-6 ESMR over the central

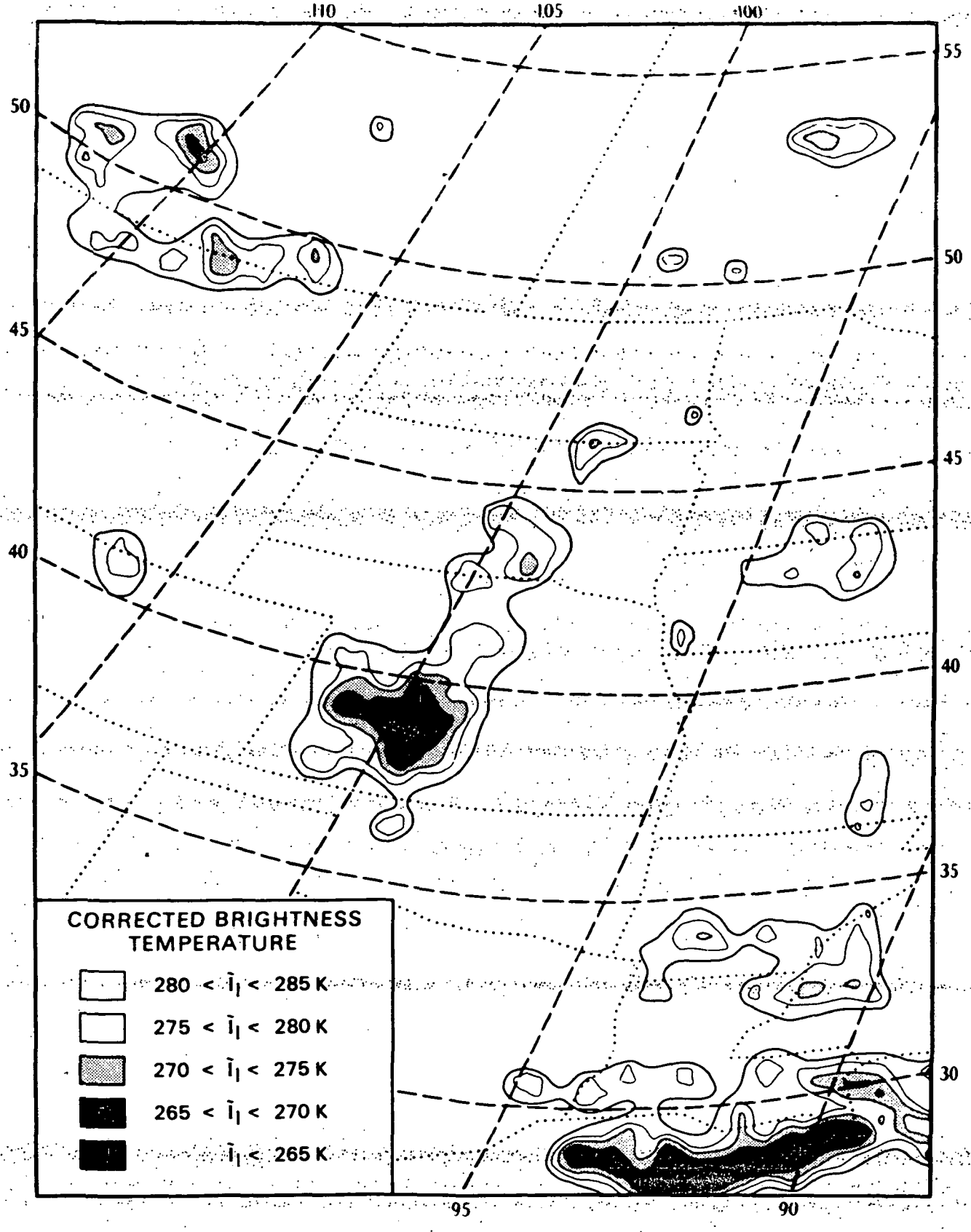


Figure 5.12. Nimbus-6 ESMR corrected brightness temperature over the central United States on July 31, 1975. (Weinman and Guetter, 1977). Dotted lines show state boundaries.

United States on 31 July 1975 have been corrected, by making use of polarization information as described by Weinman and Guetter (1977) to eliminate land-water differences; but thunderstorms over Kansas and Nebraska and the Louisiana coast are very prominent.

If sizeable ice particles are carried above the supercooled water region of a thunderstorm, there should be a lower window microwave brightness temperature than if they were not there, due to scattering. The higher they are carried, the more there are, and the larger the size, the lower the temperatures. It is anticipated that the brightness temperature would be related to the severity (hail size, number of particles, etc.) of the hailstorm. More research to study the frequency and polarization characteristics of these effects is called for. Perhaps there would be a signature that would precede damaging hail at the surface such that some warning could be given.

5.5.1.2.4. Temporal Resolution

The thunderstorm, with its relatively short life time and rapid associated changes, needs high time frequency of observations to be effectively monitored. This observational frequency points to either geostationary platforms with their attendant problems of antenna size and resolution, or to a system of low orbiting satellites, perhaps with pointable sensors for increased time resolution. Research into this area should be pursued.

5.5.2. Potential Users

Potential users for precursor condition information include both operational weather forecasting centers and research institutions. In the last few years numerical-dynamical models for weather prediction have decreased their horizontal mesh size with resulting better forecasts of thunderstorm activity. However, there is now a need for data for model initialization on a spatial scale more

commensurate with the model grid size. The satellite is the only source for getting much of this information. Data from microwave sensors can contribute to this needed meso-scale information base.

It is anticipated that such models will in a few years be running operationally at NOAA's National Meteorological Center and other forecast centers, e.g. the Air Force's Global Weather Central. Satellite input data will be used by these operational centers and other researchers there and in other facilities, including universities.

Microwave data being used to test concepts will be analyzed by researchers in universities, government laboratories, and in private industry. From these evaluations direction for sensors will evolve.

5.6 References

Adler, R. F. and E. B. Rodgers, Satellite-observer latent heat release in a tropical cyclone, Mon. Weather Rev., 105, 956-963 (1977).

Air Force Cambridge Research Laboratory (AFCRL), "Handbook of Geophysics and Space Environments," McGraw-Hill, New York (1965).

Fritsch, J. M., C. F. Chappell, and L. R. Hoxit, The Use of large scale budgets for convective parametrization, Mon. Weather Rev., 104, 1408-1418 (1976).

Griffith, C. G., W. L. Woodley, S. Browne, J. Teijeiro, K, M. Maier, D. W. Martin, J. Stout, D. M. Sidfar, Rainfall estimation from synchronous satellite imagery during daylight hours, NOAA Tech. Rept. ERL-356-WMPO (1976).

Gunn, K. L. S. and T. U. R. East, The microwave properties of precipitation particles, Quart. J. Roy. Meteor. Soc., 80, 522-545 (1954).

Marshall, T. S. and W. McK. Palmer, The distribution of raindrops with size, J. Meteor., 5, 165-166 (1948).

National Oceanic and Atmospheric Administration (NOAA), "Some Devastating North Atlantic Hurricanes in the 20th Century," NOAA-PA-70025 (Rev), GPO 872,197 (1974).

National Research Council, The Atmospheric Sciences: Problems and Applications. Washington, National Academy of Sciences, 124 pp. (1977).

Rosenkranz, P.W., D. H. Staelin, and N. C. Grody, Typhoon June (1975) viewed by a scanning microwave spectrometer, J. Geophys. Res., 83, in press (1978).

Savage, R. C. and J. A. Weinman, Preliminary calculations of the upwelling radiance from rainclouds at 37.0 and 19.35 GHz, Am. Met. Soc. Bulletins, 56, 1272-1274,(Dec. 1975).

Weinman, J. A., and P. J. Guetter, Detection of rainfall distribution from microwave radiation measured by the Nimbus 6 ESMR, J. App. Met., 16, 437-442 (1977).

Wilheit, T. T., J. S. Theon, W. E. Shenk, L. J. Allison, and E. B. Rodgers, Meteorological interpretations of the images from the Nimbus-5 electrically scanned microwave radiometer, J. App. Met., 15, 166-172 (1976).

Wilheit, T. T., A. T. C. Chang, M. S. U. Rao, E. B. Rodgers, and J. S. Theon, A satellite technique for quantitatively mapping rainfall rates over the oceans, J. App. Met., 16, 551-560 (1977).

CHAPTER 6

MICROWAVE RADIOMETRY APPLIED TO SYNOPTIC METEOROLOGY AND CLIMATOLOGY*

6.1 Executive Summary

6.1.1 Summary of Measurement Capability

A. Priorities	Nominal Desired Spatial Resolution (km)	Radiometer Frequencies (GHz)	Radiometer Sensitivities (°K rms)	Achievable Measurement Accuracy (rms)
Temperature Profiles	50	∿55 or 118 [∿5-12 freq.]	0.3	1-5°K
Integrated Water Vapor	15	∿22 [1 or 2 freq.]	0.5	0.1-0.4 cm
Water Vapor Profile	15	∿183 (3-5 freq.)	0.5	
Liquid Water (Rain)	2-10	+2 freq. 15-90 GHz (e.g. 19 and 37 GHz)	2	0.006-0.012 cm
Ocean Temperature and Surface Wind	50	∿2 freq. 1.4-10 GHz (e.g. ∿1.4 and 6)	0.3	∿0.5°K 2 m/sec

B. The operational viewing interval in each case should be ∿ 6 hours for global coverage, although 12 hours is of some use, particularly for ocean and atmospheric temperatures. The viewing angle is best if held constant near ∿ 50° zenith, with vertical and horizontal polarizations being measured separately for all window channels, although through-nadir scanning could be employed with degraded performance.

C. Such data should be very useful for:

1) supporting improved NMC, GWC, and FNWC operational products,
2) supporting the collection of uniform global climatological data (this objective would also be supported by snow and ice data, as discussed in chapter 2).

*Prepared by N. C. Grody.

D. Present experience provides confidence that uniquely useful data concerning temperature profiles, water vapor, and liquid water (precipitation) can be provided. Yet to be fully demonstrated is the ability of passive microwave systems to measure ocean temperature and surface winds; satellite observations in 1978 should remedy this deficiency.

E. The climatology of trace constituents like O_3 can be monitored with high accuracy relative to other techniques (see chapter 7).

6.1.2 Recommendations

A. Support trial and operational efforts to use for synoptic and climatological purposes microwave data from the 1) Tiros-N Microwave Sounding Unit, 2) Block 5D Microwave Sounder, 3) Nimbus-G and Seasat Scanning Multichannel Microwave Spectrometers, and 4) the Nimbus-5 and Nimbus-6 Microwave Radiometers (ESMR, NEMS, and SCAMS). Several years of utilization study and experience would then precede full operational use of the high-resolution data proposed here.

B. Support efforts to obtain data from aircraft, etc. with higher spatial resolution than that proposed here; this would facilitate the utilization study of recommendation (1).

C. Commence development of a multi-purpose passive microwave system to meet the needs of high-resolution synoptic meteorological monitoring and climatology. Integration with other sensor systems would be beneficial for these applications.

6.2 Background

Although the meteorological satellite program is 17 years old, beginning with the Tiros 1 launch in 1960, the application of microwave radiometry as part of that program began only during the last five years. In that period the Nimbus series of experimental polar orbiting satellites first carried radiometers sensing emission in the microwave spectral region.

Nimbus 5, which was launched on December 11, 1972, carried the Nimbus E Microwave Spectrometer (NEMS) which consisted of five separate microwave radiometers to detect thermal radiation at three frequencies in the 60 GHz oxygen absorption band, at the 22 GHz water vapor absorption line and the 31 GHz window region of the spectrum. Measurements of both total water vapor and cloud liquid water were derived over the oceans using the 22 and 31 GHz radiometric data. The three oxygen channels provided global vertical temperature soundings throughout the troposphere using the simplest possible retrieval techniques, i.e. cloud effects were simply ignored in the NEMS analysis. NEMS data analysis clearly established the importance of microwave techniques in determining atmospheric temperature (Waters et al. 1975, Staelin et al. 1975) and water content (Staelin et al. 1976, Grody, 1976) under virtually all weather conditions. However, the non-scanning feature of the NEMS limited its horizontal coverage of meteorological systems.

The SCAnning Microwave Spectrometer (SCAMS) aboard Nimbus 6 launched June 12, 1975, is essentially a scanning version of the NEMS with an improved calibration system. Grody and Pellegrino (1977) have compared SCAMS derived temperatures with radiosonde measurements for frontal systems over Europe. This study showed the ability of the SCAMS to display synoptic scale features comparable with

radiosonde temperature analyses under clear and typical cloudy conditions. A more stringent test of SCAMS cloud penetrating capabilities was presented in the paper by Rosenkranz, Staelin and Grody (1978) where the instrument was used to study the development of Typhoon June over the Pacific. SCAMS measurements showed the possibility of deriving cloud liquid water content and sea surface winds from the 22 and 31 GHz radiometric data from the typhoon. SCAMS 55.45 GHz brightness temperatures displayed the typhoon's warm core temperature structure around 200 mb where the channel has its maximum response.

High resolution microwave measurements of about 25 km (compared to the approximately 200 km linear dimensions resolved by the NEMS and SCAMS) at 19 GHz and 37 GHz were obtained from the Electrically Scanned Microwave Radiometers (ESMR) aboard Nimbus 5 and Nimbus 6, respectively. The ESMR data has been particularly useful for monitoring the movement of sea-ice boundaries (Gloersen et al. 1974), precipitation estimates over oceans (Allison, et al. 1974) and soil moisture variations (Schmugge, et al. 1977). The utility of such data has led to the development of a five channel (6.6, 10.7, 18.0, 21.0, 37.0 GHz) Scanning Multichannel Microwave Radiometer (SMMR) to be launched in 1978 on both Nimbus G and SeaSat A (Gloersen and Barath, 1977). The instruments will be capable of determining sea surface temperature, surface winds, water vapor and precipitation estimates over the oceans. Ice mapping and soil moisture monitoring will also be available from SMMR data.

We are now entering a phase when satellite microwave systems will be exploited operationaly to supplement the traditional passive sensors in the infrared and visible regions of the spectrum. The achievements of the NEMS and SCAMS instruments have led to development of the first operational microwave spectrometer to be flown on the

TIROS-N series. These satellites will carry a four channel Microwave Sounding Unit for the purpose of temperature sounding. Also, the Defense Meteorological Satellite Program is developing a seven channel microwave temperature sounder (SSM) to be flown on its Block 5D meteorological satellite.

The evolution of passive microwave techniques for meteorological purposes has been outlined above and summarized in Table 8.3.1, where the individual instrumental capabilities and characteristics are indicated. As shown in the table, all temperature sounding instruments have horizontal resolutions in excess of 100 km, making them only useful for observing synoptic scale meteorological systems. Such sensors would be of even greater value if instruments having smaller fields of view were available to probe cloud-shielded subsynoptic and mesoscale weather situations.

6.2.1 Microwave Supplement to Conventional Data Sources

Traditionally the major source of upper air meteorological data has been obtained from direct measurements by radiosonde and rawinsonde instruments. The instruments are balloon launched at synoptic times (00 and 12 UT) from a global network of fixed land stations (spaced about 500 km apart) and a limited number of island stations and weather ships. The radiosonde measurements of temperature, pressure, relative humidity and rawinsonde winds serve as reliable inputs to the analysis of initial state parameters for numerical models in weather prediction. However due to their limited areal coverage and infrequent observations, additional data sources are required to investigate disturbed weather areas. This is particularly true for the tropical and extratropical cyclones which develop over the oceans and move into land areas.

To expand the spatial and temporal coverage (particularly

over the oceans), aircraft measurements are used to supplement the global data network. Commercial aircraft provide temperature and wind measurements along their 200-250 mb flight level at various asynoptic times. For tropical storms over the oceans, aircraft reconnaissance flight data are available. The data contain vertical temperature, pressure and humidity profiles from dropsonde measurements, and flight level winds around 700 mb from doppler radar measurements for a limited number of flight paths through the storms. But it is a highly complex and exhausting task, if at all possible, to obtain a complete time history of a major storm development using aircraft data.

Various types of data derived from satellites are used to supplement radiosonde data. This includes not only the temperature and moisture data derived from polar orbiting satellites but other data from the geostationary satellites. Presently, infrared and visible cloud imagery from the NOAA Geostationary Operational Environmental Satellite (GOES) are routinely applied in the analysis of dynamical systems. Estimates of tropical storm intensities have been developed based on subjective analysis of satellite imagery (Dvorak, 1975). Meteorologists experienced in the interpretation of infrared and visible images have developed techniques for identifying circulation patterns which may not be detected from the coarse global data network (Anderson, et al. 1975). Subjective interpretations from satellite television pictures are entered into the final stages of analysis and forecast of weather systems. Finally, the cloud motion fields observed by GOES are used to derive atmospheric winds at upper and lower levels (Green et al. 1975). This last technique of following cloud motion is however limited by the difficulty of properly identifying clouds at different altitudes, and much of the circulation at low levels is obscured by higher clouds.

Because of the cloud penetrating property of microwave radiation, together with the high stability and sensitivity of microwave radiometers, microwave measurements have the potential of adding very significantly to the current operational data base. However, it is well to recognize that realization of the full benefits of microwave-derived data requires that they be properly introduced into numerical models for analysis and forecasting of meteorological events.

6.2.2 Application of Microwave Data

It remains a sensitive issue that tests conducted with the Nimbus 6 sounding system have not shown any dramatic impact on weather analysis and forecasting in the Northern Hemisphere (Tracton and McPherson, 1977). One answer may be that the "silent" areas (e.g. ocean regions) are not as data void as initially believed. Surface data, aircraft data, satellite wind vectors, and subjective interpretations from satellite television pictures, together with forecasts from data rich areas, appear to specify the atmosphere adequately in the great majority of synoptic scale situations. Add to this the characteristic deficiencies in the infrared satellite sounding data caused by cloud contamination as well as the vertical resolution problem of remote sounders in general and one finds that "impact" has been minimal. A shortcoming of the Nimbus 6 sounding system was that under conditions judged too cloudy for the infrared sounder, retrievals were not made. Thus the benefit of the SCAMS measurements, i.e. cloud penetrating capability, was not realized in many situations. This will not be the case for Tiros-N, where it is planned to obtain microwave retrievals under conditions which are too cloudy for infrared retrievals.

An example of a modest but significant analysis change indicated by the SCAMS data is given in Figures 6.1 and 6.2.

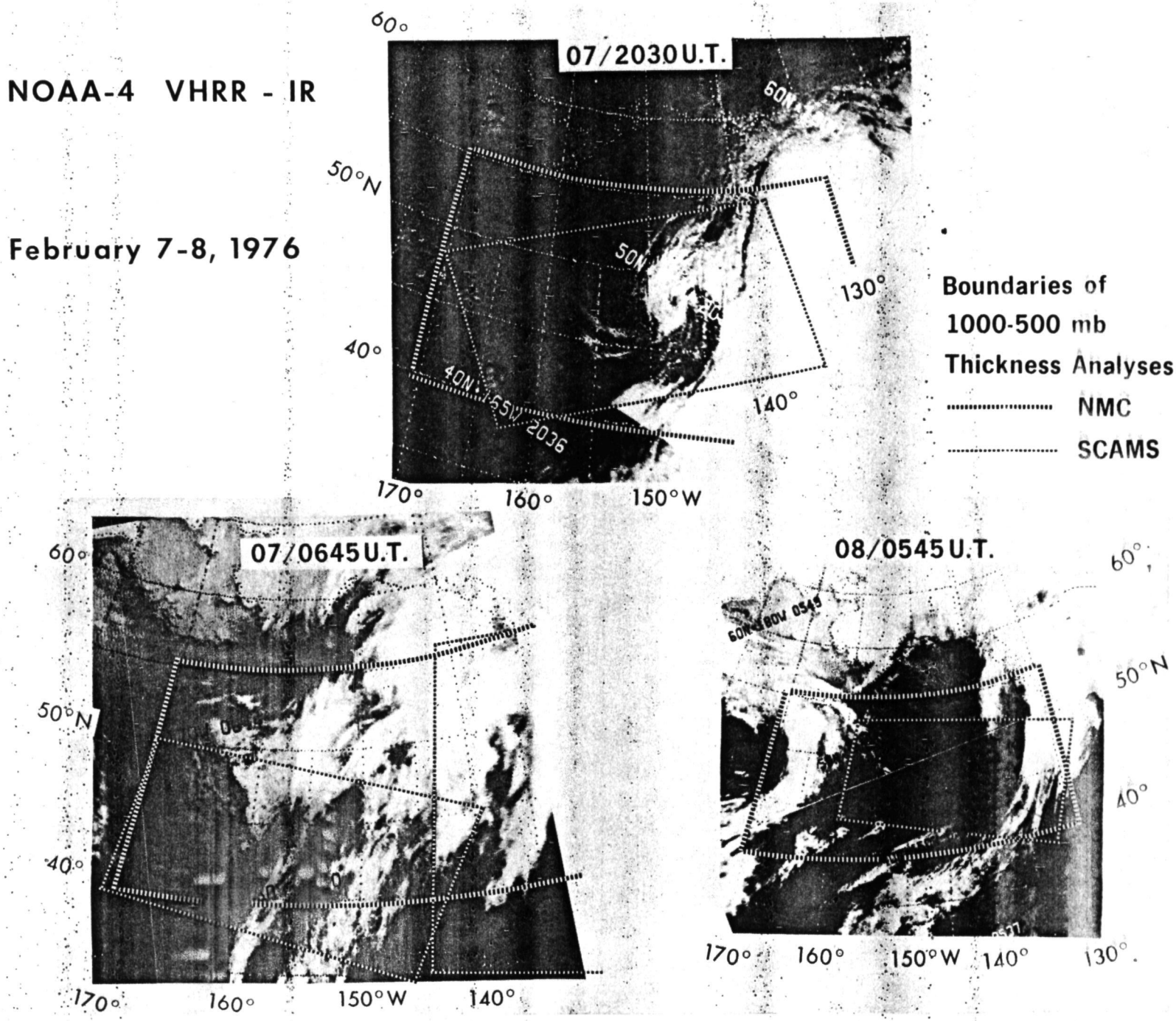


Figure 6.1. NOAA-4 VHRR satellite images showing cloud features and boundaries for NMC and SCAMS analyses for February 7-8, 1976.

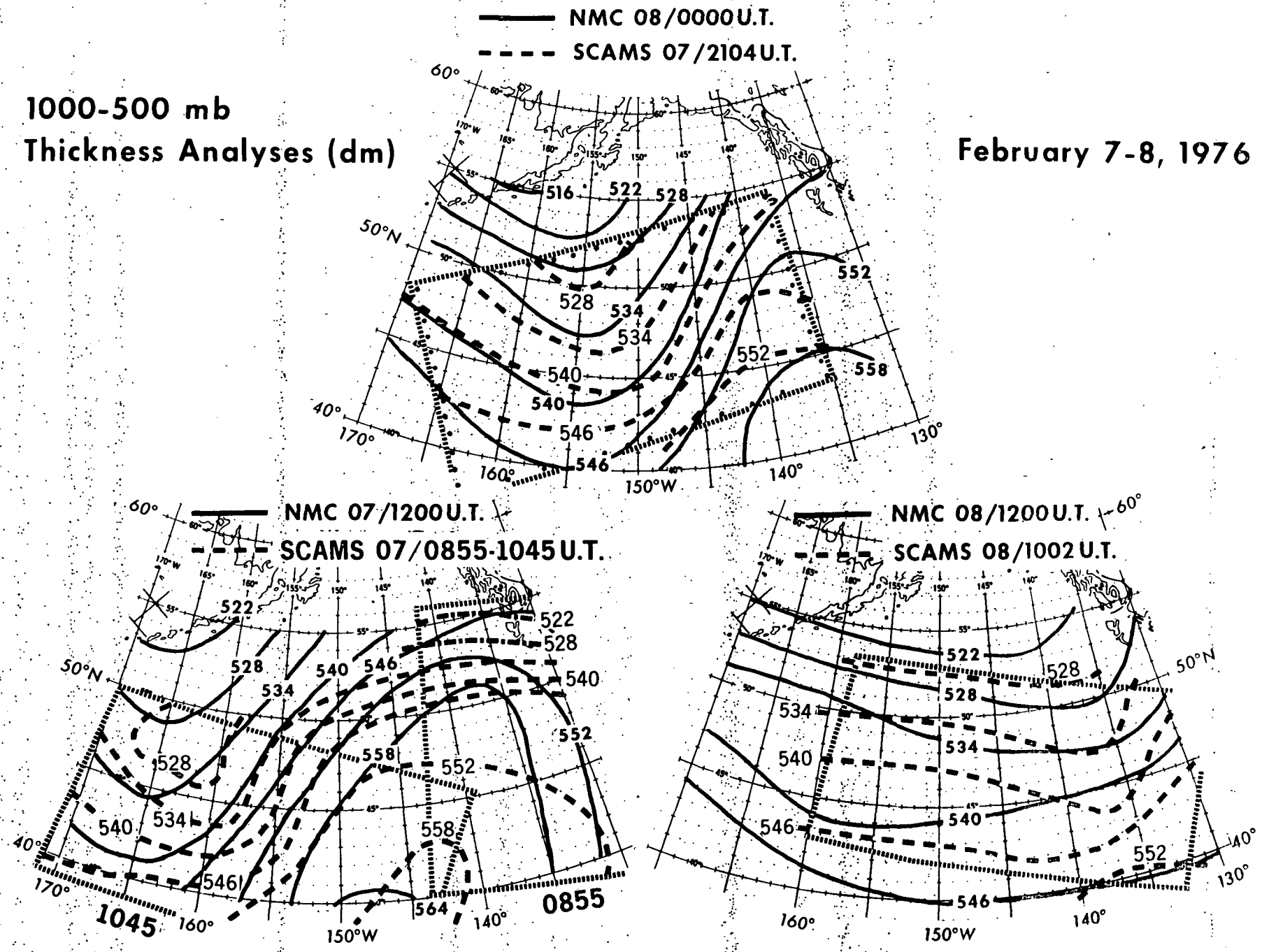


Figure 6.2. Comparisons between NMC and SCAMS retrieved 1000-500 mb thickness fields for February 7-8, 1976. The SCAMS data coverage contained within dashed lines correspond to Figure 6.1.

Figure 6.1 shows the satellite-observed clouds of a rapidly moving weather disturbance traveling across the Gulf of Alaska on the Pacific northwest coast on February 7-8, 1976. Figure 6.2 shows the depiction of the same system as defined by NMC (National Meteorological Center) analysis (which does not include the research satellite data) and by the SCAMS soundings. Notice that movement of the trough associated with the system is contained in both analyses, but there are important differences in shape, position, and intensity. Figures 6.3 and 6.4 again show the differences between NMC and SCAMS analysis of a cyclonic disturbance into the Pacific northwest coastal region on February 18-21, 1976. These differences may not be adequately reflected in the product of coarse, large scale forecast models but must make an impact on sensitive, fine scale forecast models. Current and ongoing applications of satellite data will stress this area which is of ultimate importance for short to medium range forecasts.

It is generally accepted that within the tropical environment knowledge of the large variations in water vapor are of utmost importance for understanding the development of tropical cyclones and cloud clusters. As illustrated in Figure 6.5, the total water vapor derived from the SCAMS (or NEMS) instrument can produce estimates approaching the accuracy of radiosonde instruments and show the large variations in the water vapor distribution over the oceans which previously could only be surmised from the limited number of island radiosonde stations and by subjective analysis of satellite-cloud observations (e.g. Ruprecht and Gray, 1976). However, most numerical prediction models require at least two vertical layers of the water vapor amounts in the atmosphere, rather than the total (integrated) amounts derived from past microwave instruments. To be useful, either the total moisture must be parameterized into a profile, or new instruments must be developed. Current

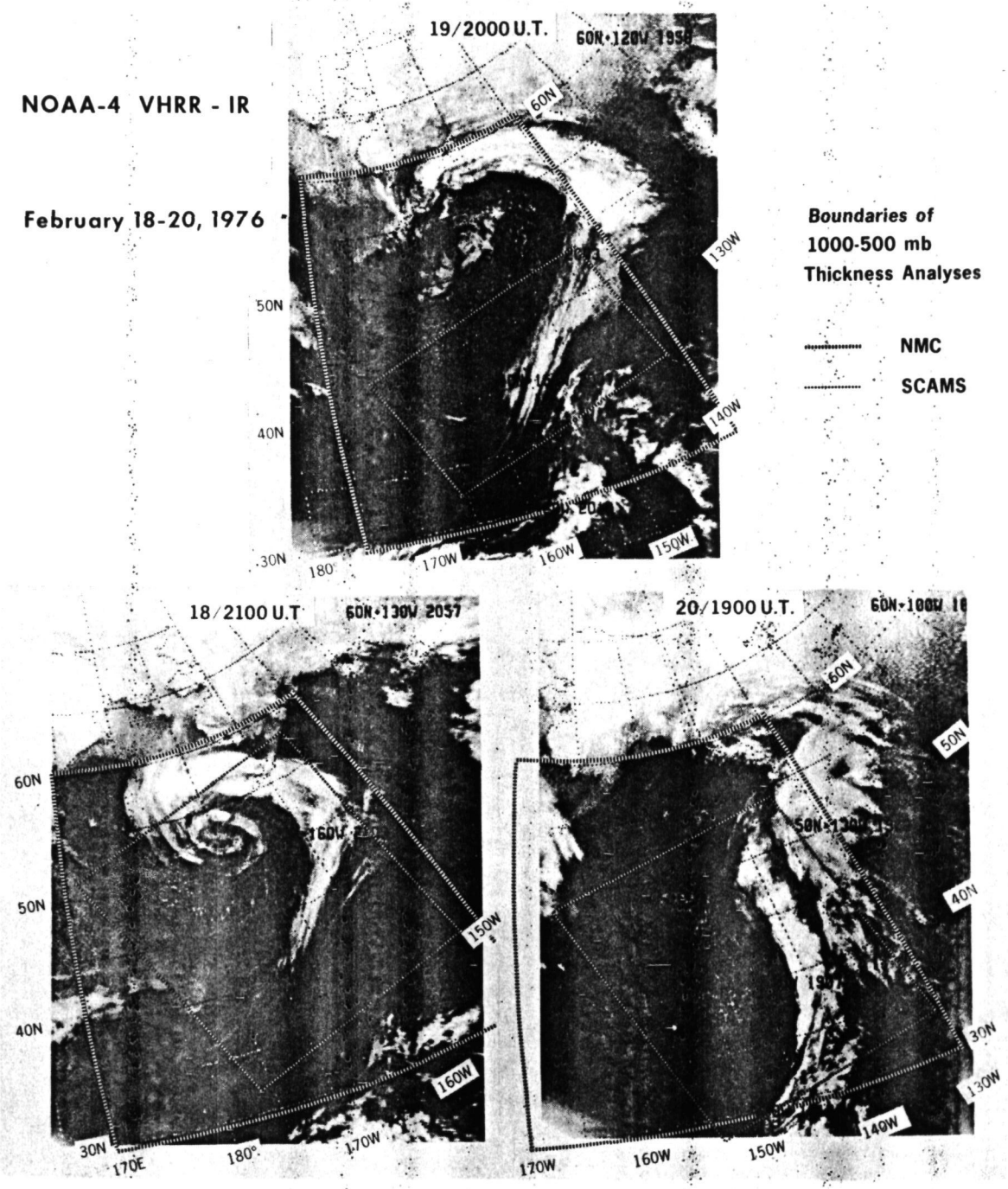


Figure 6.3. As in Figure 6.1 except for February 18-20, 1976.

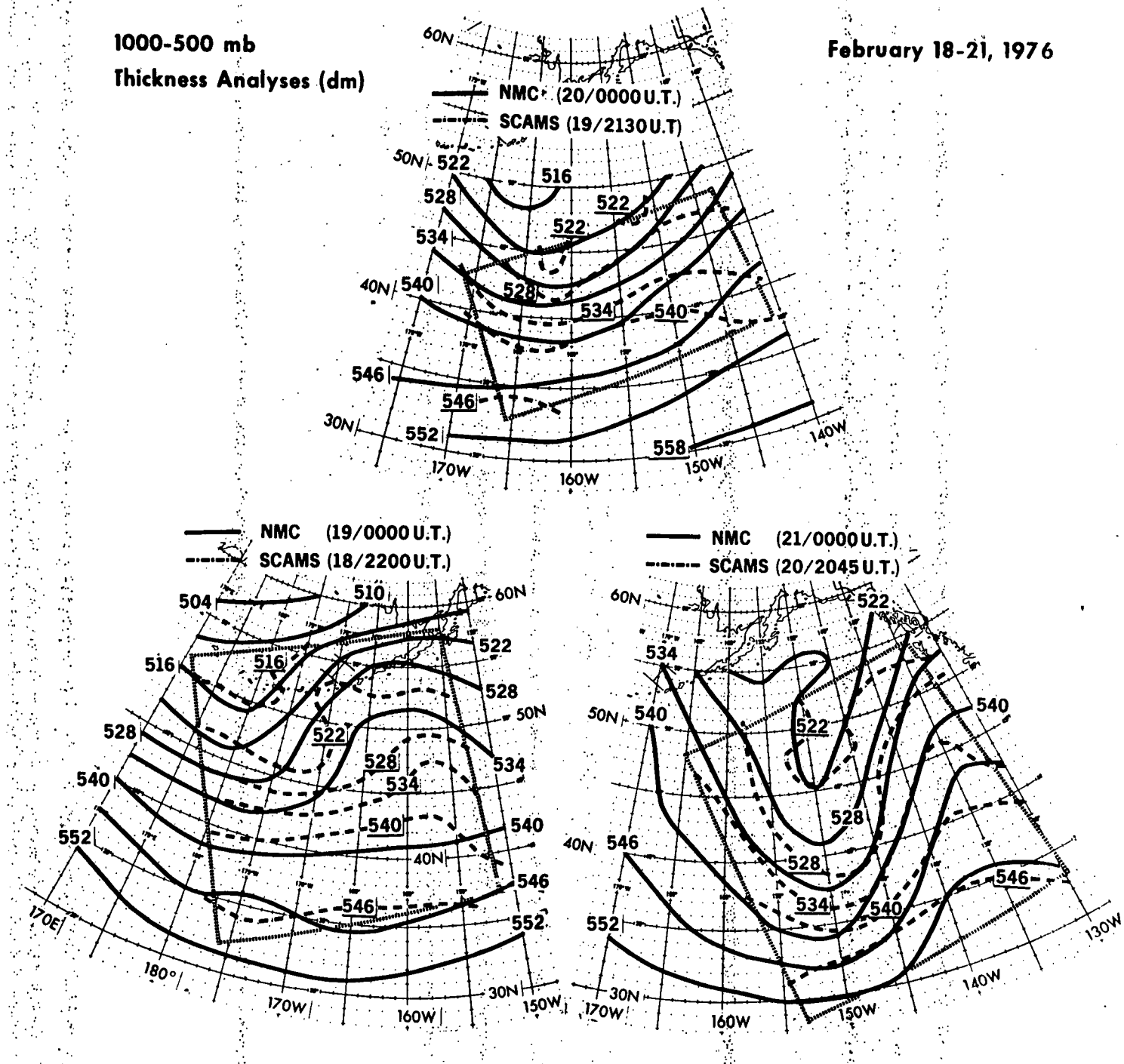


Figure 6.4. As in Figure 6.2 except for February 18-20, 1976.

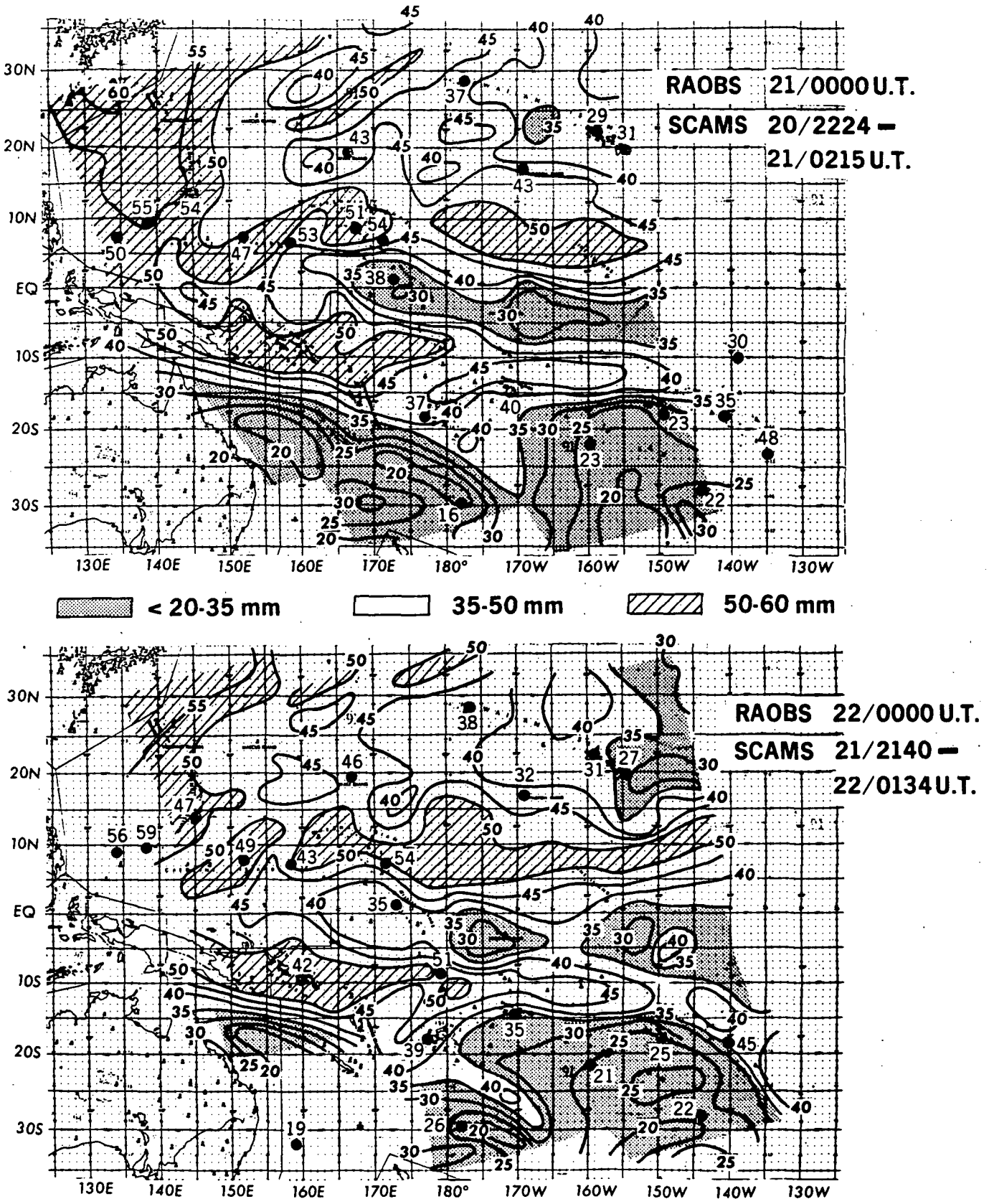


Figure 6.5. Comparisons between SCAMS retrieved precipitable water (mm) and radiosonde measurements for August 20-22, 1975.

and ongoing research at the National Atmospheric and Space Administration (NASA) and the Massachusetts Institute of Technology (MIT) involves the design of multichannel spectrometers employing the 183 GHz water vapor region in addition to the more transparent 22 GHz spectral region for obtaining water vapor profile information.

6.3 Measurement Techniques and Evaluation

Atmospheric temperature and water content are the principal meteorological variables derivable from radiometric measurements in the oxygen and water vapor spectral regions, respectively. The methodology of determining vertical temperature (thickness) and geostrophic wind from radiometric data will be described, followed by a review of the technique used in determining atmospheric water vapor and liquid water content. Although the theories of measurement outlined are applicable to a wide class of microwave sensors, reference will be made occasionally to the SCAMS set of channels (22.2, 31.6, 52.8, 53.8, 55.4 GHz). Examples of SCAMS measurements will serve to illustrate the capabilities of the microwave techniques in various meteorological applications.

6.3.1 Atmospheric Temperature (thickness) and Geostrophic Wind Determinations

The calibrated response of a satellite-borne, earth-viewing microwave radiometer to received radiation at frequency ν is a brightness temperature $T_B(\nu)$ averaged over the instrument's field of view. Brightness temperature is related to the vertical profile of atmospheric temperature $T(P)$, in accordance with the radiative transfer equation which can be written in the descriptive form as the sum of an atmospheric and surface term:

$$T_B(\nu) = \int_{-\infty}^{\ln P_s} T(P)\, W(\nu,p)\, d\ln P + \tau_\nu(P_s)^{\mathrm{Sec}\theta}\, \varepsilon_s\, T_s \qquad (1a)$$

$$W(\nu,p) = \left[1 + (1-\varepsilon_s) \left(\frac{\tau_\nu(P)}{\tau_\nu(P_s)} \right)^{2\mathrm{Sec}\theta} \right] \frac{\partial \tau_\nu(P)}{\partial \ln P}^{\mathrm{Sec}\theta} \qquad (1b)$$

where $\tau_\nu(P)$ is the atmospheric transmittance from pressure P to the satellite level, P_s is the surface pressure, T_s the surface temperature and ε_s the surface emissivity. The off-nadir (limb) effect is included by the $\mathrm{Sec}\theta$ factor, where θ is the earth-located zenith angle for a particular viewing direction. In the microwave spectral regions of interest, oxygen and water vapor are the major atmospheric absorption media, whose transmittances are accurately given by Rosenkranz (1975) and Liebe (1969, 1977). For the spectral regions of interest the emissivity is about 0.5 for sea surfaces and approaches unity for dry land. The expression $W(\nu,p)$ is called the temperature weighting function since it weights the atmospheric temperature contribution to the brightness temperature. Surface effects are included in the weighting function definition by the bracketed part of Eq. (1b) which contains the reflected radiation contribution in the case of sea surfaces.

Within the oxygen band (centered at 60 GHz), the weighting functions are essentially independent of temperature and have a unique pressure dependence for a given frequency, surface emissivity and view angle. They are unimodal, peaking at decreasing pressure as the frequency approaches the center of the oxygen band at 60 GHz. This property is illustrated by the SCAMS weighting functions in Figure 6.6 which was computed for land and sea surfaces viewed at nadir and the extreme scan position. The spread in the weighting functions is an approximate indication of the vertical resolution of temperature structure recoverable from individual brightness temperature measurements, although linear combinations of weighting functions

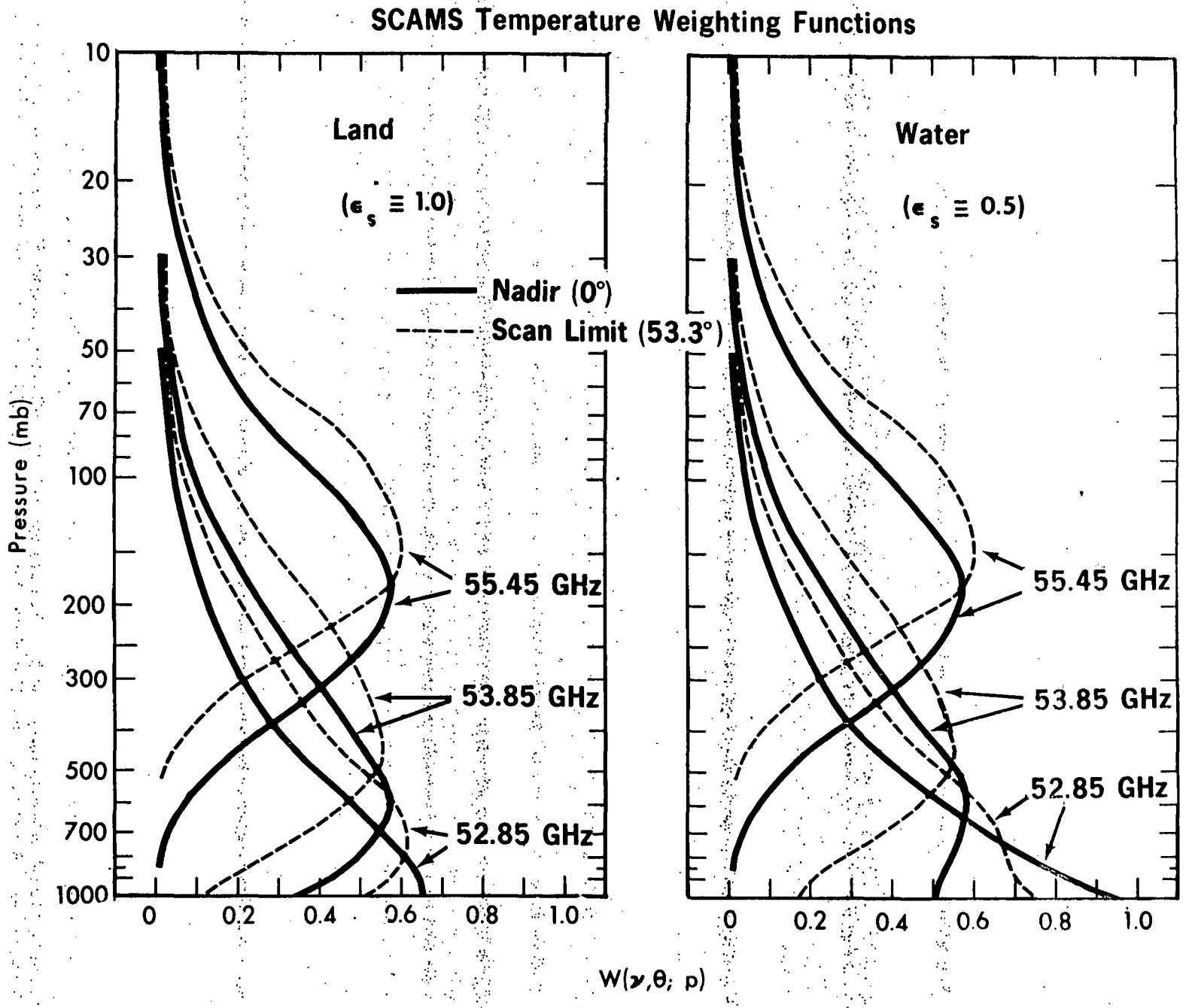


Figure 6.6. SCAMS temperature weighting functions calculated for nadir and scan limit positions, for land and sea class surfaces.

(corresponding to linear combinations of brightness temperatures) improve the vertical resolution attainable from a given set of channels (Backus and Gilbert, 1970).

Equation (1a) then can be inverted to give a linear relationship between atmospheric temperature profile and brightness temperatures, viz;

$$T(P) = a_o(P) + \sum_n a_n(P)\ T_B(\nu_n) \qquad (2)$$

where the coefficients $a_n(P)$ are dependent on the weighting function properties. Various techniques have been investigated for obtaining the coefficients. However, most practical methods are basically variations of a statistical linear regression approach (Hayden, 1976) with brightness temperatures as predictors and atmospheric temperature as the predictand. In this case $a_n(P)$ of equation (2) are regression coefficients. The accuracy of the temperature measurements relies on statistical information in addition to the basic resolution and characteristics of weighting functions. In fact improvements in temperature retrieval accuracy result because the regression coefficients contain statistical information correlating temperatures averaged over the weighting functions with the temperature at a discrete pressure level.

There are essentially two ways in which regression coefficients $a_n(P)$ are computed. In both instances radiosondes provide the temperature data but the brightness temperature may be either measured (by a simultaneous satellite measurement) or simulated by a forward calculation of Equation (1a). In either case the coefficients contain some effects due to local surface emissivity variations, but the large variations between land and sea surface emissivity are eliminated by obtaining separate coefficients

in the case of land and sea surfaces. The principal reason for using the colocated measurement approach is that simulated and measured brightness temperatures often disagree for infrared channels. However with SCAMS these were found to agree (Grody and Pellegrino, 1977); substantiating the independence of SCAMS results to such auxiliary data. This is apparently unique to the microwave radiometric technique and is partly due to the well defined atmospheric transmittance for the oxygen band in addition to the generally small perturbation resulting from cloud liquid water attenuation.

Results from synoptic scale studies comparing SCAMS retrieved temperatures with coincident radiosonde measurements confirm the theoretical expectations of standard error. Figure 6.7 shows the theoretical results obtained for land and sea surfaces viewed at nadir and the extreme scan position; based on regression estimates obtained with numerical simulations of the SCAMS response to a set of global, all season radiosonde observations. The SCAMS 52.85, 53.85 and 55.45 GHz brightness temperatures were the predictors used in obtaining temperatures at the standard pressure levels. In general, the largest temperature errors occur at pressures where (a) weighting functions are inadequate and (b) strong correlation is lacking between level temperatures and weighted temperatures sensed by the instrument. It is not always possible to separate these two sources of error, although an indication of the weighting function factor is shown by the smaller errors above 100 mb in the scan limit position (when the weighting function peaks higher in the atmosphere) compared to the errors for the nadir case. An indication of the latter is shown by the relatively poor information content of the measurements near 200 mb where the tropopause has not been resolved.

Figure 6.8 compares 700 mb temperatures derived from

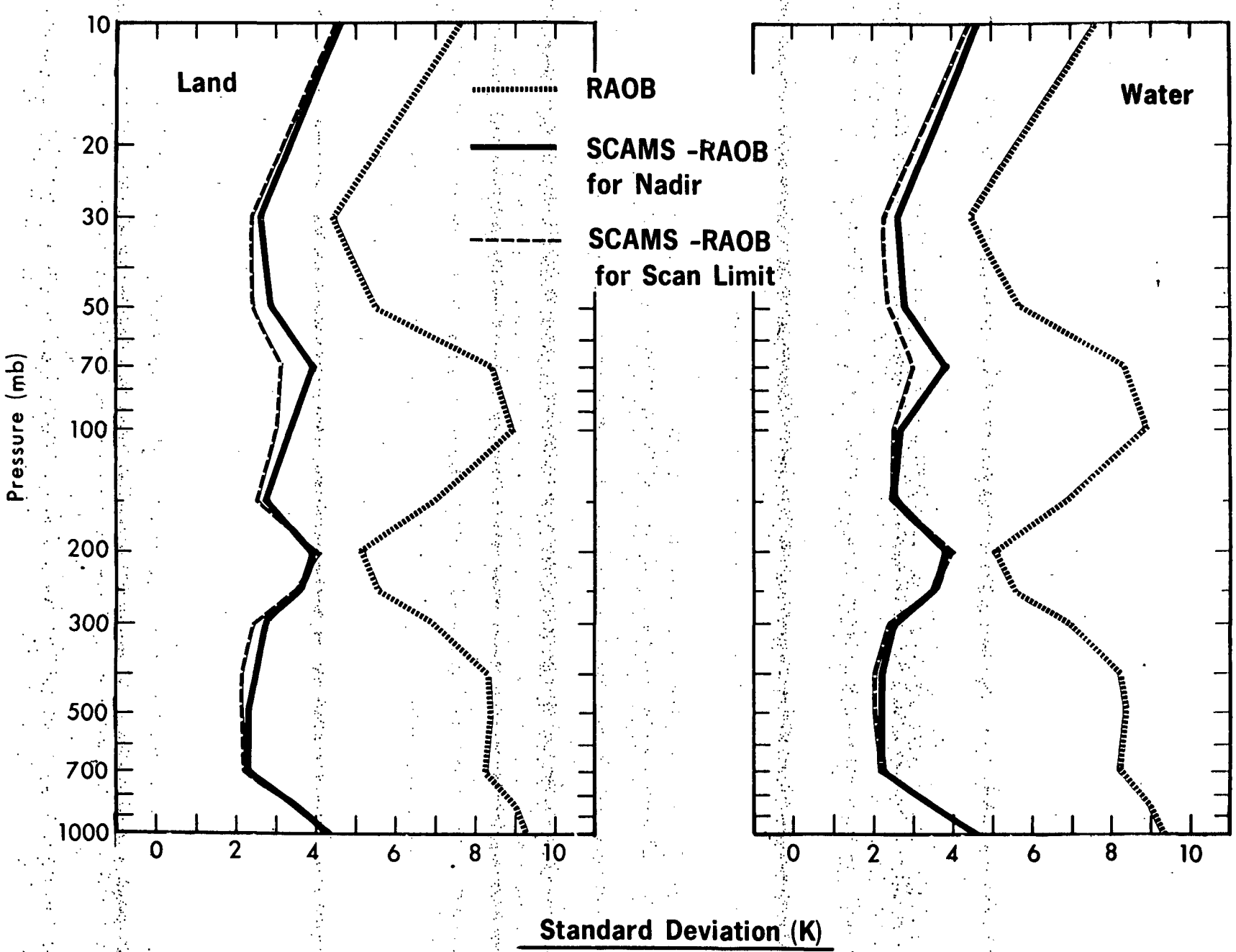


Figure 6.7. Theoretical accuracy of SCAMS retrieved temperatures. Curves show standard error (SCAMS - RAOB) between simulated SCAMS retrievals and radiosonde data. Results are presented for both sea and land surfaces when SCAMS is viewing nadir and the extreme scan position. Also shown is the standard deviation (RAOB) in the radiosonde temperature sample.

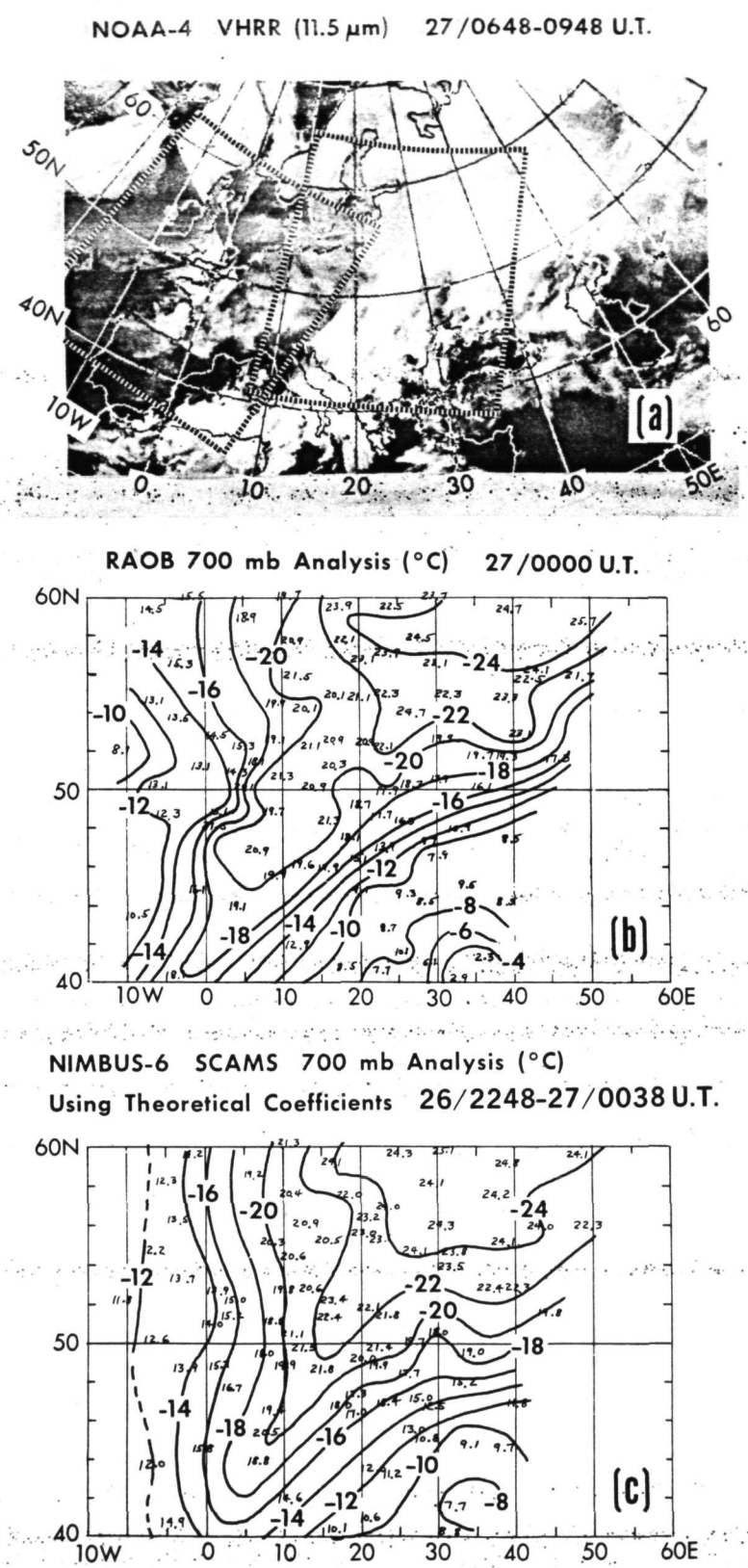


Figure 6.8. Comparisons between SCAMS 700 mb retrieved temperature measurements and radiosonde data for January 26-27, 1976: (a) NOAA-4 VHRR satellite image showing cloud features and SCAMS grid coverage, (b) analysis of 0000 UT radiosonde temperatures, (c) analysis of 2248-0038 UT SCAMS retrieved temperatures. (After Grody and Pellegrino, 1977).

SCAMS measurements over Europe with the RAOB analysis. The positions of the major trough and ridge are well defined in the SCAMS analysis although both the amplitude of the ridge and temperature gradient in the frontal bands are underestimated. Some of this gradient reduction is due to SCAMS' large field of view, which smooths out temperature gradients.

For applications to numerical models the layer temperatures or "thickness" values are more appropriate than level temperatures. From the hydrostatic equation the thickness between pressure P and a reference level P_o becomes

$$Z\ (P) = \frac{R}{g} \int_{\ln P_o}^{\ln P} T^*(P)\ d\ln P \qquad (3)$$

where R is the gas constant, g the gravitational constant and $T^*(P)$ the virtual temperature. Thickness may be approximated using the level temperatures of Eq. (2), which reduces (3) to a regression solution

$$Z\ (P) = b_o(P) + \sum_n b_n(P)\ T_B(\nu_n) \qquad (4)$$

where the coefficients $b_n(P)$ can be computed from simulations or from the temperature regression coefficients, viz;

$$b_n(P) = \frac{R}{g} \int_{\ln P_o}^{\ln P} a_n(P)\ d\ln P \qquad (5)$$

SCAMS 1000mb to 500mb thickness fields shown in Figures 6.2 and 6.4 were derived using Eq. (4) with simulated coefficients relating the oxygen channel brightness temperatures with thickness values. It is certainly conceivable that insufficient NMC data was responsible for the differences between the SCAMS results. In the North Atlantic area the

NMC analyses are generally improved from prior knowledge of systems traveling across the east coast (where much conventional data exists) as evidenced by the SCAMS comparison shown in Figure 6.9. Both thickness fields display similar shapes, positions and intensities, although small scale features shown by the SCAMS results appear smoothed out in the NMC analysis.

In addition to temperature or thickness determinations, brightness temperature gradients for the oxygen channels are useful in deriving wind fields at different levels in the atmosphere. The relationship between brightness temperature gradient and wind is particularly straightforward for the case of geostrophic flow as described below.

For steady state conditions, and in regions where "frictional" forces are negligible, balance relationships exist between the motion and mass fields enabling direct determination of winds from temperature analyses. The thermal wind equation is developed from the balance between Coriolis and pressure gradient forces and can be expressed in isobaric coordinates as

$$\frac{\partial V}{\partial P} = - \frac{R}{f} \frac{1}{P} \frac{\partial T}{\partial \eta} \qquad (6)$$

where V is the geostrophic wind along a constant pressure surface, R is the gas constant, f the Coriolis parameter and η the coordinate in the direction of the horizontal temperature gradient. Multiplying Eq. (6) by the temperature weighting function of Eq. (1b) and integrating through the atmosphere gives:

$$\int_0^{P_s} \frac{\partial V}{\partial P} W(\nu,P)\, dP = - \frac{R}{f} \frac{\partial}{\partial \eta} \int_{-\infty}^{\ln P_s} TW(\nu,P)\, d\ln P \qquad (7)$$

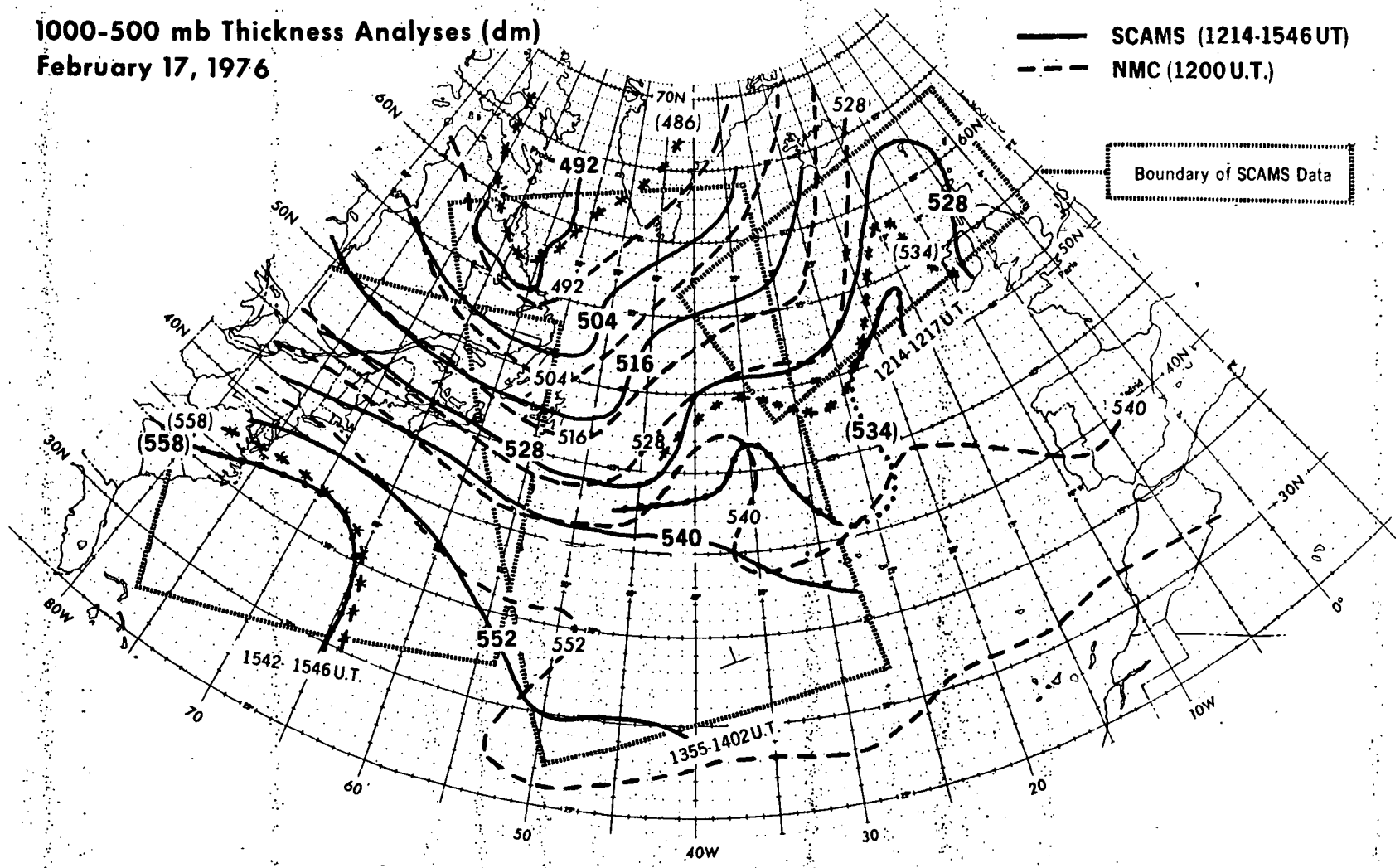


Figure 6.9. Comparisons between NMC and SCAMS retrieved 1000-500 mb thickness field for February 17, 1976. The areas within dashed lines define the SCAMS data coverage.

Using Eq. (1a) the right hand side of Eq. (7) becomes proportional to the brightness temperature gradient; neglecting the small contributions due to gradients in surface temperature and surface pressure. Also, integrating the left hand side of Eq. (7) by parts one obtains the final result;

$$\frac{R}{f}\frac{\partial T_B}{\partial \eta} = \int_{-\infty}^{\ln P_s} V \frac{dW(\nu,P)}{d\ln P} - V_s W(\nu,P_s) \qquad (8)$$

where V_s is the surface wind. Equation (8) has a form similar to Eq. (1a) and relates the horizontal gradient in brightness temperature to the wind profile through a "wind weighting function" which is the vertical derivative of the temperature weighting function. Differentiation of the unimodal temperature weighting function results in a doublet producing regions of positive and negative contributions with a crossover point at the pressure of maximum temperature weighting. The wind weighting functions for the SCAMS oxygen channels illustrate this property and are shown in Figure 6.10 for land and sea surfaces viewed at nadir.

Analogous to the temperature inversion problem, the vertical wind profile can be expressed as a linear combination of brightness temperature gradients,

$$V(P) = C_o(P) + \sum_n C_n(P) \frac{\partial T_B(\nu_n,\eta)}{\partial \eta} \qquad (9)$$

where the coefficients $C_n(P)$ can be obtained from regression analysis using simulated data. Alternatively, the wind equation (9) could be arrived at by applying the temperatures of Eq. (2) to the thermal wind equation (6) and obtain the coefficients

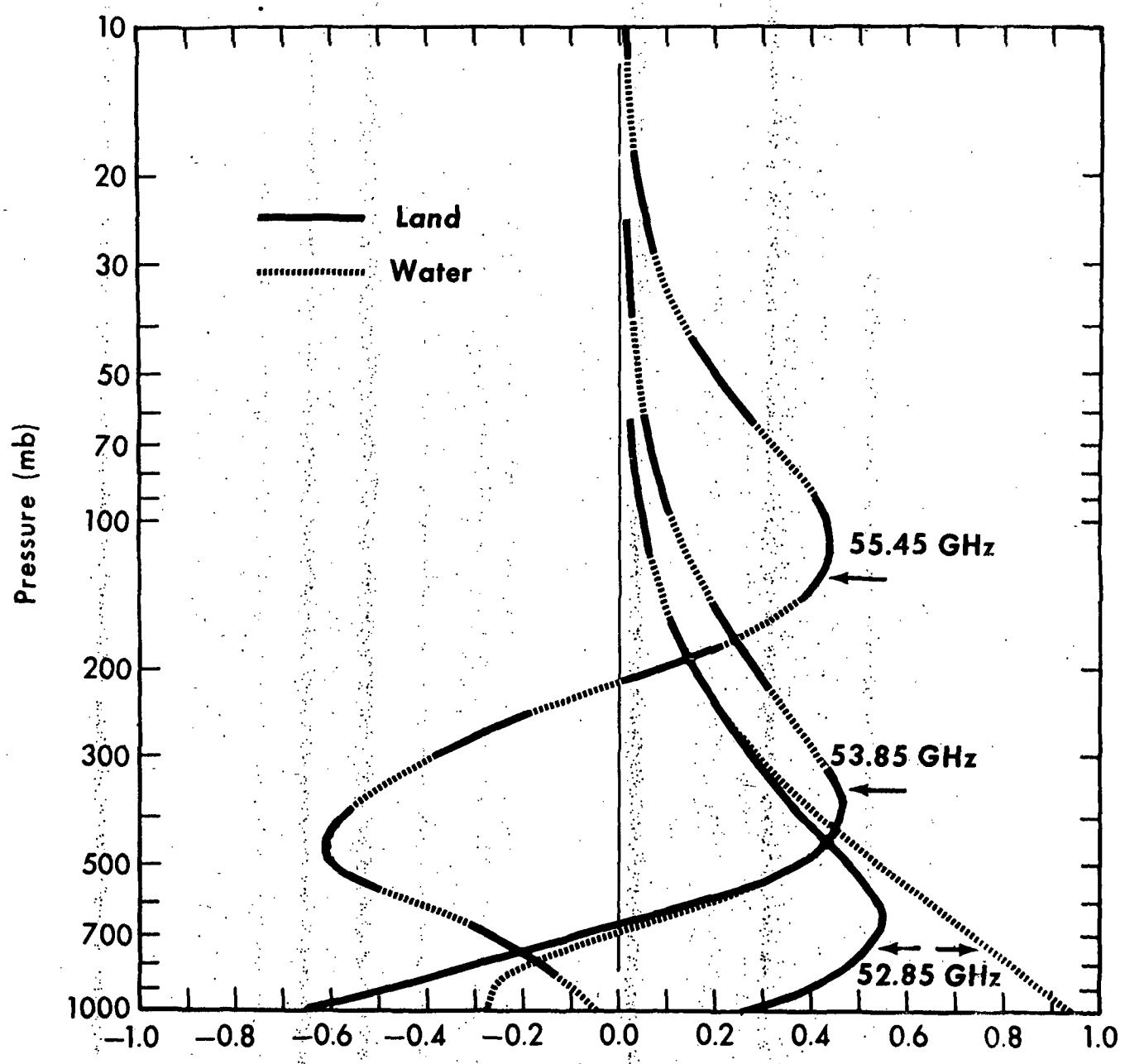


Figure 6.10. SCAMS wind weighting functions calculated for nadir, for land and sea class surfaces.

$$C_o \approx V(P_o)$$

$$C_n \approx -\frac{R}{f} \int_{\ln P_o}^{\ln P} a_n(P)\, d\ln P = -\frac{g}{f} b_n(P) \qquad (10)$$

Application of microwave derived winds in numerical analysis and prediction has not been explored, although the wind weighting function concept suggests new methods for exploiting the gradient information in the oxygen channels.

6.3.2 Atmospheric Water Vapor and Liquid Water Determinations Over Oceans

At frequencies near 22 GHz the variations in signal caused by changes in atmospheric temperature are inconsequential as compared to variations caused in transmittance. In the hypothetical case of an isothermal earth-atmosphere system with temperature T_o, the radiative transfer solution can be written as

$$T_B = T_o \left[1 - \tau_\nu^{2\mathrm{Sec}\theta} (1 - \varepsilon_s) \right] \qquad (11)$$

where τ_ν is the total vertical atmospheric transmittance (due to water vapor and liquid water). As Grody (1976) shows, even such a simple model incorporates most of the important radiative transfer effects for frequencies below 40 GHz. Thus, three atmospheric parameters essentially determine the response of a radiometric channel. These are the column water vapor content, column liquid water, and the wind speed near the ocean surface. This last parameter affects the brightness temperature in two ways; wind-generated whitecaps and foam increase the surface emissivity, and surface roughness causes emission from a distribution of zenith angles (peaking

in the specular direction) to be reflected toward the radiometer. Because of the variability in sea surface emission, generally measurements at more than two frequencies are required for the unambiguous determination of water vapor and liquid water, based on the different spectral characteristics for water vapor absorption, liquid water absorption and sea surface emission. However, under fairly general conditions 2 channels are sufficient. For example, several investigators (eg. Staelin et al. (1976)) have applied SCAMS 22 and 31 GHz brightness temperatures to estimate the water vapor and liquid water over areas having relatively unperturbed sea surfaces.

Figure 6.11 shows the percent increase in sea surface emissivity as a function of wind speed for different viewing angles; based on extrapolation of experimental data (Stogryn, 1971). For sea surface winds below 10 m/sec the emissivity perturbations are negligible compared to the atmospheric effects on brightness temperature. Hence, except for large scale intense disturbances, the water vapor and liquid water are the most significant synoptic scale features exhibited by radiometric observations around 22 GHz. Based on Eq.(11) and the dependence of atmospheric transmittance on water vapor and liquid water, the water parameters are derivable from dual frequency brightness temperature measurements as shown below.

The total transmittance is a product of the water vapor and liquid water droplet transmittances (neglecting the near unity oxygen transmittance component),

$$\tau_\nu = \tau_\nu\ (H_2O) \cdot \tau_\nu\ (Liq) \qquad (12)$$

and the water vapor transmittance can be approximately* expressed in terms of the integrated water vapor in a column W,

---

* The largest standard error in the transmittance model occurs at 22.23 GHz with a value of 10^{-2}, which is mainly due to variations in water vapor distribution with altitude.

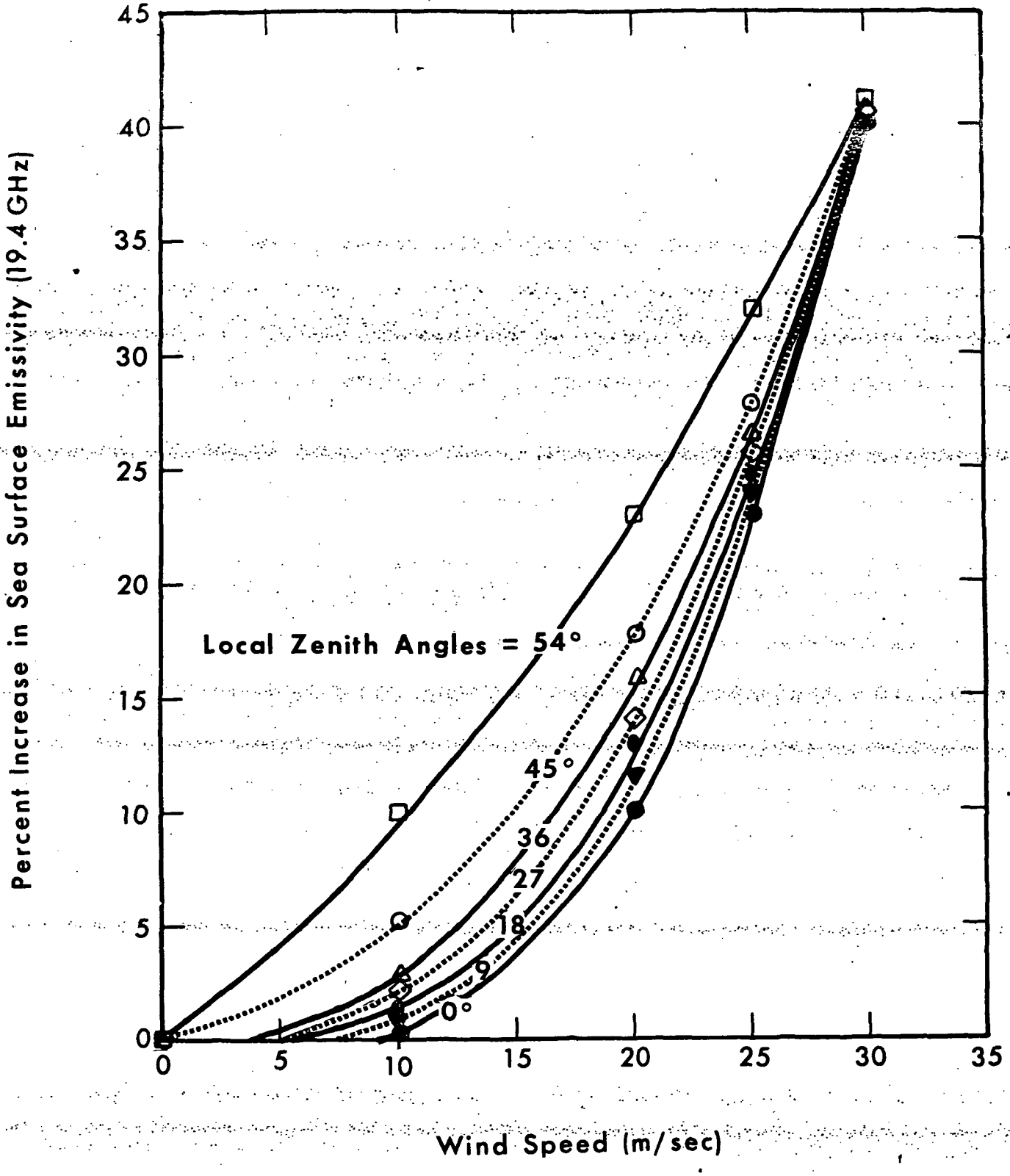


Figure 6.11. Increase in sea surface emissivity (19.4 GHz) as a function of wind speed (m/sec) for different local zenith angles, for SCAMS antenna polarization. (After Stogryn, 1971)

$$\tau_\nu\ (H_2O) = e^{-W/W_o(\nu)};\ W \text{ in } g/cm^2 \qquad (13)$$

where $W_o(\nu)$ is a frequency dependent quantity (see Figure 6.12), reaching a maximum of about 18 g/cm^2 at the center of the 22 GHz water vapor line and increasing on either side of the resonance.

For frequencies below 50 GHz and water droplets smaller than 50 microns (corresponding to non-precipitating clouds) the liquid water cloud transmittance is approximated by the Rayleigh limit. In this limit, absorption depends only on the total liquid water volume and not on the distribution of droplet sizes. Thus

$$\tau_\nu\ (Liq) = e^{-Q/Q_o(\nu)};\ Q \text{ in } Kg/m^2 \qquad (14)$$

where $Q_o(\nu)$ decreases monotonically with increasing frequency (see Figure 6.12), and also depends on the mean cloud temperature (Staelin, 1966).

It should be recognized that absorption of radiation due to ice clouds is about two orders of magnitude less than liquid water cloud of the same water content and is therefore neglected. Also, whereas rain absorption is greater than that of liquid water clouds of the same water content, for the present purpose precipitation effects are neglected by assuming that the area of precipitation is small compared to the instrument's field of view. This assumption is valid for the majority of synoptic scale observations made with the SCAMS and NEMS instruments. In principle the different characteristics of precipitating drops compared to that of small suspended cloud droplets should enable some separation of the two constituents using multispectral measurements. This is not readily possible with current instruments, but requires a multichannel high resolution spectrometer.

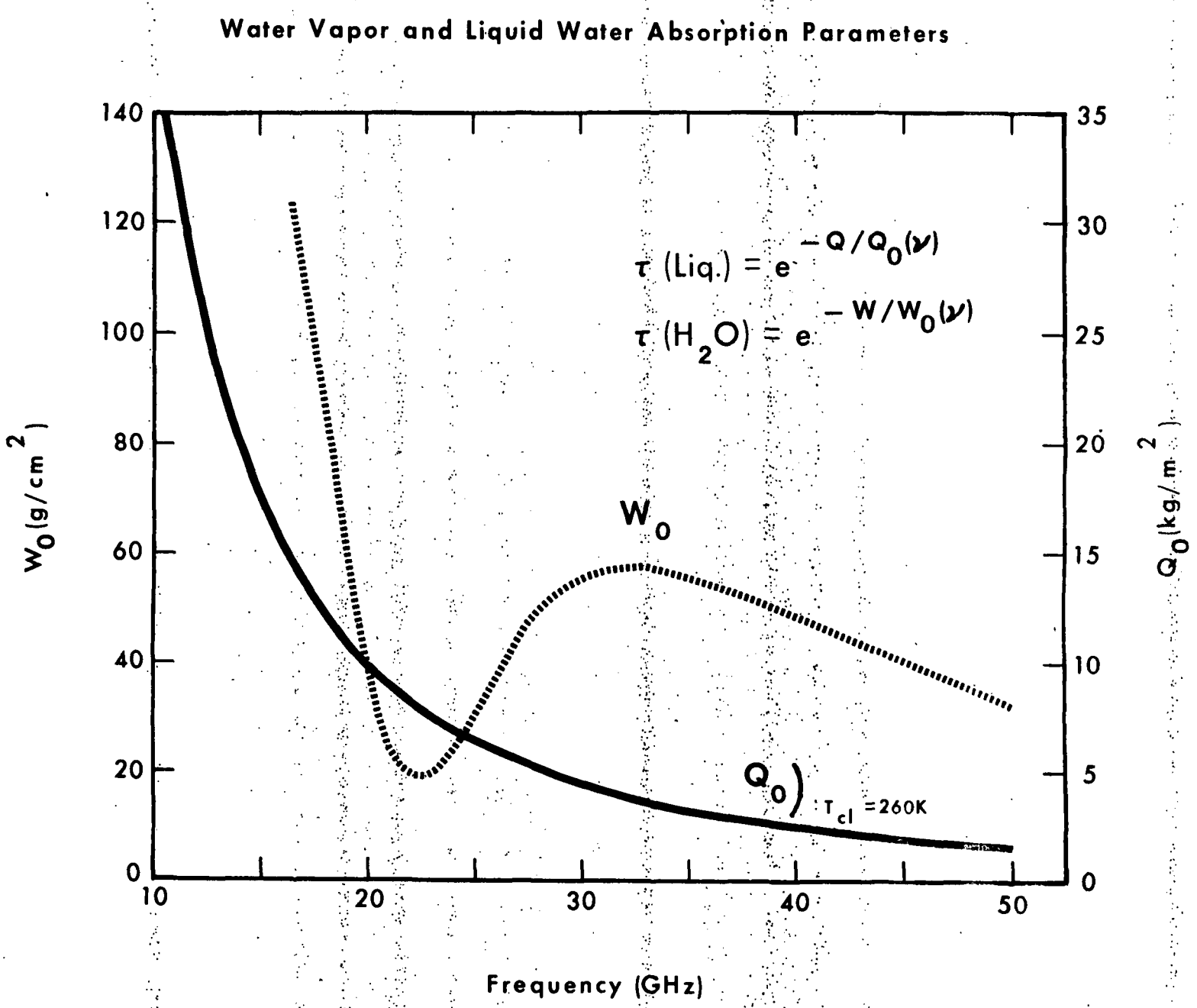


Figure 6.12. Water vapor and liquid water absorption parameters as a function of frequency.

For water vapor less than 18 g/cm^2 and liquid water less than about 5 kg/m^2 the transmittances (13) and (14) can be linearized so that equation (11) can be approximated

$$T_B(\nu) \cong \varepsilon_s T_o + 2 \left[\frac{Q}{Q_o(\nu)} + \frac{W}{W_o(\nu)} \right] (1-\varepsilon_s) T_o \mathrm{Sec}\theta \quad (15)$$

Thus brightness temperature measurements at two frequencies enable the determination of Q and W, given reasonable estimates of the temperature T_o, surface emissivity ε_s, and mean cloud temperature (contained in Q_o and only needed for liquid water determination). The solution has the general form

$$W = \omega_o + \omega_1 T_B(\nu_1) + \omega_2 T_B(\nu_2) \quad (16a)$$

$$Q = q_o + q_1 T_B(\nu_1) + q_2 T_B(\nu_2) \quad (16b)$$

where $T_B(\nu_1)$ and $T_B(\nu_2)$ are the brightness temperatures at frequencies ν_1 and ν_2. The coefficients ω_i and q_i depend on the frequencies chosen, the averaged temperature near the surface and the emissivity (q_i also depends on mean cloud temperature). Note from (15) that the coefficients weighting the brightness temperatures are simply related to the absorption parameters by the relationships,

$$\omega_1/\omega_2 = W_o(\nu_1)/W_o(\nu_2) \ , \ q_1/q_2 = Q_o(\nu_1)/Q_o(\nu_2).$$

The form of Eq. (16) suggests the use of a statistical linear regression solution with brightness temperatures as predictors, where the coefficients contain the variations in temperature and emissivity of the dependent data sample.

Table 6.1 lists the residual errors obtained from simulations using the exact radiative transfer equation (Rosenkranz et al. 1972; Grody, 1976). A small improvement over the linear estimate is obtained by inclusion of a term that is quadratic in 22 GHz brightness temperature. A crude simulation of the effects of occasional ocean roughness and foam cover is given in the righthand column of the table, where the surface emissivity was increased by 10% in 20% of the statistics. This is probably a pessimistic estimate of the effects of sea state. Staelin et al. (1976) compared actual NEMS retrievals of water vapor with radiosonde measurements from island stations. They found standard deviations of 0.12 g/cm^2 for the NEMS-radiosonde differences in January 1973, and 0.44 g/cm^2 in June 1973. The higher value in June was attributed to a greater occurrence of small-scale structure in the humidity. No improvement due to the addition of nonlinear terms was evident in the NEMS-radiosonde comparison. As in the case of temperature retrievals, the water vapor is accurately determined using simulated coefficients, substantiating again the independence of microwave results to auxiliary data.

The examples of SCAMS derived water vapor shown in Figure 6.5 were obtained as described by Grody (1976) and are comparable with the indicated radiosonde measurements. Any large differences between SCAMS and radiosonde observations are probably due to the horizontal resolution problem, i.e. radiosondes obtain point measurements while SCAMS results are averaged over an approximate 200 km linear dimension. Nevertheless, the good spatial coverage of the SCAMS delineates detailed structure which is only suggested by the limited radiosonde observations. Unlike the relatively smooth changes in temperature, water vapor variations can be highly variable, and as such are difficult to analyze based on the limited conventional data coverage. The detailed spatial and temporal variations should play an important role in initializing forecast models for predicting

Parameter/ form of estimate	RMS residual errors (g/cm^2)	
	smooth sea surface	varied sea surface
water vapor/ linear	0.19	0.32
water vapor/ quadratic	0.13	0.24
liquid water/ linear	0.006	0.012

Table 6.1. Simulation results for water vapor and liquid water retrievals using 22 and 31 GHz.

precipitation. The application of water vapor measurements for monthly and seasonal averages has not been previously considered due to insufficient conventional data coverage. However, with the availability of microwave data it is now possible to map the global distribution of water vapor over the oceans with sufficient detail to be an important factor in determining climatic variations in the water transport cycle. Figure 6.13 shows the SCAMS derived water vapor for a two week period through August-September 1975 (upper) and during February 1976 (lower). The shaded areas in the tropics contain water vapor in excess of 45 mm (4.5 g/cm^2). In the mid-latitude the shaded area includes water vapor less than 15 mm (1.5 g/cm^2). These data for the first time furnish the meteorologist with detailed information concerning the water vapor distribution over the oceans. The maps indicate large inhomogeneity over the tropics. Consider for example, that the mean tropical atmosphere (Riehl, 1954) has a value of 46 mm and note the fraction of the tropics where this value is exceeded as shown by the shaded areas of the maps. Very moist areas with values in excess of 55 mm occur over the western parts of the Pacific; during winter over Indonesia - New Guinea and during summer near the Philippines and Taiwan. Conversely, many areas are considerably drier than the mean. In particular, the dry zone of the equatorial Pacific exhibits water vapor less than 35 mm. This dry zone extends from the equator southeastward towards South America, reflecting the subsiding dry air of the South Pacific trades which were particularly strong during these periods. Also of interest is the water vapor variation along the west coast of South America between summer and winter.

6.4 Recommendation for High Resolution Instruments

Satellite borne microwave radiometry is comparatively new in relation to the more traditional infrared and visible techniques. Its potential use in meteorology has been only partially explored with the Nimbus 5 and Nimbus 6 microwave

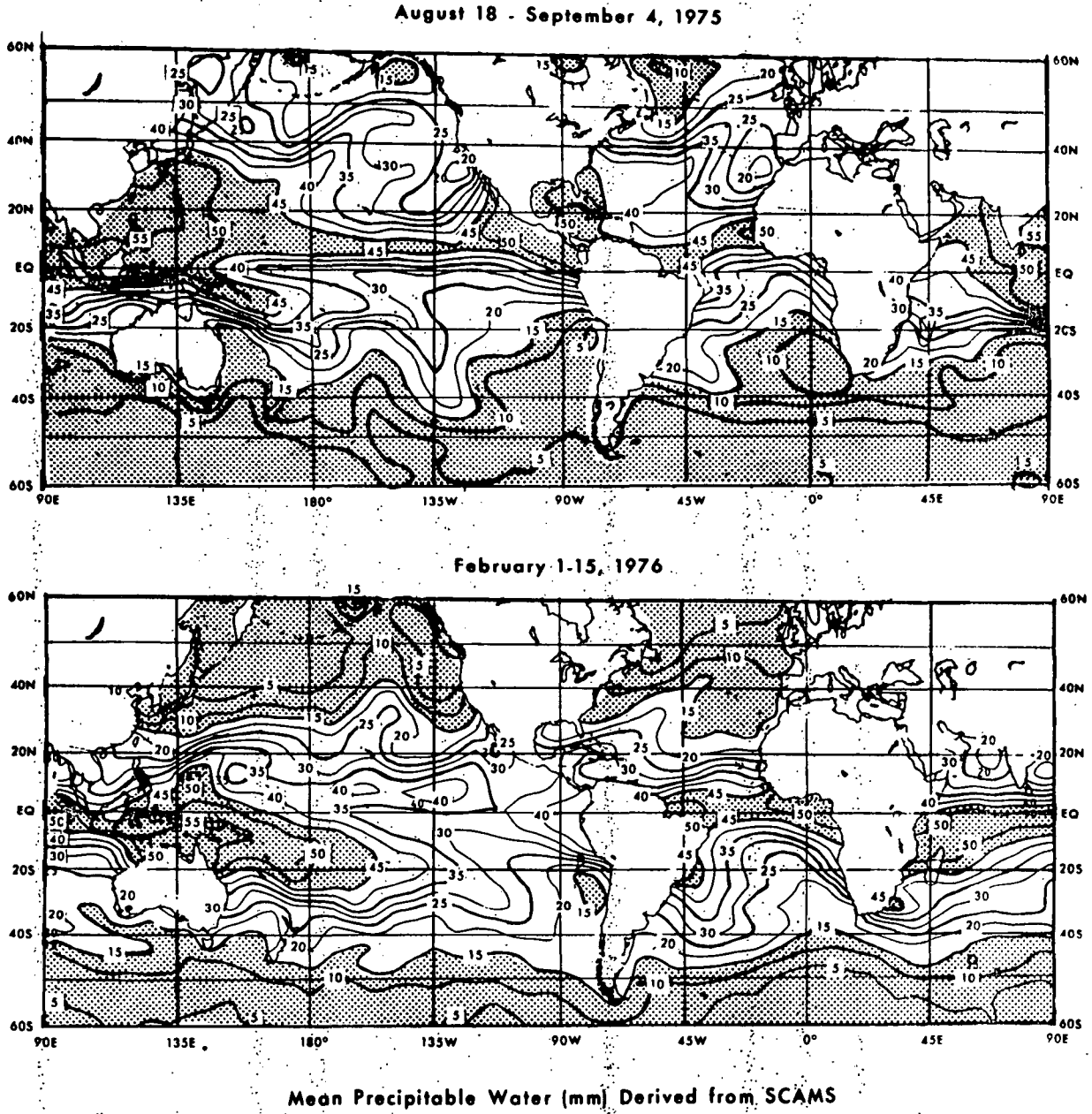


Figure 6.13. SCAMS retrieved precipitable water (mm) averaged over a two week period through August-September, 1975 (Upper) and during February 1976.

instruments. A major limitation of current microwave sensors is the relatively poor horizontal resolution compared with the infrared and visible counterparts. However, it is technically feasible to develop satellite instruments with as small as 5 km horizontal resolution for temperature sounding at polar orbiting altitudes; slightly coarser resolution (10 km) is practical for water vapor and liquid water observations. This limitation is simply based on spacecraft antenna size, as discussed in Chapter 8.

The need for high resolution data is obvious when one recognizes that the main virtue of the microwave technique resides in its capability of probing both large and small scale cloud shielded weather phenomena. The lack of insufficient resolution was well dramatized by the SCAMS observations made through Typhoon June by Rosenkranz et al. (1978) (see Chapter 5). It was found that the 200 km SCAMS resolution was inadequate for resolving the complete storm structure, and resulted in underestimates of the temperature anomaly near the storm center. Even for moderate disturbances such as frontal systems, the limited SCAMS resolution can smooth out large temperature gradients as evidenced by the radiosonde comparison made over Europe shown in Figure 6.8. The strong 700 mb temperature gradients around the leading and trailing edge of the trough appear smoothed in the SCAMS temperature analysis. In this case however, the question remains: how much of the horizontal smoothing is due to vertical resolution problems? The separation of these effects is complicated by SCAMS' large field of view which smooths horizontal temperature gradients, and the need for better weighting functions to improve the vertical resolution.

Spatial variations of liquid water and water vapor normally exceed temperature variations (e.g. in tropical regions temperatures vary less than 1 K). Convective storms are highly localized and can only be properly analyzed using high resolution data; liquid water data are essentially meaningless

if the instrument cannot resolve precipitating areas from non-precipitating cloudy regions. The coarse spatial averaging of the NEMS and SCAMS instruments prevented any quantitative estimates of precipitation. The 25 km ESMR resolution allowed such observations but even the ESMR precipitation estimates are questionable in cases of squall lines whose accompanying thunderstorm cells are usually less than 5 km in horizontal extent.

6.5 Acknowledgments

The author wishes to thank Dr. C. M. Hayden for his support and encouragement during the course of this investigation. Mr. P. P. Pellegrino is gratefully acknowledged for providing much of the SCAMS data analysis. Information supplied by Messrs. A. Krueger and Dr. W. C. C. Chen was particularly valuable.

6.6 BIBLIOGRAPHY

Allison, L. J., E. B. Rodgers, T. T. Wilheit, and R. W. Fett, 1974: Tropical cyclone rainfall as measured by the Nimbus 5 electrically scanning microwave radiometer. Bull. Amer. Meteor. Soc., 55, 1074-1089.

Anderson, R. K., 1974: Application of meteorological satellite data in analysis and forecasting. ESSA Tech. Rep. NESC 51.

Backus, G., and F. Gilbert, 1970: Uniqueness in the inversion of inaccurate gross earth data. Phil. Trans. Roy. Soc. London, 260, 123-192.

Gloerson, P., T. T. Wilheit, T. C. Chang, W. Nordberg, and W. J. Campbell, 1974: Microwave maps of the polar ice of the Earth. Bull. Amer. Meteor. Soc., 55, 1442-1448.

Gloerson, P., and F. T. Barath, 1977: A scanning multichannel microwave radiometer for Nimbus-G and Sea Sat-A. IEEE Jour. Oceanic Engr., Vol. OE-2, 172-178.

Green, R., G. Hughes, C. Novak, and R. Schreitz, 1975: The automatic extraction of wind estimates from VISSR data. Contained in NOAA Tech. Memo. NESS 64, 94-110.

Grody, N. C., 1976: Remote sensing of atmospheric water content from satellites using microwave radiometry. IEEE Trans. Ant. Propagat., Vol. AP-24, 155-162.

Grody, N. C., and P. P. Pellegrino, 1977: Synoptic scale studies using the Nimbus-6 scanning microwave spectrometer. J. Appl. Meteor., vol. 16, 816-826.

Hayden, C. M., 1976: The use of radiosondes in deriving temperature sounding from the Nimbus and NOAA satellite data. NOAA Tech. Memo. NESS 76, 19 pp.

Liebe, H. J., 1969: Calculated tropospheric dispersion and absorption due to the 22-GHz water vapor line. IEEE Trans. Ant. Propagat., Vol. AP-17, 621-627.

Liebe, H. J., 1977: Atmospheric oxygen microwave spectrum - experiment versus theory, IEEE Trans. Ant. Propagat., vol. AP-25, 327-335.

Riehl, H., 1954: Tropical Meteorology. McGraw Hill, New York.

Rosenkranz, P. W., F. T. Barath, J. C. Blinn, E. J. Johnston, W. B. Lenoir, D. H. Staelin, and J. W. Waters. Microwave radiometric measurements of atmospheric temperature and water from an aircraft. J. Geophys. Res. 77, 5833-5844, 1972.

Rosenkranz, P. W., 1975: Shape of the 5 mm oxygen band in the atmosphere. IEEE Trans. Ant. Propagat., Vol. AP-23, 498-506.

Rosenkranz, P. W., D. H. Staelin, N. C. Grody, 1978: Typhoon June (1975) viewed by a scanning microwave spectrometer. J. Geophys. Res., in press.

Ruprecht, E., and W. M. Gray, 1976: Analysis of satellite-observed tropical cloud clusters, 11. Thermal, moisture and precipitation. Tellus XXVIII, 5, 414-425.

Schmugge, T. J., J. M. Meneely, A. Rango, and R. Neff, 1977: Satellite microwave observations of soil moisture variations. Water Res. Bull., Vol. 13, 265-281.

Staelin, D. H., 1966: Measurements and interpretation of the microwave spectrum of the terrestrial atmosphere near 1 centimeter wavelength. J. Geophys. Res. 71, 2875-2881.

Staelin, D. H., A. L. Cassel, K. F. Kunzi, R. L. Pettyjohn, R. K. L. Poon, R. W. Rosenkranz, and J. W. Waters, 1975: Microwave atmospheric temperature sounding: Effects of clouds on the Nimbus-5 satellite data. J. Atmos. Sci., 32, 1970-1976.

Staelin, D. H., K. F. Kunzi, R. L. Pettyjohn, R. K. L. Poon, and R. W. Wilcox, 1976: Remote sensing at atmospheric water vapor and liquid water with the Nimbus 5 microwave spectrometer. J. Appl. Meteor., Vol. 15, 1204-1214.

Stogryn, A., 1972: A study of radiometric emission from a rough sea surface. NASA CR-2088, 47.

Tracton, S. T., and R. D. McPherson, 1977: On the impact of radiometric data upon operational numerical weather prediction at NMC. Bull. Amer. Meteor. Soc., 58, 1201-1209.

Waters, J. W., K. F. Kunzi, R. L. Pettyjohn, R. K. L. Poon, and D. H. Staelin, 1975: Remote sensing of atmospheric temperature profiles with the Nimbus 5 microwave spectrometer. J. Atmos. Sci., 32, 1953-1969.

CHAPTER 7

APPLICATIONS OF HIGH RESOLUTION PASSIVE MICROWAVE SATELLITE SYSTEMS TO THE STRATOSPHERE, MESOSPHERE, AND LOWER THERMOSPHERE*

7.1 Summary

Earth's upper atmosphere involves complex chemistry, photochemistry, and transport processes. Although significant progress has been recently made in understanding these processes, much uncertainty still remains. Measurements of several parameters are needed. Of particular importance at the present time are measurements which can improve our knowledge of how man's increasing technological activities may threaten Earth's protective ozone layer. That this threat warrants concern has been well established.

Microwave techniques have recently been applied to upper atmospheric measurements. Results from ground-based and aircraft-based experiments have established the techniques as both feasible and valuable for upper atmospheric measurements. Microwave experiments on satellites, although principally oriented towards tropospheric and surface measurements, have established the feasibility of performing such experiments from spacecraft.

High resolution satellite microwave systems can allow, for the first time, the application of limb sounding techniques at microwave wavelengths. These techniques provide very substantially improved sensitivities and vertical resolution over down-looking experiments. With such techniques several important measurements can be performed with existing technology. The extension of microwave technology to submillimeter wavelengths will allow many more important measurements to be made. The normal observation mode of these techniques, measurements of atmospheric thermal emission, allows continuous global coverage.

Recommendations for future satellite microwave systems for upper atmospheric applications must include considerations of which measurements are likely to still be needed after the three or four years normally required to develop such a system. This consideration is particularly difficult for stratospheric research as the measurement priorities will continue to change as new measurements are made and theoretical understanding is improved. Nevertheless there are particular measurements which we can say with confidence will be needed four years hence. For the mesosphere and lower thermosphere, it is easier to predict which measurements will still be of value four years hence simply because so little is now known of the details of the physical processes in these higher regions and very few measurements exist. In these regions microwave techniques are particularly well-suited because the spectral lines observed remain in thermal equilibrium throughout the region and the widths of the lines are well suited for the instrumentation.

Taking into account all of these considerations we recommend the following two areas as being appropriate for immediate support:

1. Development of a versatile microwave limb sounder for research use on Shuttle sortie missions or on a free flier satellite.

---

*Prepared by J. W. Waters and S. C. Wofsy.

2. Development of technology for space-qualifiable heterodyne radiometers in the 100 to 3000 GHz spectral range.

The microwave limb sounder instrument should have an antenna of at least 1 meter diameter in order to give better than 3 km vertical resolution at frequencies of 200 GHz and above. It should be capable of accommodating several radiometers for simultaneous measurement of several species. The radiometers should be modularly constructed so they can be easily exchanged as measurement priorities evolve and technology advances. Initial measurements with this instrument in the 100-250 GHz range where technology presently exists should include O_2 in the lower thermosphere where it is dissociated, temperature and winds in the mesosphere and lower thermosphere, and precision measurements of stratospheric ozone profiles. The radiometer used for the ozone measurements can also be used simultaneously for ClO and H_2O_2 if measurements of these species are still required. O_3, H_2O and CO in the mesosphere and lower thermosphere should also be measured. The overall instrument should be constructed so that instruments in other spectral regions, e.g., the infrared, can easily be boresighted with it for simultaneous complementary measurements.

A thorough analysis, including numerical simulations, should be performed to verify that ozone profiles can be monitored to 1 percent accuracy with these techniques. Optimum spectral lines for the measurements should also be verified.

Development of submillimeter heterodyne radiometers up to 3000 GHz frequency will allow measurement of many more important species in the stratosphere, mesosphere, and lower thermosphere. These include O, OH, NO, and many others. Improvement of the present sensitivity of spaceworthy radiometers in the 100-250 GHz frequency range should also be a goal. An overall goal for the receiver sensitivity should be that the system noise temperature in Kelvins equals the frequency in GHz.

The laboratory spectroscopy required to support measurements in the submillimeter range should be defined and performed.

Figures 7.1 and 7.2 outline the summary and recommendations.

7.2 Earth's Upper Atmosphere: A Summary Description

The atmospheric region considered here covers altitudes between about 15 and 150 km which includes the stratosphere, mesosphere and lower thermosphere. In this regions there are important interactions with the troposphere below and with the magnetosphere above. Absorption and emission of radiation occur over a wide range of the electromagnetic spectrum, a large variety of minor constituents playing a part in the radiative transfer processes. The distribution of these minor constituents is in turn determined by many chemical and photochemical reactions and by atmospheric motions on both the small scale and the very large scale. Because of this complex interplay between radiative, chemical and dynamical processes, it is a very interesting part of the

HIGH RESOLUTION SATELLITE MICROWAVE SYSTEMS FOR UPPER ATMOSPHERIC APPLICATIONS

SUMMARY

- THERE IS MUCH UNCERTAINTY IN OUR PRESENT UNDERSTANDING OF THE PHYSICAL AND CHEMICAL PROCESSES IN EARTHS STRATOSPHERE, MESOSPHERE, AND LOWER THERMOSPHERE. MANY MEASUREMENTS ARE NEEDED TO IMPROVE THIS UNDERSTANDING.
  - OF PARTICULAR IMPORTANCE ARE MEASUREMENTS TO IMPROVE KNOWLEDGE OF HOW MAN'S INCREASING TECHNOLOGICAL ACTIVITIES MAY AFFECT EARTH'S PROTECTIVE OZONE LAYER.
  - LONG-TERM PRECISION MEASUREMENTS OF STRATOSPHERIC OZONE AND TEMPERATURE ARE NEEDED.
- HIGH RESOLUTION SATELLITE MICROWAVE SYSTEMS WILL, FOR THE FIRST TIME, MAKE POSSIBLE THE USE OF LIMB SOUNDING TECHNIQUES IN THE MICROWAVE SPECTRAL RANGE. MICROWAVE LIMB SOUNDING TECHNIQUES CAN PROVIDE VALUABLE AND UNIQUE MEASUREMENTS OF THE STRATOSPHERE, MESOSPHERE, AND LOWER THERMOSPHERE.
- A VERSATILE MICROWAVE LIMB SOUNDER INSTRUMENT SHOULD BE DEVELOPED FOR RESEARCH USE ON SHUTTLE SORTIE MISSIONS OR ON FREE-FLIERS.
- MICROWAVE TECHNOLOGY SHOULD BE ADVANCED TO THE SUBMILLIMETER WAVELENGTH REGION SO THAT MANY IMPORTANT UPPER ATMOSPHERIC SPECIES CAN BE MEASURED.

Figure 7.1: High Resolution Satellite Microwave Systems for Upper Atmospheric Applications: Summary

HIGH RESOLUTION SATELLITE MICROWAVE SYSTEMS FOR UPPER ATMOSPHERIC APPLICATIONS

RECOMMENDATIONS

DEVELOP A MICROWAVE LIMB SOUNDER INSTRUMENT USING PRESENT TECHNOLOGY FOR VERSATILE USE ON EITHER SHUTTLE SORTIE MISSIONS OR ON A FREE-FLIER

- IT SHOULD HAVE AN ANTENNA OF AT LEAST 1 METER DIAMETER TO GIVE BETTER THAN ~3 km VERTICAL RESOLUTION AT FREQUENCIES ABOVE 200 GHz, AND SHOULD BE CAPABLE OF ACCOMODATING SEVERAL RADIOMETERS
- IT SHOULD BE USED INITIALLY FOR MEASUREMENTS OF O_2 DISSOCIATION, PRECISION PROFILES OF O_3, TEMPERATURE AND WINDS IN THE MESOSPHERE AND LOWER THERMOSPHERE, AND PROFILES OF H_2O, ClO, H_2O_2 AND CO. THE O_3 MEASUREMENTS SHOULD BE USED TO EVALUATE THESE TECHNIQUES FOR LONG-TERM MONITORING PURPOSES
- THE RADIOMETERS FOR THIS INSTRUMENT SHOULD BE MODULARLY CONSTRUCTED SO THEY CAN BE EASILY EXCHANGED AS TECHNOLOGY ADVANCES AND MEASUREMENT PRIORITIES EVOLVE
- THE INSTRUMENT SHOULD BE DESIGNED SO THAT INSTRUMENTS IN OTHER SPECTRAL REGIONS CAN EASILY BE BORESIGHTED WITH IT FOR SIMULTANEOUS COMPLEMENTARY MEASUREMENTS

- A THOROUGH ANALYSIS SHOULD BE PERFORMED TO DETERMINE THE OPTIMUM O_3 LINES TO USE FOR PRECISION MONITORING AND THE ACCURACY WHICH CAN BE ACHIEVED

DEVELOP NEW TECHNOLOGY FOR SPACE-QUALIFIED HETERODYNE RADIOMETERS IN THE 100 TO 3000 GHz (SUBMILLIMETER) SPECTRAL RANGE

- THESE RADIOMETERS CAN CONTINUOUSLY MEASURE, ON A GLOBAL SCALE, THE FOLLOWING PARAMETERS IN EARTH'S UPPER ATMOSPHERE
  1) ABUNDANCES OF O, O_2, O_3, OH, H_2O, H_2O_2, HO_2, HNO_3, NO, N_2O, ClO, CO HCl, HF, NO_2 AND PROBABLY MANY OTHER SPECIES
  2) TEMPERATURE, WINDS, MAGNETIC FIELD, AND REFERENCE PRESSURE LEVEL
- A GOAL FOR SENSITIVITY SHOULD BE THAT THE SYSTEM NOISE TEMPERATURE IN KELVINS EQUALS THE FREQUENCY IN GHz. (HOWEVER, TEN TIMES WORSE SENSITIVITY WILL SOMETIMES BE USABLE)

- DEFINE AND PERFORM LABORATORY SPECTROSCOPY REQUIRED TO SUPPORT MEASUREMENTS WITH THESE RADIOMETERS

Figure 7.2: High Resolution Satellite Microwave Systems for Upper Atmospheric Applications: Recommendations

atmosphere scientifically. Also because important clues to our understanding of climate, climatic change and the long term evolution of the atmosphere lie in this region about which comparatively little is known, its study is of great importance to atmospheric science considered as a whole.

Figure 7.3 summarizes some of the more important physical processes occurring in the stratosphere, mesosphere, and lower thermosphere. There are three major sources of heating in this region, and in the troposphere below it, which account for the temperature profile with altitude as shown in Figure 7.3 Earth's surface absorbs visible solar radiation and provides heating from below. The stratospheric ozone layer absorbs solar ultraviolet (UV) radiation between about 200 and 300 nm, producing the temperature maximum near 50 km altitude and protecting life in the biosphere from the damaging UV. Above 90 km, in the lower thermosphere, molecular oxygen (O_2) produces heating by absorption of solar ultraviolet radiation. The solar radiation of wavelength less than 242 nm dissociates molecular oxygen into atomic oxygen (O). The oxygen atoms then recombine with molecular oxygen, in the presence of a third molecule (required for conservation of energy and momentum) to form ozone. This mechanism is responsible for the formation of the stratospheric ozone layer. Ozone molecules are destroyed through several chemical and photochemical processes; these processes are described further in Section 7.3 below. Solar energetic particles also interact with the atmosphere in the region of the mesosphere and lower thermosphere and may be important in certain chemical schemes.

7.3 Major Problems Related to the Stratosphere, Mesosphere, and Lower Thermosphere

The most important problem of this region of the atmosphere at present is to obtain an adequate understanding of the processes by which the stratospheric ozone layer is maintained. The ozone layer protects life on Earth from damaging ultraviolet (UV) radiation of wavelengths shorter than about 300 nm. It has been recently realized that man's increasing technological activities could affect the balances by which the ozone layer is maintained and thus perturb the amount of UV reaching the biosphere. Studies by the National Academy of Sciences [1975, 1976] have indicated that a 1% reduction in ozone would increase the amount of UV radiation at Earth's surface by 2%. The studies also reasonably well establish that a 5% decrease in ozone could cause an increase of between 20,000 and 60,000 non-melanoma human skin cancer cases per year in the U.S. alone. Additional deleterious effects from increased UV exposure could include damage to the nucleic acids which store and transmit genetic information and to proteins which form part of enzymes and membranes. Such damage prevents these molecules from properly performing their biological functions, to the detriment of the living system in which they reside. Increased UV exposure is also expected to adversely affect photosynthesis in plants. However, it must be emphasized that the magnitude of the effects on plants, and on animals through damage

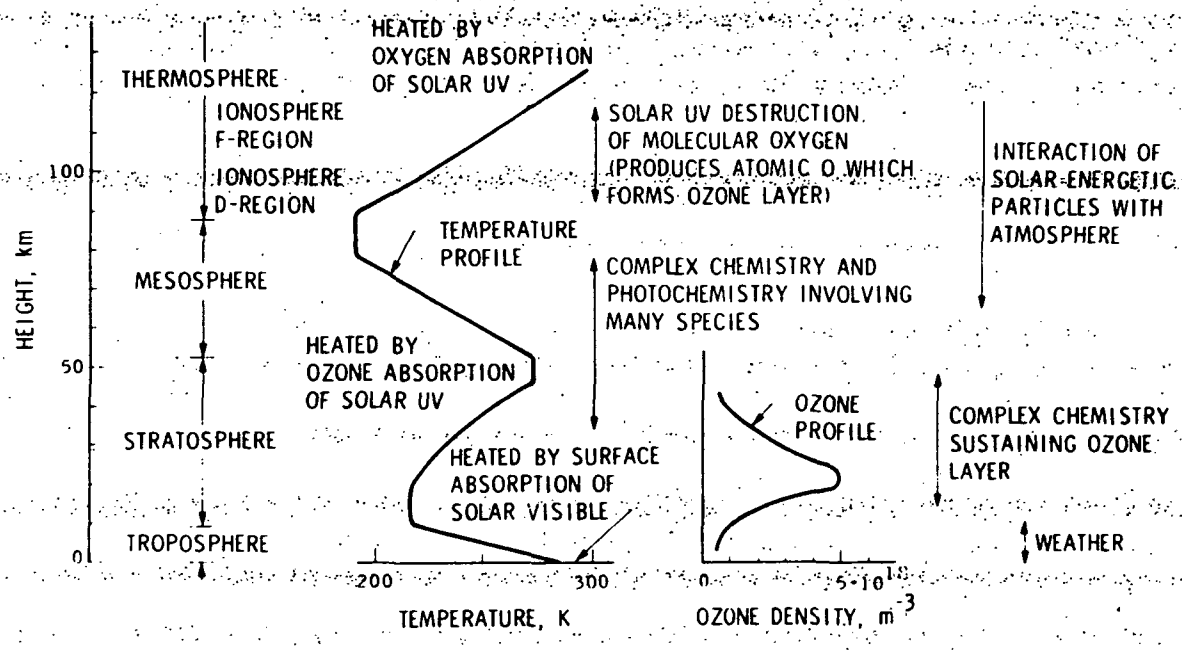


Figure 7.3: Earth's Atmosphere

to macromolecules, is presently unknown. Reduction in the ozone layer could also have significant effects on climate, both indirectly due to additional UV and visible radiation reaching the surface and producing increased heating there, and directly due to decreased heating in the stratosphere. Quantitative evaluations are, to date, insufficiently precise to establish the magnitude, or even the sign of the climatic influence.

Ozone molecules are continually being produced and destroyed in the upper atmosphere; the net amount being determined by equilibrium between the production and destruction mechanisms. Figure 7.4 summarizes the chemical schemes presently thought to be dominant in establishing this equilibrium. Ozone is produced naturally by the combination of O_2 and O, where the O is formed by photodissociation of O_2 in the lower thermosphere. Ozone is destroyed by direct reaction with O and through catalytic reactions involving nitrogen, hydrogen, and chlorine compounds. The formation of ozone and its destruction by reaction with $O(^3P)$ was postulated by Chapman in 1930. The destruction of ozone through catalytic reactions with oxides of hydrogen was postulated by Bates and Nicolet in 1950, and destruction through reactions with oxides of nitrogen postulated by Crutzen in 1970. In 1974 Molina and Rowland drew attention to the potential destruction of ozone by catalytic reactions involving chlorine liberated from industrial usage of stable chlorine compounds.

Estimates based on theoretical calculations suggest that the destruction of stratospheric ozone by combination with oxygen atoms may account for about 20% of the natural destruction of ozone, reactions with hydrogen oxides for about 10%, and reactions with nitrogen oxides for 50-70% [e.g., Department of the Environment, 1976]. This leaves a possible 0-20% to be accounted for by other mechanisms. The industrial usage of chlorofluorocarbons prior to 1976 may have already caused a reduction of about 2% in total ozone [Crutzen, et al., 1977]. It is worth noting that for the first forty years of stratospheric ozone research the only mechanisms considered responsible for ozone destruction are now thought to account for only about 30% of the total destruction. This should be a warning against becoming too complacent with our understanding of how man's activities may affect stratospheric ozone. In fact, since the initial writing of this paragraph the destruction budget of ozone has changed significantly due to Howard's [1977] recent measurement of a faster rate constant for the reaction $NO + HO_2 \rightarrow NO_2 + OH$; the importance of nitrogen oxides has been reduced [R. T. Watson, private communication].

Recognizing the possibility that man's activities could perturb Earth's upper atmosphere, the U.S. Congress in FY 1976 instructed NASA to "develop and implement a comprehensive program of research, technology, and monitoring of the phenomena of the upper atmosphere to provide for an understanding of and to maintain the chemical and physical integrity of Earth's upper atmosphere" [NASA Upper Atmosphere Research Office, 1976]. The overall goal of the NASA Upper Atmospheric Research Program is to acquire sufficient understanding of the physical and chemical processes occurring in the Earth's atmosphere so that (1) perturbations in the stratosphere caused by man's actions can be accurately assessed and (2) any resulting change in surface ultraviolet radiation can be determined.

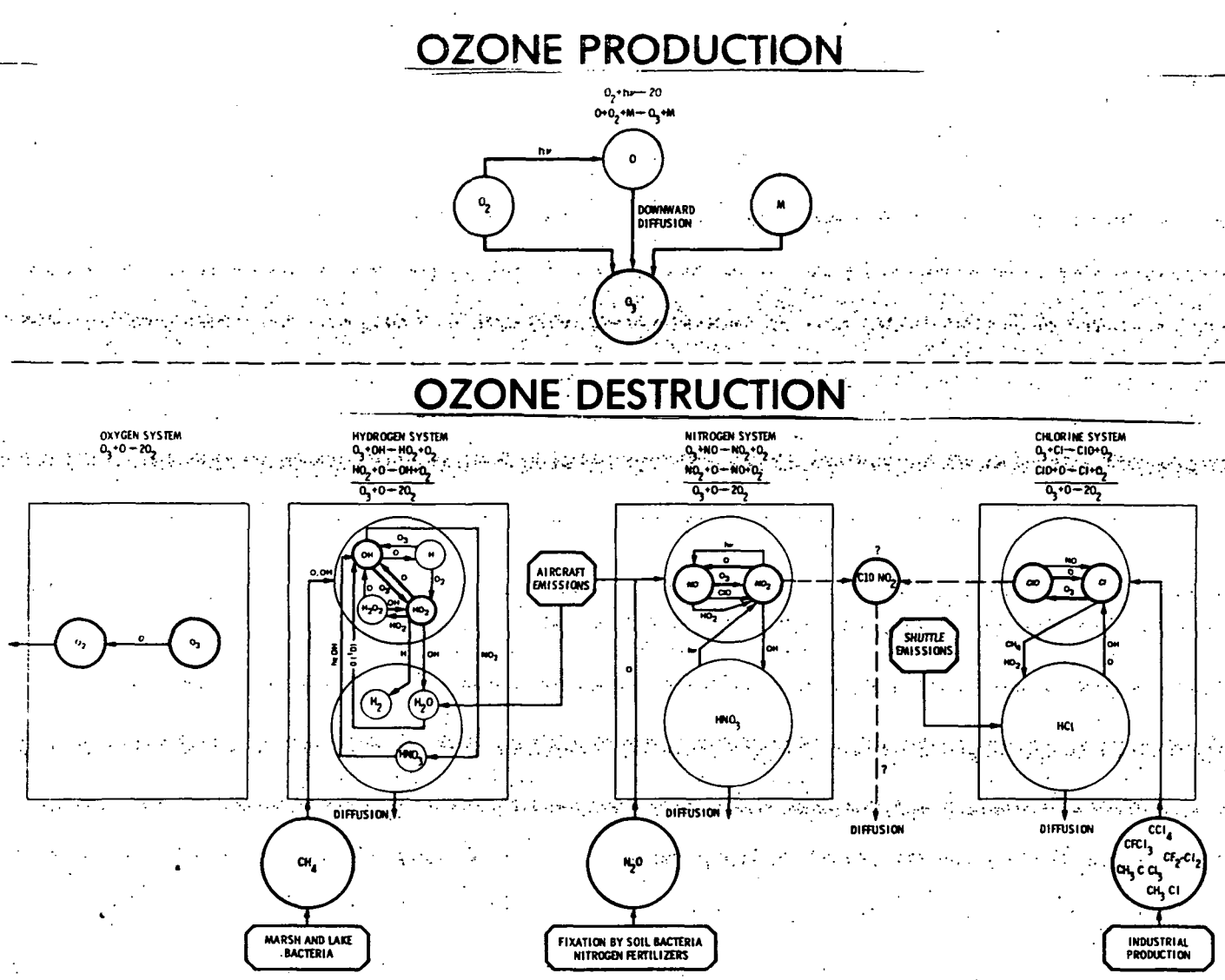


Figure 7.4: Ozone Production and Destruction

The long term objective of the NASA program is to develop an organized, solid body of knowledge of the physics, chemistry, and transport processes occurring in the stratosphere. A continuing goal is to be able to understand and evaluate potential threats to the upper atmosphere.

Three potential threats to the stratosphere have already been identified as being of sufficient concern to warrant their evaluation an immediate objective of the program. These are: chlorofluoromethane (CFM) releases, space shuttle effluents, and aircraft exhausts. The manner in which these manifestations of man's technological activities are thought to influence the processes maintaining the ozone layer are indicated schematically in Figure 7.4, and discussed below.

Chlorofluoromethanes (CFMs) are extremely stable compounds (CF_xCl_y where $x + y = 4$) used industrially, principally as refrigerants and aerosol propellants. Upon release, or leakage, into the atmosphere these stable compounds ultimately diffuse upward above the ozone layer where they are photodissociated by solar UV and liberate, among other things atomic chlorine (Cl). The Cl then catalytically destroys ozone with ClO radical formed as an intermediate step. Processes by which chlorine atoms can be removed from this catalytic cycle include reactions with hydrogen-containing trace gases to form HCl, and possibly reactions with NO_2 to form $ClONO_2$, which tie up the Cl in less reactive species, and diffuse downwards where they are washed out by rainfall. The National Academy of Sciences [1976] study concluded that continued release of CFMs at the 1973 level is calculated to given an ultimate reduction in ozone of about 7% where there is an uncertainty of about a factor of 3 in the amount of reduction. A review of the impact of CFM releases on stratospheric ozone is given by Crutzen, et al., [1977] who calculated an 8% reduction in ozone due to continued releases at the 1973 level.* Figure 7.5 gives the results of Crutzen's calculations. Note that in addition to the threat caused by chlorofluoromethanes, a serious threat due to methylchloroform, $C_2H_3Cl_3$, is also predicted. Knowledge of the CFM problem as of June 1977 is represented in the NASA publication "Chlorofluoromethanes and the Stratosphere" [NASA, 1977].

The solid rocket motors for the Space Shuttle produce two exhaust products, gaseous HCl and particulate Al_2O_3, which may interact with stratospheric processes. HCl is important, as discussed above, because it is the end product by which Cl atoms can be removed from the stratosphere. Additional HCl injected into the stratosphere would tend to perturb equilibrium conditions. Theoretical calculations predict an ozone reduction of 0.2% (with a factor of 3 uncertainty) due to the continuous launching of 60 Space Shuttles per year planned for 1983 and beyond [NASA Upper Atmospheric Research Office, 1976]. Particulate Al_2O_3 could affect stratospheric processes by serving as scattering centers for solar radiation and by providing active sites on their surfaces for the occurrence of chemical reactions.

* These calculations of ozone reduction may be revised upward by a factor of approximately 2 due to the new rate constant for the reaction $NO + HO_2 \rightarrow NO_2 + OH$ [P. J. Crutzen, private communication, 1977].

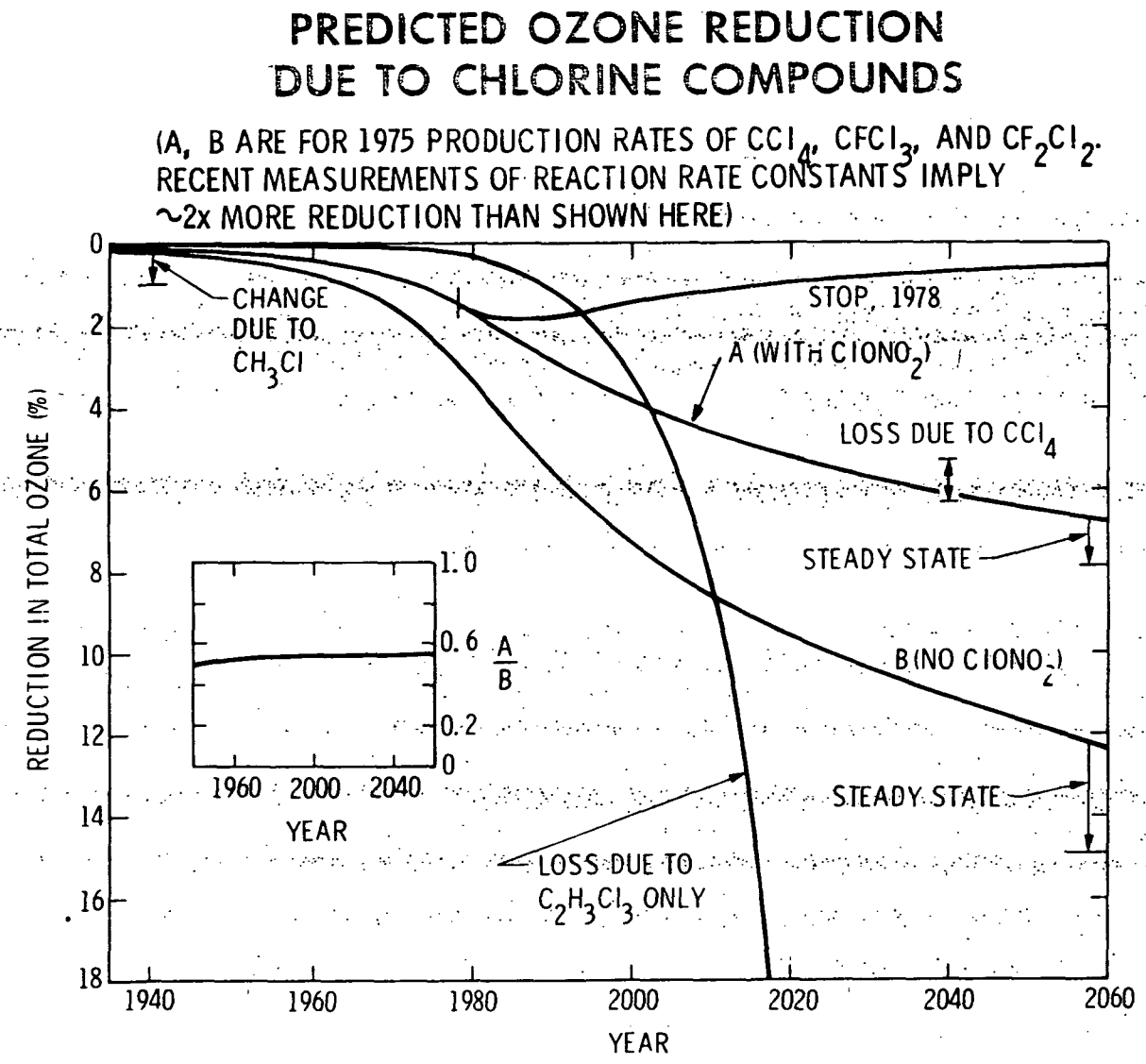


Figure 7.5: Predicted Ozone Reduction Due to Chlorine Compounds [from Crutzen, 1977].

Curve A assumes continued releases of CCl_4, $CFCl_3$, and CF_2Cl_2 at the 1975 production rate. Curve B employs the same scenario but with the omission of chlorine nitrate whose existence was only first suggested in 1976. The inset shows the ratio of the two. Also indicated is the effect of stopping production in 1978 and the loss due to $C_2H_3Cl_3$ production increasing at the present rate.

Both of these possibilities have been investigated and it is now believed that the potential is negligible for Al_2O_3 from Space Shuttle operations to affect the stratosphere [NASA Upper Atmospheric Research Office, 1976].

Aircraft flying in or just below the stratosphere emit exhaust products which can interact in the chemical schemes maintaining the ozone layer. The dominant interaction is believed due to the NO_x generated by the aircraft; additional interactions may be due to the generation of SO_2 and H_2O. Much data on this topic were obtained during the Climatic Impact Assessment Program (CIAP) sponsored by the U.S. Department of Transportation and published in a series of monographs [CIAP, 1975]. These data were reviewed by the National Academy of Sciences Climatic Impact Committee whose report [NAS, 1975] concluded there is reason for concern that projected aircraft operation could adversely affect the stratosphere. A more recent report has been prepared for the High Altitude Pollution Program (HAPP) of the U.S. Department of Transportation [Oliver, et al., 1977]. The HAPP report concludes that for subsonic aircraft, inclusion of methane oxidation reactions has completely altered the CIAP [1975] and NAS [1975] picture of the effects of this class of aircraft on the ozone column. Instead of depleting the ozone layer, the effects of a projected 1990 fleet of subsonic aircraft cruising in the 6-14 km altitude region would enhance (by $\sim$ 0.01%) or have almost no effect on the ozone column. Supersonic aircraft, cruising at 16-19 km, destroy ozone, but for given NO_x injection rates, by amounts less than expected previously. P. Crutzen's 2-D model including the methane oxidation reactions was run for the HAPP study and predicted 2.7% ozone depletion at 45°N for August 30. The study also concluded that for a "high" estimate of the 1990 total fleet of subsonic and supersonic aircraft (including 142 Concordes and Tupolevs and assuming current engines and accepted NO_x emission indices) the total ozone in the northern hemisphere would be enhanced by about 0.4 to 0.9%, varying with season. These predictions have a very large uncertainty, however, due to the complexity of the chemical scheme and uncertainty in reaction rates, transport effects, and natural abundances in the stratosphere. Figure 7.6 shows the range of predicted ozone reduction due to projected supersonic aircraft operation which have been reported in the last three years. A recent paper by Hidalgo and Crutzen [1977] discusses predicted aircraft perturbations of atmospheric composition.

In addition to the three threats to the stratosphere discussed above other identified potential threats to stratospheric chemistry include bromine compounds [Wofsy, et al., 1975], perturbations of the global nitrogen cycle through N_2O produced from fertilizers [McElroy, 1976; McElroy, et al., 1976; Sze and Rice, 1976], and industrial use of methylchloroform, $C_2H_3Cl_3$ [Crutzen, 1977].

It is clear from the above discussion that present understanding of the extent to which man's activities are, and could, affect the stratosphere is at a somewhat primitive state. However, although there are large uncertainties in the predictions of man's effects, it is well established that there is a reason for concern. To acquire the insights necessary for understanding the presently identified and potential future threats, we must understand the workings of the upper atmosphere as completely as possible.

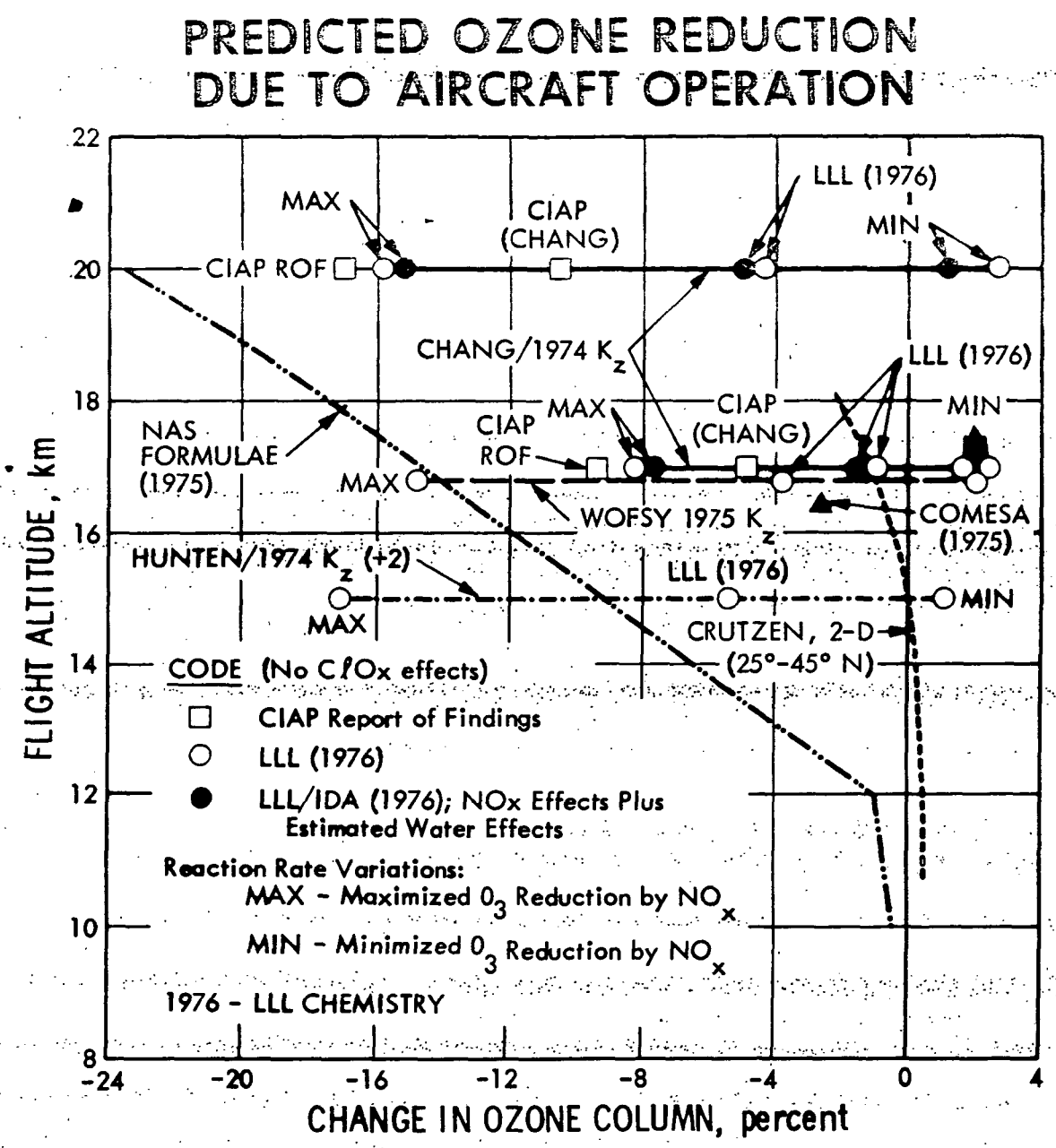


Figure 7.6: Predicted Ozone Reduction Due to Aircraft Operation [from Oliver, et al., 1977].

The variation in these predictions illustrates the uncertainties in the theoretical models due both to chemistry and dynamics. Chlorine chemistry is not included. The NO_x injection rate at each altitude is constant at 2000 mol/cm^3-sec over 1 km, or 1.23×10^9 kg (as NO_2)/year if assumed in one hemisphere. In round numbers for the 17-km injection case, using NAS [1975] NO_x rates per Concorde per year (6.28×10^5 kg/yr), the 1.23×10^9 kg/yr figure corresponds to 2000 Concordes. The equivalent number of Boeing 2707s (at 20 km) is arguable; if based on the 1974 figures (p. 101, CIAP, 1974) of 9.2×10^5 kg NO_2/yr per B-2707, the figure corresponds to 1340 Boeing 2707s. These figures ignore a slight altitude correction; i.e., 17 km and 20 km are not the proper weighted cruise altitudes for these aircraft. The results shown here do not incorporate the new rate constant for the $NO + HO_2 \rightarrow NO_2 + OH$ reaction.

All present predictions of the impacts of natural and manmade materials on the stratosphere, and particularly on its ozone balance, are based on numerical models of the upper atmosphere. These models are of differing degrees of sophistication; the most elaborate of them attempt to treat the chemistry and the distribution of minor constituents, the radiation field and the large scale dynamics as full three-dimensional time dependent problems. It is through comparisons of the results of such models with detailed sets of observations, that our understanding of this region of the atmosphere will develop. It is essential that these models be validated and improved to the greatest possible extent.

A principal method of validating the numerical models is checking their predictions of the distribution and variation of the chemically-active constituents in the upper atmosphere. Because of the complexity of the upper atmospheric chemistry, there are many chemically active species. Figure 7.7 gives representative measurements and calculations of the relative abundances of such species as a function of altitude.

An important consideration stressed by the NASA Stratospheric Research Advisory Committee [1977] is that "measurement strategies for stratospheric research should be planned primarily for their utility in verifying and validating theory. They should be constructed such that the search for the unexpected is encouraged. To check the photochemical models, all significant factors which influence and result from a reaction must be measured. These factors include concentrations of the reactant and product species, the temperature and the mean radiance in photochemically active spectral range." The NASA Stratospheric Advisory Committee has identified several sets of simultaneous measurements which are presently needed. In some cases measurements are needed over a diurnal cycle to adequately test the chemical theories. This is especially true for measurements of $ClONO_2$ and ClO; ClO is predicted to be substantially transformed to $ClONO_2$ at night.

Some specific problems for which measurements are needed are listed below. It must be emphasized that a solution to these problems generally requires simultaneous measurements of many related parameters.

1. The largest and most significant discrepancies between theory and observations in regards to the CFM problem occur for ClO, the most crucial compound in the chlorine cycle of ozone [Crutzen, 1977]: "If the high ClO abundances measured by Anderson [1977] are representative for average conditions, our knowledge of the ozone and chlorine chemistry simulation in the atmosphere needs considerable adjustment." Preliminary microwave results, discussed in Section 7.5 below, suggest lower ClO abundance, in better agreement with theory.

2. Although there is on the average good agreement between theoretical profiles of NO_x and those determined by optical and infrared methods, rather disturbing deviations exist between the theoretical profiles and those determined by chemiluminescent detectors. It remains very important to obtain additional information on the distribution of NO_x in

SOME CHEMICALLY-ACTIVE SPECIES IN EARTH'S UPPER ATMOSPHERE

--- CALCULATED, —— MEASURED

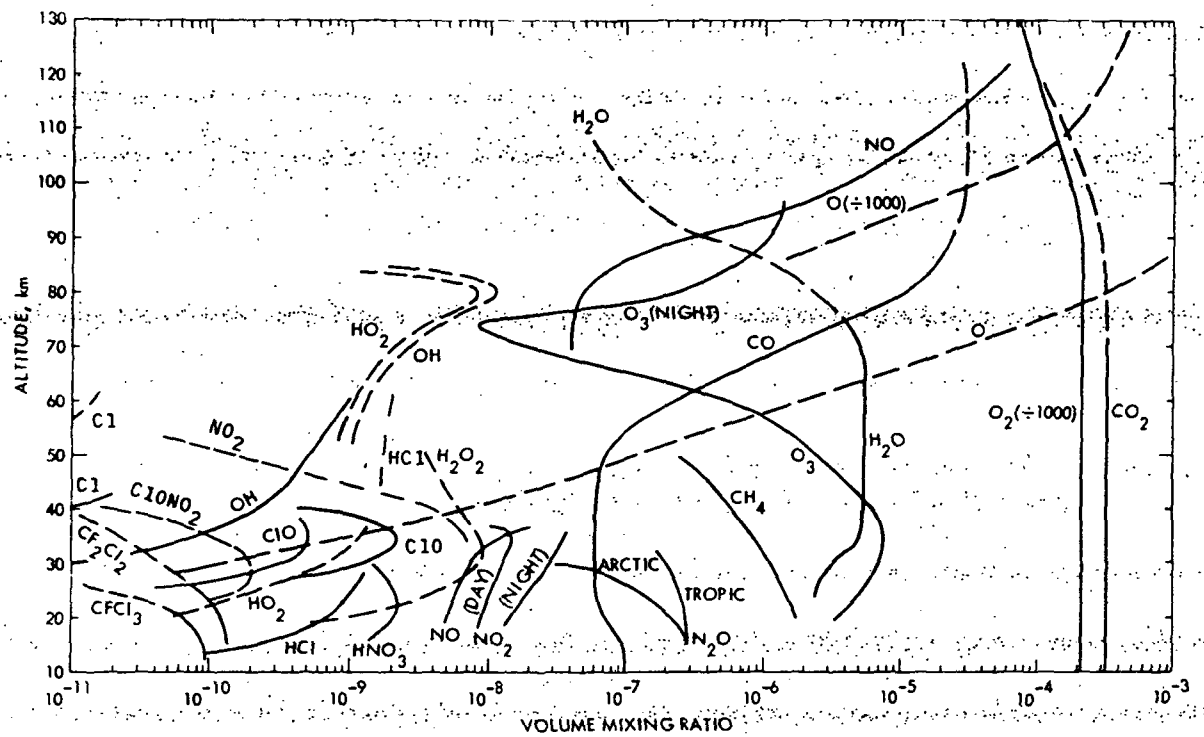


Figure 7.7: Some Chemically-Active Species in Earth's Upper Atmosphere

the stratosphere [Crutzen, 1977]. Some predicted NO_x species (e.g. N_2O_5 and HO_2NO_2) have not yet been measured in the stratosphere.

3. Observations of carbon monoxide (CO) between the troposphere and 30 km deviate considerably from theoretical predictions. This deserves more attention [Crutzen, 1977].

4. More measurements are needed on the distribution and variability of O which is involved in all the destruction schemes of ozone.

5. More data is needed on the distribution and variability of OH. The OH radicals drive most of the chemistry in the stratosphere and play a pivotal role in the partitioning of NO_x and ClO_x among species which are relatively reactive or stable toward O_3 or O [Wofsy, 1977]. Note in Figure 7.4 that OH participates in all three of the catalytic reduction cycles for ozone.

6. More observations of H_2O and O_3 above 25 km altitude are needed to determine whether significant variations occur in these species. Such variations could control variations in the OH profile and thus affect chemical processes controlling ozone. It is presently impossible to determine whether the observed OH and NO variability is driven by variations in H_2O or variations in O_3.

7. Most observations of O_3 above 30 km indicate larger values than predicted [Wofsy, 1977). At these higher altitudes the chemical system responsible for maintaining ozone is thought to be much simpler and better understood than at lower altitudes. It is important to determine whether there is a problem with the theoretical models in this region of the atmosphere. If the models cannot predict the measured ozone profiles in a region where the chemistry is thought to be relatively simple, it is certainly questionable whether they can predict the effect of man-made perturbations which involve more complex chemistry.

8. In winter at high latitudes (>55°N) NO_2 is observed by Noxon [1976] to decrease by a factor of 6, but calculations do not predict this [Wofsy, 1977]. Since NO_2 is the most important molecule in the nitrogen system for destruction of ozone, it is important that its behavior in the atmosphere be understood as completely as possible.

9. Other species for which immediate measurements are needed as specified by the NASA Stratospheric Research Advisory Committee [1977] include chlorine nitrate ($ClONO_2$), perhydroxyle radical (HO_2), hydrogen peroxide (H_2O_2), carbonyl compounds (COFCl, COF_2, $COCl_2$), total chlorine and bromine compounds and peroxynitric acid (HO_2NO_2).

The specific stratosphereic research problems mentioned above are of concern now. Certainly, as more measurements are made and theories are improved, these problems will be replaced by others.

Chemical processes in the upper atmosphere cannot be separated from transport processes if an understanding of its overall workings is to be obtained. The coupling between the two processes is illustrated in the case of ozone. Although maximum ozone production occurs over the tropics, the abundance of ozone is typically twice as large over the polar regions as over the tropics. The global distribution of ozone measured on one day is shown in Figure 7.8.

For research purposes, the NASA Stratospheric Advisory Committee [1977] concludes that future studies of dynamics and transport should involve measurements of :

1. Temperature, with high vertical resolution. For comparison with theory, temperature measurements will be required with spatial resolutions on the order of 1000, 250, and 3 km in the zonal, meridional, and vertical directions, respectively.

2. Winds. Direct measurements are needed especially in tropical regions and at altitudes above 50 km where non-geostrophic components become comparable to geostrophic ones. Such measurements would provide important tests of model outputs and also verification of winds determined by indirect methods such as from temperature fields.

3. Tracer species. Accurate high vertical resolution measurements are needed for photochemically simple species which can serve as tracers of atmospheric motions. Spatial and temporal resolution requirements will be similar to those for temperature measurements. O_3, N_2O, CH_4, and the chlorofluoromethanes offer potential for such studies.

In order to use such measurements for dynamics and transport studies, the data must be obtained over considerable periods of time. Short duration space shuttle missions may not offer observation periods of sufficient length to be very useful. Longer term ($\gtrsim$ 1 year) satellite missions will probably be required to obtain appropriate data sets.

In addition to research aimed at understanding how man may be affecting stratospheric processes, general knowledge is needed on the role which the stratosphere plays in climatic changes [e.g., Chamberlain, 1977], the explanation of sudden stratospheric warmings [e.g., Taylor and Perr, 1977] and their impact on stratospheric chemistry, and the temporal and spatial distributions of aerosols [NASA Stratospheric Advisory Committee, 1977].

Research is also needed to determine the extent of interaction of the stratosphere with the troposphere below and mesosphere above. Regarding the dynamics of the overall regime of the troposphere, stratosphere, mesosphere, and lower thermosphere, Figure 7.9 illustrates the mean zonal winds at the solstices. This diagram is, however, only a small part of the dynamical picture. The processes by which trace species are exchanged between the troposphere and stratosphere are not

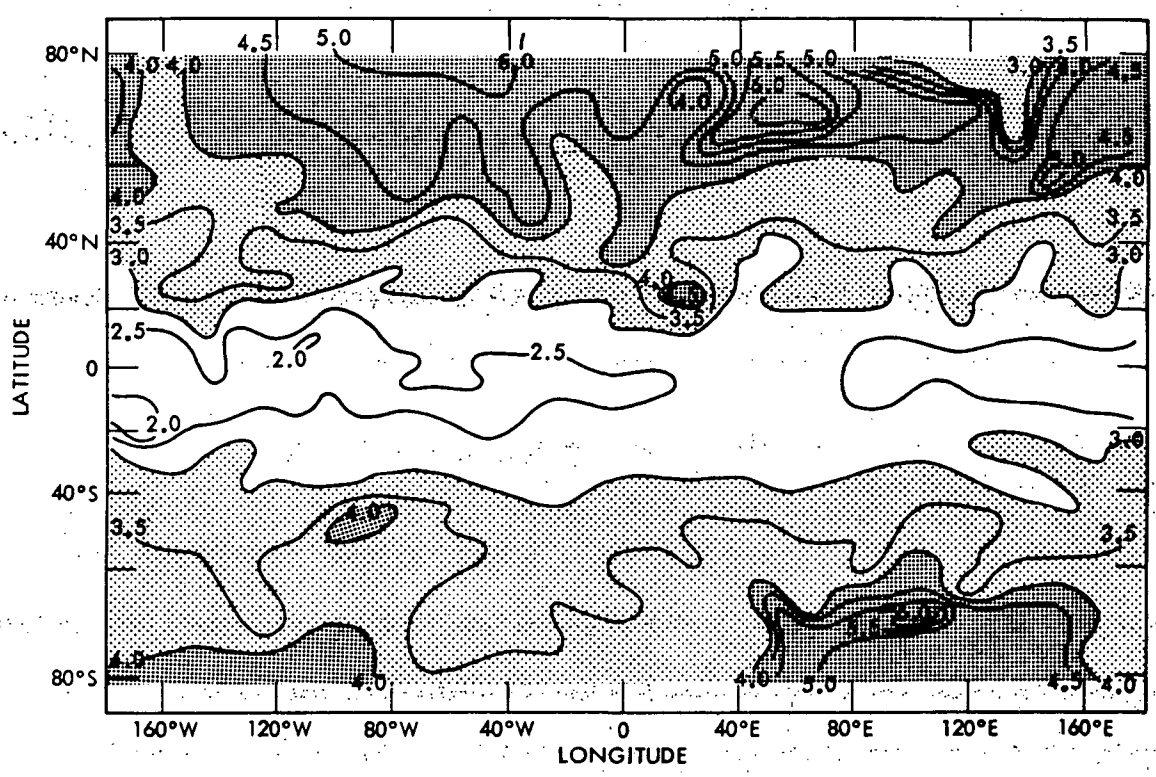


Figure 7.8: The global distribution of total ozone in millimeters at STP on 28th April, 1969, taken from Prabhakara, et al., [1971] and given in CIAP [1975].

MEAN ZONAL WINDS AT THE SOLSTICES

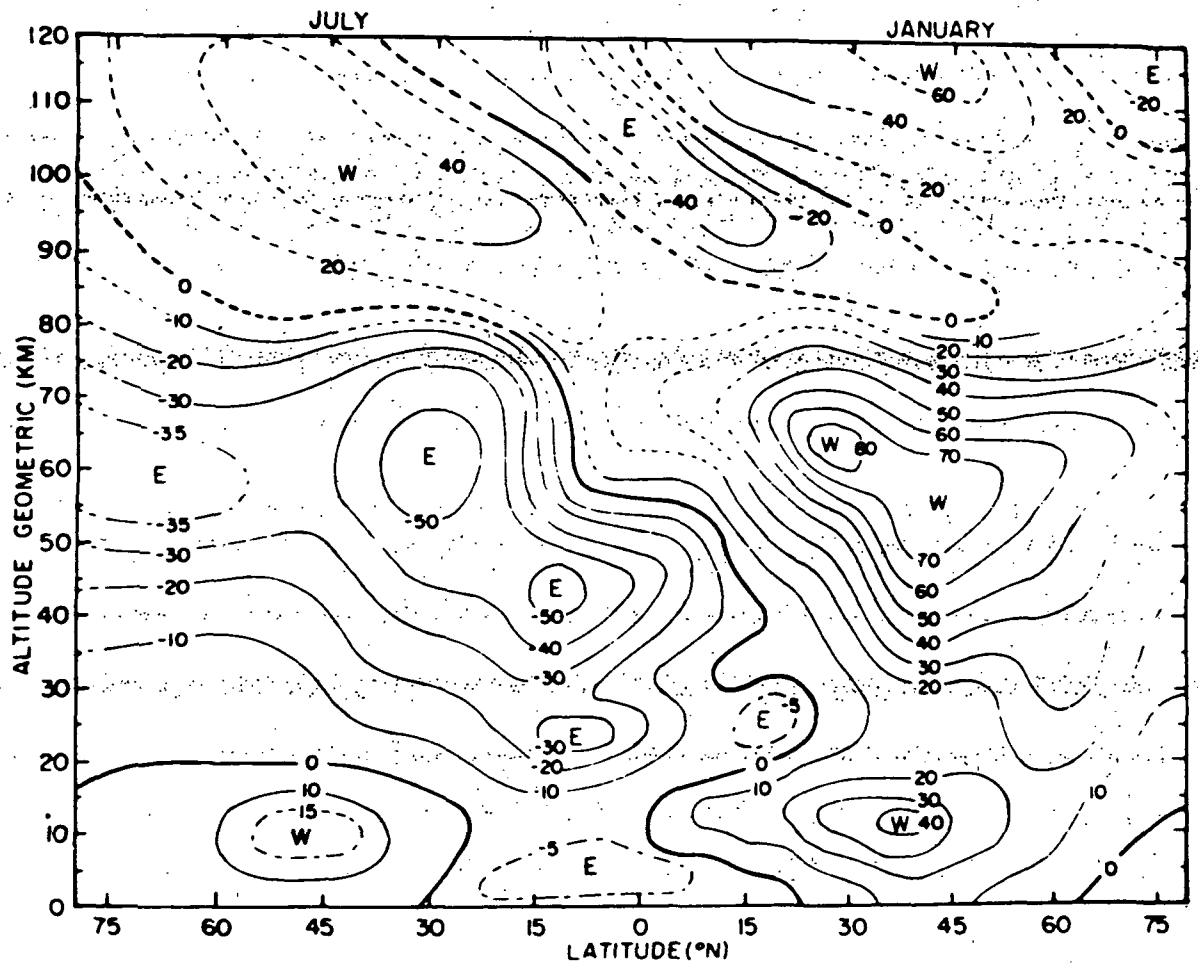


Figure 7.9: Mean Zonal Winds at the Solstices [from CIRA 1972]. Contours are wind values in m/s.

sufficiently understood at present. Little is also known about the details and variability of transport between the stratosphere and the mesosphere and thermosphere which are source regions for NO, O, OH, and CO. Motions in the mesosphere and lower thermosphere are dominated by tidal phenomena and by gravity waves propagated upwards from below; these latter are an important energy input to the region. Planetary waves also propagate into it; the most intense of these occur during stratospheric warmings and are associated with the ionospheric winter anomaly. The conditions under which propagation occurs and the details of the association between stratospheric and ionospheric phenomena in the winter are not well understood.

Concerning the mesosphere and lower thermosphere, much less is known than about the stratosphere. Measurements of its composition and variability are needed to verify and improve the chemical models. Note from Figure 7.7 that knowledge of the relative composition of atmospheric trace species decreases rapidly above 50 km altitude. Very little is known about the variabilities in the production of atomic oxygen by photodissociation of O_2 in the lower thermosphere. This region is also significantly influenced by ion chemistry, about which our knowledge is meager.

Figure 7.10 shows the temperature structure of the upper stratosphere, mesosphere, and lower thermosphere for a period near the solstices. Strong emission from the 15 μm band of carbon-dioxide leads to the very cold temperature (the coldest anywhere in the atmosphere) around 85 km. A surprising feature of the structure of the region around 85 km (the mesopause) is that it is at its coldest ($\sim$140 K) near the summer pole where there is a large energy input from solar radiation. Very substantial amounts of energy must be advected by atmospheric motions in order to maintain this distribution of temperature; our current knowledge is far too scanty to provide quantitative understanding of the mechanisms of energy exchange.

Because excitation to molecular vibrational energy by collisions is not sufficiently rapid to balance the rate of loss by emission of radiation, thermodynamic equilibrium does not apply to a number of molecular vibrations in the mesosphere and above. This is particularly the case for the 15 μm vibration level of CO_2, radiation from which is the main energy sink in the region. Our knowledge of the radiation loss from CO_2 above 80 km is very inadequate.

There are needs for monitoring of the upper atmosphere in addition to the research needs described above. (The distinction between research and monitoring is, however, sometimes not clear.) Measurements of vertical ozone profiles above 35 km, where variation is believed to be dominated by photochemistry rather than transport, should provide sensitive clues to any changes taking place in the stratosphere, and to the nature of those changes [NASA Stratospheric Advisory Committee, 1977]: "This region can also be considered a precurser region which gives early warning of changes which will be manifested later in total ozone. ... This region can and should be subjected to observation over long periods of time." For example, the ozone change at 40 km due to CFMs is expected to be approximately 0.6% per year (perhaps a factor of 2 larger due to the new measurement of the $NO + HO_2 \rightarrow NO_2 + OH$ reaction). This change might be detectable within a few years

TEMPERATURE AT THE SOLSTICES

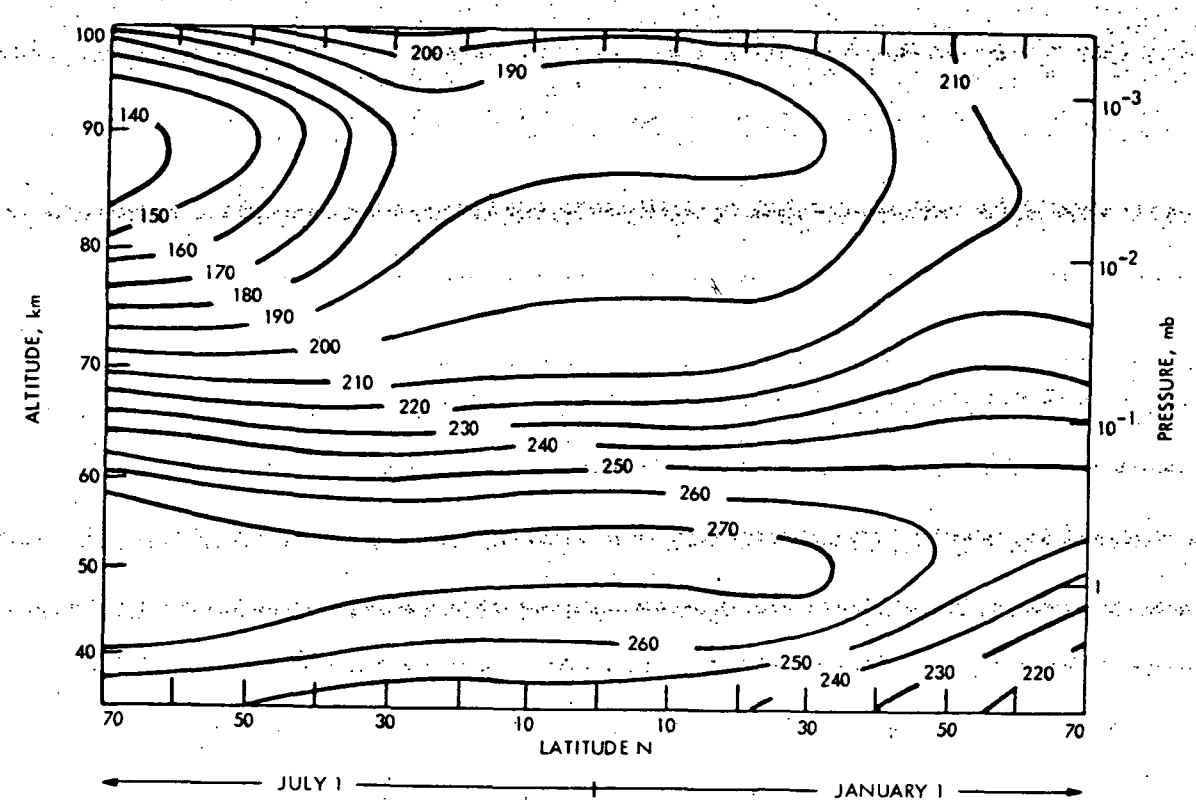


Figure 7.10: Temperature Structure at the Solstices [from CIRA 1972]. Contours are temperature in Kelvins.

with an instrument having precision of 1% or better, providing natural changes in ozone can be accounted for. The NASA Stratospheric Advisory Committee concludes that an ozone profile instrument capable of determining the mean ozone concentration over a month in the 30-45 km region with 3-5 km vertical resolution and 1% precision is needed for monitoring.

To investigate the needs for stratospheric monitoring an Interagency Working Group on Monitoring of the Stratosphere has been established and is preparing a report on this topic. Preliminary requirements established by this working group are [W. Planet, private communication, 1977]:

1. Stratospheric Meteorology - In terms of 95% confidence limits ($\sim 2\sigma$) in the region 16-55 km with 3-5 km vertical resolution:

   (a) temperature to a precision of ±4 K

   (b) vector horizontal wind to a precision of ±5 m/s or ±10%

   (c) density to a precision of ±2%

   (d) height of pressure surface to a precision of ±200 geopotential meters

The sampling requirements for these data are a minimal spatial separation on the order of 1000 km in the east-west directions and meridional spacing of 2.5° latitude on a daily basis.

2. Stratospheric Ozone

   (a) Total Ozone: Mean daily total ozone over globe to precision of ±0.5% (95% confidence limit)

   (b) Ozone Profile: 16-55 km altitude coverage with vertical resolution 3-5 km in 5° latitude bands averaged over one week to precision of ±1% (95% confidence limit)

It should be noted that these monitoring requirements are preliminary until the final report of the working group is released.

For longer term measurements by satellites NASA is also studying the feasibility of a dedicated satellite system for upper atmospheric research.

Figure 7.11 summarizes some of the major problems related to the statosphere, mesosphere, and lower thermosphere. The problems are separated into the categories of stratospheric research, stratosphere monitoring, and mesospheric and lower thermospheric research.

SOME MAJOR PROBLEMS RELATED TO THE STRATOSPHERE, MESOSPHERE, AND LOWER THERMOSPHERE

- **STATOSPHERIC RESEARCH**
  - TO WHAT EXTENT ARE THE PRESENT CHEMICAL AND PHOTOCHEMICAL MODELS CORRECT?
  - HOW ARE THE PROCESSES WHICH MAINTAIN THE OZONE LAYER AFFECTED BY MAN's ACTIVITIES AND SOLAR ACTIVITY?
  - WHAT ARE THE DYNAMICS AND HOW SHOULD TRANSPORT EFFECTS BE INCLUDED IN MODELS?
  - WHAT PART DOES THE STRATOSPHERE PLAY IN CLIMATIC CHANGES?
  - WHAT ARE THE INTERACTIONS WITH THE TROPOSPHERE BELOW AND MESOSPHERE ABOVE?
  - WHAT IS THE CAUSE OF SUDDEN WARMINGS AND THEIR IMPACT ON THE CHEMISTRY?
  - WHAT IS THE DISTRIBUTION OF AEROSOLS?
  - WHAT IS THE BUDGET OF PRECURSORS FOR NO_x ClO_x HO_x AND CO_x ?
- **STRATOSPHERIC MONITORING**
  - HOW TO MEASURE TEMPERATURE WITH ±2K ACCURACY AND 3 km VERTICAL RESOLUTION?
  - HOW TO MONITOR OZONE TO ±1% ACCURACY AND 3 km VERTICAL RESOLUTION?
  - WHAT CHEMICALLY REACTIVE SPECIES (OTHER THAN O_3) SHOULD BE MONITORED?
- **MESOSPHERIC AND LOWER THERMOSPHERIC RESEARCH**
  - TO WHAT EXTENT ARE THE PRESENT CHEMICAL AND PHOTOCHEMICAL MODELS CORRECT?
  - WHAT IS THE ION CHEMISTRY OF THE REGION?
  - WHAT IS THE METEOROLOGY OF THE REGION (TEMPERATURE, PRESSURE, AND WIND VARIATIONS)?
  - WHAT FACTORS CONTROL THE ENERGY EXCHANGES IN THE REGION?
  - WHY IS THE MESOPAUSE COLDEST WHERE MAXIMUM SOLAR HEATING OCCURS?
  - TO WHAT EXTENT DO ENERGETIC SOLAR PARTICLES AFFECT THE CHEMISTRY AND PHOTOCHEMISTRY?
  - WHAT IS THE DISTRIBUTION OF AEROSOLS IN THIS REGION?
  - ARE THERE VARIATIONS IN THE DISSOCIATION OF O_2?

Figure 7.11: Some Major Problems Related to the Stratosphere, Mesosphere and Lower Thermosphere.

7.4 Applications of Microwave Radiometric Techniques to Upper Atmospheric Research and Monitoring

This section describes general application areas and features of microwave* radiometric techniques for upper atmospheric research and monitoring. Specifies on the potential of high-resolution satellite systems for upper atmospheric research are discussed in Section 7.6.

Figure 7.12 summarizes the general application areas. The techniques can be used for measurement of stratospheric composition and temperature for research applications and for precision monitoring of ozone profiles (Specific measurement capabilities for satellite systems are given in Section 7.6.) Minor constituents important for developing a basic understanding of mesospheric chemistry can also be measured.

Because the microwave transitions of molecular oxygen (as well as those of other species) remain in thermal equilibrium at altitudes throughout the mesosphere and lower thermosphere, they can be used to measure the kinetic temperature of these regions. Such measurements, together with infrared measurements of CO_2 emission which give CO_2 vibrational temperatures at these altitudes, would significantly contribute to understanding the energetics of the region. The microwave measurements also yield the abundances of and variations of molecular oxygen in the region where it is dissociated. Such measurements on a continuous global scale have not been previously possible but are important because the dissociation of O_2 is the process by which reactive atomic O is produced. The O_2 microwave lines are due to magnetic dipole transitions and are split into Zeeman components by the terrestrial magnetic field. This splitting allows, in principle, remote measurement of the magnetic field. Such measurements with requisite accuracy, performed simultaneously with composition measurements, could indicate the extent to which energetic charged particles from the sun affect upper atmospheric chemistry. The charged particles are sensed by their disturbance of the terrestrial magnetic field. Sensitivities required for meaningful measurements are discussed in Section 7.6.

Figure 7.13 summarizes some of the general features of microwave radiometric techniques relevant to upper atmospheric measurements. The techniques can be used for observation of either thermal emission or of absorption by molecules of interest. Emission observations are more attractive than absorption observations because they provide the capability for continuous global measurements from satellites, limited only by orbital and observational geometry. However, as long as the noise temperature of the radiometer is more than the atmospheric temperature, absorption experiments using the sun as a source can potentially provide better sensitivity than emission experiments.

---

* The term "microwave" is used generically here to refer to that portion of the electromagnetic spectrum between approximately 3 and 3000 GHz (100 to 0.1 mm wavelength).

APPLICATIONS OF MICROWAVE RADIOMETRIC TECHNIQUES TO UPPER ATMOSPHERIC SENSING

STRATOSPHERIC RESEARCH AND MONITORING

- MEASUREMENT OF TEMPERATURE AND MINOR CONSTITUENTS IMPORTANT TO STRATOSPHERIC CHEMISTRY
- PRECISION MONITORING OF OZONE PROFILES (1% ACCURACY WITH BETTER THAN 3 km VERTICAL RESOLUTION SHOULD BE ACHIEVABLE)

MESOSPHERIC AND LOWER THERMOSPHERIC RESEARCH

- DETERMINE METEOROLOGY (TEMPERATURE, WINDS) AT MESOPAUSE REGION

  WHY IS MESOPAUSE COLDEST WHERE MAXIMUM SOLAR HEATING OCCURS?

- MEASURE MINOR CONSTITUENTS IMPORTANT TO MESOSPHERIC CHEMISTRY
- MEASURE O_2 IN REGION WHERE IT IS PHOTODISSOCIATED BY SOLAR UV

  ALTHOUGH O_2 IS THE FIRST MAJOR ATMOSPHERIC GAS TO BE DISSOCIATED BY SOLAR UV AND IS THEREBY RESPONSIBLE FOR FORMATION OF OZONE AND HEATING OF THE LOWER THERMOSPHERE, NO TECHNIQUES NOW EXIST OR ARE PLANNED FOR MEASURING IT. GLOBAL MEASUREMENTS OVER DAILY AND SEASONAL CYCLES SHOULD PROVIDE SIGNIFICANT NEW INFORMATION ON SOLAR-TERRESTRIAL INTERACTIONS

- MEASURE MAGNETIC FIELD DISTURBANCES IN MESOSPHERE AND LOWER THERMOSPHERE (BY ZEEMAN SPLITTING OF O_2 LINES)

  THE CHARGED SOLAR PARTICLES ARE SENSED BY THEIR DISTURBANCE OF THE TERRESTRIAL MAGNETIC FIELD. SIMULTANEOUS COMPOSITION MEASUREMENTS WILL INDICATE THEIR CHEMICAL INTERACTIONS

Figure 7.12: Applications of Microwave Radiometric Techniques to Upper Atmospheric Sensing.

MICROWAVE RADIOMETRIC TECHNIQUES: GENERAL FEATURES RELATIVE TO UPPER ATMOSPHERIC SENSING

- NATURAL THERMAL EMISSION IS MEASURED
  - ALLOWS CONTINUOUS GLOBAL COVERAGE, LIMITED ONLY BY ORBITAL PARAMETERS
  - TRANSMITTER AND EXTERNAL SOURCES (e.g., THE SUN) NOT REQUIRED
- ROTATIONAL MOLECULAR TRANSITIONS ARE OBSERVED
  - REMAIN IN THERMAL EQUILIBRIUM TO HIGHER ALTITUDES THAN VIBRATIONAL INFRARED TRANSITIONS
  - COLLISIONAL BROADENING OF SPECTRAL LINES DOMINATES THROUGHOUT THE STRATOSPHERE ALLOWING INFORMATION TO BE OBTAINED FROM LINE SHAPE (NOT TRUE FOR I.R. ABOVE MIDDLE STRATOSPHERE)
- HETERODYNE RECEIVERS PROVIDE NEEDED SPECTRAL RESOLUTION FOR EXTRACTING LINE SHAPE INFORMATION
- SMALL (~1 meter) ANTENNA CAN PROVIDE ~3 km VERTICAL RESOLUTION

Figure 7.13: Microwave Radiometric Techniques: General Features Relative to Upper Atmospheric Sensing.

In addition to the microwave spectral lines remaining in thermal equilibrium to higher altitudes than infrared lines, collisional broadening of these lines dominates to higher altitudes than for infrared lines. Collisional broadening produces a spectral line width which is a very strong function of altitude and thus allows altitude information to be derived from the spectral line shape for altitudes below $\sim$60 km. Figure 7.14 shows typical spectral line widths in the terrestrial atmosphere. For submillimeter and longer wavelengths, collisional broadening dominates to altitudes of the lower mesosphere or higher. The heterodyne receivers used by microwave techniques provide the spectral resolution needed for extracting the line shape information.

In order to provide the vertical resolution of $\sim$3 km or better required for atmospheric measurements a relatively modest antenna of $\sim$1 meter diameter is required for low altitude orbit (See Section 7.6).

At the present time microwave receiver technology is rapidly advancing to submillimeter wavelengths, allowing measurement of more and more species by these techniques. Figure 7.15 shows the submillimeter spectra of some molecules important in upper atmospheric chemistry, and indicates the status of low noise receiver technology. (Here "low-noise" refers to receivers having noise equivalent power equal to, or less than, that of blackbody radiation at a few thousand Kelvins temperature.) Of particular importance to upper atmospheric science is development of a low noise receiver operating near 2 THz frequency which could be used to remotely measure OH and O.

7.5 Results Obtained to Date from Microwave Sensing of the Upper Atmosphere

In order to provide background for the potential of high-resolution satellite systems for microwave sensing of the upper atmosphere, and to understand the maturity of the techniques for these applications, it is worthwhile to review the results which have been obtained to date. Application of these techniques to upper atmospheric sensing is rapidly advancing; most of the results have been obtained only within the past two years.

Figure 7.16 summarizes these results; they are described in detail below.

The first measurement of carbon monoxide (CO) in the mesosphere was by ground-based observation of solar absorption near the J=0 $\rightarrow$ 1 CO transition at 115 GHz frequency [Waters, et al., 1976]. The data are shown on the left in Figure 7.17. The width of the observed absorption line proves it originated at altitudes higher than $\sim$65 km in the terrestrial atmosphere. Photochemical theories [Hays and Olivero, 1970;

SPECTRAL LINEWIDTHS IN THE TERRESTRIAL ATMOSPHERE

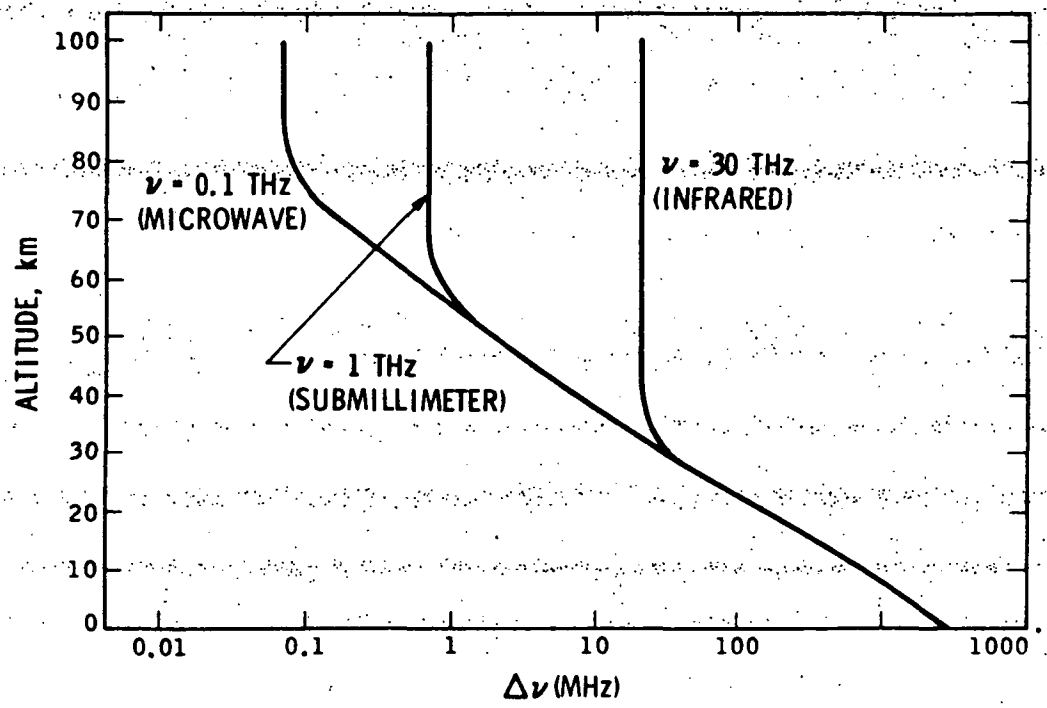


Figure 7.14: Spectral Linewidths in the Terrestrial Atmosphere. Typical values are shown. Actual values will vary by about a factor of 2 from species to species.

SUBMILLIMETER SPECTRA OF SOME MOLECULES IMPORTANT IN STRATOSPHERIC OZONE DEPLETION CYCLES

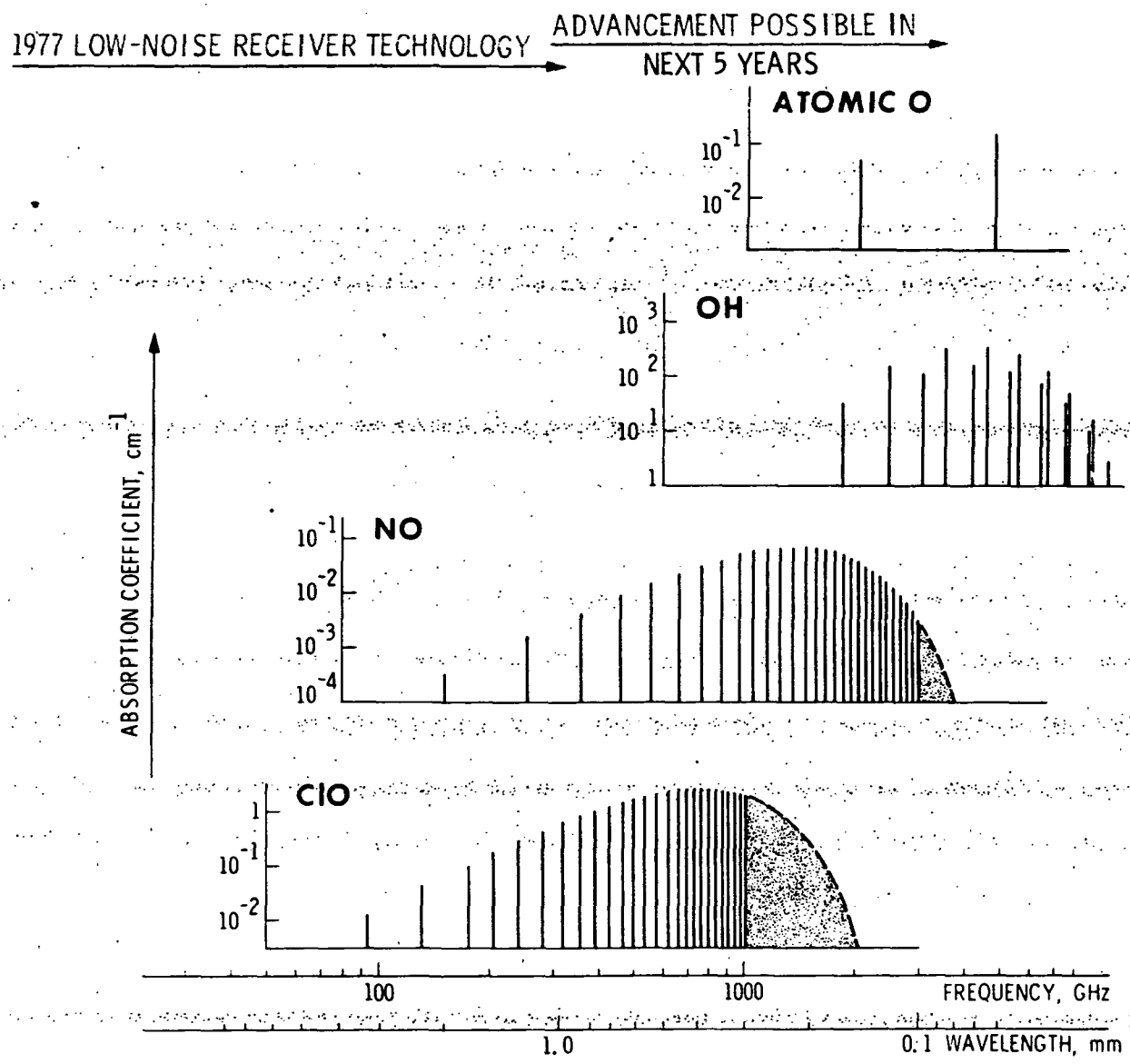


Figure 7.15: Submillimeter Spectra of Some Molecules Important in Stratospheric Ozone Depletion Cycles.

MICROWAVE SENSING OF THE UPPER ATMOSPHERE MEASUREMENT RESULTS TO DATE

- GROUND-BASED
  - FIRST MEASUREMENT OF MESOSPHERIC CARBON MONOXIDE
  - FIRST CONTINUOUS MEASUREMENT OF MESOSPHERIC OZONE THROUGH A DIURNAL CYCLE
  - DETECTION OF MESOSPHERIC WATER VAPOR EMISSION
  - MEASUREMENT OF HIGH-ROTATIONAL EMISSION LINES OF STRATOSPHERIC O_2
- AIRCRAFT-BASED
  - MEASUREMENT OF STRATOSPHERIC EMISSION FROM 15 OZONE MICROWAVE LINES AND RECOVERY OF OZONE PROFILES
  - FIRST MEASUREMENT OF LATITUDINAL VARIATION IN UPPER STRATOSPHERIC AND MESOSPHERIC WATER VAPOR
  - UPPER LIMIT AND TENTATIVE DETECTION OF STRATOSPHERIC ClO RADICAL
  - DETECTION OF EMISSION FROM STRATOSPHERIC NITROUS OXIDE (N_2O)
  - DEMONSTRATION OF CAPABILITY TO MEASURE VARIATIONS IN UPPER STRATOSPHERIC TEMPERATURE
- SATELLITE-BASED
  - GLOBAL MEASUREMENTS OF LOWER STRATOSPHERIC TEMPERATURES

Figure 7.16: Microwave Sensing of the Upper Atmosphere: Measurement Results to Date.

Wofsy, et al., 1972 Crutzen, 1974] had predicted a relatively large abundance of CO at these altitudes which is produced by photodissociation of CO_2 in the lower thermosphere. The microwave measurements shown in Figure 7.15 provided the first experimental confirmation of this prediction. The curves A, B, and C in Figure 7.15 show three CO mixing ratio profiles and the absorption calculated for these respective profiles. CO profile B best fits the measurement. Atmospheric emission, as well as absorption for this CO transition has been measured, (and it has been detected) on both Venus and Mars [Kakar, et al., 1976 and 1977].

Ground-based microwave techniques have also been used to measure mesospheric ozone [e.g., Penfield, et al., 1976; Shimabukuro, et al., 1977]. Mesospheric ozone is predicted to increase significantly at night, and the microwave measurements have provided a continuous measurement of the diurnal variation. Figure 7.18 shows the data and recovered ozone profiles from Shimabukuro, et al. (Their published profiles of ozone number density have been converted to mixing ratio using total air density from the 1976 U.S. Standard Atmosphere.) The narrow spike at the center of the emission line due to increased mesospheric O_3 is clearly evident in the night data. The ozone abundance inferred at the 84 km nocturnal peak agrees quite well (to within ~10%) with that predicted by Shimazaki and Laird [1970].

Stratospheric emission from approximately 20 ozone lines at frequencies between 160 and 380 GHz has been recently measured using microwave limb sounding techniques from aircraft [Waters, et al., unpublished results]. These lines are very strong by microwave radiometric standards, approximately 30-100 K at 20° elevation angle from 13 km altitude, and are easily measurable. One measurement of the $10_{0,\,10} \rightarrow 9_{1,\,9}$ transition of O_3 at 184.378 GHz is shown in the left part of Figure 7.19. The ozone profile retrieved from this measurement is shown in the right part of the figure as the protion of curve 1 above 28 km. (Because of the complement of filters in the radiometer at the time of measurement, the data was not very sensitive to ozone below about 30 km.) The portion of curve 1 below 28 km was fit to the ozone profile measured by a coincident ozonesonde. Some other measurements of ozone profiles above 40 km are indicated in the figure as are profiles calculated from photochemical models. Most other measurements of ozone above 50 km give values much higher than predicted by the models [Wofsy, 1977]. The significance of the microwave measurements is that they are consistent with the photochemical models in an altitude region where the models should be accurate. In the altitude region overlapped there is good agreement in the ozone profile inferred from the ground-based measurement at 101.737 GHz and that inferred from the aircraft measurement at 184.378 GHz.

Microwave emission from water vapor in the upper stratosphere and mesosphere has been detected both from ground [Radford, et al., 1977] and aircraft [Waters, et al., 1977]. Aircraft measurements of the 183.310 GHz emission line at three latitudes are shown in the left part of Figure 7.20. Water vapor profiles are shown in the right part of

CARBON MONOXIDE (CO)

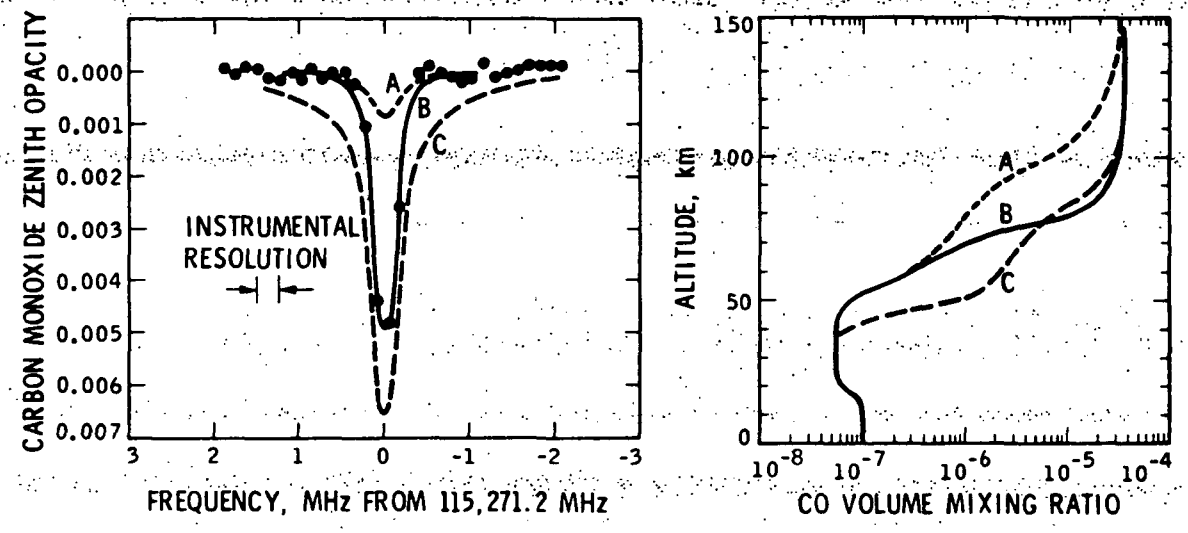


Figure 7.17: Ground-Based Microwave Measurement of Carbon Monoxide in the Upper Atmosphere [from Waters, et al., 1976].

OZONE (O_3)

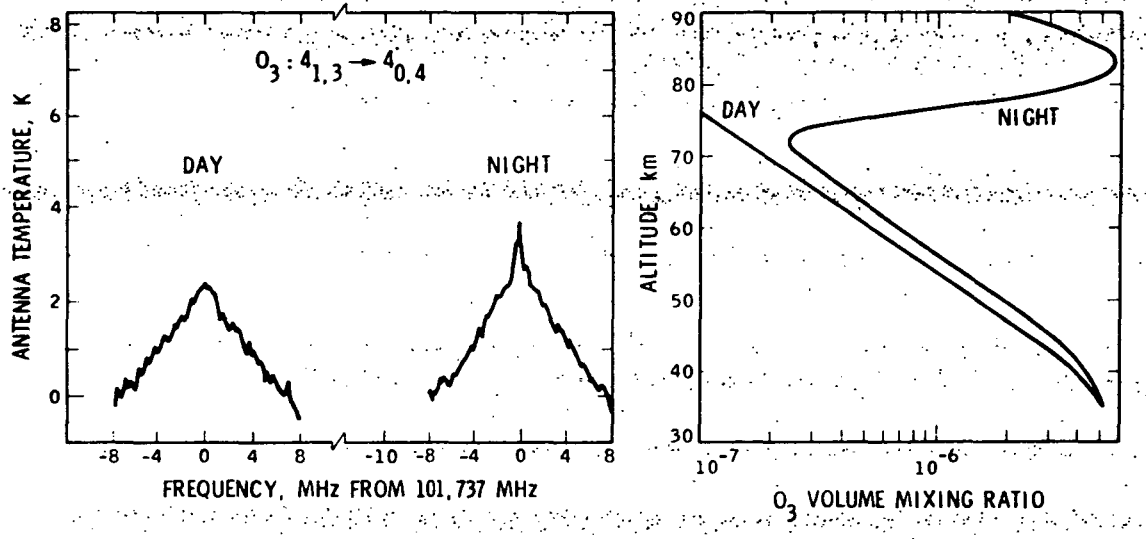


Figure 7.18: Ground-Based Microwave Measurement of Ozone in the Upper Atmosphere [data from Shimabukuro, et al., 1977].

OZONE (O_3)

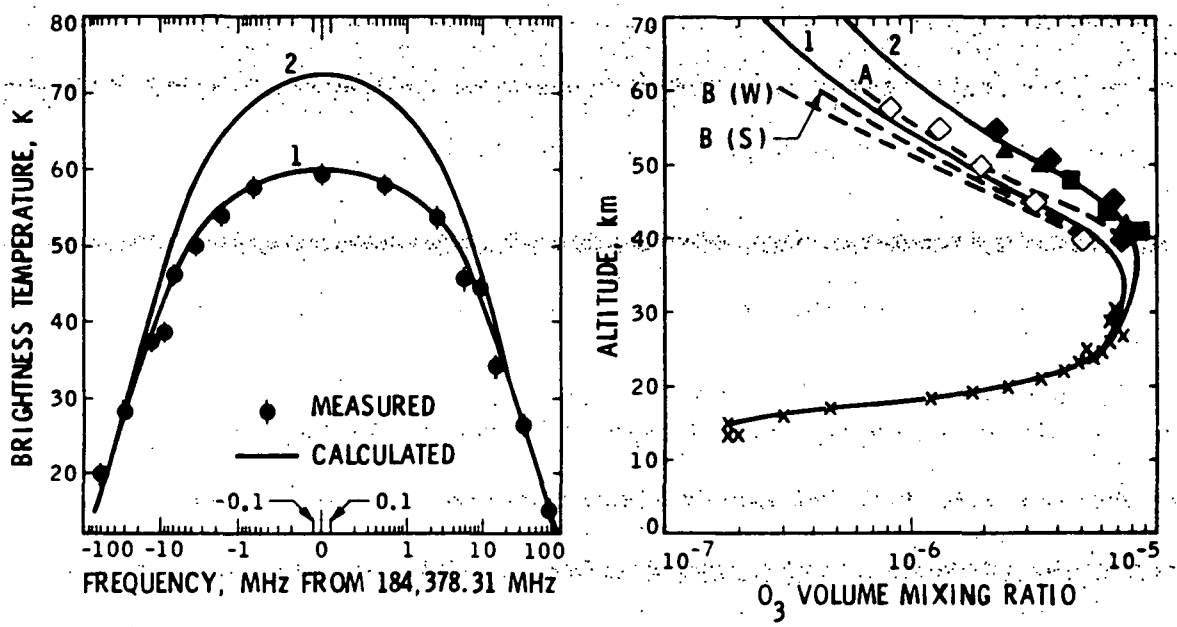


Figure 7.19: Aircraft-Based Microwave Measurements of Ozone in the Upper Atmosphere [Waters, et al., unpublished results].

Left: The ozone emission line measured on 11 November 1976 at 9:00 a.m. local time near 40°S and 146°E (just south of Aspendale, Australia). The elevation angle of the observation was 20°. Also shown are emission lines calculated for the similarly-labeled ozone profiles.

Right: Ozone Mixing Ratio Profiles. The profile retrieved from the microwave data is curve 1 above 28 km. Below 28 km curve 1 is fit to data (X) from the ozonesonde which was launched from Aspendale, Australia (38°S, 145°E) at 9:30 a.m. local time on 11 November 1976. The dashed lines are chemical calculations by Wofsy [1977]. The symbols are some other measurements quoted by Wofsy.

WATER VAPOR (H_2O)

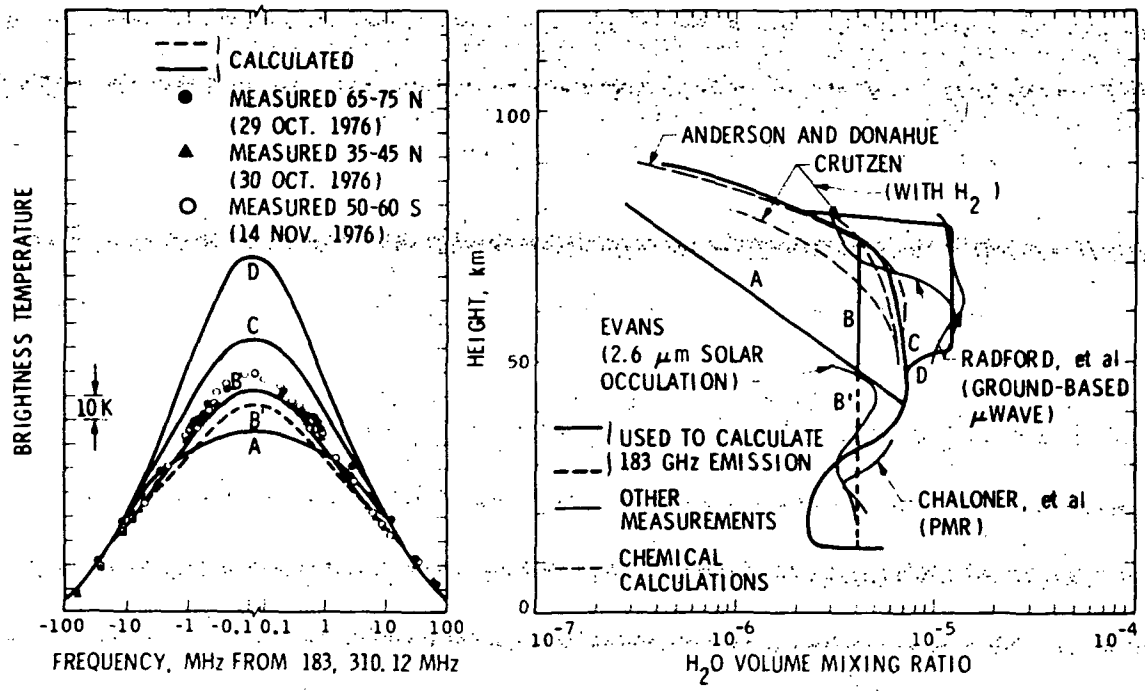


Figure 7.20: Aircraft-Based Microwave Measurements of H_2O in the Upper Atmosphere [Waters, et al., 1977].

Left: Calculated and measured emission from the 183 GHz H_2O profiles shown on the right; the U.S. Standard Atmosphere temperature profile was used. The zero level is arbitrary and the calculated and measured curves have been shifted slightly ($\lesssim$10 K) to coincide at 100 MHz from line center. Measurements within 0.2 MHz of center are not available in the two northern hemisphere bands because of interference in those channels.

Right: H_2O mixing ratio profiles used for the calculated 183 GHz lines shown at left. Also shown are some other measurements of H_2O and calculated profiles.

Figure 7.20. The heavily drawn profiles labeled A, B, C, and D were used to calculate the similarly-labeled emission lines shown in the left part of the figure. The aircraft measurements suggest the H_2O profile above 40 km is between curves B and C. Recent aircraft measurements of upper atmospheric H_2O emission at 380 GHz have confirmed these results [Waters, et al., unpublished].

Microwave limb sounding techniques have also been used from aircraft to search for millimeter-wavelength emission by the stratospheric ClO radical. As discussed in Section 7.3, measurement of stratospheric ClO (and all Cl containing species) is of crucial importance in assessing the threat to stratospheric ozone from commercial use of chlorofluorocarbons. To date, three millimeter-wavelengths transitions of ClO have been searched for from aircraft [Waters, et al., unpublished]. Results from preliminary data reduction are shown in left part of Figure 7.21. Also shown in the left of the figure are signals calculated for no ClO and for two ClO profiles shown in the right of Figure 7.21. The dashed ClO profile is an early calculation from a photochemical model [Wofsy, 1977]; the solid profile was a preliminary measurement reported by Anderson [1976]; the symbols give final results from three measurements by Anderson, et al., [1977]. The microwave measurements at 167 and 278 GHz indicate that, for the form of the profile expected, the ClO mixing ratio does not exceed 0.5×10^{-9} (0.5ppb). The 241 GHz microwave measurement indicates the ClO mixing ratio does not exceed 2ppb. ClO profiles having these values at the times and places of the microwave measurements would, however, be consistent with the data.

The 251 GHz J=9→10 transition of nitrous oxide (N_2O) has also been detected by microwave limb sounding techniques from aircraft [Waters, et al., unpublished] and is shown in Figure 7.22.

Up-looking measurement of 53 GHz emission by molecular oxygen from aircraft and from ground [Rosenkrantz, et al., 1975] have demonstrated the ability of these techniques to sense temperatures in the upper stratosphere and to sense the change in Zeeman splitting of the O_2 lines with a change in magnetic latitude. Figure 7.23 shows temperature variations in two layers of the upper stratosphere between 75°N and 20°N inferred from the aircraft measurements and compared with coincident rocket measurements. Figure 7.24 shows the variation in Zeeman splitting for the 27 O_2 transition measured for Haystack Observatory (Massachusetts) and Arecibo Observatory (Puerto Rico). The Haystack measurement is closer to the magnetic pole where the more intense magnetic field produces a broader line.

The microwave spectrometers on the NIMBUS-5 and NIMBUS-6 satellites [Staelin, et al., 1973 and 1977] were sensitive to lower stratospheric temperatures. Comparison of the temperatures retrieved from these NIMBUS experiments with coincident radiosondes [Waters, et al., 1975; Grody and Pellegrino, 1977] indicated that the predicted theoretical accuracies of ∿2 -3 K rms were achieved for the temperature profile over the altitude region to which the experiment was sensitive.

ClO RADICAL

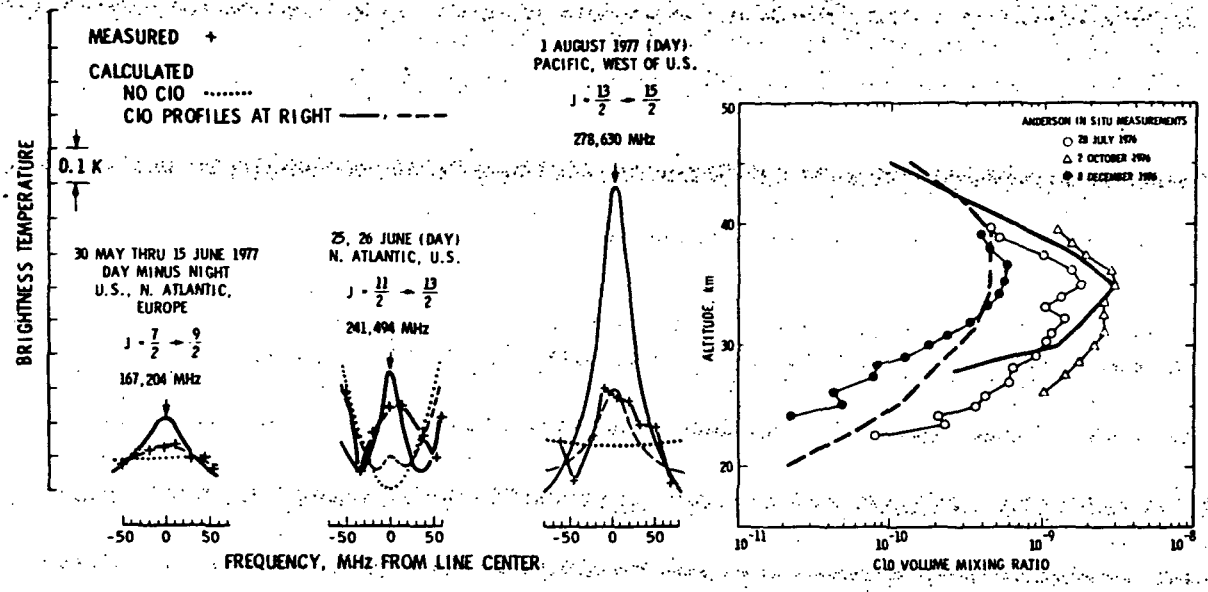


Figure 7.21: Aircraft-Based Microwave Measurements of Stratospheric Emission Near ClO Millimeter-Wavelength Transitions. [Waters, et al., unpublished results]

Left: Measured and calculated stratospheric emission near frequencies for ClO rotational lines.

Right: ClO profiles. The dashed profile is an early calculation by Wofsy [1977] and the solid profile is a preliminary measurement reported by Anderson [1976]. These two profiles were used to calculate the similarly-labeled emission lines shown at left. The symbols are final results from Anderson's [1977] measurements made from Palestine, Texas, on the indicated dates.

NITROUS OXIDE (N_2O)

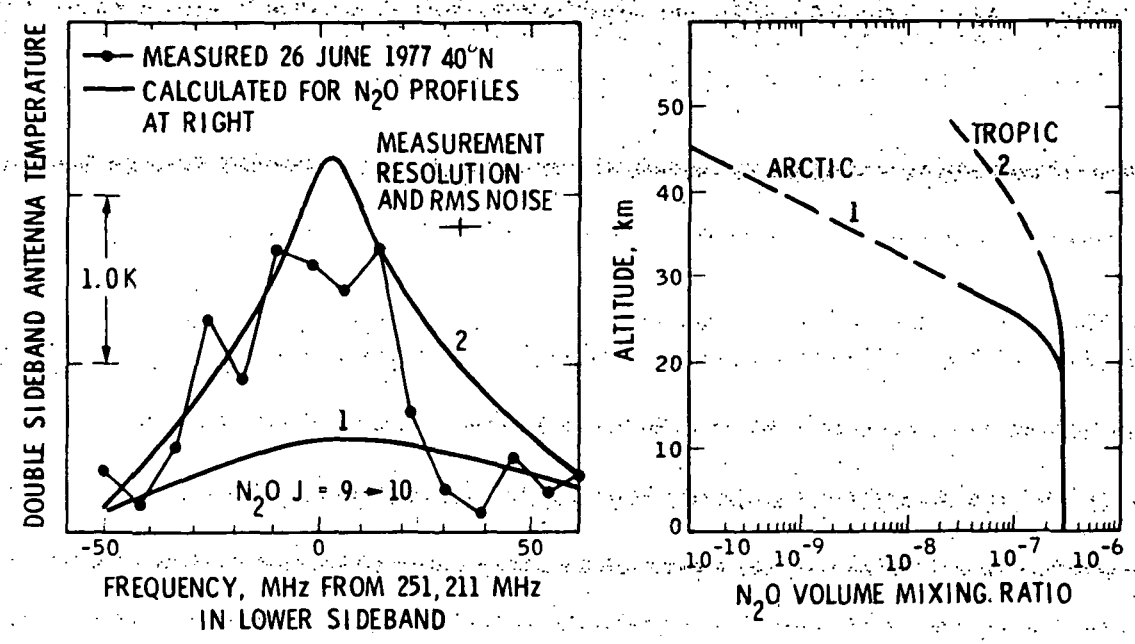


Figure 7.22: Aircraft-Based Microwave Measurements of Stratospheric N_2O. [Waters, et al., unpublished results]

Left: Measured and calculated stratospheric emission near the J=9 → 10 N_2O transition.

Right: N_2O mixing ratio profiles used for calculations shown on left. Curve 1 is for arctic and curve 2 for tropical profiles as indicated by Schmeltekopf, et al., [1977].

STRATOSPHERIC TEMPERATURE

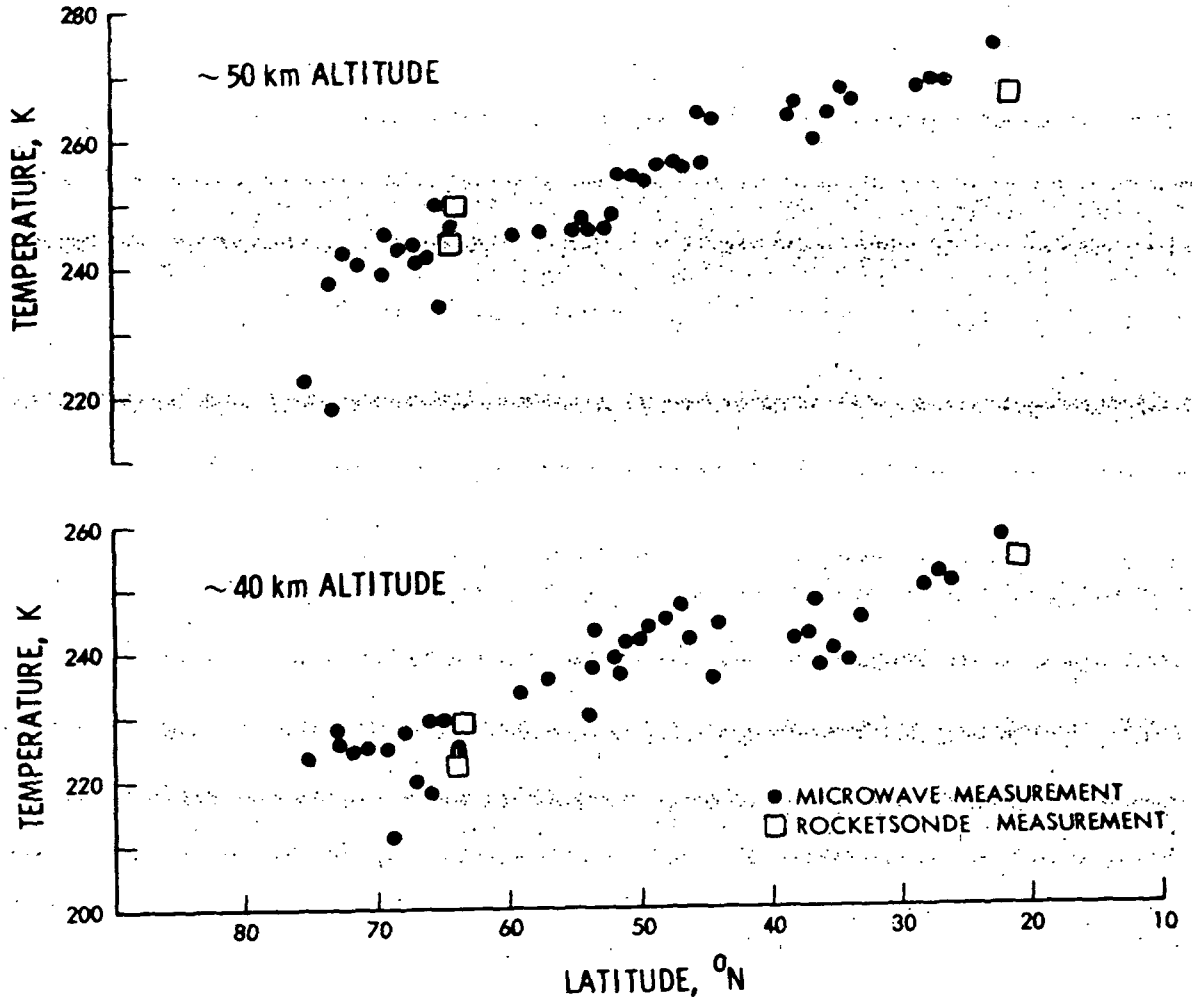


Figure 7.23: Comparison of Upper Stratospheric Temperatures Inferred from Microwave Aircraft Measurements and Measured by Rockets [From Rosenkranz, et al., 1975].

MEASURED ZEEMAN SPLITTING OF 27_ O_2 LINE

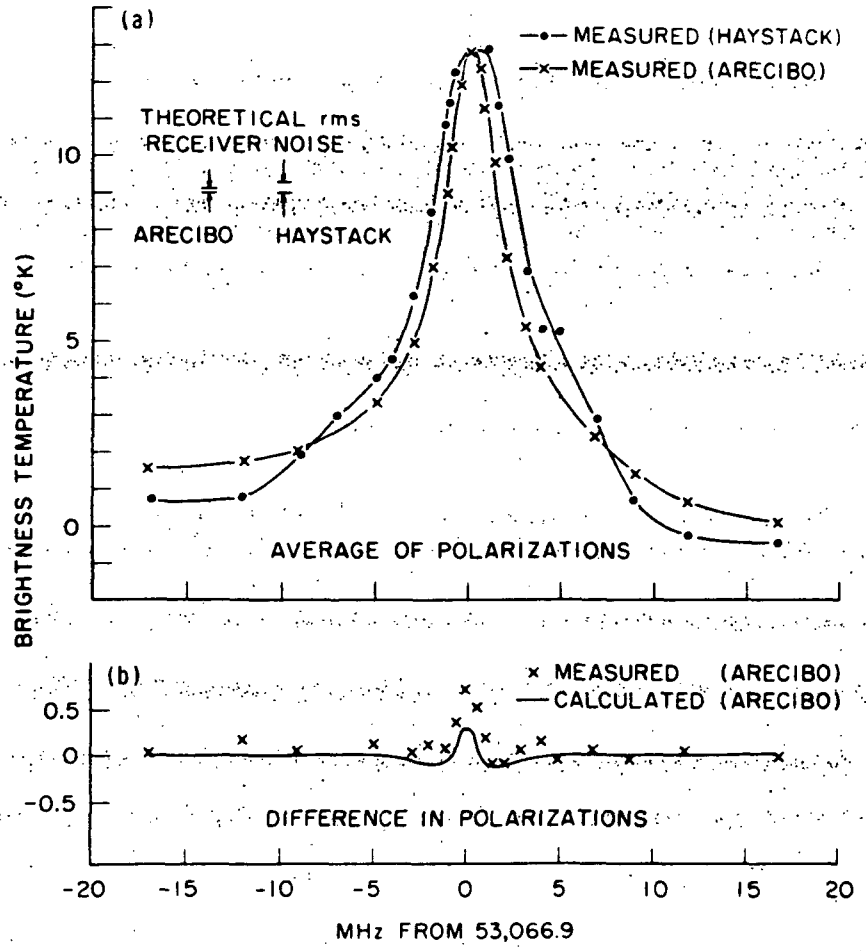


Figure 7.24: Measured Zeeman Splitting and Polarization of Stratospheric Emission by 27_ O_2 Line [From Waters, 1973].

(a) Atmospheric zenith emission by the 27_ O_2 line as measured on August 30, 1972 from Haystack Observatory (magnetic latitude 55°) and on November 1, 1972 from Arecibo Observatory (magnetic latitude 29°). The Haystack measurement is noisier because it represents a shorter integration time than the Arecibo measurement.

(b) Measured and calculated electric polarization of the 27_ O_2 for Arecibo. The linear polarization in the magnetic east-west direction is stronger than that in the magnetic north-south direction.

7.6 High-Resolution Satellite Systems for Microwave Sensing of the Upper Atmosphere

For the purpose of this report "high-resolution" microwave systems are defined as systems having significantly improved angular resolution over those previously flown or planned. Such systems can allow, for the first time, the application of limb sounding techniques at microwave wavelengths. Down-looking microwave systems may also be useful for upper atmospheric measurements, particularly for temperature sounding, but are not covered here because they do not allow the range of parameters to be measured that limb sounding techniques allow, and because they do not require "high-resolution."

The general geometry for limb sounding emission observations is sketched in Figure 7.25. The major advantages of such observations for sensing the upper atmosphere are:

1. They use the largest possible atmospheric path length at a given level which enhances weak signals and allows sensing to higher altitudes.

2. Cold space behind the atmospheric observation path provides the optimum background for emission measurements.

3. The field of view of the instrument principally determines the altitude region sensed, and altitude resolution can be made better than with other modes of passive emission measurements.

4. The observations are not dependent upon a background radiation source (e.g., the Sun) allowing diurnal and other variations in the atmospheric parameters to be easily measured.

The intensity and spectral character of the limb emission depends upon the atmospheric composition, thermal structure, motion along the line of sight relative to that of the observation point, and for the microwave O_2 lines on the magnetic field. These atmospheric parameters can be recovered, to a certain degree, from the measured radiation field.

If the atmospheric path is just completely opaque at all wavelengths in the instrument passband the signal received is directly proportional to the source function $B(\overline{T})$ appropriate to the mean temperature $\overline{T}$ of the path and this mean is measured. As the altitude probed is increased the atmosphere becomes partially transparent in the passband of the instrument, and the intensity of radiation received from the limb path is then $\varepsilon.B(\overline{T})$ where ε is an effective emissivity. If ε is known and not too small, as is the case of a uniformly mixed gas such as O_2 below ~ 80 km, $B(\overline{T})$ may be found and the atmosphere's temperature deduced. $B(\overline{T})$ having been measured ε can be found for any other gas and hence the gas concentration determined.

This simple treatment ignores the fact that even for a very precise direction of view emission from a range of altitudes will be observed. Further, for a given viewing direction emission from different gases

LIMB SOUNDING GEOMETRY

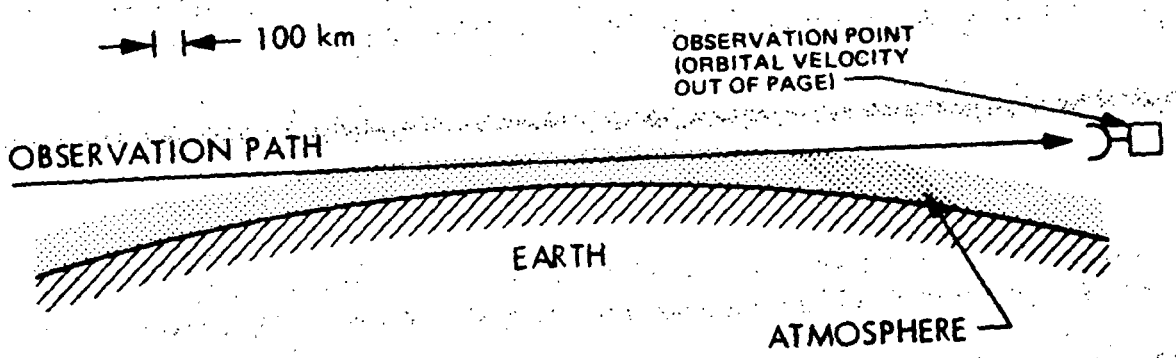


Figure 7.25: Limb Sounding Geometry.

will not be weighted in exactly the same way with altitude so that the mean temperature appropriate to the expression $\varepsilon.B(\overline{T})$ is not in general immediately comparable for different gases. A more complete retrieval process is therefore required. The theory of such processes is, however, well advanced and a number of efficient retrieval methods are available [see, e.g., Rodgers, 1971].

The range of altitudes contributing to a measurement can be described by a weighting function. Figure 7.26 compares weighting functions for down-looking and limb-looking microwave measurements. The improved vertical resolution from the limb measurements is clearly evident in the figure. For the limb observations, half the observed signal from a single ray arises from an atmospheric layer between $\sim$1 and $\sim$3 km above the tangent height of the observation path and within $\sim\pm$100 to $\pm$200 km to either side of the tangent point of the observation path [Waters, 1976b]. The finite beamwidth of the antenna used for the observations will degrade the resolution since radiation from all directions within the beam will contribute substantially to the measured signal. For observations from 250 km altitude, the nominal orbital altitude for the Shuttle, a 3 km altitude difference at a tangent point of 50 km altitude corresponds to an angular difference of $\sim$0.1°. Thus beamwidths of $\sim$0.1° are required in order to achieve the verticle resolution needed. The size antenna required to achieve $\sim$3 km vertical resolution is given in Figure 7.27 as a function of the wavelength (and frequency) of observation for orbital altitudes of 250 km (Shuttle), 1000 km (sun-synchronous), and 36,000 km (Earth synchronous).

Calculations of weighting functions which include both the effects of radiative transfer through the atmosphere and the finite antenna beamwidth are given in Figure 7.28 for a 1 meter diameter antenna, 250 km orbital altitude, and the indicated measurement frequencies. Such an antenna can give better than $\sim$3 km vertical resolution for measurements at frequencies of $\sim$180 GHz and higher. Fabrication of this size antenna with the required surface tolerances can be accomplished with present technology.

There is no reason to reduce the horizontal resolution normal to the observation path to much less than the horizontal resolution along the path which is determined by radiative transfer and is $\sim$200-400 km. Thus 100 km horizontal resolution normal to the line of sight is reasonable, which corresponds to acceptable beamwidths in the horizontal plane of as much as $\sim$3° for a 250 km orbit. For those channels with a spectral resolution comparable to the Doppler line width, the horizontal resolution must be less if the effects of Doppler shift due to orbital motion are to be removed. A frequency shift of 1/10 the Doppler width is produced by changing the horizontal direction of observation by 0.3° from the normal to the velocity vector of a satellite at 250 km altitude. Thus, measurements with channels having spectral resolution comparable to the Doppler line width will be affected by orbital motion for a 250 km

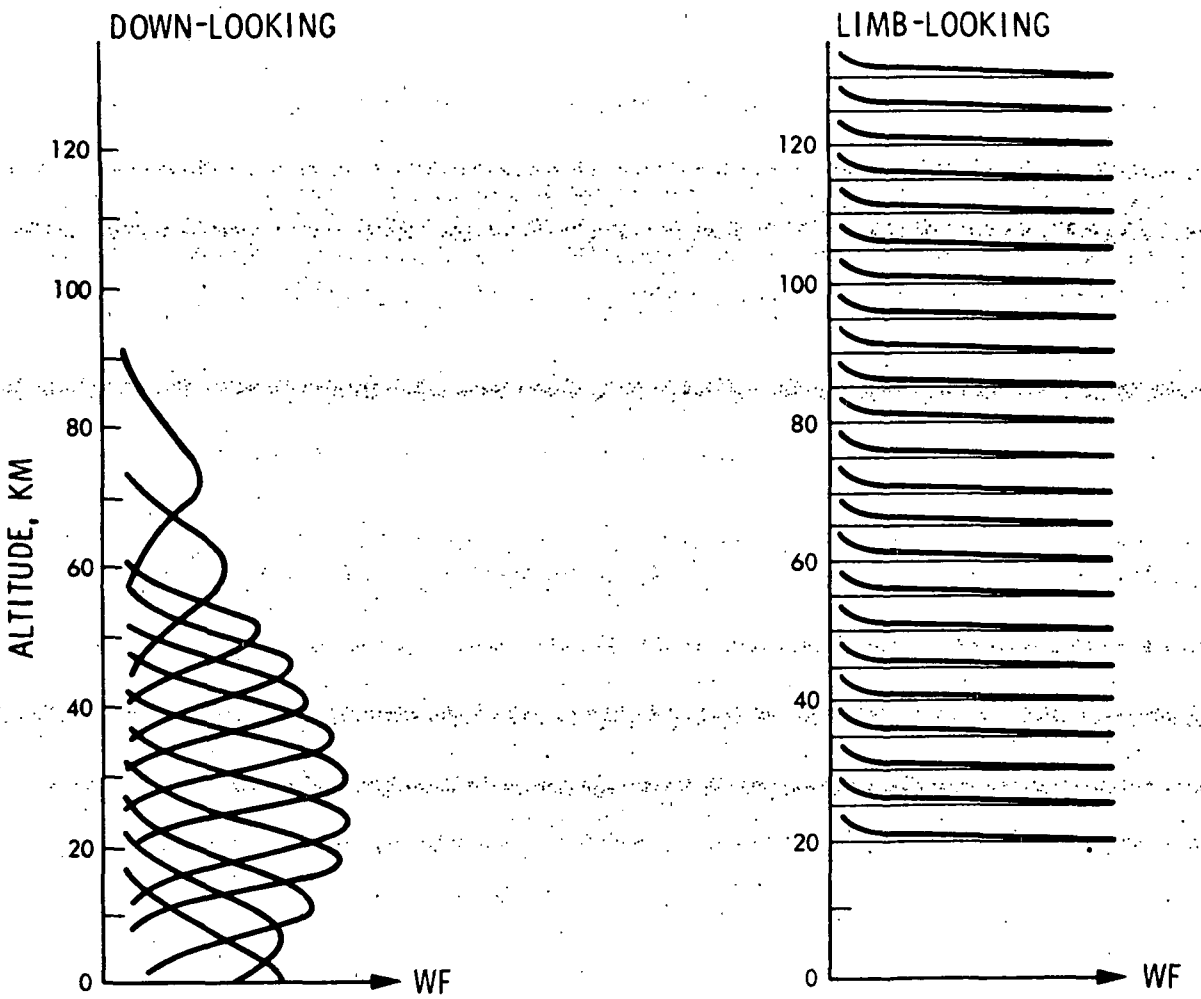


Figure 7.26: Down-Looking and Limb Looking Weighting Functions.

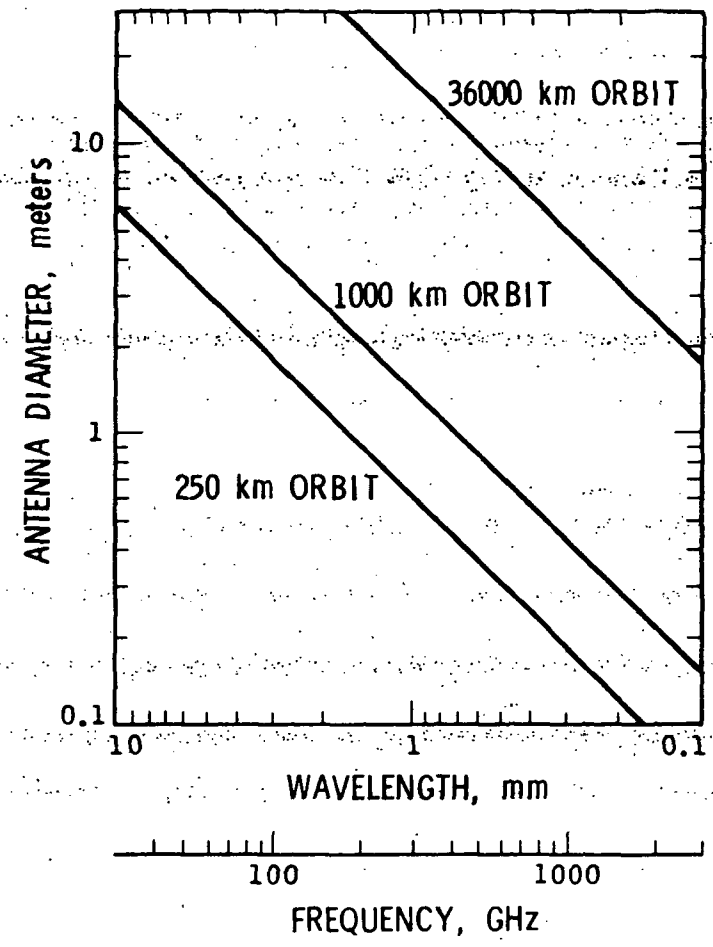


Figure 7.27: Antenna Diameter Required for 3 km Beamwidth at Tangent Point for Limb Observations.

(The antenna diameter required for other beamwidths is inversely proportional to the beamwidth. For example, a 1 1/2 km beamwidth requires an antenna twice as large as indicated by the above curves.)

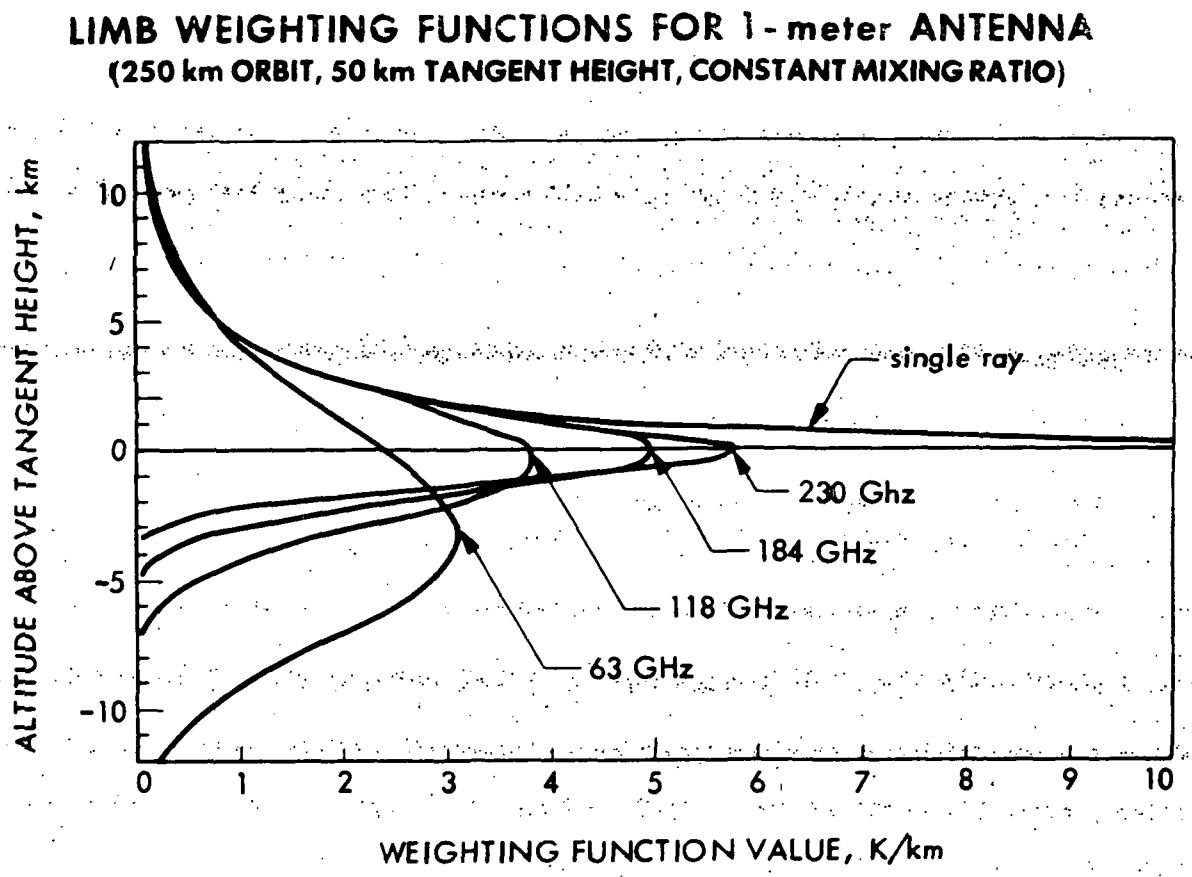


Figure 7.28: Limb Weighting Functions for 1-Meter Antenna in 250 km Altitude Orbit. [From Waters, 1976b]

orbit if their horizontal beamwidth is larger than $\sim 0.5^{o}$, even though the observations are in a direction normal to the orbital velocity.

Spectral resolution or selection is required of limb sounding instruments in order to identify emission from a particular gas. For microwave instrumentation arbitrarily fine spectral resolution can be achieved by means of electronic filtering after the signal has been converted to a sufficiently low frequency by mixing it with a local oscillator. The major requirement on the instrumentation for spectral resolution is then that the local oscillator frequency be sufficiently stable that its variation does not smear the resolution by an unacceptable amount. Such stabilities are readily achievable by locking the local oscillator to a reference crystal. Given this arbitrarily fine spectral resolution the ultimate limit on signal detectability of microwave radiometers is due to unaccounted for spectral responses in the instrument. In practice these effects can generally be reduced to ~ 0.1 K for the instrument bandwidths required. This limit is lower than the radiometer noise for measurement times available from satellite platforms, and the major limitation on measurements from space is expected to be the radiometer sensitivity.

Microwave radiometer sensitivities are typically expressed in terms of their equivalent system noise temperature T_s. This temperature is that which a blackbody would need in order to radiate the same amount of power as the noise power of the radiometer. At the present time, state of the art microwave radiometers at room temperature have system temperatures of ~ 1500 K at 100 GHz and ~ 4000 K at 200 GHz. The rms noise ΔT in the measurement is related to the system temperature by

$$\Delta T = \frac{2T_s}{\sqrt{B\tau}}$$

where B is bandwidth (frequency resolution) of the measurement and τ is the integration time. The factor of 2 is due to switching between the signal and a comparison target which is required to reduce the effects of gain variations to an acceptable level.

As an example of the sensitivity which can be achieved with present state-of-the-art instrumentation we consider measurements of emission by the 118 GHz oxygen line. For measurements of the middle stratosphere a resolution of ~ 10 MHz is required; with this resolution a temperature measurement having 3 K rms accuracy is possible in only 0.1 seconds observation time. For measurements of the lower thermosphere a resolution of ~ 0.1 MHz is required and with this resolution a temperature measurement having 3 K rms accuracy requires 10 seconds observation time. A reasonable amount of time available to scan the antenna beam over the altitude region being sensed is ~ 40 seconds for observations from a low altitude orbit as this is the amount of time it takes the observation path to move an amount comparable to the resolution along the line of sight. An optimum antenna scan program would use relatively short observation times at the lower altitudes and longer observation times at the higher altitudes.

Figure 7.29 shows the calculated signal for limb measurements of emission from the 118 GHz oxygen line. These calculations include the effect of a one meter diameter antenna. The horizontal axis gives the strength of the signal and the vertical axis gives the tangent height of the observation path. The various curves are for various frequencies away from the center of the line. As can be seen, the line center stays optically thick up to ∿100 km altitude and measurable signal exists up to at least 120 km. This insures that temperatures can be measured at least to 100 km altitude, and O_2 abundances to at least 120 km.

Figure 7.30 shows a similar set of curves calculated for measurements of water vapor by emission at its 183 GHz transition. The water vapor distribution used for these calculations is that given in Figure 7.7, except that curves a and b are for 0.5x and 2x that H_2O distribution. The inset shows the signal as a function of frequency for an observation path with 80 km tangent height. These calculations indicate that the 183 GHz H_2O line and present state of the art instrumentation could be used for meaningful measurements of H_2O between altitudes of ∿15 and 90 km.

The calculated signals shown in Figure 7.29 and 7.30 assume thermal equilibrium throughout the altitude region in which the signal is sufficiently large to be measurable. This has been checked for the 183 GHz H_2O line [Kakar, unpublished results] and the results of Kakar's calculations are given in Figure 7.31. That figure shows the excitation temperature of the 183 GHz H_2O line as a function of collision rate for various assumptions on the collision cross section R_{ij}. A kinetic temperature of 250 K and a radiational temperature of 200 K was used in these calculations. For a collisional frequency greater than ∿100 s^{-1} corresponding to altitudes below about 140 km the excitation temperature of the line equals the kinetic temperature, indicating this transition is in thermal equilibrium. The 118 GHz oxygen line will be in thermal equilibrium to much higher altitudes because its spontaneous transition probability is ∿10^4 lower than that for the 183 GHz H_2O line.

As Figures 29 and 30 show, the signal from the atmospheric limb is a drastic function of the tangent height of the observation in the region where the observation is optically thin (regions in which the signal is $\lesssim$150 K); it is these regions which must be used to sense composition. Because of this the signal varies rapidly with observation angle, even when the abundance of the species being observed is constant, and places requirements on the instrument pointing accuracy and stability in order to achieve accurate composition measurements. A reasonable goal for most composition measurements is 3% which requires measurements of limb emissivity to 3%. For partially transparent paths and observations of emission arising principally from the wings of spectral lines, the emissivity typically varies with tangent pressure p as p^2. For a 3% emissivity measurement, the tangent pressure must be known to ∿1% which corresponds to a height change in the atmosphere of ∿0.07 km or ∿0.003° angular change in the vertical plane for a 250 km orbit. The pointing must be known and constant for this amount during the measurement time if 3% composition accuracy is to be achieved.

LIMB EMISSION FROM 118 GHz O_2 LINE (1 meter ANTENNA IN 250 km ORBIT)

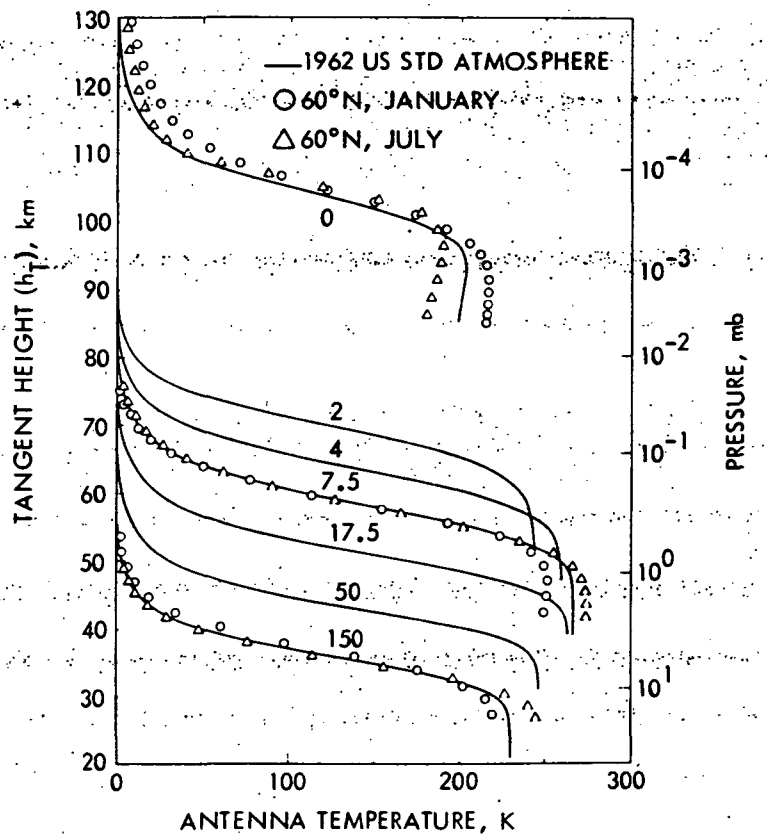


Figure 7.29: Limb Emission From 118 GHz O_2 Line. [From Waters, 1976b]

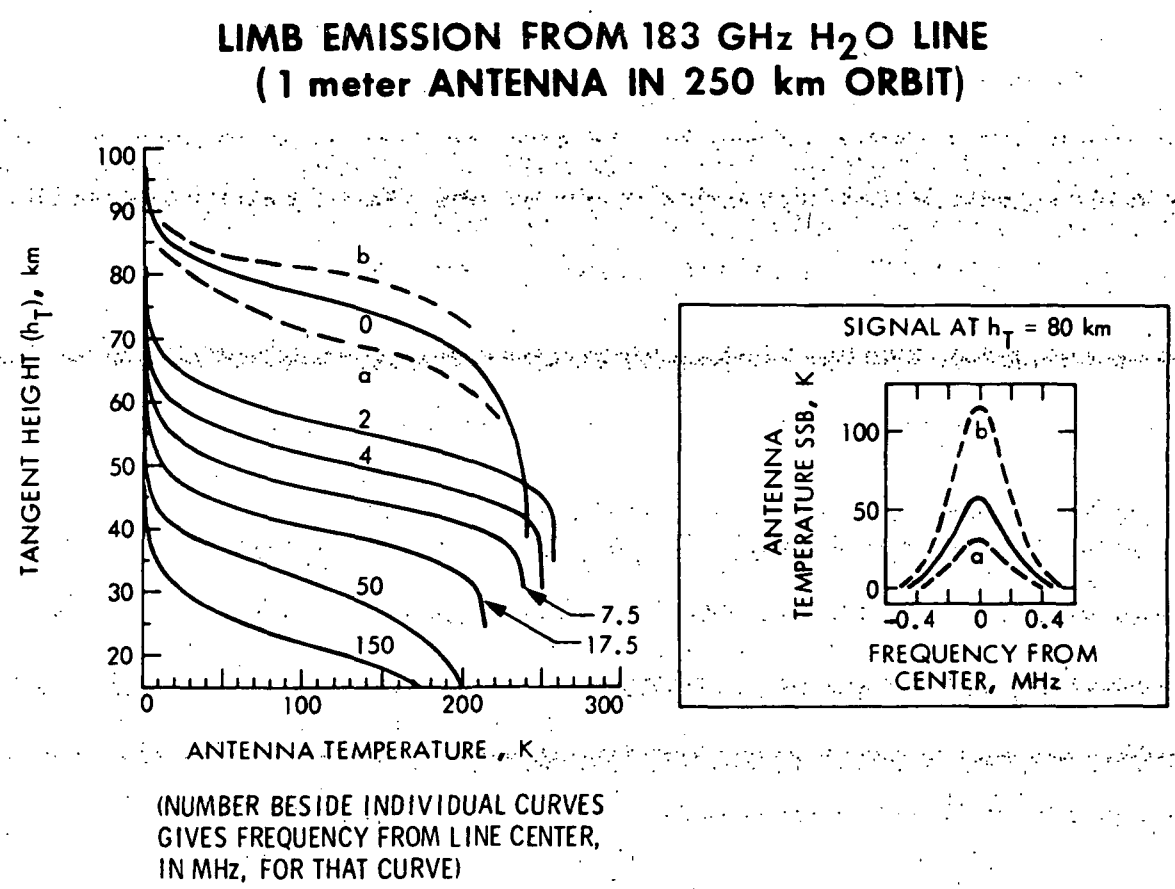


Figure 7.30: Limb Emission From 183 GHz H_2O Line. [From Waters, 1976b]

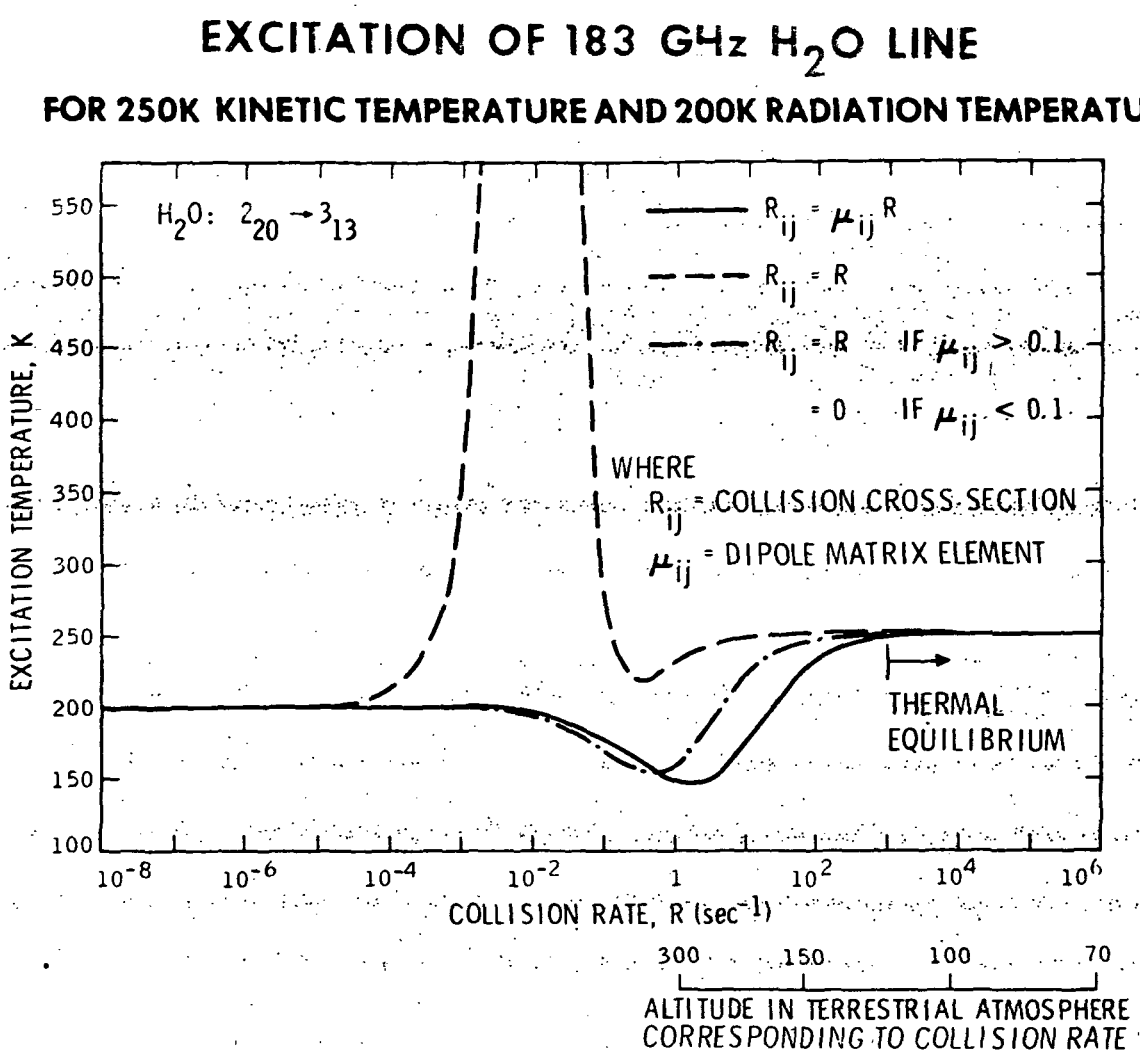


Figure 7.31: Excitation of 183 GHz H_2O Line. [Kakar, unpublished results]

If the required pointing accuracy and stability is not available from the platform being used for the measurements, microwave emission from appropriate oxygen lines in the 60 GHz band can provide the pointing reference and stability. This is done by selecting oxygen lines which are insensitive to temperature. Figure 7.32 shows the energy level diagram for the oxygen molecule. The microwave transitions are due to changes in the unpaired electron spin, and separate transitions occur for different rotational states. The intensities of the lower rotational lines decrease as the temperature increases because the number of molecules in these states is decreased with increasing temperature. However, the intensities of the higher rotational lines increase with increasing temperature because the number of molecules in these higher states increases as the temperature increases. At intermediate states the lines are relatively insensitive to temperature. Figure 7.33 shows the calculated limb emission from oxygen lines chosen for maximum insensitivity to temperature. The effects of a one meter antenna are included in the calculation. For the range of atmospheric conditions used in the calculations, which is rather extreme, the variation in atmospheric temperature causes a change $\lesssim 1\%$ in the atmospheric emissivity for a given pressure at tangent point. The radiometer sensitivity also allows measurements of the emissivity to $\lesssim 1\%$ for an 0.25 second observation time. Since the emissivity goes approximately as the square of the tangent pressure, the accuracy in measuring tangent pressure should be about 0.5%. Further calculations have indicated this accuracy can be achieved for observation paths having tangent heights between at least 35 km and 70 km altitude. Antenna beams covering other altitude ranges could be offset from the beam measuring the reference level allowing the same accuracy over an extended range. Thus, this technique for obtaining the pointing reference direction should certainly allow composition measurements to 3% accuracy.

The very rich microwave spectrum of ozone provides lines which are relatively insensitive to temperature variations. Such lines can be chosen which are negligibly affected by absorption or scattering from other species. These lines are ideally suited for precision monitoring of ozone profiles. An analysis of the potential monitoring accuracy is summarized in Figure 7.34. This analysis suggested that $\sim 1\%$ accuracy in monitoring ozone profiles might be possible even with temperature uncertainties as large as 5 K. Pointing accuracy of $.001^{\circ}$ will be required to achieve this composition accuracy as discussed above. Instrumental stability and calibration accuracy may also be limiting factors; at present these effects typically introduce $\sim 3\%$ uncertainties.

It is possible to simultaneously measure more than one species with a single radiometer if spectral lines from separate species are sufficiently close in frequency that they can fit within the radiometer intermediate frequency passband, and if the lines are not so close that they significantly overlap one another. One example of such a situation occurs for lines of O_3, ClO, and H_2O_2 near 205 GHz. Figure 7.35 shows calculated limb emission for these lines as would be observed from a 40 km altitude balloon. The manner in which they can be multiplexed into a single radiometer is indicated in Figure 7.36. Development of a balloon instrument [Waters, et al., 1977] to measure these species is underway.

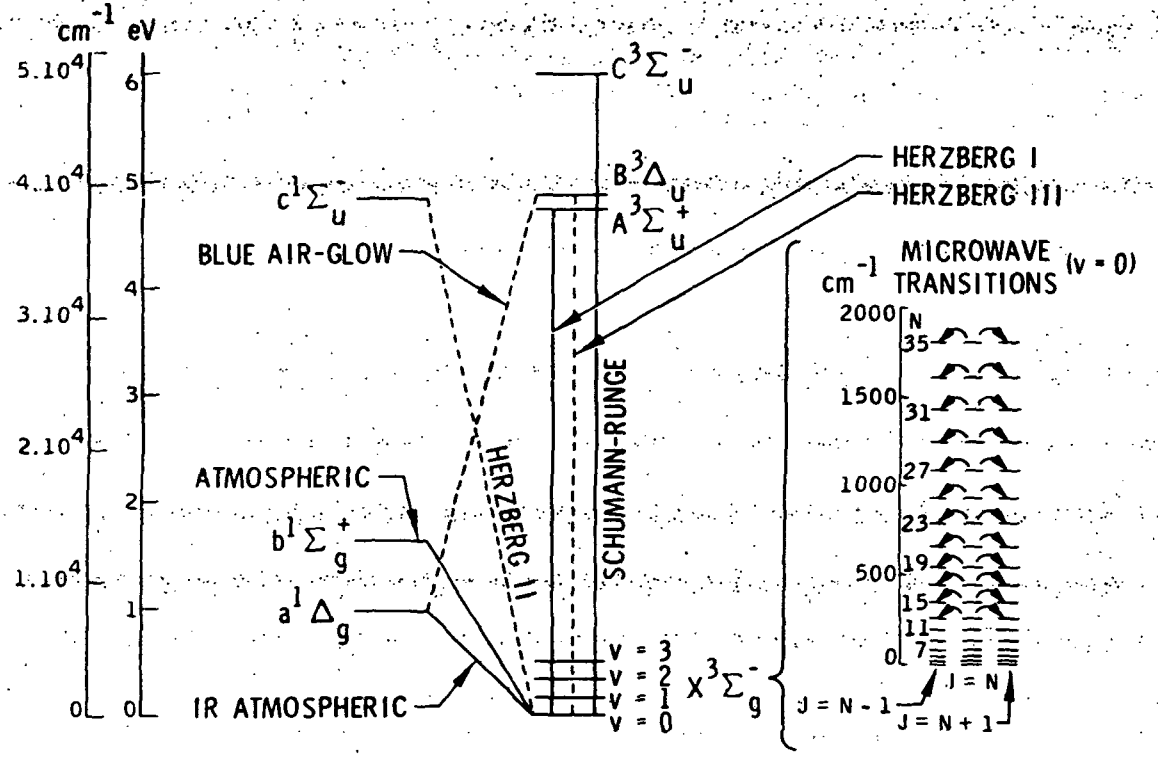


Figure 7.32: O_2 Energy Levels.

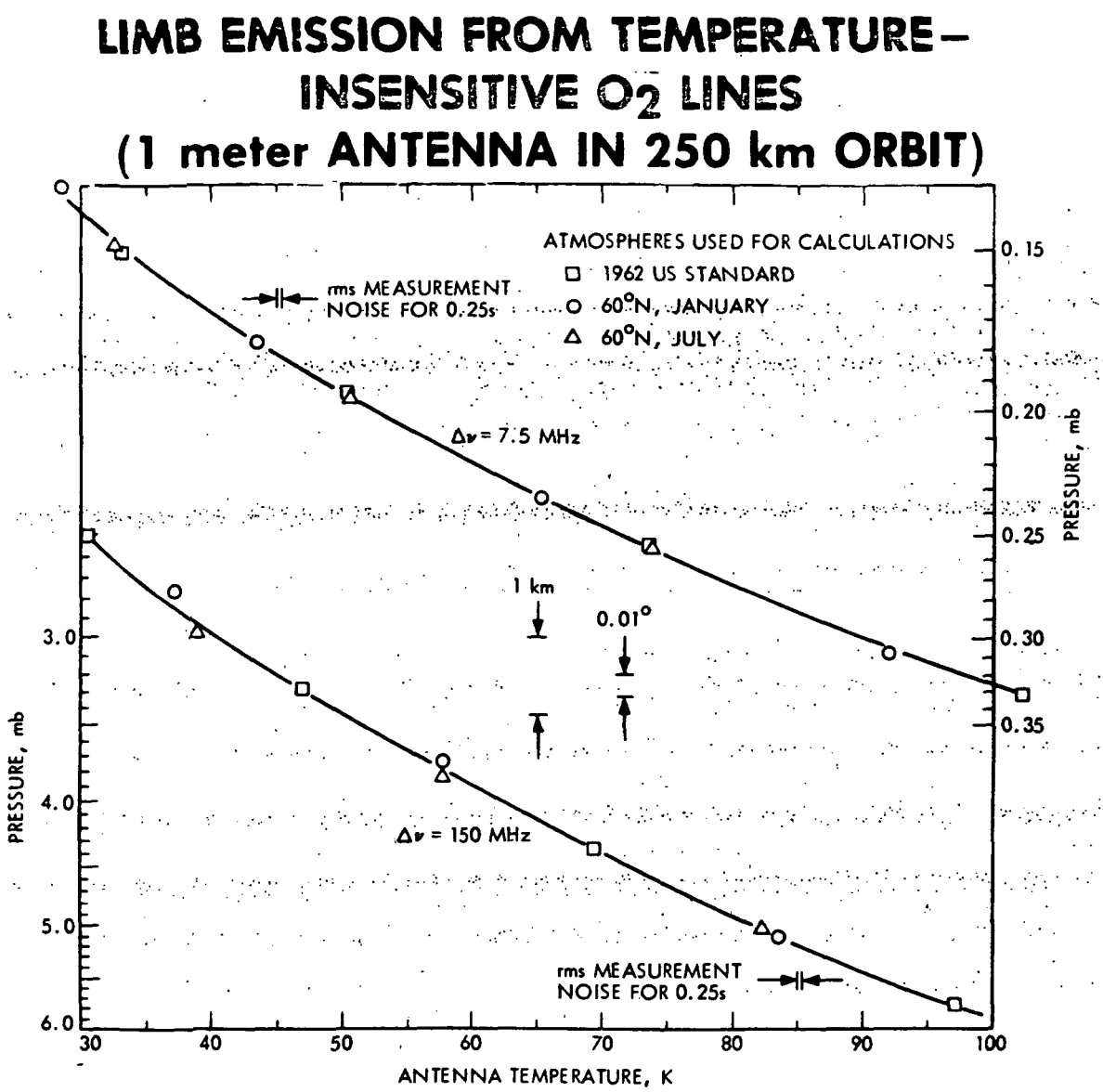


Figure 7.33: Limb Emission From Temperature Insensitive O_2 Lines. [From Waters, 1976b]

PRECISION MONITORING OF OZONE PROFILES BY MICROWAVE TECHNIQUES

- OZONE HAS VERY RICH MICROWAVE SPECTRUM. LINES CAN BE CHOSEN WHICH ARE NEGLIGIBLY AFFECTED BY ABSORPTION FROM OTHER SPECIES AND BY SCATTERING
- LINES CAN ALSO BE CHOSEN WHICH ARE INSENSITIVE TO ATMOSPHERIC TEMPERATURE VARIATIONS
  - ON THE WING OF AN OPTICALLY THIN LINE, THE MEASURED LIMB BRIGHTNESS TEMPERATURE FROM LINE HAVING LOWER ENERGY E_l DEPENDS UPON TEMPERATURE T AND OZONE NUMBER DENSITY N APPROXIMATELY AS

$$T_B \propto N T^{\frac{-5}{2}} \exp\left\{-E_l/KT\right\}$$

  - RELATIVE VARIATIONS IN T_B ARE GIVEN BY

$$\frac{dT_B}{T_B} = \frac{dN}{N} + \left(\frac{E_l}{KT} - \frac{5}{2}\right)\frac{dT}{T}$$

  - THE TERM INVOLVING dT/T INTRODUCES UNCERTAINTY IN DETERMINING N. IT CAN BE ELIMINATED BY CHOOSING A LINE SUCH THAT $E_l = 5/2\ kT$
  - FOR OZONE LINES AVAILABLE TO 1977 STATE OF ART INSTRUMENTATION, THE 206.132 GHz LINE IS LEAST SENSITIVE TO ATMOSPHERIC TEMPERATURE VARIATIONS. FOR THIS LINE, A 5°K TEMPERATURE UNCERTAINTY LEADS TO THE FOLLOWING UNCERTAINTIES IN DETERMINING OZONE ABUNDANCES

0.1% AT T = 190 K

-0.9% AT T = 220 K

-1.3% AT T = 250 K

- THESE RESULTS INDICATE OZONE CAN IN PRINCIPLE BE MEASURED WITH 1% PRECISION BUT A MORE SOPHISTICATED ANALYSIS INVOLVING NUMERICAL SIMULATIONS NEEDS TO BE PERFORMED
- MEASUREMENTS TO 1% PRECISION REQUIRE POINTING KNOWLEDGE TO ~0.001° (FOR 250 km ORBIT) AND PLACE SEVERE REQUIREMENTS ON INSTRUMENT CALIBRATION. SUCH CONSIDERATIONS ARE LIKELY TO DETERMINE THE PRECISION WHICH CAN BE ACHIEVED IN PRACTICE

Figure 7.34: Precision Monitoring of Ozone Profiles by Microwave Techniques: Outline of Analysis.

LIMB EMISSION BY ClO, H_2O_2, AND O_3 NEAR 205 GHz (CALCULATED FOR 40 km OBSERVATION ALTITUDE)

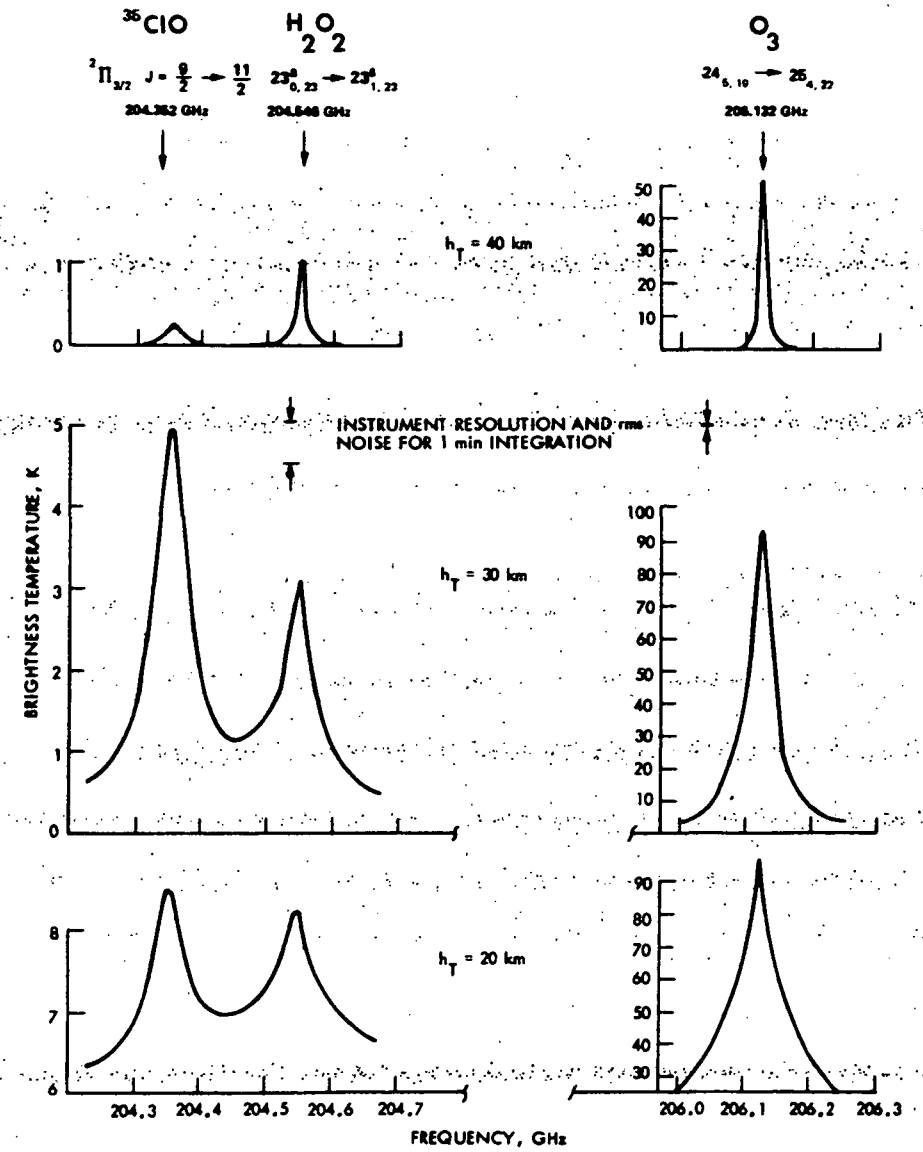


Figure 7.35: Limb Emission by ClO, H_2O_2, and O_3 Near 205 GHz. [From Waters, et al., 1977]. The tangent height h_T for the observation path is indicated.

ARRANGEMENT FOR SIMULTANEOUS MEASUREMENT OF ClO, H_2O_2, AND O_3 BY A SINGLE RADIOMETER

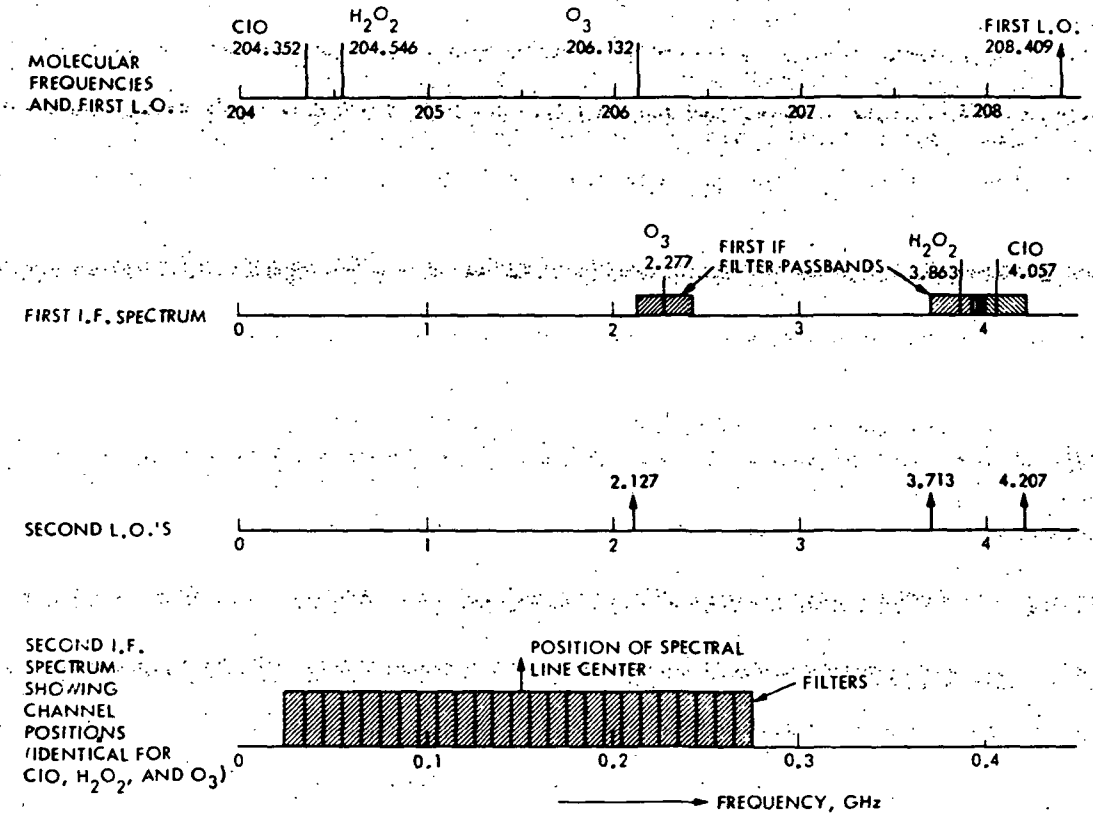


Figure 7.36: Arrangement for Simultaneous Measurement of ClO, H_2O_2, and O_3 by a Single Radiometer. [From Waters, et al., 1977]

Large scale atmospheric winds can also be remotely measured by the Doppler shift they produce in the frequency of a spectral line. Random molecular speeds in the atmosphere are of the order of 300 m/s whereas a meaningful measurement accuracy for large scale winds in the upper atmosphere is $\sim$10 m/s. This implies the frequency shift in a spectral line must be measured to $\sim$3% of its Doppler width, which is feasible. Wind measurements to a given accuracy require, however, that the component of orbital velocity in the observation direction be known to better than this accuracy. The orbital velocity for a 250 km orbit is $\sim$7 km/s; in order that the orbital velocity component in the observation direction be known to $\sim$3 m/s, which is required for $\sim$10 m/s wind accuracy, the angle of observation relative to the velocity vector for this orbital altitude must be know to $\sim 0.03^{\circ}$ for observation direction nearly normal to the direction of travel. Any spectral line can, in principle, be used for the wind measurement; the only requirement is that the line be sufficiently strong that adequate signal to noise is obtained. Preliminary analysis [Waters, 1976b] indicates that with the 118 GHz O_2 line and state-of-the-art instrumentation a 3 m/s wind accuracy, at least in the 70-100 km altitude range is possible for an observation time of $\sim$20 s or less. Such measurements would be very important in understanding the dynamics of the mesosphere and lower thermosphere.

Because the microwave O_2 lines arise from magnetic dipole transitions, they are split into Zeeman components by the terrestrial magnetic field. This splitting is noticeable only at altitudes above $\sim$40 km where the collisional broadening is sufficiently small that it does not mask the splitting. The absorption and emission by the Zeeman components is both polarized and anisotropic and a tensor form of the radiative transfer equation must be used to calculate the expected signals. Lenoir [1968] first formulated the expressions necessary for such calculations. Figure 7.37 shows the calculated emission from the Zeeman components of the 118 GHz O_2 lines for an observation path with 100 km tangent height. These calculations are for the circularly-polarized component of the signal. Also shown in Figure 7.37 is the rms noise for a state-of-the-art room temperature instrument with 0.05 MHz resolution and 10^8 observation time.

In principle, the Zeeman splitting of the oxygen lines can be used to measure the terrestrial magnetic field. For $\sim$10s observation time, a preliminary analysis indicates terrestrial magnetic field variations can be measured to $\sim$1% accuracy using the Zeeman components of the 118 GHz O_2 line. This is meaningful accuracy for only the most intense geomagnetic storms ; the normally-occurring storms will require an accuracy an order of magnitude better. Such accuracies should be possible with cryogenically-cooled instrumentation which could be available for use in space within the next few years.

In addition to temperature, winds, reference pressure level, magnetic field, O_2, and H_2O which were discussed above, microwave techniques can be used to measure many other upper atmospheric species. Figure 7.38 is a summary of the parameters which our analysis has indicated can be measured to meaningful accuracies over the indicated

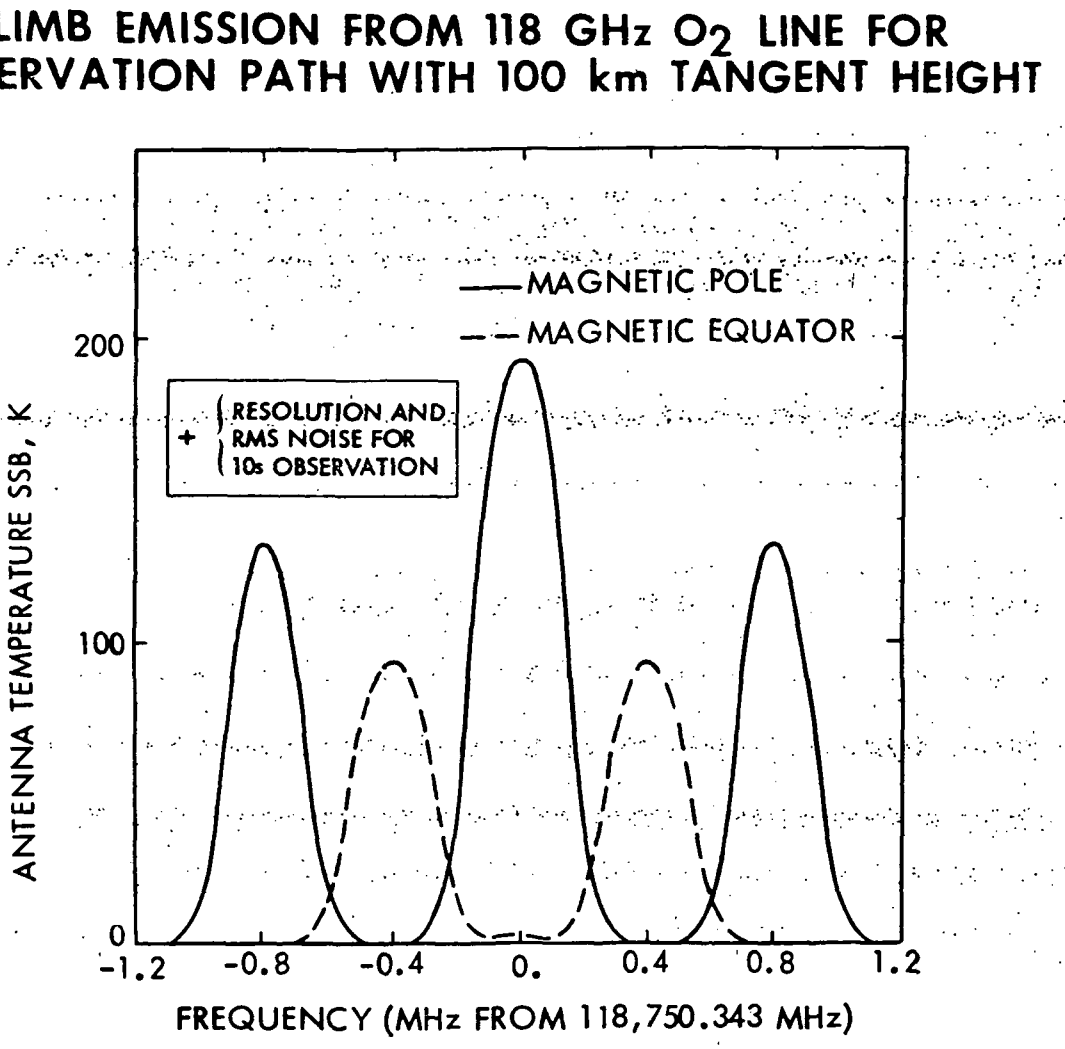


Figure 7.37: Limb Emission From 118 GHz O_2 line for Observation Path With 100 km Tangent Height.

altitude range from emission observations. The parameters are shown separately for those which should be measurable with present technology and with the technology it should be possible to develop in the next few years. Also indicated in Figure 7.38 is the 1977 capability for performing global measurements from satellites, and the advertised capability of sensors in other spectral ranges approved for operation up to 1980.

It should be emphasized that Figure 7.38 is by no means necessarily complete in terms of what parameters can be measured by microwave techniques. The application of microwave techniques to upper atmospheric research is relatively new. As investigations continue measurements of many additional species may prove possible.

7.7 Recommendations and Impact

In making recommendations for future microwave satellite systems for upper atmospheric applications some general principles must be considered. First, the time period in which the experiment will be performed is a very important factor. Atmospheric measurement priorities continually change as new measurements are made and theoretical understanding of the upper atmosphere is improved. Measurements which are important now may not be as important after the two or three years it typically takes to develop a space instrument. In recommending a satellite system it is important to be sure that the measurements to be made will be needed, or at least that there is a high probability that they will be needed, at the time the experiment is to be performed. Second, in planning a microwave experiment, consideration must be given to other methods of performing the same measurement. In certain cases, such as for very critical measurements and for cross-calibration checks, redundancy is desirable or even essential. In other cases economical constraints may dictate that only one technique be developed for particular measurements; in these cases the best technique must be developed.

The time period in which a microwave system for upper atmospheric measurements could be available is 1982 or later. This is based on a 4-year lead time due to 1 year needed for definition work and decision-making and 3 years needed for fabrication and integration onto a spacecraft.

Measurements which can be performed by microwave techniques and which are projected to be needed in the time period 1982 and later are summarized in Figure 7.39. These measurements are separated into those pertaining to the stratosphere and those pertaining to the mesosphere and lower thermosphere.

Some of the measurements indicated in Figure 7.39 can be performed with present technology; others require advancement of technology. We therefore recommend:

GLOBAL CONTINUOUS ATMOSPHERIC MEASUREMENT CAPABILITY

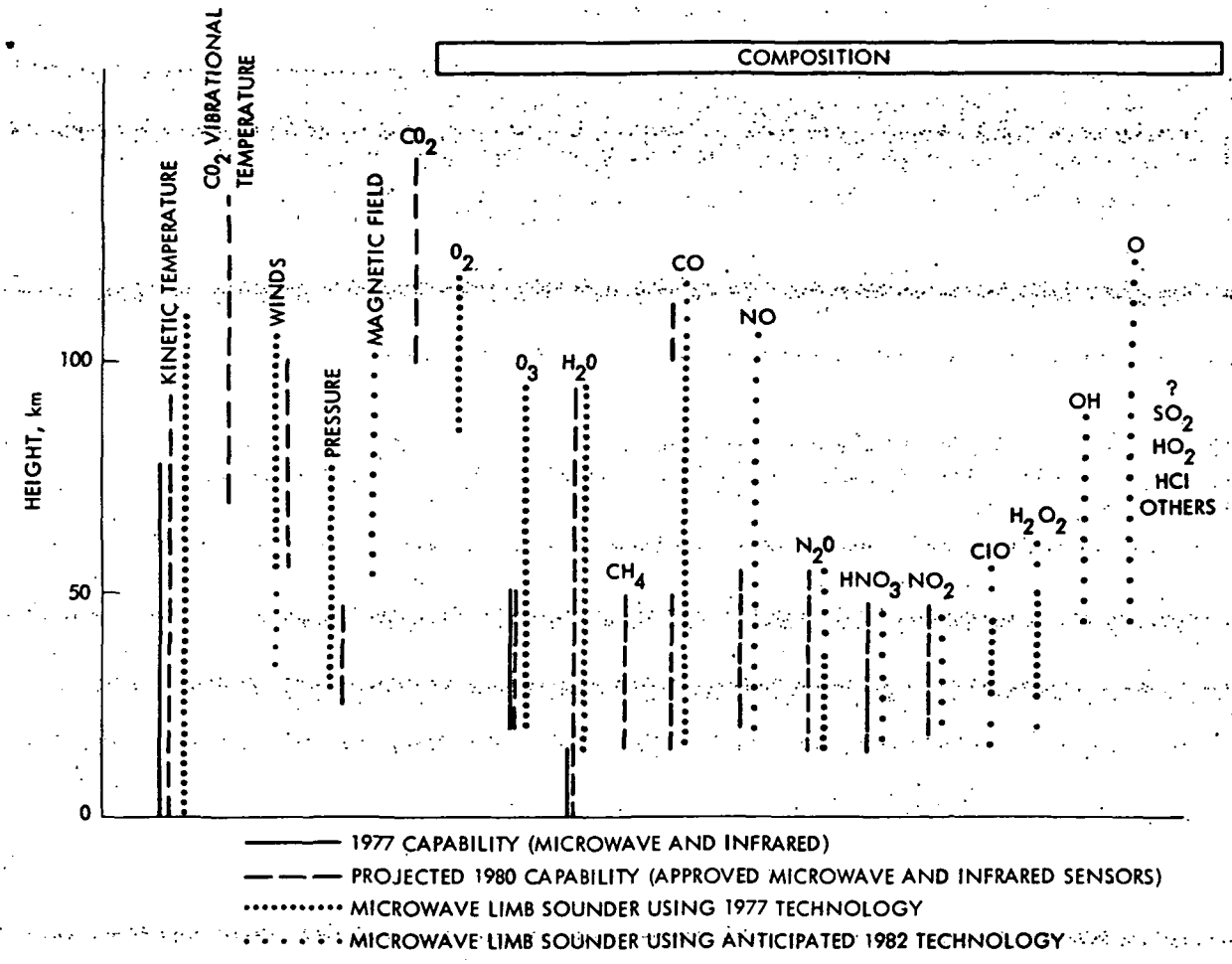


Figure 7.38: Global Continuous Atmospheric Measurement Capability.

PROJECTED 1982 UPPER ATMOSPHERIC MEASUREMENT NEEDS WHICH CAN LIKELY BE MET BY MICROWAVE TECHNIQUES

STRATOSPHERE

- OH AND ATOMIC O WITH 10% PRECISION (UPPER STRATOSPHERE ONLY)
- O_3 PROFILES WITH 1% PRECISION
- TEMPERATURE WITH 2 K PRECISION
- ClO, H_2O_2, CO, H_2O, N_2O, NO WITH 10% OR BETTER PRECISION

MESOSPHERE AND LOWER THERMOSPHERE

- OH, O, O_2, NO, CO, O_3, H_2O WITH 10% OR BETTER PRECISION
- TEMPERATURE WITH 5 K OR BETTER PRECISION
- WINDS WITH 10 M/S OR BETTER PRECISION
- MAGNETIC FIELD WITH 0.1% OR BETTER PRECISION (TO BE MEASURED SIMULTANEOUSLY WITH CERTAIN SPECIES)

Figure 7.39: Projected 1982 Upper Atmospheric Measurement Needs Which Can Likely be Met by Microwave Techniques.

1. Development of a microwave limb sounder instrument using present technology for versatile research use on either Shuttle sortie missions or on free-flier satellites. The instrument should have an antenna of at least one meter diameter which would give better than 5 km vertical resolution at frequencies above 118 GHz. In order that several species can be simultaneously measured with this instrument, it should be capable of accomodating several ($\sim$5 or more) radiometers. The radiometers should be modularly constructed so that they can be easily exchanged as technology advances and measurement priorities evolve. The versatility of this instrument is particularly important in order to allow it to be easily used for measurement requirements as yet unforeseen. The antenna, scanning, data handling and power supply systems should be common to any complement of radiometers used with the system. The instrument should be designed for a normal mode of operation in which it observes atmospheric thermal emission so that continuous global measurements can be performed. Consideration should be given to making it adaptable to also observe the sun for absorption measurements. The instrument should also be designed so that instruments operating in other spectral regions can easily be boresighted with it for simultaneous and complementary measurements.

   An initial complement of radiometers to be considered for this instrument should cover the following frequency bands:

118 GHz	temperature	15-100 km
	O_2 density	90-120 km
	wind	70-100 km
	magnetic field	70-100 km
184 GHz	H_2O	15-90 km
	O_3	15-90 km
205 GHz	precision O_3 profiles	15-50 km
	ClO and H_2O_2 if needed	
230 GHz	CO	15-120 km

   A thorough analysis, including numerical simulations, should be performed to verify that ozone profiles can be monitored to 1% accuracy with these techniques. Optimum spectral lines for the measurements should also be verified.

2. Development of new technology for space qualified heterodyne radiometers in the 100 to 3000 GHz spectral range. These radiometers would be capable of continuously measuring:

   abundances of: O, O_2, O_3, OH, H_2O, H_2O_2, HCl, HNO_3 NO, N_2O, ClO, CO and probably many other species

   temperature, winds, and magnetic field

Of particular importance is the measurement of O and OH in Earth's upper atmosphere. These species have spectral lines near 2000 GHz frequency and a top priority should be development of low-noise heterodyne radiometers in this region. In the spectral range of 100 to 300 GHz, the emphasis should be on obtaining lower-noise radiometers suitable for use in space. Improvement in system noise temperatures of from 1500 K to 100 K at 118 GHz will make possible a meaningful measurement of magnetic field. A goal for radiometer sensitivities throughout the 100 to 3000 GHz range should be that the system noise temperature in Kelvins equals the frequency in GHz, although ten times worse sensitivity will sometimes be usable.

The laboratory spectroscopy required to define instrument parameters and interpret the measurements should also be supported.

These recommendations have been summarized in Figure 7.2.

The impact of microwave measurements of the upper atmosphere should be very significant in the 1982+ time period. Obtaining as complete as possible an understanding of the workings of the upper atmosphere is a very challenging scientific problem; many related measurements by complementary techniques are needed. Several measurements (including precision monitoring of ozone profiles, measurement of temperatures throughout the stratosphere, mesosphere, and lower thermosphere, measurement of the important species of O and OH, and measurements of winds and magnetic fields in the mesosphere and lower thermosphere) can either be performed uniquely with microwaves, or microwave techniques are apt to be the best way to perform the measurements. Such measurements are becoming more and more essential in order that rational decisions can be made regarding any necessary regulation of man's technological activities that threaten Earth's protective ozone layer. This regulation involves serious aspects of national and international policy since the industries affected are very important economically.

As an example of the broad impact which the measurements have, Figure 7.40 lists the various U.S. agencies and an industrial association (MCA: Manufacturing Chemists Association) which are supporting related activities.

MICROWAVE APPLICATIONS TO THE STRATOSPHERE, MESOSPHERE, AND LOWER THERMOSPHERE

APPLICATION / USER AGENCY / PARAMETER MEASURED	RESEARCH							MONITORING				
	NASA	NSF	NOAA	EPA	ERDA	FAA	MCA	NOAA	FAA	EPA	ERDA	DOD
TEMPERATURE	•	•			•		•	•				
PRESSURE	•	•			•							
WINDS	•	•			•							
+MAGNETIC FIELD	•	•			•							
COMPOSITION												
O_3	•	•	(*)	(*)	•	•	•	•				
H_2O	•	•		(*)	•	•	•					
CO	•	•		(*)	•	•	•					
ClO	•	•		(*)	•	•	•					
H_2O_2	•	•		(*)	•	•	•					
N_2O	•	•		(*)	•	•	•					
NO	•	•	(*)	(*)	•	•	•					
HCl	•	•		(*)	•	•	•					
OH	•	•		(*)	•	•	•					
O	•	•		(*)	•	•						
HNO_3	•	•		(*)		•	•					
HO_2	•	•		(*)	•	•	•					
NO_2	•	•	(*)	(*)	•	•						
OTHERS	•	•		(*)	•	•	•					

AN INTERAGENCY WORKING GROUP ON "MONITORING OF THE STRATOSPHERE" IS NOW PREPARING A REPORT ON REQUIREMENTS.

*TECHNOLOGY ADVANCEMENT REQUIRED. ( ) USED AS COMPLEMENTARY OR CORROBORATIVE MEASUREMENT ONLY

Figure 7.40: Microwave Applications to the Stratosphere, Mesosphere, and Lower Thermosphere: User Agencies. The data for this figure were taken from information given in the Program Plan for the NASA Program on Upper Atmospheric Research [NASA Upper Atmospheric Research Office, 1976].

7.8 Acknowledgments

R. K. Kakar provided many of the unpublished calculations given in this report. J. J. Gustincic, T. G. Phillips, T. de Graauw, A. R. Kerr, R. J. Mattauch, P. N. Swanson, and their associates made essential contributions to the unpublished microwave measurements which are described. J. T. Houghton prepared certain paragraphs in Sections 7.2, 7.3, and 7.6 which have been used earlier [Waters, 1976b]. P. J. Crutzen kindly allowed use of his figure showing calculated depletion of ozone by chlorine compounds prior to its appearing in print. W. Planet communicated preliminary conclusions of the Inter-agency Working Group on Monitoring of the Stratosphere. H. K. Roscoe and R. T. Watson provided many helpful discussions.

7.9 References

Anderson, J.G., "A Simultaneous Measurement of Cl and ClO in the Earth's Stratosphere," Int. Conf. on Stratosphere and Related Problems, Utah State University, [1976].

Anderson, J.G., J.J. Margitan, D.H. Stedman, "Atomic Chlorine and the Chlorine Monoxide Radical in the Stratosphere: Three in situ Observations," Science, 198, 501, [1977].

Bates, D.R. and M.J. Nicolet, "The Photochemistry of Atmospheric Water Vapor," J. Geophys. Res., 55, 301, [1950].

Chamberlain, J.W., "A Mechanism for Inducing Climatic Variations Through the Stratosphere: Screening of Cosmic Rays by Solar and Terrestrial Magnetic Fields," J. Atmos. Sci., 34, 737, [1977].

Chapman, S., "A Theory of Upper Atmospheric Ozone," Mem. Royal Met. Soc., 3, 103, [1930].

CIAP, "Report of Finds. The Effects of Stratospheric Pollution by Aircraft," U.S. Department of Transportation, DOT-TST 75-50, Washington, [1974].

CIAP Monograph 1, "The Natural Stratosphere of 1974," U.S. Department of Transportation, Washington, [1974].

CIAP Monograph 3, "The Stratosphere Perturbed by Propulsion Effluents," U.S. Department of Transportation, [1974].

CIAP Monograph 4, "The Natural and Radiatively Perturbed Troposphere," U.S. Department of Transportation, Washington, [1974].

CIAP Monograph 5, "Impacts of Climatic Change on the Biosphere," U.S. Department of Transportation, Washington, [1974].

CIRA, "COSPAR International Reference Atmosphere 1972," Akademie-Verlag, Berlin [1972].

Crutzen, P.J., "The Influence of Nitrogen Oxides in the Atmospheric Ozone Content," Roy. Meteorol. Soc. Quart. J., 96, 320-325, [1970].

Crutzen, P.J., "A Review of Upper Atmospheric Photochemistry,"Can. J. Chem., 52, 1569-1581, [1974a].

Crutzen, P.J., I.S.A. Isaksen, J.R. McAfee, "The Impact of the Chlorocarbon Industry on the Ozone Layer," J. Geophys. Res., [in press, 1977].

Department of the Environment, "Chlorocarbons and Their Effect on Stratospheric Ozone," Her Majesty's Stationery Office, London, [1976].

Grody, N.C., P.P. Pelegrino, "Synoptic-Scale Studies Using the Nimbus 6 Scanning Microwave Spectrometer," J. Appl. Meteorology, 16, 816, [1977].

Hays, P.B., J.J. Olivero, "Carbon Dioxide and Monoxide Above the Troposphere," Planet. Space Sci., 18, 1729, [1970].

Hidalgo, H., and P.J. Crutzen, "The Tropospheric and Stratospheric Composition Perturbed by NO_x Emissions of High-Altitude Aircraft," J. Geophys. Res., 82, 5833, [1977].

Howard, C.J., and K.M. Evenson, "Kinetics of the Reaction of HO_2 with NO," Geophys. Res. Lett., 4, 437, [1977].

Kakar, R.K., J.W. Waters, W.J. Wilson, "Venus: Microwave Detection of Carbon Monoxide," Science, 191, 379, [1976].

Kakar, R.K., J.W. Waters, W.J. Wilson, "Mars: Microwave Detection of Carbon Monoxide," Science, 196, 1090, [1977].

Lenoir, W.B., "Microwave Spectrum of Molecular Oxygen in the Mesosphere," J. Geophys. Res., 73, 361, [1968].

McElroy, M.B., "Chemical Processes in the Solar System," Int. Rev. Sci., 9, 127, Butterworths, London, [1976].

McElroy, M.B., J.W. Elkins, S.C. Wofsy, and Y.L. Yung, "Sources and Sinks of Atmospheric N_2O," Rev. Geophys. Space Phys., 14, 143-150, [1976].

Molina, M.J., and F.S. Rowland, "Stratospheric Sink for Chlorofluoromethanes: Chlorine Atom Catalyzed Destruction of Ozone," Nature, 249, 811-812, [1974].

NASA Stratospheric Research Advisory Committee, "A Measurement Strategy for Stratospheric Research," [preliminary manuscript dated July 1977].

NASA Upper Atmospheric Research Office, "The NASA Program on Upper Atmospheric Research: Program Plan," Washington, D.C. [1976].

NASA "Chlorofluoromethanes and the Stratosphere," NASA Reference Publication 1010, NASA Scientific and Technical Information Office [1977].

National Academy of Sciences, "Environmental Impact of Stratospheric Flight. Biological and Climatic Effects of Aircraft Emissions in the Stratosphere," Washington, D.C., [1975].

National Academy of Sciences, "Panel on Atmospheric Chemistry, Halocarbons: Effects on Stratospheric Ozone," Washington, D.C., [1976].

Noxon, J.F., "Seasonal and Latitudinal Behavior of Stratospheric NO_2," Int. Conf. on Problems Related to the Stratosphere, Utah State University, Logan, Utah [1976].

Oliver, R.C., E. Bauer, H. Hidalgo, K.A. Gardner, W. Wasylkiwskyj, "Aircraft Emissions: Potential Effects on Ozone and Climate," Rpt. FAA-EQ-77-3, U.S. Department of Transportation, Washington, D.C., [1977].

Penfield, H., M.M. Litvak, C.A. Gottlieb, A.E. Lilley, "Mesospheric Ozone Measured from Ground-Based Millimeter-Wave Observations," submitted to J. Geophys. Res. [1976].

Prabhakara, C. et al., "Seasonal and Geographic Variation of Atmospheric Ozone Derived from Nimbus 3," NASA Goddard Space Flight Center NASA-TN-D-6443, [1971].

Radford, H.E., M.M. Litvak, C.A. Gottlieb, E.W. Gottlieb, S.K. Rosenthal, A.E. Lilley, "Mesospheric Water Vapor Measured from Ground-Based Microwave Observations," J. Geophys. Res., 82, 472, [1977].

Rodgers, C.D., "Some Theoretical Aspects of Remote Sounding in the Earth's Atmosphere," J. Quant. Spectrosc. Radiat. Transfer, 11, 767, [1971].

Rosenkranz, P.W., B.G. Anderson, K.F. Kunzi, R.M. Paroskie, R.J. Parr, D.H. Staelin, J.W. Waters, "Development of a Stratospheric and Mesospheric Microwave Temperature Sounder Experiment," Final Report to NASA Advanced Applications Flight Experiments Program, [1975].

Schmeltekopf, A.L., D.L. Albritton, P.J. Crutzen, P.D. Goldan, W.J. Harrop, W.R. Henderson, J.R. McAfee, M. McFarland, H.I. Schiff, and T.L. Thompson, "Stratospheric Nitrous Oxide Altitude Profiles at Various Latitudes, J. Atmos. Sci., 34, 729, [1977].

Shimabukuro, F.I., P.L. Smith, W.J. Wilson, "Estimation of the Daytime and Nighttime Distribution of Atmospheric Ozone from Ground-Based mm-Wavelength Measurements," J. App. Meteorology, 16, 929, [1977].

Shimazaki, T., and A.R. Laird, "A Model Calculation of the Diurnal Variation in Minor Neutral Constituents in the Mesosphere and Lower Thermosphere Including Transport Effects," J. Geophys. Res., 75, 3221, [1970].

Staelin, D.H., A.H. Barrett, J.W. Waters, F.T. Barath, E.J. Johnston, P.W. Rosenkranz, N.E. Gaut, W.B. Lenoir, "Microwave Spectrometer on the Nimbus 5 Satellite: Meteorological and Geophysical Data," Science, 182, 1339, [1973].

Staelin, D.H., P.W. Rosenkranz, F.T. Barath, E.J. Johnston, J.W. Waters, "Microwave Spectroscopic Imagery of the Earth," Science, 197, 991-993, [1977].

Sze, N.D., H. Rice, "Nitrogen Cycle Factors Contributing to N_2O Production from Fertilizers," Geophys. Res. Lett., 3, 343, [1976].

Taylor, B.F., J.D. Perry, "The Major Stratospheric Warning of 1976-77," Nature, 267, 417, [1977].

Waters, J.W., "Observations of High-J Atmospheric O_2 Lines at Arecibo Observatory," M.I.T. Research Laboratory of Electronics Quarterly Progress Report No. 108, p. 59, [1973].

Waters, J.W., K.F. Kunzi, R.L. Pettyjohn, R.K.L. Poon, D.H. Staelin, "Remote Sensing of Atmospheric Temperature Profiles with the Nimbus 5 Microwave Spectrometer," J. Atmospheric Sciences, 32, 1953, [1975].

Waters, J.W., W.J. Wilson, F.I. Shimabukuro, "Microwave Measurement of Mesospheric Carbon Monoxide," Science, 191, 1174, [1976].

Waters, J.W., "Microwave Infrared Mesospheric Stratospheric Experiment (MIMSE)," Proposal submitted to NASA for Spacelab I by Jet Propulsion Laboratory, Oxford University (U.K.), National Physical Laboratory (U.K.), University of Berne (Switzerland) and University of Bonn (W. Germany), [1976b].

Waters, J.W., J.J. Gustincic, R.K. Kakar, A.R. Kerr, H.K. Roscoe, P.N. Swanson, "The Microwave Limb Sounder Experiment: Observations of Stratospheric and Mesospheric H_2O," in Interhemispheric Survey of Minor Upper Atmospheric Constituents During October-November 1976, NASA TM X-73630 Lewis Research Center [1977].

Waters, J.W., J.J. Gustincic, R.K. Kakar, H.K. Roscoe, P. Zimmermann, "A Balloon-Borne Microwave Limb Sounder for Upper Atmosphere Measurements," proposal to NASA, [1977].

Wofsy, S.C., J.C. McConnell, M.B. McElroy, "Atmospheric CH_4, CO, and CO_2," J. Geophys. Res., 77, 4477, [1972].

Wofsy, S.C., M.B. McElroy, Y.L. Yung, "The Chemistry of Atmospheric Bromine," Geophys. Res. Lett., 2, 215, [1975].

Wofsy, S.C., "Temporal and Latitudinal Variations of Stratospheric Trace Gases: A Critical Comparison Between Theory and Experiment" [preprint draft dated February, 1977].

CHAPTER 8

SYSTEMS*

8.1 Executive summary

8.1.1 Summary

A. Passive microwave spectrometers and imaging systems have been successfully flown in space since 1961; more than 12 such systems will have flown before 1979.

B. Current instrument technology is adequate to support most contemplated future missions; selected areas for improvement include low-noise millimeter and submillimeter wavelength receivers and the design of large multi-frequency antennas.

C. A wide variety of applications exist for high-resolution passive microwave data; the required instrument specifications for these diverse applications overlap considerably. A "baseline" observatory concept that serves many applications incorporates a 3-4 meter reflector antenna rotating $\sim$ 0.5 Hz about the nadir axis. The microwave spectrometer would have $\sim$ 15 channels observing $\sim$ 1-200 GHz at $\sim$ 60° zenith angle with $\sim$ 6-12-hour revisit times and $\sim$ 5-14 km resolution for full earth coverage from a $\sim$ 1200-km orbit; two such systems in different orbits could provide 6-hour coverage. The 1) very high time resolution requirements for severe storm monitoring, 2) the long-wavelength high-spatial-resolution requirements of soil moisture sensing, 3) the limb-scan geometry desired for probing above $\sim$ 30 km altitude, and 4) the high resolution required for coastal zone and ocean pollution monitoring might best be obtained by separate special purpose systems.

D. Systems concepts proposed elsewhere and summarized here include 1) a baseline-type spectrometer with a fixed reflector (SIMS), 2) three baseline-type spectrometers

*Prepared by D. H. Staelin, J. J. Gustincic, and P. W. Rosenkranz.

with scanning reflector antennas, 3) a 10-m square low-frequency phased array, 4) a 100-m reflector with moveable subreflector, 5) a 100-m reflector with ∿ 100 feeds for ocean observations, 6) a limb-scanning spectrometer for atmospheric studies, 7) a pressure-sensing 5-mm wavelength radar transmissometer, and 8) a low resolution wide-swath synthetic aperture radar (SAR) to support a passive microwave observatory with a "zoom" capability. Although this list is not exhaustive, it includes most classes of instruments of current interest.

8.1.2 Recommendations

		Estimated Cost Effectiveness
1)	Prompt development of an operational imaging spectrometer 1-200 GHz, such as the baseline system described above.	Highest
2)	Development of a limb-scanning microwave spectrometer for shuttle sortie missions and eventual operational use.	Very high
3)	Development of a ∿ 1-3 GHz dual-polarized phased array ∿ 10-m square for sensing soil moisture, etc., and to supplement a baseline observatory.	High
4)	Study and development of a pressure-sensing 5-mm radar transmissometer.	High
5)	Development of a 100-200 GHz imaging spectrometer for monitoring severe storms from geostationary orbit.	High
6)	Study and possible development of a wide-swath low-resolution synthetic aperture radar to provide a "zoom" capability for a passive microwave observatory.	Moderate
7)	Development of 100-m reflector antenna system for geophysical sensing.	Low

8.2 Introduction

This chapter begins with a history of passive microwave sensors in space and a brief survey of instrument technology. In order to clarify the relationships between various applications, a baseline passive microwave observatory system is then defined and evaluated. This is followed by a brief discussion of some of the systems concepts that have been proposed for consideration.

In order to arrive at a sound set of recommendations, the next two sections explore possible mission concepts and various cost benefit considerations. These are then followed by a series of recommendations for systems and technology development.

8.3 History of passive microwave sensors in space

The first use of microwave radiometry on a spacecraft was for remote sensing of cloud-shrouded Venus. Mariner 2 determined that the planetary emission was characterized by limb darkening (Barath et al., 1964) which confirmed that Venus had a high surface temperature.

Table 8.3.1 presents a summary of microwave radiometers that should have been launched prior to the end of 1978. The first satellite-based microwave observations of Earth were made by Cosmos-243 (Basharinov et al., 1969). The most extensive microwave observations to date, however, have been made by satellites in the Nimbus series (Gloersen et al., 1974; Staelin et al., 1973, 1977; Wilheit et al., 1976). Numerous atmospheric and surface effects have been observed, but only the most quantitative interpretations of the data are mentioned in the table.

Table 8.3.1 conveys rather well the acceleration of activity in this field, with three different instruments on five satellites scheduled for launch in 1978. Not so evident from the table is the fact that research began with the

Table 8.3.1. History of microwave radiometry on spacecraft.

Year of launch	Spacecraft	Instrument acronym	Frequencies (GHz)	Antenna type	Swath-width of scan (km)	Smallest resolution element (km)	Principal parameters measured or inferred
1962	Mariner 2 (Venus flyby)	—	15.8, 22.2	mechanically scanned parabola	plane-tary	1300*	limb darkening of planetary emission
1968	Cosmos 243	—	3.5, 8.8, 22.2, 37	nadir viewing parabola	—	13	atmosphere: water vapor content; liquid water content. surface: sea temperature, sea ice concentration.
1970	Cosmos 384						
1972	Nimbus 5	ESMR	19.3	electrically scanned array	3000	25	atmosphere: rain rate. surface: sea ice concentration, ice classification.
		NEMS	22.2, 31.4, 53.6, 54.9, 58.8	five lens-loaded horns, nadir viewing	—	200	atmosphere: temperature profile, water vapor content, liquid water content. surface: ice classification, snow cover.
1973	Skylab	S-193	13.9	mechanically scanned parabola	180	16	surface: soil moisture
		S-194	1.4	nadir viewing array	—	115	surface: soil moisture
1974	Meteor	—	37	dual polarization 35° from nadir	—		atmosphere: liquid water content
1975	Nimbus 6	ESMR	37	dual polarization electrically scanned array	1300	20 × 43	same as Nimbus 5 ESMR
		SCAMS	22.2, 31.6, 52.8, 53.8, 55.4	three rotating hyperbolic mirrors	2700	150	same as Nimbus 5 NEMS
1978	Block 5D	SSM	50.5, 53.2, 54.3, 54.9, 58.4, 58.8, 59.4	single rotating mirror	1600	175	atmosphere: temperature profile
1978	Tiros N (2 satellites)	MSU	50.3, 53.7, 55.0, 57.9	dual rotating mirrors	2300	110	atmosphere: temperature profile
1978	Nimbus G	SMMR	6.6, 10.7, 18, 21, 37	single oscillating mirror	800	18 × 27*	atmosphere: water vapor content; liquid water content, rain rate. surface: sea state (wind speed), sea temperature, sea ice concentration, ice classification, snow cover, soil moisture.
1978	SeaSat A				600	14 × 21*	

*resolution at highest frequency only

identification and measurement of gross surface and atmospheric phenomena. Further progress with these techniques requires greater specificity of the geophysical parameters, which in most cases implies finer spatial resolution.

8.4 Survey of current instrument technology

The most critical elements in passive microwave remote sensing systems are the receivers, antennas, and data systems. The state-of-the-art for ground-based receivers is summarized in Figure 8.4.1. Most of the receiver specifications can be duplicated in space, although those that employ cryogenics may be troublesome. Uncooled receivers generally fall near the line labeled "useful" in the figure. It appears that present receiver technology is adequate to meet most of the applications requirements discussed in this report; exceptions are treated separately.

Performance parameters of large millimeter-wave radio telescopes are presented in Figure 8.4.2. The angular resolutions of these antennas are more than adequate for the applications discussed here. These antennas are not rapidly scanned, however; to do this requires mechanical motion or electronic beam steering. Approaches to this problem that have been implemented for space are listed in Table 8.3.1, and several proposed concepts are discussed in section 8.7. Most of the applications discussed in this report require antennas that might comprise about half the total cost of the instrument; antennas requiring unfurling or space fabrication would generally cost more and involve greater risks.

Current communications technology is more than adequate for the data rates discussed here, so implementation of any necessary additions to communications facilities by $\sim$ 1985 seems entirely feasible. These data rates can be estimated by assuming 20 parameter maps with full earth coverage at 5-km resolution are produced continuously. This

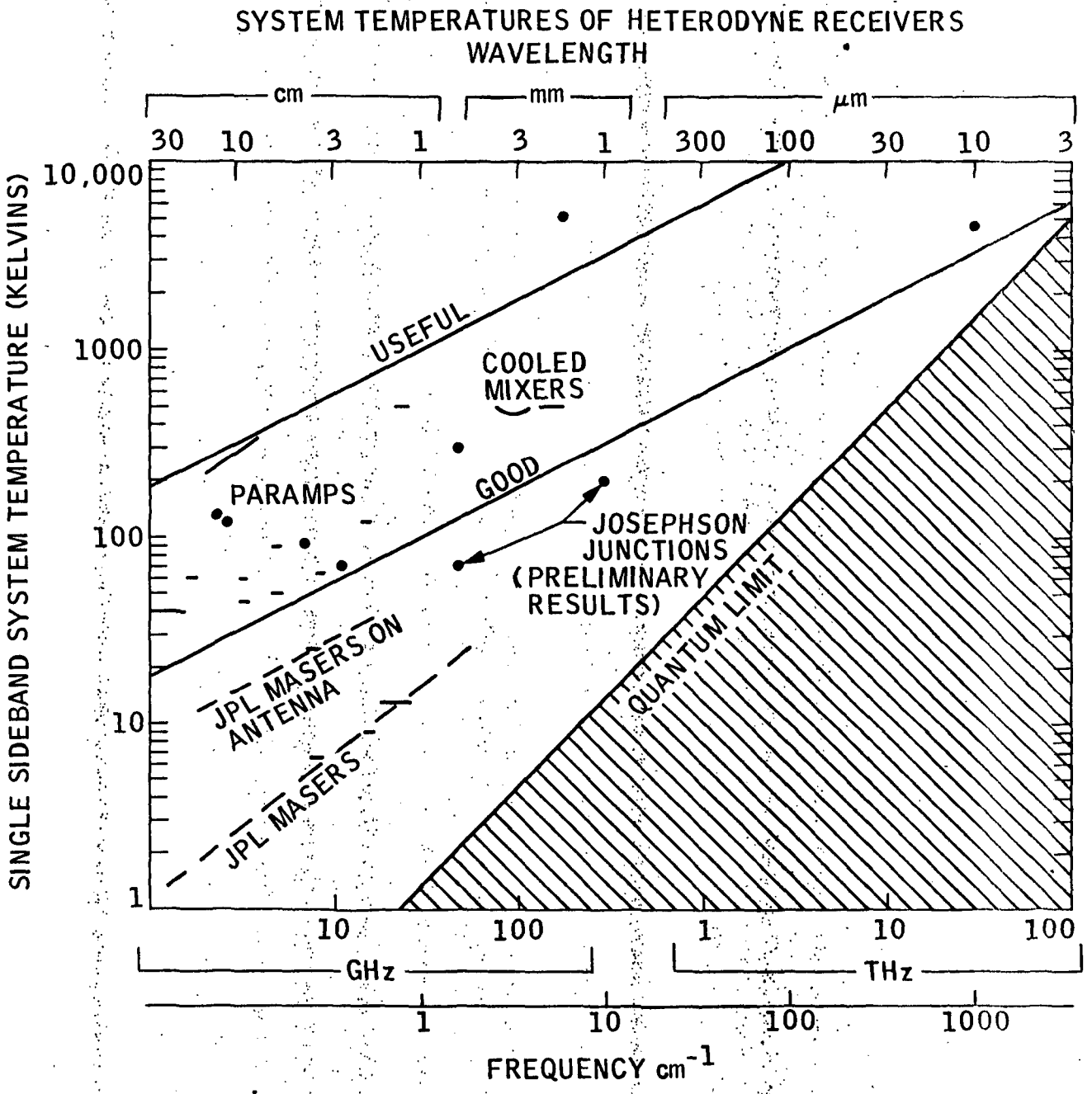


Figure 8.4.1. State-of-the-art single-sideband system noise temperatures (°K).

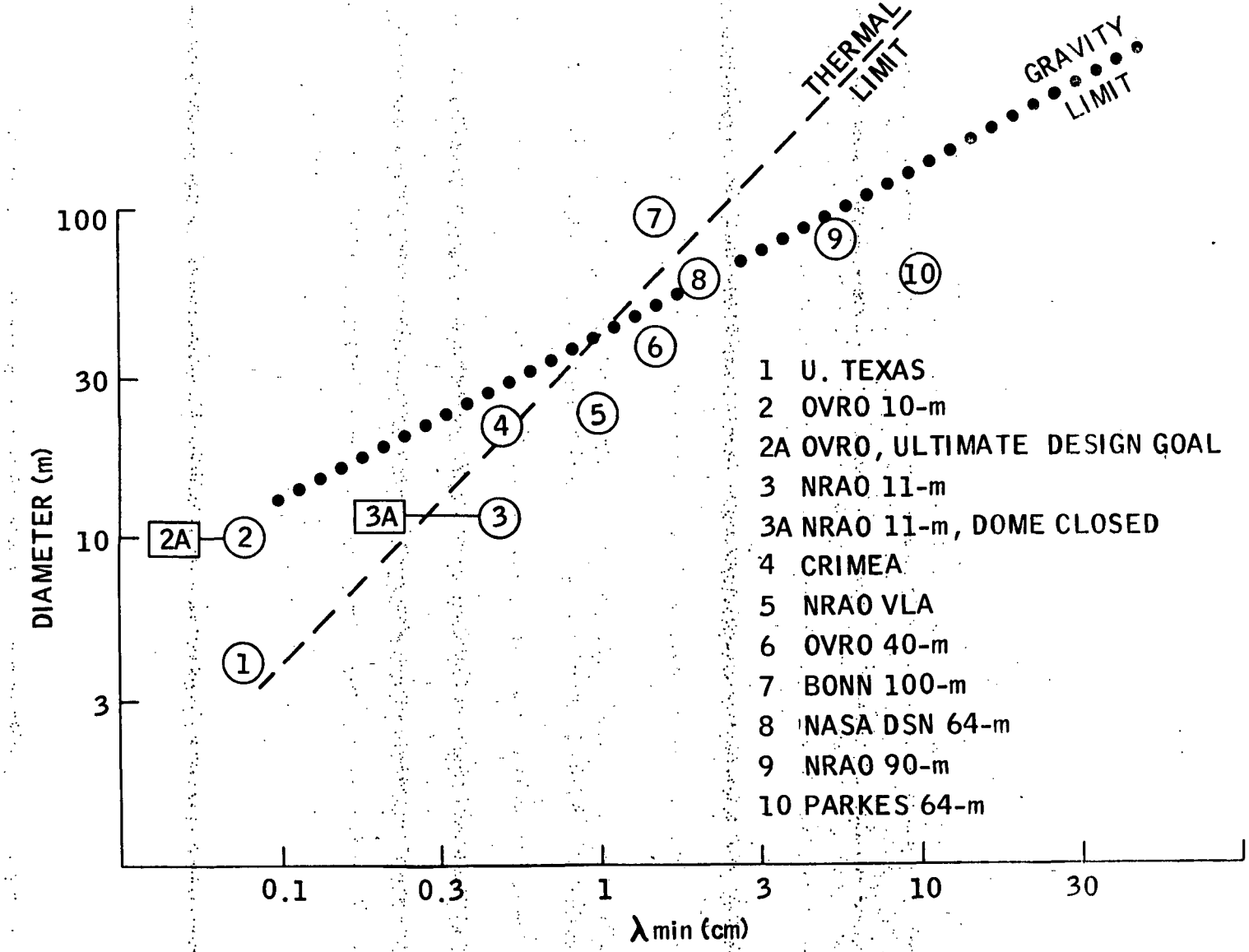


Figure 8.4.2. Performance parameters of large ground-based millimeter-wave radio telescope antennas.

would represent about 15,000 words per second, or 150,000 bits/sec for 10-bit words. Since many parameters of interest do not warrant such resolution, the data rates for most reasonable systems could be more modest.

8.5 Summary of applications

Potential applications of passive microwave systems in space may be divided into two broad groups, those that require imaging the earth and atmosphere beneath the satellite, and those that require viewing of the atmosphere only at the planetary limb. The former group of applications are listed in Table 8.5.1 and the limb-scanning applications are discussed in Chapter 7.

Table 8.5.1 also lists the nominal instrument sensitivity, spatial resolution, and revisit time needed in order to satisfy the listed applications with respect to various parameters of interest. In many cases the desired spatial resolution and revisit times are presented as a range of values, which represent attempts to span the specifications that most users would like. There is no attempt here to represent users desiring extremely high resolution (such as Landsat photographs) at infrequent intervals; the users of concern here are generally those desiring more frequent coverage of large geographic areas, and for whom data handling constraints also limit useful resolution. For example, the soil moisture requirements here serve users interested in the daily hydrological history and status of agricultural regions containing several fields, rather than those wishing infrequent observations of single fields. The former group includes agriculturalists employing crop yield models with soil moisture history as input.

The finest resolution listed in the table generally corresponds to the minimum scale size of the phenomenon that

Table 8.5.1 Application Areas and Observable Parameters

APPLICATION AREAS AND OBSERVABLE PARAMETERS	DESIRED SPECIFICATIONS			SPOT SIZE (KM) AT CRITICAL FREQUENCY			ΔT_{rms} AT DESIRED RESOLUTION			[SPOT SIZE (⊕)]/[DESIRED SIZE]			$[\Delta T_{rms}$ (AVAILABLE)]/$[\Delta T_{rms}$ (REQUIRED)]			FREQUENCY (GHz)									
																SMMR					TIROS-N			
	SPOT SIZE (KM)	ΔT_{rms}	REVISIT TIME (HR)	HEIGHT (KM) 400	900	1200	HEIGHT (KM) 400	900	1200	HEIGHT (KM) 400	900	1200	HEIGHT (KM) 400	900	1200	1.4	3.0	6.6	10.7	18	21	37	55	90	183
SYNOPTIC METEOROLOGY & CLIMATOLOGY																								
Temperature Profile	50	0.3	3-12	1.5	3.3	4.3	0.2	0.3	0.4	0.03	0.06	0.08	0.8	1.1	1.2							•	⊕	
Water Vapor Profile	15	0.5	3-12	4.1	8.6	11.2	0.4	0.6	0.7	0.3	0.6	0.8	0.9	1.2	1.4					+	⊕	+			+
Water Vapor Profile (Non-Tropical)	15	0.5	3-12	0.5	1.0	1.3	2.1	3.0	3.4	0.03	0.06	0.08	4.2	6.0	6.7									+	⊕
Liquid Water Abundance, Rain Rate	2-10	2	3-12	2.3	4.9	6.3	0.9	1.3	1.4	0.2	0.5	0.6	0.4	0.6	0.7		•	•	•	+	+	⊕	•	+	
Sea Surface Temperature	50	0.3	6-36	13	28	36	0.08	0.1	0.1	0.3	0.6	0.7	0.3	0.4	0.4	•	+	⊕	•	+	•	+			
Sea Surface Wind (Magnitude)	50	1	3-12	7.9	17	22	0.1	0.1	0.2	0.1	0.3	0.4	0.1	0.1	0.2	+	•	+	⊕			+			
Sea Surface Wind (No Precipitation)	50	1	3-12	2.3	4.9	6.3	0.2	0.2	0.3	0.05	0.1	0.1	0.2	0.2	0.3					+	+	⊕			
SEVERE STORMS																								
Temperature Profile	3-30	0.3	1-6	1.5	3.3	4.3	0.4	0.6	0.6	0.05	0.11	0.14	1.3	1.9	2.1							•	⊕		
Water Vapor Profile	3-15	0.5	1-6	4.1	8.6	11.2	0.4	0.6	0.7	0.3	0.4	0.6	0.9	1.2	1.4					+	⊕	+			+
Water Vapor Profile (Non-Tropical)	3-15	0.5	1-6	0.5	1.0	1.3	2.1	3.0	3.4	0.03	0.06	0.08	4.2	6.0	6.7									+	⊕
Liquid Water Abundance, Rain Rate	2-10	2	1-6	2.3	4.9	6.3	0.9	1.3	1.4	0.2	0.5	0.6	0.4	0.6	0.7		•	•	•	+	+	⊕	•	+	
Sea Surface Temperature	3-30	0.3	2-6	13	28	36	0.1	0.2	0.2	0.4	0.9	1.2	0.5	0.6	0.7	•	+	⊕	•	+	•	+			
Sea Surface Wind (Magnitude)	3-30	1	1-6	7.9	16.9	22	0.2	0.2	0.2	0.3	0.6	0.7	0.2	0.2	0.2	+	•	+	⊕			+			
Sea Surface Wind (No Precipitation)	3-30	1	1-6	2.3	4.9	6.3	0.3	0.4	0.5	0.1	0.2	0.2	0.3	0.4	0.5					+	+	⊕		+	
OCEAN SURFACE																								
Surface Wind Velocity	2-50	1	3-12	7.9	16.9	22	0.1	0.1	0.2	0.2	0.3	0.4	0.1	0.1	0.2	+	•	+	⊕			+			
Surface Wind Velocity (No Precipitation)	10-50	1	3-12	2.3	4.9	6.3	0.2	0.2	0.3	0.05	0.1	0.1	0.2	0.2	0.3					+	+	⊕		+	
Sea Surface Temperature	1-50	0.3	6-36	13	28	36	0.08	0.1	0.1	0.3	0.6	0.7	0.3	0.4	0.4	•	•	⊕	•	+	•	+			
Salinity	0.5-10	0.3	3-12	60	130	168	0.3	0.5	0.5	6.1	13.0	16.8	1.1	1.6	1.8	⊕	•	+	•	+		+			
Oil Slicks, etc. (No Precipitation)	0.5	0.3	1-12	2.3	4.9	6.3	18	25	28	4.6	9.8	12.7	60	84	94	•	•	+		+		⊕		+	
LAND PARAMETERS																								
Soil Moisture (Low Frequency)	3-25	1	6-36	61	130	168	0.1	0.2	0.2	2.4	5.2	6.7	0.1	0.2	0.2	⊕		+	•						
Soil Moisture (Higher Frequency)	3-25	1	6-36	13	28	36	0.2	0.2	0.3	0.5	1.1	1.4	0.2	0.2	0.3	•		⊕				•			
Snow Cover and Type, Frozen Ground	3-25	1	6-12	2.3	4.9	6.3	0.4	0.5	0.6	0.1	0.2	0.2	0.4	0.5	0.6		•	+		+		⊕		+	
SEA AND LAND ICE																								
Sea Ice Concentration	1-5	2	3-12	2.3	4.9	6.3	1.8	2.5	2.8	0.5	1.0	1.3	0.9	1.3	1.4					+		⊕		•	
Sea Ice Type	1-5	1	6-12	2.3	4.9	6.3	1.8	2.5	2.8	0.5	1.0	1.3	1.8	2.5	2.8		•	•	+	+		⊕		•	
Land Ice Properties (e.g., Firn)	10-50	1	12-36	2.3	4.9	6.3	0.2	0.2	0.3	0.05	0.1	0.1	0.2	0.2	0.3		•	•	+	+		⊕		•	

is physically significant for synoptic purposes. For example, the minimum resolution listed for severe storms is approximately the size of a single small convective cell. More complete rationale for these various requirements may be found in the corresponding chapters of this report.

The "desired ΔT_{rms}" in Table 8.5.1 is an estimate of the nominal microwave receiver sensitivities required to yield useful system performance. The remainder of the table is discussed in the next section, 8.6.

In addition to the limb-scanning systems discussed in Chapter 7, there are two other microwave systems that might usefully augment a passive microwave observatory. These are a nadir viewing spectral transmissometer for pressure sounding, and a simple synthetic aperture radar having $\sim$ 100-m resolution for simultaneously mapping ice pressure ridges on pack ice, small open leads in ice, precipitation zones, etc. Because such systems have been studied only incompletely in the present context, they are included in the recommended areas for research and development.

8.6 Analysis of a baseline observatory system

Because of the very large range of possible parameters for a passive microwave observatory system, it is useful to consider a baseline system concept with respect to which these diverse system opportunities might be compared.

The baseline concept described below was selected to meet the following constraints:

1) Applicability to the maximum range of users.
2) Full Earth coverage every 12 hours with one satellite (most applications require at least a 12-hr repeat cycle).
3) Frequency coverage over most of the 1-100 GHz band (most applications require several frequencies spanning one or more octaves).

4) Unfurled antennas not required for a shuttle launch (such rapidly scanned large millimeter wavelength reflector antennas are deemed risky and expensive at present).

5) Maximum cost-effectiveness, including maximum use of space-tested concepts, maximum modularity and system lifetime, and maximum range of present and potential future users.

The maximum range of users dictates a multi-channel spectrometer system, and 12-hr full Earth coverage requires a scanned system at an orbital altitude above $\sim$ 1000 km. At these altitudes the user requirements for spatial resolution and frequency coverage mandate the largest feasible mechanically scanned reflector antenna compatible with a shuttle launch without being furled; a dish about 4-m diameter meets these requirements and the needs of most users. Because data interpretation requires low antenna sidelobes, an off-axis feed is important. Many applications also benefit from simultaneous observations of both horizontal and vertical polarization, and so a constant circular scan pattern about a vertical axis is desirable. A sketch of an antenna system meeting these requirements is presented in Figure 8.6.1.

With such a nominal antenna configuration it is then possible to explore the degree to which various user data requirements could be met with currently available receiver systems. The specific system specifications assumed in this exercise include: 1) the terrestrial surface is viewed from a zenith angle of 55°, 2) the sum of the receiver noise temperature T_R and the antenna temperature T_A is $400°K + 20\nu°K$, where ν is the radiometer frequency (GHz), and 3) the receiver bandwidth for each channel is 100 MHz. Although these numbers might vary in actual systems, they are good baseline approximations.

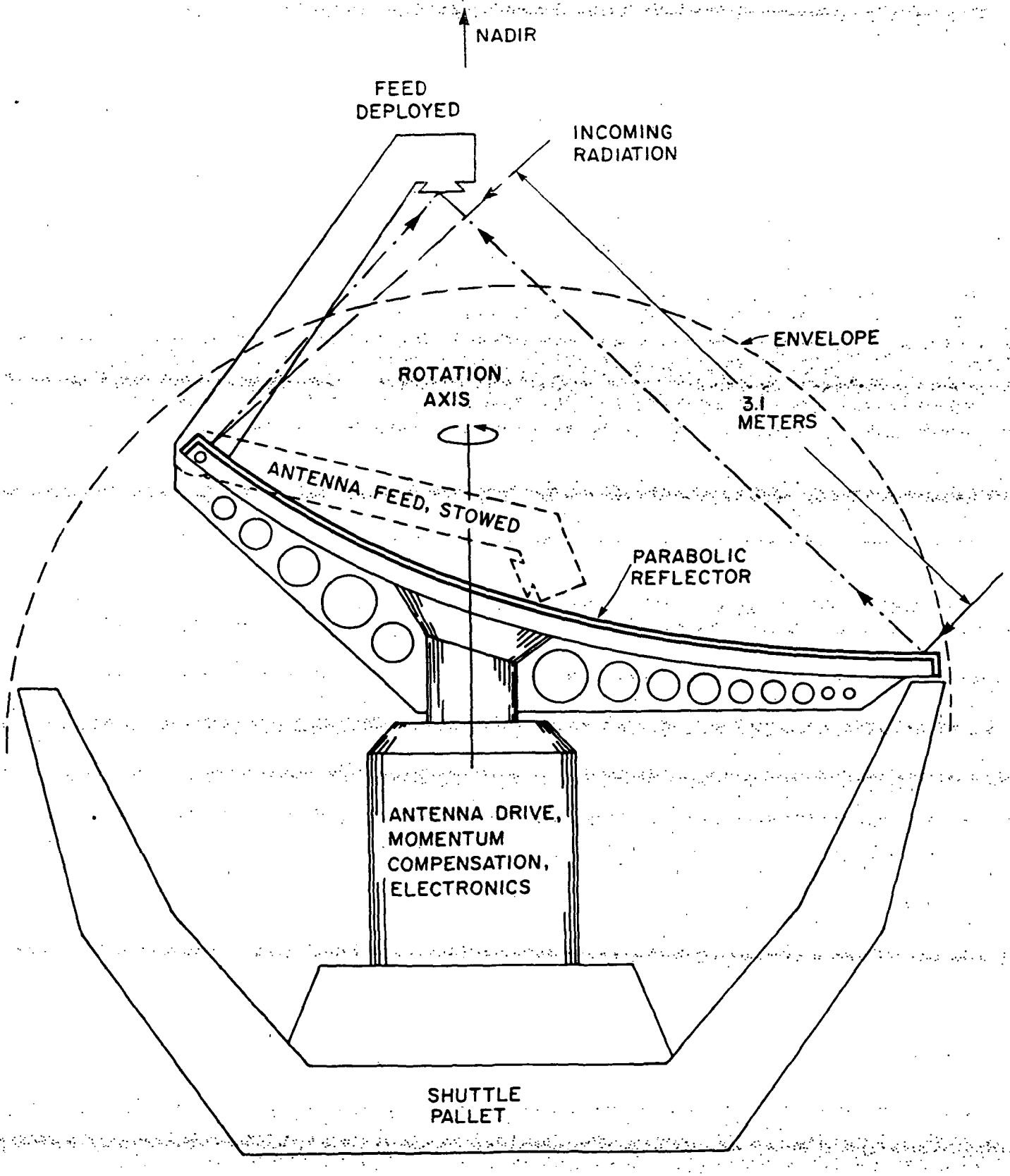


Figure 8.6.1. Possible baseline passive microwave observatory system.

Table 8.6.1 lists a series of frequencies that might be incorporated in such a system, together with their nominal system noise temperatures ($T_A + T_R$), and the instantaneous footprint dimensions at the half-power points for three possible orbital altitudes; 400, 900, and 1200 km. The assumed circular antenna beam intercepts an oval on the ground having dimensions a × b, the geometric mean of which, $\overline{ab}$, is also presented in the table. Each frequency is assumed to illuminate the same 4-meter dish uniformly, although in operational systems some frequencies may be deliberately under-illuminated in order to broaden the antenna beam, achieve a longer integration time, a lower data rate and a higher sensitivity, and to provide a beamwidth that is more nearly independent of frequency. The table shows that resolution $\overline{ab}$ of 78, 11, and 2.6 km can be obtained at 3, 21, and 90 GHz, respectively, for a 1200-km orbit, an incident zenith angle of 55°, and a 2600-km swath width. An antenna aperture of 3 m × 5 m would yield a more nearly circular spot of the same resolution $\overline{ab}$.

The effective spatial resolution obtainable for any particular geophysical parameter depends upon the principal frequencies used in its estimation. Table 8.5.1 lists most applications areas and representative frequencies that might be employed to serve them. These frequencies are indicated by three symbols: + indicates frequencies that are of primary importance, • indicates helpful secondary frequencies, and ⊕ indicates the "critical" frequency for which the spatial resolution was determined for purposes of this analysis.

The average integration time per resolution cell may be determined by dividing the resolution cell size by the swath area covered per second; we use the largest cell size in the range of desired specifications. We assume the antenna rotates and records data continuously at all frequencies, and that a small on-board digital processor averages the

Table 8.6.1 Nominal Receiver Characteristic and Footprint for a 4-M Antenna Aperture

FREQUENCY (GHz)	NOMINAL $T_A + T_R$	SPOT SIZE FOR DIFFERENT ALTITUDES								
		400 KM			900 KM			1200 KM		
		a	b	$\overline{ab}$	a	b	$\overline{ab}$	a	b	$\overline{ab}$
1.4	428°K	46	80	61	98	171	130	127	222	168
3.0	460	22	37	28	46	80	60	59	104	78
6.6	532	9	17	13	21	36	28	27	41	36
10.7	614	6.0	10.5	7.9	13	22	17	17	29	22
18	760	3.6	6.2	4.7	7.6	13.3	10.1	9.9	17.3	13.1
21	820	3.1	5.3	4.1	6.5	11.4	8.6	8.5	14.8	11.2
37	1140	1.7	3.0	2.3	3.7	6.5	4.9	4.8	8.4	6.3
55	1500	1.2	2.0	1.5	2.5	4.3	3.3	3.2	5.7	4.3
90	2200	0.7	1.2	0.9	1.5	2.6	2.0	2.0	3.4	2.6
183	4060	0.4	0.6	0.5	0.7	1.3	1.0	1.0	1.7	1.3
SWATH WIDTH (KM)		1020			2028			2578		

data obtained for each resolution cell prior to transmitting the resulting rectified images to ground stations. This approach results in somewhat greater integration times at the edges of the swath than at the center; the number derived here is an average.

Using the derived integration time τ, the receiver sensitivity (ΔT_{rms}) is determined assuming 100 MHz bandwidth B and a Dicke-comparison radiometer scheme in which the reference load is viewed only a negligible fraction of the time. This yields a sensitivity of

$$\Delta T_{rms} = \frac{T_A + T_R}{\sqrt{B\tau}}$$

The ability of the baseline system defined above to satisfy various user requirements can be determined by comparing 1) the spot sizes at the critical frequencies to the desired resolutions, and 2) the rms sensitivities determined above to those believed necessary to meet the user requirements. These numbers and ratios are all presented in Table 8.5.1.

Consider first the ratio of the achievable critical-frequency spot size to the maximum desired spot size. This ratio significantly exceeds unity only for the soil moisture measurement employing 1.4 GHz and the salinity and oil slick measurements; salinity measurements require high spatial resolution for coastal zones and utilize low frequencies, and oil slicks are intrinsically very small. To meet the needs of these users a much larger antenna system would be required; such systems are discussed in section 8.7.

Although the remaining applications are generally satisfied by these specifications, the highest desired resolution can not always be achieved. Applications with this difficulty are the following. First is liquid water abundance, for which one would like 3-km resolution in some cases, whereas only $\sim$ 5 km is available for a 1200-km

orbit. This is probably satisfactory for the majority of users. 3-km resolution could be obtained in any event only at the expense of inadequate receiver sensitivities or by employing multiple detectors. Sea-surface temperatures with 1-km resolution, appropriate for coastal zones, are similarly well outside the capabilities of the baseline system and, like coastal zone salinity and oil slicks, must be handled by a separate system. Although soil moisture measurements based upon 1.4-GHz data can not yield 25-km resolution, less accurate measurements based upon 6.6 GHz data would. Ice concentration and type can be observed with 5-km resolution, but 1-km resolution is too difficult. 3-km resolution might be obtained at 1200 km altitude using 90 GHz and two offset feeds which rotate with the antenna once per second or per ~ 6 km of travel. A low-resolution synthetic aperture radar covering a wide swath might reasonably supplement such a passive system for this group of users, but analysis of this option would require further study.

High spatial resolution implies short integration times and certain applications may therefore require receiver sensitivities that are unobtainable. Because receiver sensitivities can be doubled with modest effort, difficulties occur only for those applications for which the available-to-required-ΔT_{rms} ratios listed in Table 8.5.1 exceed two. Serious problems thus arise only for water vapor determinations based on 183 GHz, which presently has the necessary spatial resolution but insufficient receiver sensitivity (cryogenic receivers can solve this problem), and for oil slicks, for which full Earth coverage implies impossibly short integration times. Measurements of ice type with 5-km resolution also pose a small problem whereas sea ice concentration measurements do not because of the lower sensitivity requirements for that parameter.

Again, this analysis was performed assuming the largest

desired resolution cell size rather than the smallest, and the highest resolution can not always be obtained. In fact, it is receiver sensitivity more often than antenna diameter that limits resolution. In general a baseline system would achieve about 6-15 km resolution for most parameters, and ground-based smoothing might be employed to obtain the receiver sensitivity desired by each particular group of users. One or two channels might employ multiple feeds, very broad bandwidths, or cryogenics to obtain the very highest resolution and sensitivity for the more important applications.

8.7 Representative proposed system concepts

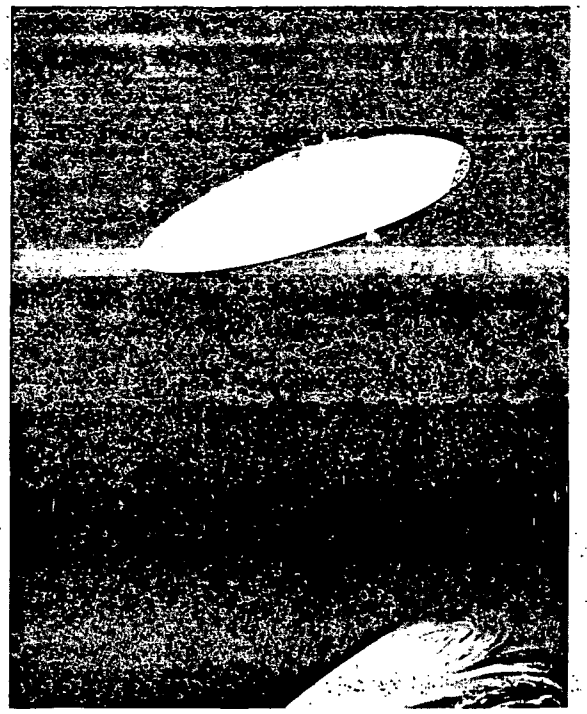
Several proposals for high-resolution passive microwave systems have been prepared by various groups for various geophysical purposes. The significant features of several of these are summarized below; the systems include scanning spectrometers with fixed and moving reflectors, very large reflector antenna systems with multiple or moving feeds, and phased array systems involving one or two frequencies. A pressure-sounding system is also described and one limb-scanning system is discussed in Chapter 7.

One large imaging system proposed in detail was SIMS, Shuttle Imaging Microwave System. This device employed a multiplicity of off-axis feeds spinning within a fixed reflector so as to rapidly scan the Earth with an effective aperture of $\sim$ 2 meters. The frequencies and radiometers proposed were comparable to those of the baseline system. One version scanned through nadir about an axis aligned with the flight path, and another version employed a vertical axis and constant angle of incidence. Principal virtues of this system were 1) the reflector did not move, so high spin rates and therefore high spatial resolution could more readily be obtained, 2) a very large number of feeds could be employed and modified without interfering with each other, 3) calibration of each frequency could be readily introduced,

and 4) aerodynamic loading of the spinning element was small, and dynamic balancing was straightforward. The principal disadvantage was that the effective aperture for a unit contained within the shuttle envelope was ∿ 2 m, approximately half what can be achieved with a scanning reflector, such as that in the baseline system. Figure 8.7.1 shows the nadir scanning version of SIMS as proposed by a team headed by J. W. Waters of the Jet Propulsion Laboratory. Similar systems might yield apertures up to 3 m if mounted longitudinally in the shuttle bay. If such a system were only to be transported by the shuttle before use on a free-flying system, then it might be stowed in the shuttle bay so as to permit an effective aperture closer to 4 meters.

A system roughly comparable to the baseline system has been proposed by a team from the Goddard Space Flight Center. It incorporates multiple spun-reflector radiometer systems on at least two spin axes, plus one or more phased arrays for higher spatial resolution at longer wavelengths. The principal advantage of multiple spinning systems is that this reduces the spinning angular momentum on a single system. For example, the 55 GHz temperature sounding system does not require dual polarization, and perhaps polarization could be omitted at most shorter wavelengths as well. In this case all these radiometers could be motionless and employ a mirror scanning about a vertical axis. This might reduce the spinning radiometer mass on the large reflector by ∿ 30%. Examination of Table 8.5.1 suggests that such a secondary spinning mirror might have a diameter of approximately one meter. Multiple mirrors also reduce the number of feeds required for one antenna, but use of a small cluster of multi-frequency feeds seems practical and largely negates this advantage over the single-dish baseline concept.

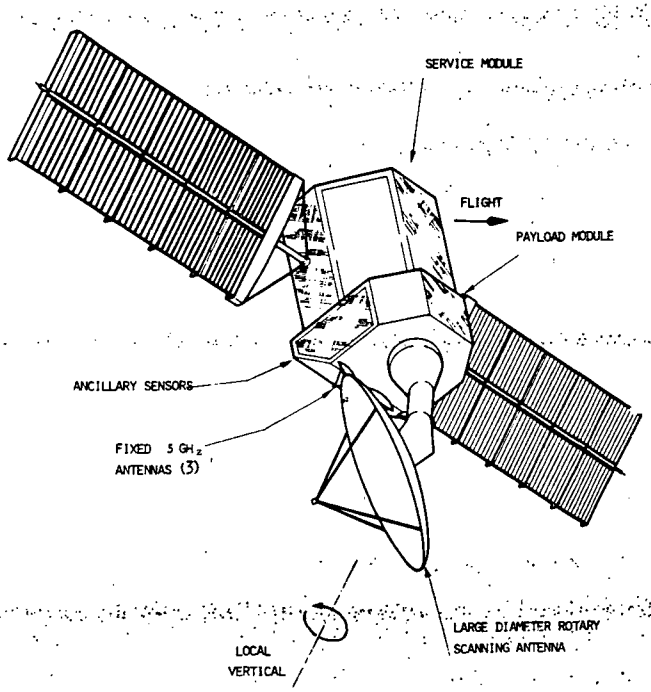
Large phased arrays have been proposed for use alone or in combination with other smaller antennas. For example,



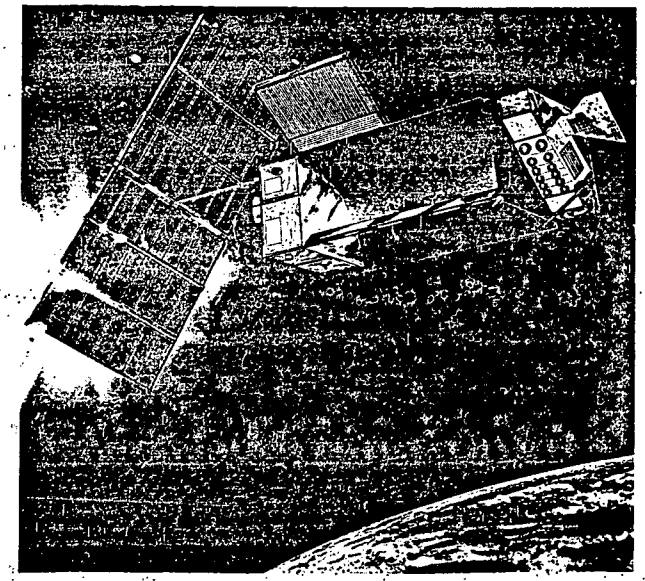
100-meter reflector with scanning subreflector



SIMS, Shuttle Imaging Microwave Spectrometer - 1/3 scale model



PAMIRASAT with 2-meter scanning parabola



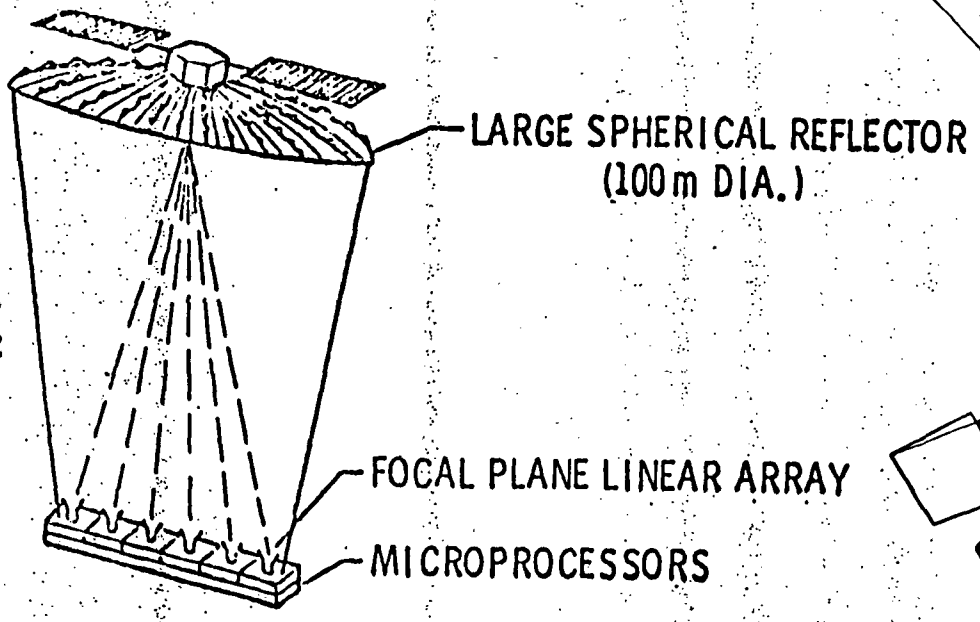
ARGUS with 1.8-meter array and 4-meter cylindrical parabola

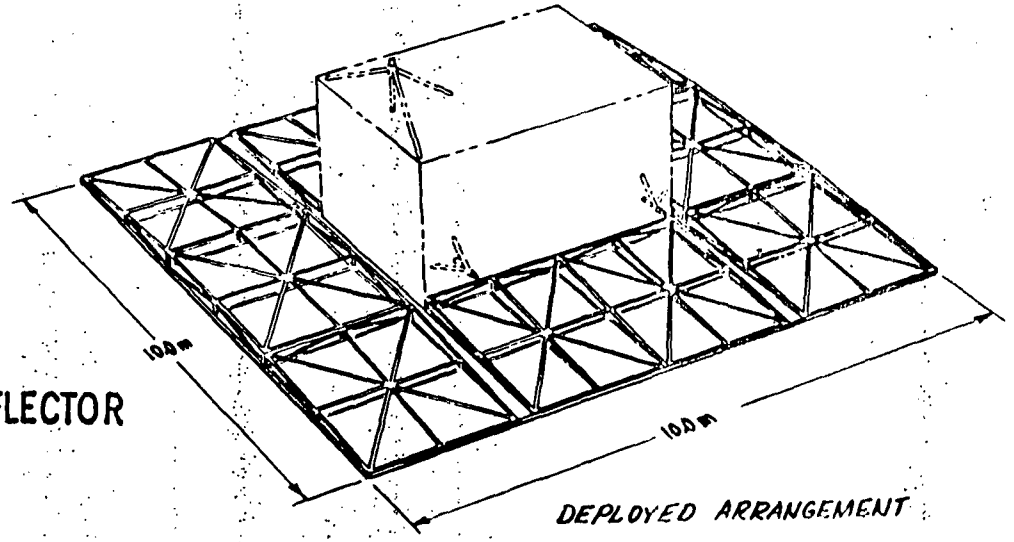
Figure 8.7.1

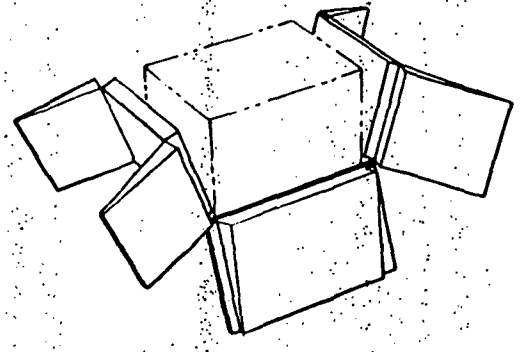
a 10-m square phased array operating near 1.4 GHz is being contemplated for soil moisture measurements, sea ice studies, and other purposes by a team from the NASA Goddard Space Flight Center. Principal advantages of these systems are the large apertures and the rapid scanning speeds available. Principal difficulties with such systems are that an expensive antenna is required for each frequency of interest, and precise calibration of such large radiometric systems has not been attempted; it is anticipated to be quite difficult. Achieving full coverage with the desired sensitivity may also be difficult because of bandwidth constraints imposed by RFI and the antenna.

Two concepts for very large reflector antennas have also been studied. One proposal by a team headed by J. Stacey of the Jet Propulsion Laoratory envisioned a baseline-type radiometer system mounted on a rigid reflector 100 m in diameter which is scanned over small angles by a nutating subreflector. The very high resolution (less than a kilometer) and infrequent revisit times of this system are more nearly compatible with the LANDSAT concept than with the synoptic systems discussed here. Figure 8.7.1 illustrates this concept.

A variation of this scheme has been studied by C. Swift of NASA/Langley and his colleagues. Its primary objective is coastal zone studies where sub-kilometer resolution is useful. Again, a 100-m reflector would be employed, but with perhaps 100 feeds operating simultaneously in order to obtain acceptable integration times. (See Figure 8.7.2.) The system would be oriented so as to view as much coastline as practical, but those coasts perpendicular to the flight path would generally be viewed only at intervals of a week or so. The advantages of extremely high resolution offered by these systems are offset by a more restricted market for such data and the presently high cost of 100-m antennas, which now is at least a few hundred million dollars.







100-meter reflector with pushbroom feeds

10-meter phased array

Figure 8.7.2

Two European studies sponsored by ESA are of interest here. The British Aircraft Corporation in combination with the Technical University of Denmark analyzed a concept designated PAMIRASAT, a passive microwave radiometer satellite having a rotary scanning radiometer 5-37 GHz with an antenna $\gtrsim$ 2-m diameter, spatial resolution of $\sim$ 10 km, and a swath width of $\sim$ 1000 km (see Figure 8.7.1). Three fixed antennas at 5 GHz were incorporated for sea-surface temperature measurement, and a 3-beam spectrometer would operate near the H_2O and O_2 resonances.

A similar proposal for a European Earth Resources Satellite, designated ARGUS, was prepared by Messerschmitt-Bolkow-Blohm in cooperation with Zentralstelle fur Geophotogrammetrie und Fernerkundung of Munich. A sketch appears in Figure 8.7.1 where a 1.8-m planar phased array can be seen together with a 4-m cylindrical parabolic reflector illuminated by a linear phased array at 10.6 and 5.3 GHz. The planar array at 19 and 33 GHz would yield resolution of $\sim$ 4 and 7 km, respectively, and the cylindrical antenna would yield resolutions of 5 and 11 km. The swath width would be only 200-300 km, so $\sim$ 12-day intervals between revisit times would result. The microwave radiometers in this concept and in PAMIRASAT would be accompanied by various sophisticated optical and radar sensors to form a complete observing platform. The principal difficulty with both concepts is the limited earth coverage for synoptic purposes.

A rather complete description of a possible limb-scanning system is contained in Section 7.6 of this report.

One promising pressure-sensing technique that might be incorporated on a microwave observatory satellite has been proposed by a team from the Herriot-Watt University. The system incorporates an antenna of $\sim$ 0.5 m^2 aperture viewing nadir with 3-6 frequencies in the 20-70 GHz regions; at each frequency the round trip attenuation of a radar signal is

measured precisely. Pressure can be determined because the strong absorption on the wings of the 60 GHz O_2 absorption complex is highly frequency dependent and dependent upon the amount of O_2 in the path, particularly in the 0-4 km altitude region. The pressure measured refers to this zone, but can be interpreted over ocean in terms of a surface pressure at sea level accurate to perhaps 1-4 mb rms. The eventual limits to accuracy are still under study, but the technique appears to be very promising. Considerable importance has been attached to such measurements as a potential means for improving numerical weather predictions.

The foregoing systems all operate best in low earth orbits which provide global coverage. Severe storm monitoring, however, is best when images can be obtained at $\sim$ 1-hour intervals, which is practical only with geosynchronous satellites. Because antenna size presently imposes a severe cost constraint, wavelengths near 1-3 mm are attractive due to the improved spatial resolution they permit. The largest antenna that can be launched intact is $\sim$ 4.4 m diameter, and the specifications that result for such a system are listed in Figure 8.7.3, together with a sketch prepared by Hughes Aircraft Corporation. The cirrus-penetration ability of microwaves makes such systems very attractive components in any operational severe storm monitoring system.

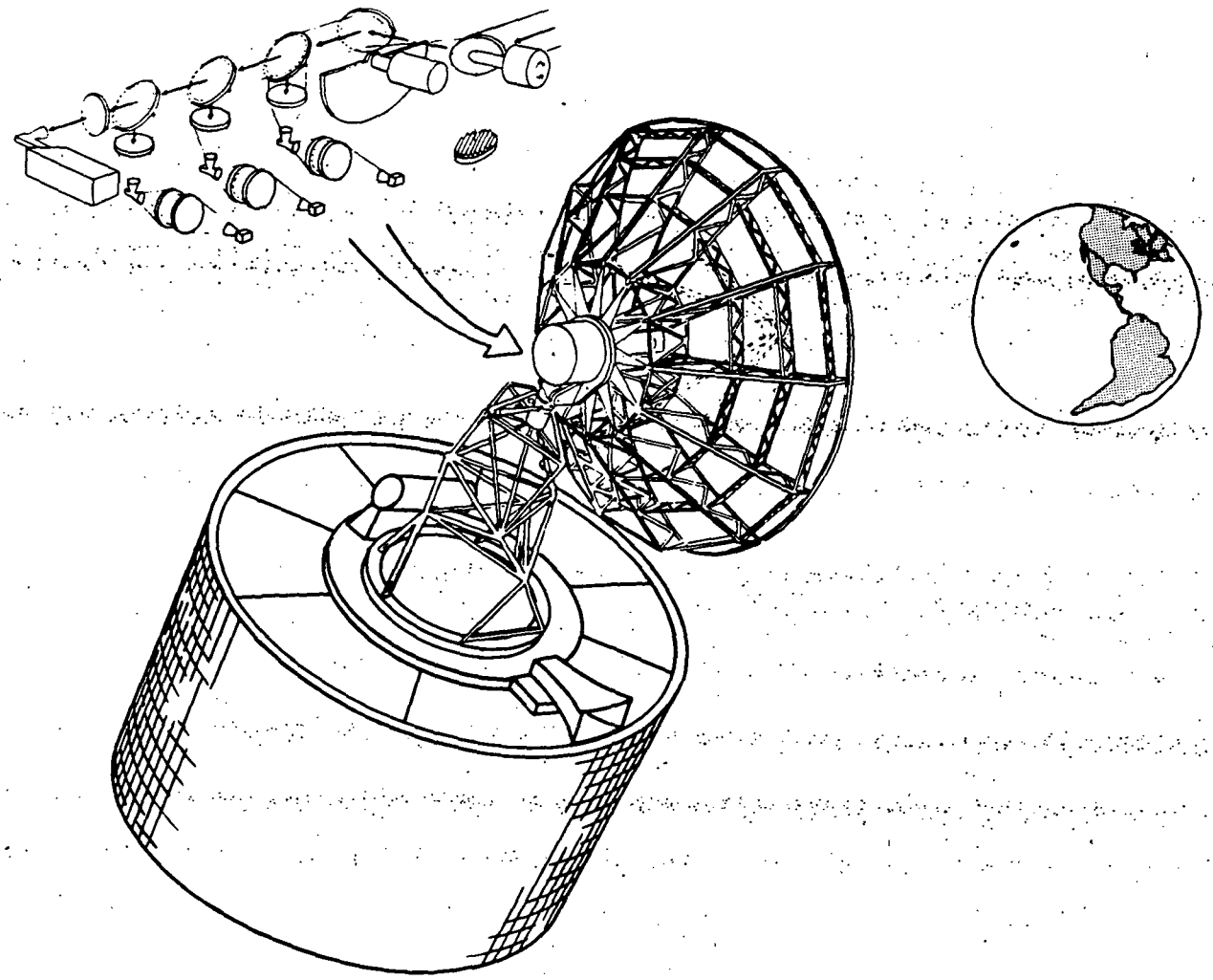
8.8 Alternative mission purposes

There are four primary purposes that can be served by shuttle-launched microwave missions:

1) Provide data to answer specific scientific questions; problems for which several days of data per year are adequate.
2) Provide scientific and engineering data to aid in design of future observatories.

Figure 8.7.3

GEOSYNCHRONOUS MICROWAVE ATMOSPHERIC SOUNDING RADIOMETER (MASR)



BAND (GHz)	NUMBER OF CHANNELS	NOMINAL RESOLUTION (km)	SENSITIVITY (°K)	FUNCTION (800 × 800 km maps in ½ hour)
183	6	25	0.2	Water Vapor Profile
140	1	32	0.1	Liquid Water
118	11	38	0.1-0.4	Temperature Profile 0-30 km, Precipitation over Land
104	1	45	0.1	Window, Precipitation

3) Provide a "proof-test" for some or all of the modules of candidate free-flyer observatory subsystems prior to operational use.

4) Provide an operational system.

With the possible exception of experiments designed to monitor the composition and structure of the stratosphere, mesosphere, and lower thermosphere (Chapter 7), the first class of scientific experiments has only a few compelling examples that would warrant the necessary expenditures in preference to comparable aircraft flights or ground-based observations. Such examples would include severe storms which aircraft can not overfly at sufficient altitude (e.g. the ITCZ), and experiments like sea ice or snow monitoring where coverage of vast remote regions is desired. Most scientific experiments for which aircraft or ground-based observations are inadequate require much longer observation periods to be productive; examples include climatological monitoring of sea ice, precipitation, soil moisture, etc.

The second category of experiments, for design purposes, is sufficiently expensive that serious consideration should be given to moving directly to the third category of shuttle flights -- the proof-test mode for candidate observatory systems. This would provide all of the benefits of the second mode plus the benefits of the third mode if the design were well conceived. If the presently planned passive microwave satellite experiments (SMMR, Tiros-N MSU, and Block 5D Microwave Sounder) function as planned, then they plus appropriate laboratory and aircraft tests should be capable of answering many system design questions more economically and swiftly than would a major shuttle instrument.

The need for "proof-test" shuttle missions will vary from system to system. Some systems may involve so little uncertainty that it would be appropriate to launch directly a proof-test experiment in an operational configuration,

probably on a free-flyer. An example of such an instrument would be a conventional 5-mm atmospheric temperature sounder.

Any limb-scanning instrument might reasonably be flown for any or all of the four listed purposes, whereas a pressure-sounding 5-mm radar might be flown initially primarily to collect data for design purposes. A large phased array (say 10 m square) might be flown first primarily to obtain design data concerning calibration, interference, soil behavior on a global scale, etc. An SMMR/Temperature Sounder instrument such as the baseline concept, might fly for scientific and design purposes, and, if successful, as a proof test. The precise rationale for any specific mission should be part of any detailed flight proposal.

8.9 Cost-Effectiveness

Three issues are discussed here:

1) User-group investment as a cost constraint.
2) Multi-purpose versus single-purpose facilities.
3) Facility development sequence: multi-step versus single-step development.

8.9.1 User group investment as a cost constraint

Any new observatory facility entails initial capital costs plus system operating costs; the corresponding costs borne by user groups should also be considered. These user costs can be measured in dollars, time, and performance. User expenses generally occur in the areas of research, software development and validation, communications system development, data operations, and user training. The time required to introduce an acceptable operational product can be several years; for example, even now the impact of satellite data on numerical weather prediction is only beginning to be felt.

The principal constraint this consideration introduces is that the number of changes in observatory products that

can be efficiently assimilated by a user group per decade is probably limited. Unnecessary intermediate steps in the development of a monitoring capability not only burdens user groups by extra validation and reprogramming of procedures, but also by introducing possibly awkward lapses of data. Such a lapse could occur, for example, with the loss of ESMR data for operational sea ice monitoring by the Navy.

In general, larger costs are associated with larger user groups and more complex data products; the problem is most severe in synoptic monitoring of weather and severe storms, and least severe for atmospheric and mesospheric research.

8.9.2 Multi-purpose versus single-purpose facilities

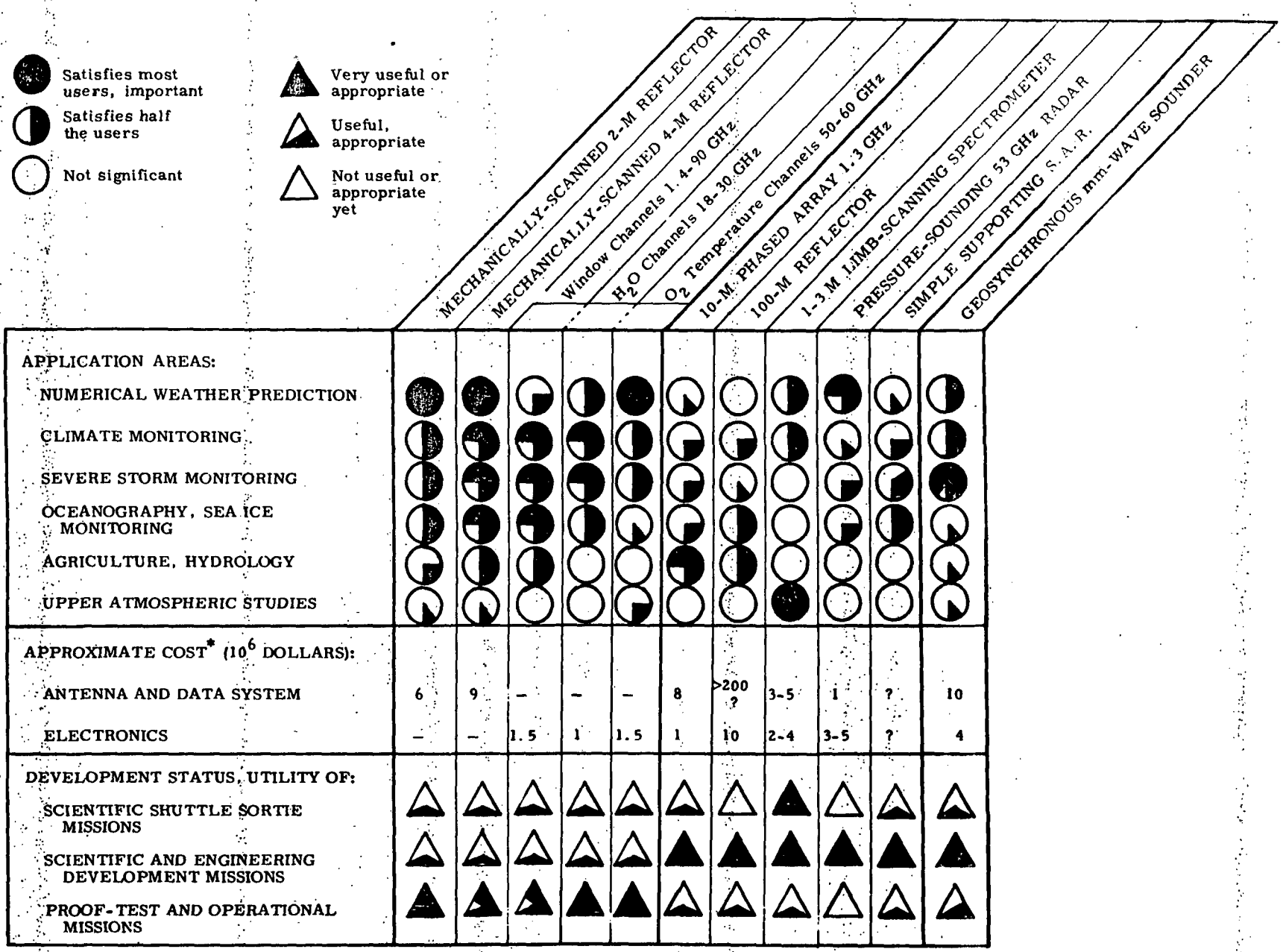
It is fortunate that a large fraction of the potential users of passive microwave data can be well served by the same observations; this suggests that multi-purpose missions may offer a significant opportunity to maximize cost effectiveness. In Table 8.9.1 are listed various data applications and various alternative microwave observing systems. The degree to which each system can serve each application is indicated qualitatively.

It is difficult to estimate costs for such systems with precision, but rough estimates are presented in the table for the costs of development plus a single flight unit and a single flight spare. These estimates have not been approved or validated by any agency, but are consistent with historical costs.

The primary conclusion to be drawn from these estimates is that the best opportunity for establishing a multi-user facility would be a $\sim$ 4 m scanned antenna similar to the baseline system described in Section 8.6. Most of the other systems have more limited, although important, constituencies.

These various systems generally would complement one another and should benefit greatly from flying on the same

Table 8.9.1 System Utility, Cost, and Status



*Cost estimates (1977 Dollars) should be correct within a factor of two. They include development, one flight model, and one prototype.

platform, but it is not essential. In Table 8.9.2 are listed the principal advantages of combining various pairs of sensors on the same platform.

8.9.3 Facility development sequence: multi-step versus single-step

As discussed in Section 8.8, considerable savings in time and in engineering and other costs can be achieved if one can move more directly to proof-test models without developing special shuttle experiments as a separate step. The degree to which each measurement concept might benefit from 1) scientific shuttle flights, 2) scientific and engineering development flights, and 3) proof-test and subsequent operational flights is estimated in Table 8.9.1.

In general, those systems involving multi-frequency scanned reflectors are sufficiently like the Nimbus-G and SeaSat SMMR instruments that little additional development work seems necessary. The dynamics and thermal behavior of steadily rotating reflector antenna systems can presumably be studied fairly well on the ground. Antennas 10-m or larger are sufficiently different from their predecessors that special development flights might be appropriate; issues include deployment, calibration accuracy, scientific character of the data, etc. The limb-scanning spectrometer, pressure-sounding transmissometer, and a simple synthetic aperture radar probably require one or more scientific or engineering development flights before an operational proof-test model is launched.

8.10 Recommendations

8.10.1 Systems development

The systems development options that appear most desirable and cost effective are listed below and in Figure 8.10.1.

Table 8.9.2 Advantages of Combining Sensors on the Same Platform

DISADVANTAGES / ADVANTAGES	SCANNED 4-M REFLECTOR + TEMPERATURE SOUNDING 50-60 GHz	SCANNED 4-M REFLECTOR + WINDOW, H_2O CHANNELS 1-100 GHz	10-M PHASED ARRAY. SINGLE FREQUENCY 1-3 GHz	100-M REFLECTOR MULTI-FREQUENCY 1-22 GHz	LIMB-SCANNING SPECTROM-ETER 60-3000 GHz	PRESSURE-SOUNDING RADAR	WIDE-SWATH S.A.R.
SCANNED 4-M REFLECTOR + TEMPERATURE-SOUNDING 50-60 GHz		None	If non-synoptic coverage, then phased array best in low orbit.	Large apertures definitely best in low orbits.	Limb scanner best in low orbit.	Low orbit slightly better for pressure.	None*
SCANNED 4-M REFLECTOR + WINDOW, H_2O CHANNELS 1-100 GHz	Simultaneous data in severe storms, etc. Retrievals benefit. ●		Same as above.	Same as above.	Same as above.	Same as above.	Same as above. None*
10-M PHASED ARRAY. SINGLE FREQUENCY 1-3 GHz	Same as above, but less overlap. ◔	Supports soil moisture, snow cover, rain, sea ice, ocean parameters (if synoptic). ◕		None, if both in low oribts.	None*	None*	Same as above. None*
100-M REFLECTOR MULTI-FREQUENCY 1-22 GHz	Same as above, but only over narrow strip. ◔	Coverage overlaps imperfectly. Infrequent visits imply separate orbits o.k. ◔	Same as on left. ◕		None*	None*	None*
1-3 M LIMB-SCANNING REFLECTOR. 60-3000 GHz	High vertical resolution of limb supports nadir retrievals of temperature ●	None ○	None ○	None ○		None*	None*
PRESSURE-SOUNDING RADAR TRANSMISSOMETER	Spectrometer corrects pressure meas. Simultaneity useful. ◕	Same as on left. ◕	None ○	None ○	None ○		None*
LOW-RESOLUTION WIDE-SWATH SYNTHETIC APERTURE RADAR	Small advantage. ◔	Simultaneity for ice ridges, types, precip., ocean roughness radar "zoom". ◕	Same as on left. ◕	Same as on left for a very narrow strip along flight path. ◑	None ○	None ○	

● Very important ◑ Moderately useful ○ No benefit

*Unless different orbital altitude desired for specific applications.

Figure 8.10.1 Research and Development Requirements

RESEARCH AND DEVELOPMENT EFFORT	BASELINE OBSERVATORY 1-200 GHz	LIMB-SCANNING SPECTROMETER 60-600 GHz	GEO-SYNCHRONOUS MM-WAVE SOUNDER 100-200 GHz	10-M PHASED ARRAY 1.4 GHz	PRESSURE SOUNDING RADAR 53 GHz	SYNOPTIC SAR	100-M REFLECTOR
SCIENTIFIC STUDIES							
Theoretical							
Field Experiments							
OBSERVATORY SYSTEMS							
Design Analyses, Cost Estimates							
Antenna Prototype, Tests							
Electronics Prototype, Tests							
Receiver Sensitivity Improvement							
Electronics Weight and Power Reduction							

 Very Major Undertaking

 Average Undertaking

 No Effort Required

IF experiment is developed, initial priorities are:

 Higher priority

 Average priority

 Lowest priority

I. IMAGING SPECTROMETER [*Cost Effectiveness: Highest*]

Applications

Numerical weather prediction
Climate monitoring
Severe storm monitoring
Oceanography, sea ice monitoring
Hydrology, snow cover, agriculture

Nominal Specifications

Window channels, O_2, H_2O bands (1-190 GHz)
$\sim$ 4 meter aperture
12-hour full earth coverage (per satellite)
5 km resolution, 90 GHz
14 km resolution, 18-190 GHz
20-170 km resolution, 10-1.4 GHz

Comments

NOAA's System '85 or an ocean satellite are promising and representative candidates for providing the platform because of their operational character, data facilities, and multi-user orientation. Advantages of such an observatory include:

a) Most users would be largely satisfied by such a system.
b) The cost of such a system is much less than the sum of several less powerful systems, each designed to serve special user groups.
c) By taking advantage of presently planned programs (SMMR, Tiros-N, MSU, etc.) little technology development is required, and one might go directly to an operational configuration with only modest proof-testing.
d) The operational character of this approach will encourage early user investment and acceptance.
e) Such a compact system might more readily be combined with other sensors in a synergistic way.

II. LIMB-SCANNING MICROWAVE SPECTROMETER

[*Cost Effectiveness: Very High*]

Initial Applications

Upper atmospheric studies

Climate monitoring

Nominal Specifications

O_2, H_2O, O_3, ClO, H_2O_2, and CO resonances (60-600 GHz)

$\sim$ 1.8 m aperture

12-hour full earth coverage, single track

3-km vertical resolution

300-km horizontal resolution

Comments

Man's activities are having an increasing and perhaps dangerous effect on the upper atmosphere, a region that is only partially understood. Microwave limb-scanning instruments are capable of significant and unique contributions to this increasingly important problem.

III. 1.4 GHz 10-METER PHASED ARRAY [*Cost Effectiveness: High*]

Applications

Soil moisture measurement

Nominal Specifications

1.4 GHz, radio astronomy band

10-meter square aperture

2-day full earth coverage above $\sim$ 30° latitude (once in daytime, once at night)

400-km polar orbit, 1000-km swath width

10-40 km resolution

Comments

Calibration and crop yield estimate procedures are of concern and deserve special attention.

IV. GEOSYNCHRONOUS MICROWAVE ATMOSPHERIC SOUNDING RADIOMETER

[*Cost Effectiveness: High*]

Applications

Severe storm monitoring

Nominal Specifications

O_2, H_2O resonances, window channels (100-190 GHz)
4.4-m aperture
800 × 800 km maps every 30 minutes
25-45 km resolution, midlatitudes
(25 km at 183 GHz)

Comments

Cloud penetration ability makes this a valuable part of a multi-sensor severe storm monitoring system.

V. PRESSURE-SENSING RADAR TRANSMISSOMETER

[*Cost Effectiveness: High*]

Applications

Numerical weather prediction

Nominal Specifications

O_2 wings, H_2O channels for compensation (20-70 GHz)
0.5 × 4 m aperture
Nadir measurements, ∿ 100 km resolution
Works only over ocean
Polar orbit
∿ 1-3 mb accuracy in surface pressure? (To be determined)

Comments

Instrument concepts and measurement accuracies must first be tested.

VI. STUDY OF SYNOPTIC LOW-RESOLUTION SYNTHETIC APERTURE RADAR [*Cost Effectiveness: Moderate*]

Applications

Support sea ice and severe storm monitoring

Nominal Specifications

Resolution ∿ 1 km? To be determined.

Full coverage capability, selected transmission

Comments

Prior SAR studies should simplify task. Ultimate utility could be significant.

VII. DEVELOPMENT OF 100-m REFLECTOR ANTENNA RADIOMETER SYSTEM [*Cost Effectiveness: Low*]

Applications

Agriculture, hydrology

Oceanography (coastal zones)

Severe storm studies

Nominal Specifications

1.4-10 GHz (2-3 channels)

100-m aperture, multi-beam or scanned

400-km orbit, 0.3-3 km resolution

2-3 day repeat cycle minimum (once in daytime, once at night)

Scheduled targets only, scan rate restrictions

Comments

Impact of coverage constraints on ultimate utility is yet to be determined. High present cost is a major obstacle now.

8.10.2 Technology development

Low noise receivers and antenna structures are the two areas in greatest need of further development, specifically:

1) Improve broadband receivers at frequencies 20-100 GHz; increase bandwidths to ∿ 1 GHz over which receiver noise

temperatures are less than $\sim$ [200 + 10ν(GHz)]°K.

2) Develop space-qualified narrowband receivers for 100-3000 GHz; reduce receiver noise temperatures below 10ν°K (ν in GHz) with a goal of ν°K.

3) Develop asymmetric Dicke-switching radiometers that approach $\Delta T_{rms} = (T_R + T_A)/\sqrt{\tau B}$ (a factor of $\sim$ 2 improvement).

4) Reduce radiometer weight and power requirements so as to reduce power, angular-momentum, and thermal problems for large radiometric systems.

5) Develop designs for 3-5 m reflector antennas with beam efficiencies above $\sim$ 90-95% and capable of scanning $\sim$ 30 rpm. Beamwidths no smaller than $\sim$ 4 arc minutes would be required.

6) Develop a 100-m diameter antenna concept for multi-beam or single-beam use. Deployment, stability, beam steering, and cost problems are of primary concern.

8.11 References

Barath, F. T., A. H. Barrett, J. Copeland, D. E. Jones, A. E. Lilley, Mariner 2 microwave radiometer experiment and results, Astron. J., 69, 49-58, 1964.

Basharinov, A. E., A. S. Gurvich, S. T. Yegorov, Dokl. Akad. Nauk SSSR, 188, 1273-1276, 1969.

Gloersen, P., T. T. Wilheit, T. C. Chang, W. Nordberg, Microwave maps of the polar ice of the earth, Bull. Am. Meteor. Soc., 55, 1442-1448, 1974.

Staelin, D. H., A. H. Barrett, J. W. Waters, F. T. Barath, E. J. Johnston, P. W. Rosenkranz, N. E. Gaut, W. B. Lenoir, Microwave spectrometer on the Nimbus 5 satellite: meteorological and geophysical data, Science, 182, 1339-1341, 1973.

Staelin, D. H., P. W. Rosenkranz, F. T. Barath, E. J. Johnston, J. W. Waters, Microwave spectroscopic imagery of the earth, Science, 197, 991-993, 1977.

Wilheit, T. T., J. S. Theon, W. E. Shenk, L. J. Allison, E. B. Rodgers, Meteorological interpretations of the images from the Nimbus-5 electrically scanned microwave radiometer, J. Appl. Meteor., 15, 166-172, 1976.

Appendix A: Orbit Selection for Earth Observation Missions*

A.1 General

In earth observation applications, the orbit selection process is usually simplified by a restriction to circular orbits, imposed by the need to maintain uniform viewing conditions. With that restriction, the primary orbit characteristics remaining to be determined reduce to only two: the altitude (h) and the inclination (i). A number of other important mission parameters depend on these choices, however, so a major part of the orbit selection task is concerned with developing these relationships in suitable forms to provide a basis for rational orbit selection procedures. The brief discussion of that subject which follows is organized around two important areas of mission performance which depend on h and i, namely, orbit plane precession and coverage pattern development.

A.2 Orbit plane precession

The dependence of orbit plane precession on h and i is shown graphically in Figure A1. The graph gives the basic nodal precession rate ($\dot{\Omega}$) as a function of h and i, along with several other useful precession-dependent quantities. The latter are largely self-explanatory, except for the "nodal day" (D_n), which is defined as the earth rotation period relative to the (precessing) orbit plane. This parameter is useful in determining coverage pattern characteristics, as described later in this section.

The specific procedures to be followed in applying design aids such as Figure A1 to particular orbit selection problems varies considerably from case to case. Some applications, for example, require sun-synchronous orbits to maintain solar illumination of the sensor fields of view, and this requirement restricts the inclination value to a narrow range near 100°, as indicated by Figure A1.

*Prepared by J. C. King.

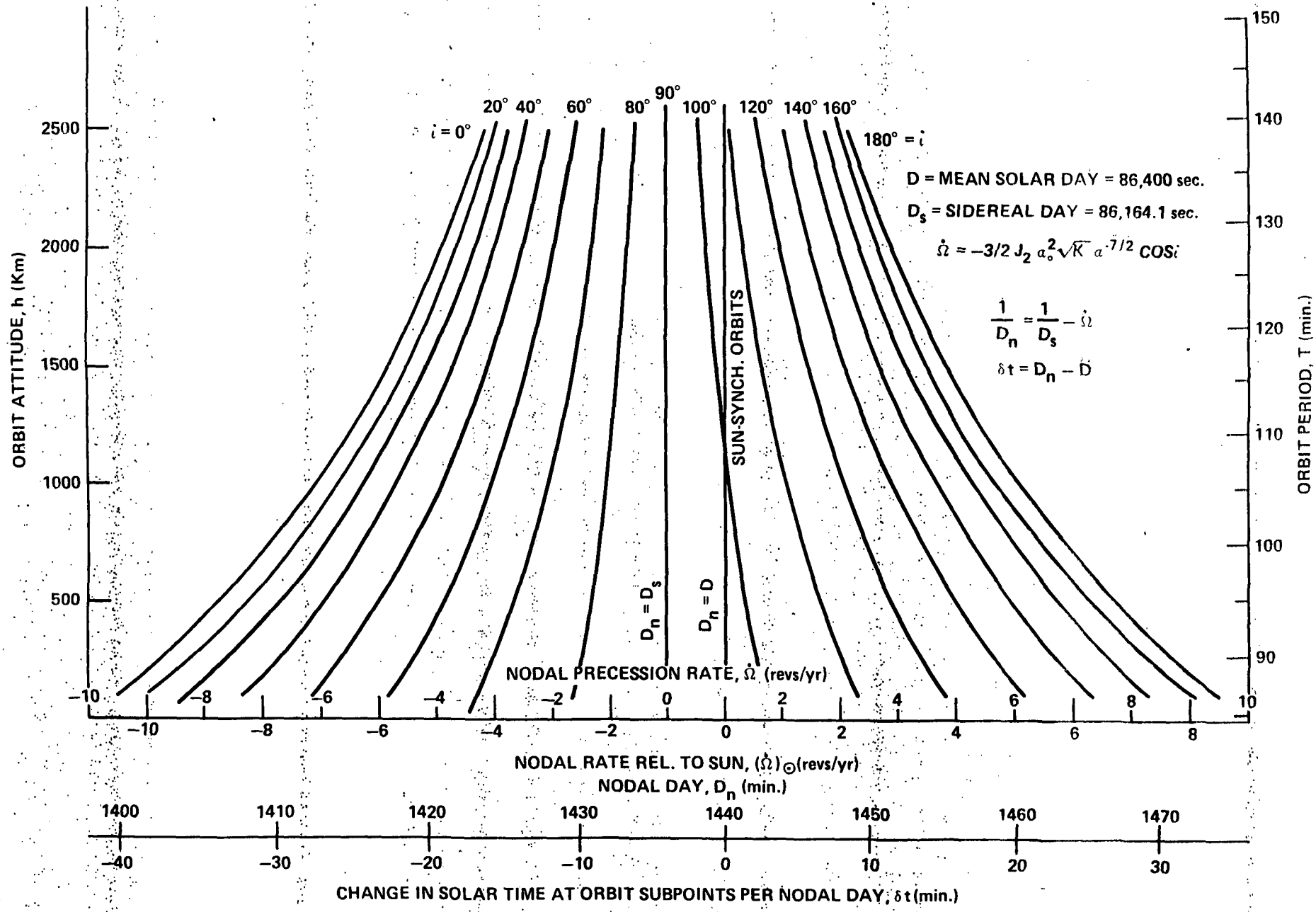


Figure A1. Satellite orbit precession and related viewing parameters.

Other applications may be free of the sun-synchronism restriction and call instead for some other precession-dependent characteristic, such as a desired rate of change of viewing time of day (solar). It is feasible, for example, to obtain a complete sweep of viewing times of day each month by selecting a nodal rate relative to the sun of 6 revolutions per year, i.e., $(\dot{\Omega})_{\odot} = \pm 6$, since the ascending and descending portions of the orbit each make separate complete (24-hr) time sweeps with every orbit plane revolution. The above sign choice might be made based on other considerations, such as the more economical launch into the low-inclination, direct (eastward) orbit obtained by choosing $(\dot{\Omega})_{\odot} = -6$.

Still other applications may require particular ranges or values of both h and i, with the resulting precession rate assuming only secondary importance.

A.3 Coverage pattern selection

A second important mission characteristic which depends on h and i is the earth coverage sequence and pattern. The desired pattern characteristics are usually determined by the sensor fields of view (swath width), the earth latitude zones of interest, and any sequencing or repetition requirement, such as a need to re-view each area of coverage every N days.

A.3.1 Pattern characteristics

Figure A2 provides a convenient means of correlating the various types and rates of periodic coverage with orbital period (or altitude). A 5-day repeat cycle period, for example, is obtainable at any of an extended series of orbital altitudes, as indicated by the points along the N = 5 ordinate line. Each point (dot) is defined by simultaneous integral values of the revolution numbers N and R, the number of nodal days and orbital revolutions, respectively,

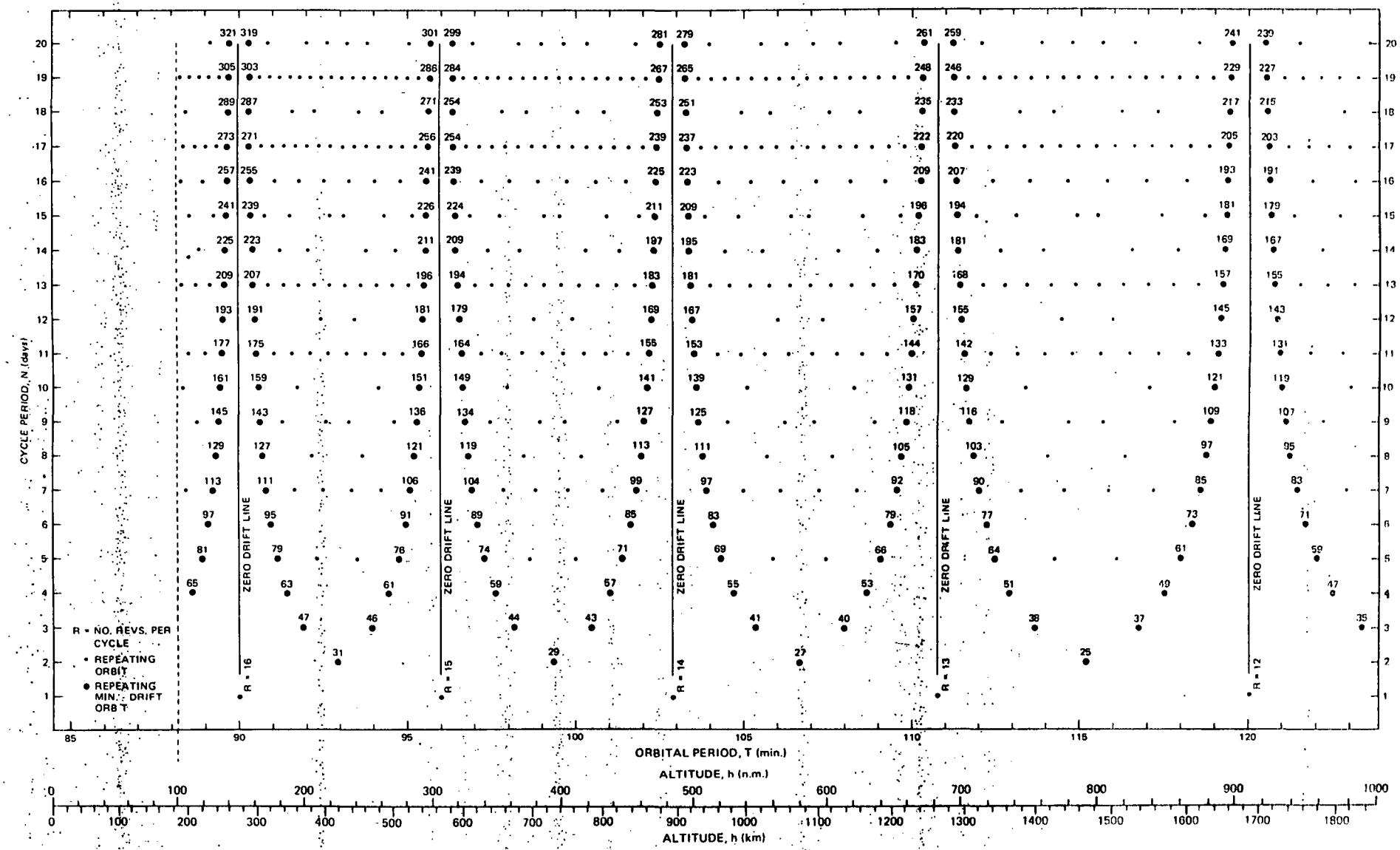
per complete pattern repetition cycle. Pattern repetition is guaranteed by the integral value constraint on N and R.

Apparent omissions in the array of points in Figure A2 occur where the integral values of N and R are not relatively prime and therefore represent redundant multiples of shorter period cycles (obtained by removing common factors from N and R). The "minimum-drift" orbits (large dots) are those in which the swath progression sequence is consecutive, i.e., adjacent swaths are covered on consecutive days. Patterns represented by the smaller dots exhibit increasing values of the "daily drift," which produces a skipping motion in the daily progression, in which the skipped-over swath positions are covered later in the cycle in subsequent sweeps across the area. The characteristic number of positions skipped in a given pattern is determined by the difference between its R-number and that of the nearest minimum-drift pattern. The apparent direction of daily drift is eastward for points (patterns) situated to the left of the nearest zero drift line and westward for points to the right.

Note that the abscissa scales in Figure A2 are strictly applicable only to sun-synchronous orbits. This restriction can be circumvented, however, if the integer N is defined in nodal days, and the abscissa scales are adjusted using the relationship

$$T = T_{ss} D_n / D$$

where T is the correct period for the unrestricted orbit precessing at a rate corresponding to D_n, and T_{ss} is the value indicated directly in Figure A2 for sun-synchronous orbits (having $D_n = D = 1440$ min, the mean solar day). In actual practice, the procedure consists of selecting the desired pattern (N,R) in Figure A2 and reading the corresponding T_{ss} directly, entering that T_{ss} value into Figure A1 and reading the value of D_n corresponding to the inclination or precession rate desired. The correct



NOTE: ABSCISSA SCALES (T and h) ARE CORRECT FOR SUN-SYNCHRONOUS ORBITS AND APPROXIMATE FOR OTHERS. SEE TEXT FOR CORRECTION PROCEDURE.

Figure 2. Array of Orbits Which Produce Repeating Swath Patterns

Figure A2. Array of orbits which produce repeating swath patterns.

period T would then be obtained using the above correction formula, and the corresponding h value obtained using the abscissa scales of Figure A2. The cycle period is known to be N nodal days (of D_n minutes each).

A.3.2 Selection factors

The characteristic revolution numbers N and R are of primary importance in the pattern selection process, since they effectively define (for a given i) the complete pattern of the nadir trace (King, 1976). The significance of N, the repetition cycle period, is already clear -- it defines the time interval between successive passes (in the same direction)[1] over a given site. The orbital revolution number R is also of primary importance in that it determines the "fineness" of the pattern, i.e., the interval s between adjacent nadir trace crossings of the equator (in one direction) in the complete pattern (s = 360°/R)(King, 1976). Thus R also determines the minimum swath width w needed to obtain full coverage (in one direction) at the equator, via the relation

$$w_{min} \cong s/\sin i = 360°/R \sin i$$

Conversely, given an available swath width, this equation will yield a minimum value of R required for full coverage in one direction. This number, along with the desired number for N, serves to guide the selection of a particular pattern (and corresponding orbit in an acceptable altitude range) from Figure A2.

A.4 Reference

King, Joseph C., Quantization and symmetry in periodic coverage patterns with applications to earth observation, J. Astro. Sciences, V. XXIV, n. 4, Oct.-Dec. 1976.

[1]Complete periodic patterns always exhibit two symmetric (mirror-image) sets of passes, ascending and descending, over all latitudes traversed. Local correlation and mapping of the two sets require more detailed analysis.

Appendix B: General Theoretical Aspects of Passive Microwave Remote Sensing*

B.1 The Forward Problem

Planck's equation for thermal emission as a function of temperature can be linearized to within 0.1 K for temperatures greater than $(\nu/23)^2$ where ν is the frequency in GHz. Consequently microwave thermal emission is usually measured as a brightness temperature, and the intensity of emission from the terrestrial surface is related linearly to the product of its temperature and its emissivity (which may itself be a function of temperature). When the contribution of the atmosphere is added, the brightness temperature of the earth may be written as

$$T_B = T_{Batm}^{\uparrow} + e^{-\tau}[\varepsilon T_S + (\varepsilon-1)T_{Bsky}] \qquad (1)$$

where $T_{Batm}^{\uparrow}$ is upward-propagating radiation from the atmosphere, τ is atmospheric opacity, ε is surface emissivity, T_S is surface temperature, and T_{Bsky} is downward-propagating radiation from the atmosphere and from extraterrestrial sources, which is reflected from the surface. In the case that the surface is nonspecular, this fact must be considered in computing T_{Bsky}.

The surface of the earth is very diverse, and the microwave signature of each category of surface (land, water, ice) differs dramatically from the others. Since the type of surface observed is application related, the reader is referred to chapters 2, 3, and 4 for discussion of emission from surfaces.

In contrast, atmospheric emission and opacity is of general relevance, in the sense that if it is the state of the atmosphere itself that is of interest, then the characteristics of propagation of radiation in the atmosphere

*Prepared by P. W. Rosenkranz.

determine the opportunities for remote sensing; whereas if the surface is of interest, then the atmosphere must be sufficiently transparent. Figure B1 illustrates the microwave spectrum of three major constituents of the atmosphere.

Molecular oxygen contributes the very strong absorption band centered on 60 GHz, and also an isolated line at 119 GHz. Since oxygen is uniformly mixed in the atmosphere, measurement of radiation from either of these resonances can be used to infer the atmospheric temperature profile. Atmospheric emission from these resonances is most conveniently described by means of weighting functions, as discussed in chapters 5 and 6. Water vapor adds lines at 22 and 183 GHz. Not shown in Figure B1 are numerous narrow lines due to ozone and other minor constituents. These are described in chapter 7.

Although the microwave region of the spectrum has several characteristics that give it unique value for remote sensing, the one that has value in almost all applications is the spectral characteristic of cloud transmittance. In a spherical cloud droplet, the lowest order mode of electromagnetic resonance occurs with a free-space wavelength somewhat longer than the circumference of the droplet (and depending weakly on the dielectric constant of the droplet). A typical nonraining cloud has droplets with radii of a few tens of microns, corresponding to submillimeter wavelength resonances. For raindrops, the corresponding wavelengths are typically several millimeters. For a given drop size, the spectra of absorption and scattering in the resonant region are quite complicated. However, due to the numerous higher order resonances and the distribution of drop sizes, a cloud containing any significant amount of liquid water is essentially opaque to wavelengths less than or of the order of the fundamental resonance wavelength. At longer wavelengths, absorption falls rapidly, approaching an asymptote of λ^{-2}. Scattering falls even more rapidly, with an

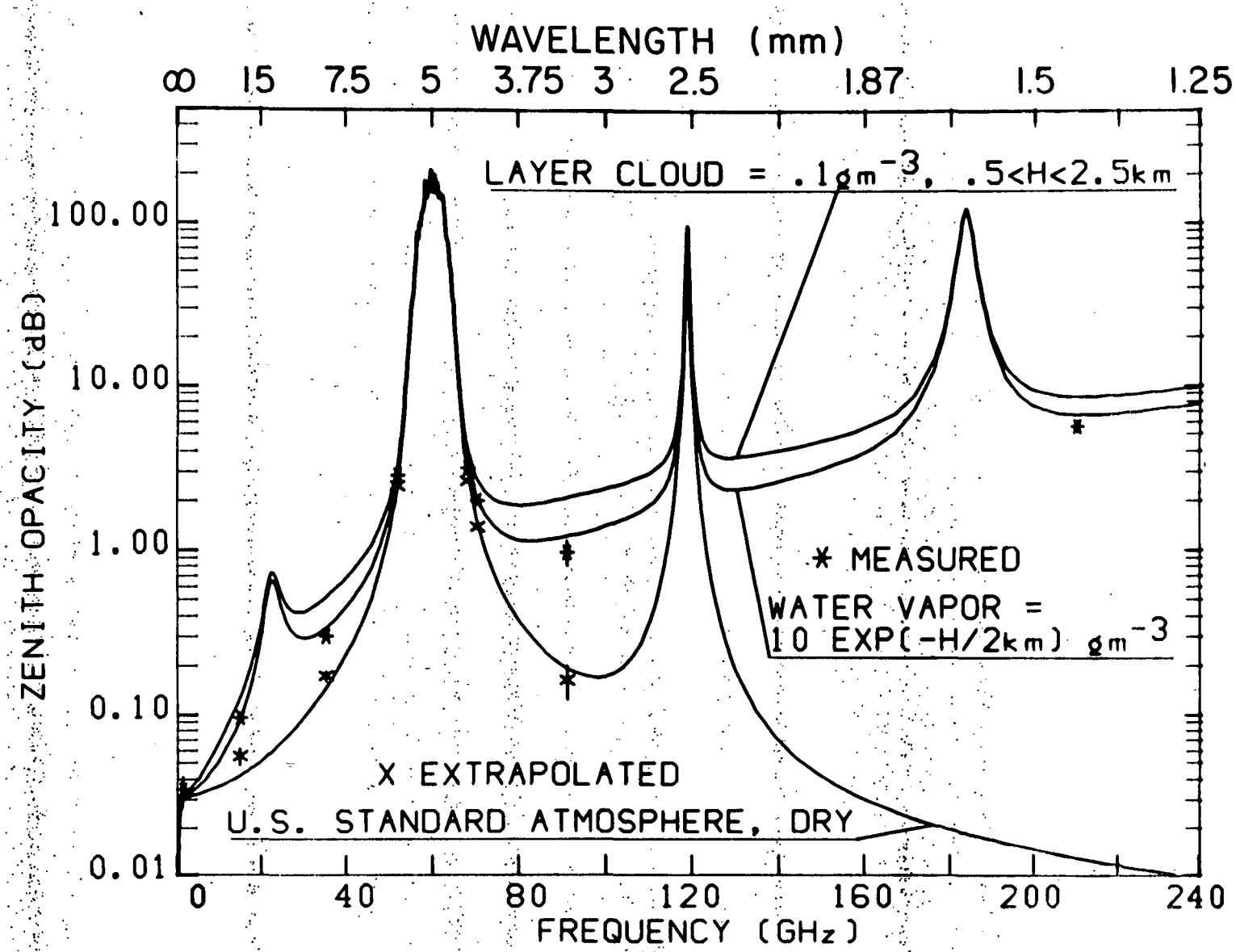


Figure B1. Lower curve - atmospheric opacity due to oxygen. Middle curve - opacity with 20 kg·m^{-2} water vapor added to the oxygen. Upper curve - opacity with 0.2 kg·m^{-2} stratus cloud added to the oxygen and water vapor.

asymptote of λ^{-4}. Therefore in the long wavelength (or small droplet) limit, extinction is essentially equal to absorption. This is the case for which the upper curve in Figure B1 is computed. It would perhaps be an oversimplification to speak of a microwave or radio window through clouds, since there is some extinction at all wavelengths. Nevertheless, the possibility of seeing through clouds provides a strong motivation for use of this part of the spectrum.

B.2 The Inverse Problem

The basic goal of remote sensing is to interpret radiometric measurements made at various wavelengths and polarizations in terms of geophysical parameters, where each of the measurements is sensitive to each of the parameters to different degrees. The number of methods of solution for such a general problem is vast, but Rodgers (1976) makes some useful classifications. One class of solutions is called "exact" by Rodgers, in the sense that a forward calculation from the solution parameters will reproduce the measurements exactly. This property might seem desirable, but in practice such solutions tend to exhibit unacceptable amplification of measurement errors, especially when the number of measurements is more than two or three. Thus one is led to seek a solution to the inverse problem that is constrained, or regularized.

Generally speaking, the forward problem at microwave wavelengths is approximately linear for rather wide ranges of the geophysical parameter values. We shall assume that the mean values have been subtracted from both the measurements and the parameters. Then the forward problem can be modeled by

$$\underline{d} = \underline{\underline{K}}\,\underline{p} + \underline{e} \qquad (2)$$

where $\underline{d}$ is a vector or column matrix whose elements are the

measurements from the instrument channels, $\underline{p}$ is the vector of parameters, and $\underline{e}$ is a vector of measurement errors, assumed to have zero mean. As an example, if $\underline{p}$ is a temperature profile, then the rows of the matrix $\underline{\underline{K}}$ are weighting functions. $\underline{\underline{K}}$ may not be square.

A linear solution to the inverse problem is expressed as

$$\hat{\underline{p}} = \underline{\underline{D}}\,\underline{d} \tag{3}$$

where $\hat{p}$ is the estimate of the parameter vector and $\underline{\underline{D}}$ is called the determination matrix. The optimum linear solution in the presence of measurement error is obtained by requiring the estimate error $(\hat{\underline{p}} - \underline{p})$ to be uncorrelated with the data vector:

$$\langle(\hat{\underline{p}} - \underline{p})\underline{d}^T\rangle = \underline{\underline{0}} \tag{4}$$

Angle brackets denote the expectation value, superscript ^{T} denotes the transpose, and $\underline{\underline{0}}$ is the zero matrix. It can be shown that eq. (4) is equivalent to requiring the mean square estimate error to be minimum. Then substitution of eqs. (3) and (2) gives

$$\begin{aligned}\underline{\underline{D}} &= \langle\underline{p}\,\underline{d}^T\rangle\,\langle\underline{d}\,\underline{d}^T\rangle^{-1} \\ &= \langle\underline{p}\,\underline{p}^T\rangle\,\underline{\underline{K}}^T\,[\underline{\underline{K}}\langle\underline{p}\,\underline{p}^T\rangle\underline{\underline{K}}^T + \underline{\underline{E}}]^{-1}\end{aligned} \tag{5}$$

where $\underline{\underline{E}}$ is the covariance matrix of measurement errors and is normally diagonal.

A closely related solution is known by the term "minimum information," in which the parameter covariance matrix $\langle\underline{p}\,\underline{p}^T\rangle$ in eq. (5) is replaced by a diagonal matrix. This solution is sub-optimum, but is often found to give satisfactory results.

A quasi-optimum nonlinear solution to the inverse problem can sometimes be constructed by identifying the

elements of the data vector $\underline{d}$ with *ad hoc* nonlinear functions of the brightness temperatures, $\underline{d}(\underline{T}_B)$. The trick is to find nonlinear functions that satisfy eq. (2) with small errors.

However, the discussion so far has ignored the fact that a radiometer does not measure the brightness temperature of the earth, but rather an antenna temperature. If the "true" brightness temperature of the earth at wavelength i is denoted by $\tilde{d}_i(x,y)$, then the antenna temperature is

$$d_i(x,y) = \iint_{-\infty}^{\infty} G_i(x' - x,\ y' - y)\ \tilde{d}_i(x',y')\ dx'\ dy' + e_i(x,y) \qquad (6)$$

where $G_i(x,y)$ is the gain pattern of the antenna at wavelength i, mapped onto the earth in coordinates x and y.

Nevertheless, eqs. (3) and (5) have generally been used to interpret satellite microwave data, by first making corrections to $\underline{d}$ in more or less rigorous ways for the antenna sidelobes. This appraoch is satisfactory when the main beams of the antenna patterns are the same size at each wavelength, which has been true for most of the multi-wavelength instruments launched to date.

Attainment of the highest possible spatial resolution at each wavelength, however, requires use of the largest practical antenna in a diffraction-limited mode. For such a system the beamwidth is proportional to the wavelength divided by the antenna diameter. One possible approach to inverting such data is to smooth the shorter wavelength images to make their resolution the same as that of the longest wavelength used to infer a particular parameter. Such an approach is workable, but clearly not optimum.

To obtain the optimum solution, consider the two-dimensional Fourier transform of the data (antenna temperatures):

$$d_i(u,v) = F\{d_i(x,y)\} \tag{7}$$

where u and v are coordinates in transform space, corresponding to x and y. It will be obvious from the arguments whether the spatial functions or their Fourier transforms are intended. The transform of eq. (6) is

$$d_i(u,v) = G_i^*(u,v)\ \tilde{d}_i(u,v) + e_i(u,v) \tag{8}$$

where superscript* denotes complex conjugate. The brightness temperature $\underline{\tilde{d}}(u,v)$ is given by

$$\underline{\tilde{d}}(u,v) = \underline{\underline{K}}\ \underline{p}(u,v) \tag{9}$$

where $\underline{\underline{K}}$ is the same matrix that occurs in eq. (2). Then

$$\underline{d}(u,v) = \underline{\underline{G}}^*(u,v)\ \underline{\underline{K}}\ \underline{p}(u,v) + \underline{e}(u,v) \tag{10}$$

where $\underline{\underline{G}}(u,v)$ is a diagonal matrix of antenna pattern transforms. The optimum linear solution, of the form (3), follows from the condition (4), where the transpose is replaced by the conjugate transpose (denoted by superscript$^+$) because we are dealing with complex quantities. The determination matrix is

$$\underline{\underline{D}}(u,v) = \underline{\underline{S}}(u,v)\ \underline{\underline{K}}^T\ \underline{\underline{G}}(u,v)[\underline{\underline{G}}^*(u,v)\ \underline{\underline{K}}\ \underline{\underline{S}}(u,v)\ \underline{\underline{K}}^T\ \underline{\underline{G}}(u,v) + \underline{\underline{E}}(u,v)]^{-1} \tag{11}$$

where

$$\underline{\underline{S}}(u,v) = \langle \underline{p}(u,v)\ \underline{p}^+(u,v) \rangle \tag{12}$$

is the spectral cross-power density matrix for the parameters, and E(u,v) is the same for the measurement errors.

A solution analogous to the minimum-information method is obtained by replacing $\underline{\underline{S}}(u,v)$ with

$$\underline{\underline{S}}_{MI} = \begin{bmatrix} \sigma_1^2 & & 0 \\ & \sigma_2^2 & \\ 0 & & \ddots \end{bmatrix} \qquad (13)$$

where σ_i is the standard deviation of parameter i. Eq. (13) is equivalent to modeling the geophysical parameters as white noise. Clearly many models intermediate between a minimum-information approach and a complete second-order statistical description of the geophysical parameters are possible.

The way in which (11) produces an optimum solution is that for spatial frequencies at which the antenna has little gain at a given wavelength, the matrix inside the brackets is dominated by the error power. Thus the corresponding channel is deemphasized in the inversion. Although the spatial and transform coordinates have been written as continuous, they would actually be gridded with resolution equal to that of the shortest wavelength. If the data grid is composed of independent measurements, then the errors will be white noise. But if the longer wavelength data is interpolated from a coarser grid, the error power will drop off at high spatial frequencies. However, the diagonal elements of $\underline{\underline{E}}(u,v)$ cannot be set to zero in eq. (11) at any spatial frequency since they provide regularization of the solution.

The estimated parameter images can be obtained in two ways:

$$\hat{\underline{p}}(x,y) = F^{-1}\{\underline{\underline{D}}(u,v)\ \underline{d}(u,v)\} \qquad (14a)$$

$$= \int_{-\infty}^{\infty}\int \underline{\underline{D}}(x - x',\ y - y')\ \underline{d}(x',y')\ dx'dy' \qquad (14b)$$

Whether a Fast Fourier Transform or a deconvolution algorithm proves to be faster for a given system is a question of implementation, and is outside the scope of this report. In either case, a non-trivial amount of data processing is implied. However, it should be remembered that the solution

(14) combines antenna pattern corrections and inversion in a single step.

In conclusion, it can be said that an optimum linear solution to the inverse problem for high-resolution microwave data is attainable. Complications arise if the projected antenna pattern changes across the scan, but scan geometries that maintain a constant incidence angle will minimize this problem. How serious it will be remains to be seen. Further research is also needed on the problems of nonlinearity and modeling of the statistics of geophysical parameters.

B.3 Bibliography

Atmospheric absorption, general:

Waters, J. W., Absorption and emission by atmospheric gases, in Methods of Experimental Physics, vol. 12: Astrophysics, Part B. (M. L. Meeks, ed.) Academic Press, 1976.

Oxygen absorption:

Liebe, H. J., G. G. Gimmestad, and J. D. Hopponen, Atmospheric oxygen microwave spectrum - experiment versus theory. IEEE Trans. Antennas Propag., AP-25, 327-335, 1977.

Rosenkranz, P. W., Shape of the 5 mm oxygen band in the atmosphere. IEEE Trans. Antennas Propag., AP-23, 498-506, 1975.

Water vapor absorption:

Liebe, H. J., and T. A. Dillon, Accurate foreign-gas-broadening parameters of the 22-GHz H_2O line from refraction spectroscopy. J. Chem. Phys., 50, 727-732, 1969.

Rusk, J. R., Line-breadth study of the 1.64 mm absorption in water vapor. J. Chem. Phys., 42, 493 , 1965.

Liquid water absorption:

Gunn, K. L. S., and T. W. R. East, The microwave properties of precipitation particles. Quart. J. Royal Meteor. Soc., 80, 522 , 1954.

Tsang, L., J. A. Kong, E. Njoku, D. H. Staelin, and J. W. Waters, Theory for microwave thermal emission from a layer of cloud or rain, IEEE Trans. Antennas Propag., AP-25, 650-657, 1977.

Inversion theory:

Deepak, A. (ed.), Inversion Methods in Atmospheric Remote Sounding. NASA CP-004. National Technical Information Service, 620 pp., 1977.

Fymat, A. (ed.) Inversion Methods in Atmospheric Radiation Research. Vol. I: Temperature Sounding. Jet Propulsion Laboratory, 1977.

Rodgers, C. D., Retrieval of atmospheric temperature and composition from remote measurements of thermal radiation. Rev. Geophys. Space Phys., 14, 609-624, 1976.

Antenna patterns:

Kraus, J. D., Radio Astronomy, McGraw-Hill, 1966.

Bracewell, R. N., Restoration in the presence of errors. Proc. IRE 46, 106-111, 1958.